Effects of photobiomodulation laser on a laser-induced choroidal neovascularization model

Dr. Marzieh Tahmasebi Sarvestani, MBBS, MedSci(Hons)

Ophthalmic Research Laboratories, Adelaide Health and Medical Sciences Building, North Terrace, University of Adelaide, Adelaide, South Australia, Australia.

Contents:

Declaration

I certify that this work contains no material which has been accepted for the award of any other degree or diploma in my name, in any university or other tertiary institution and, to the best of my knowledge and belief, contains no material previously published or written by another person, except where due reference has been made in the text. In addition, I certify that no part of this work will, in the future, be used in a submission in my name, for any other degree or diploma in any university or other tertiary institution without the prior approval of the University of Adelaide and where applicable, any partner institution responsible for the joint-award of this degree. I give permission for the digital version of my thesis to be made available on the web, via the University's digital research repository, the Library Search, and through web search engines, unless permission has been granted by the University to restrict access for a period of time. I acknowledge the support I have received for my research through the provision of an Australian Government Research Training Program Scholarship.

Marzieh Tahmasebi Sarvestani

July 2023

Acknowledgements

Thank you to Professor Robert Casson, Dr Glyn Chidlow, and Dr John Wood from the Ophthalmic Research Laboratory, University of Adelaide, for your guidance and support during my candidature. I would also very kindly like to thank ELLEX for donating the PBM laser utilised in the series of experiments, and for providing ongoing technical support and maintenance. The work contained within this thesis was supported by a charitable donation from Mrs. Barbara O'Connor through the Royal Adelaide Hospital Vision Research Fund, and the Australian Government Research Training Program Stipend Scholarship.

Abbreviations

aFGF/FGF-1: Acidic fibroblast growth factor / fibroblast growth factor-1

AMD: Age-related macular degeneration

Ang-1: Angiopoietin-1

AREDS: Age-Related Eye Disease Study

ATP: Adenosine 5'-triphosphate

BCVA: Best corrected visual acuity

BDNF: Brain-derived neurotrophic factor

bFGF/FGF-2: Basic fibroblast growth factor / fibroblast growth factor-2

CCO: Cytochrome c oxidase

CD3: Cluster of differentiation 3

CNTF: Ciliary neurotrophic factor

CNTFR: Ciliary neurotropic factor receptor

CNV: Choroidal neovascularization

COX: Cyclooxygenase

CW: Continuous wave

Cyt c: Cytochrome c

dAMD: Dry age-related macular degeneration

DAPI: 6'-Diamidino-2-phenylindole

DME: Diabetic macular oedema

DNA: Deoxyribonucleic acid

CD68/ED1: Cluster of differentiation- 68

EDTA: Ethylenediaminetetraacetic acid

EGF: Epidermal growth factor

ELISA: Enzyme linked immunosorbent assay

ERG: Electroretinogram

fd Nd:YAG: Frequency-doubled neodymium: yttrium aluminium garnet

FFA: Fundus fluorescein angiography

FGFR: Fibroblast growth factor receptor

GABA: Gamma-aminobutyric acid

GCL: Ganglion cell layer

GS: Glutamine synthetase

HIF-1α: Hypoxia-inducible factor 1-alpha

HPBM: High-dose photobiomodulation laser

HSP32: Heat shock protein-32

IB4: Isolectin-B4 (*Griffonia simplicifolia*)

IBA-1: Ionized calcium-binding adapter molecule 1

iBRB: inner blood retinal barrier

IFN- γ: Interferon-gamma

IGF: Insulin-like growth factor

IL-1α: Interleukin-1-alpha

IL-1ß: Interleukin-1-beta

IL-6: Interleukin-6

INL: Inner nuclear layer

iNOS: Nitric oxide synthase

IPL: inner plexiform layer

IS: photoreceptor inner segment

JAM: Junctional adhesion molecule

LLLT: Low-level light therapy

LPBM: Low-dose photobiomodulation laser

MMP: Matrix metalloproteinases

MPO: Myeloperoxidase

nAMD: Neovascular (wet) age-related macular degeneration

NFL: nerve fibre layer

NGF: Nerve growth factor

NHS: Normal horse serum

NHS-T: Normal horse serum with triton

NO: Nitric oxide

oBRB: Outer blood retinal barrier

OCT: Optical coherence tomography

ONL: Outer nuclear layer

OPL: Outer plexiform layer

OS: photoreceptor outer segment

PBM: Photobiomodulation

PBS: Phosphate buffered saline

PBS-T: Phosphate buffered saline with triton

PCNA: Proliferation cell nuclear antigen

PDGF-BB: Platelet-derived growth factor subunit B

PDGF: Platelet-derived growth factor

PDGFR-ß: Platelet-derived growth factor receptor beta

PDR: Proliferative diabetic retinopathy

PEDF: Pigment epithelium-derived factor

PEDFR: Pigment epithelium-derived factor receptor

R/NIR: red/near-infrared light therapy

ROP: Retinopathy of prematurity

RPC: Radial peripapillary capillaries

RPE-65: Retinal pigment epithelium-specific 65 kDa protein

RPE: Retinal pigment epithelium

SD-OCT: Spectral domain optical coherence tomography

TGF-β: Transforming growth factor beta

TIMP: Tissue inhibitor of metalloproteinases

TNF-α: Tumour necrosing factor alpha

TSP1: Thrombospondin-1

VEC: Vascular endothelial cells

VEGF: Vascular endothelial growth factor

VEGFR: Vascular endothelial growth factor receptor

WM: Wholemount

ZO: Zonula occludens

Abstract

Age-related macular degeneration is the leading cause of irreversible vision loss in the developed world. Late-stage age-related macular degeneration is classified into two basic sub-types: dry (atrophic) and wet (neovascular). The neovascular subtype accounts for the majority of severe vision loss from age-related macular degeneration. It is characterised by abnormal angiogenesis in the choroid/retina with associated haemorrhage and leakage at the macula. Inflammation and ischaemia are pathogenic components of neovascular age-related macular degeneration and overexpression of vascular endothelial growth factor is a key molecular driver. The current treatment of neovascular age-related macular degeneration involves repeated intravitreal injections of anti-vascular endothelial growth factor agents that block the pro-angiogenic pathway. Although repeat intravitreal injection of anti-vascular endothelial growth factor agents has revolutionized the management of neovascular age-related macular degeneration, often stabilizing or improving vision, it is associated with an enormous economic burden and is not without potentially significant complications. In addition, ongoing macular fibrosis limits its efficacy in a substantial proportion of individuals. Adjunctive treatments that improve visual outcomes and/or reduce the intravitreal injections burden are clinically and economically desirable.

Photobiomodulation laser has the potential to target the up-stream hypoxic and pro-inflammatory drive associated with neovascular age-related macular degeneration. It has pleotropic effects on cell survival and energy metabolism. It is believed that the biological effects of photobiomodulation are mediated through increased activity of cytochrome c

oxidase, the rate-limiting enzyme in the mitochondrial electron transport chain. Photobiomodulation stimulates adenosine triphosphate production and in various disease models has been shown to mitigate oxidative stress-induced inflammation.

This study investigated the efficacy of photobiomodulation therapy in a laser-induced rat model of neovascular age-related macular degeneration and attempted to elucidate the potential anti-inflammatory and anti-angiogenic mechanisms that may be influenced by this novel therapeutic laser treatment. Initially, the laser-induced choroidal neovascularization model was optimized and, subsequently, two energy settings of photobiomodulation laser were applied to the developed model. Neovascular membranes were quantified using complimentary methods comprising immunohistochemistry for new vessel antigens, spectral domain optical coherence tomography and fluorescein angiography. Analyses were performed to ascertain if treatment successfully reduced the size of the neovascular membrane and the degree of vessel leakage, and thus, improved the tissue outcome. The immune cell response and level of vascular endothelial growth factor in retinal tissues were analyzed to elucidate a mechanism for the observed effects of photobiomodulation treatment in the choroidal neovascularization model.

Pre-treatment with photobiomodulation laser significantly reduced the size and volume of the neovascular membranes and promoted normalization of vascular barrier function. These observations were not associated with alterations in vascular endothelial growth factor levels; however, there was evidence that photobiomodulation treatment was associated with modulation of resident retinal microglia and Müller cell inflammatory activation, as well as reduction in infiltration of vascular-derived leukocyte populations.

However, the alternative anti-angiogenic pathway mediated by photobiomodulation was not elucidated.

The findings in this thesis motivate further translational research investigating the role of adjuvant photobiomodulation laser therapy in conjunction with routine intravitreal anti-vascular endothelial growth factor injection treatment in clinical neovascular age-related macular degeneration.

Chapter 1:

A review of the literature

1.1 Basic Anatomy of the Vertebrate Retina

The vertebrate retina is organised as a highly laminar structure with three somatic layers intercalated by two synaptic layers (Figure 1.1). It comprises the photoreceptor outer segment layer (OS), outer nuclear layer (ONL), outer plexiform layer (OPL), inner nuclear layer (INL), inner plexiform layer (IPL), ganglion cell layer (GCL), and nerve fiber layer (NFL) [1]. The ONL contains the cone and rod photoreceptor cells that mediate photopic and scotopic vision, respectively. Although, rod photoreceptors make up 95% of the photoreceptor population, cone photoreceptors, which primarily populate the macula, are responsible for high acuity vision. Photoreceptor cells are composed of an outer segment (OS), inner segment (IS), cell body and synaptic terminus. They undertake phototransduction, the key process that involves conversion of photonic stimuli into neuronal signals [2]. This initial information is processed and modulated by horizontal, amacrine, and bipolar cells, three major classes of interneuron. These in turn synapse with projector neurons, retinal ganglion cells, that extend axons via the optic nerve and optic tracts to transmit visual information to the visual cortex and visual association areas of the brain to reach conscious visual perception [3]. Glial cells reside throughout the retina. Astrocytes and Müller cells, the two neuron-supporting macroglia of the retina, and microglia, the resident macrophages of the retina, constitute this key glial cell population of the retina [4]. These cells perform a multitude of functions to support the aforementioned retinal cell populations [5-9]. The retina, retinal pigment epithelium (RPE), and choroid are closely linked anatomically and functionally.

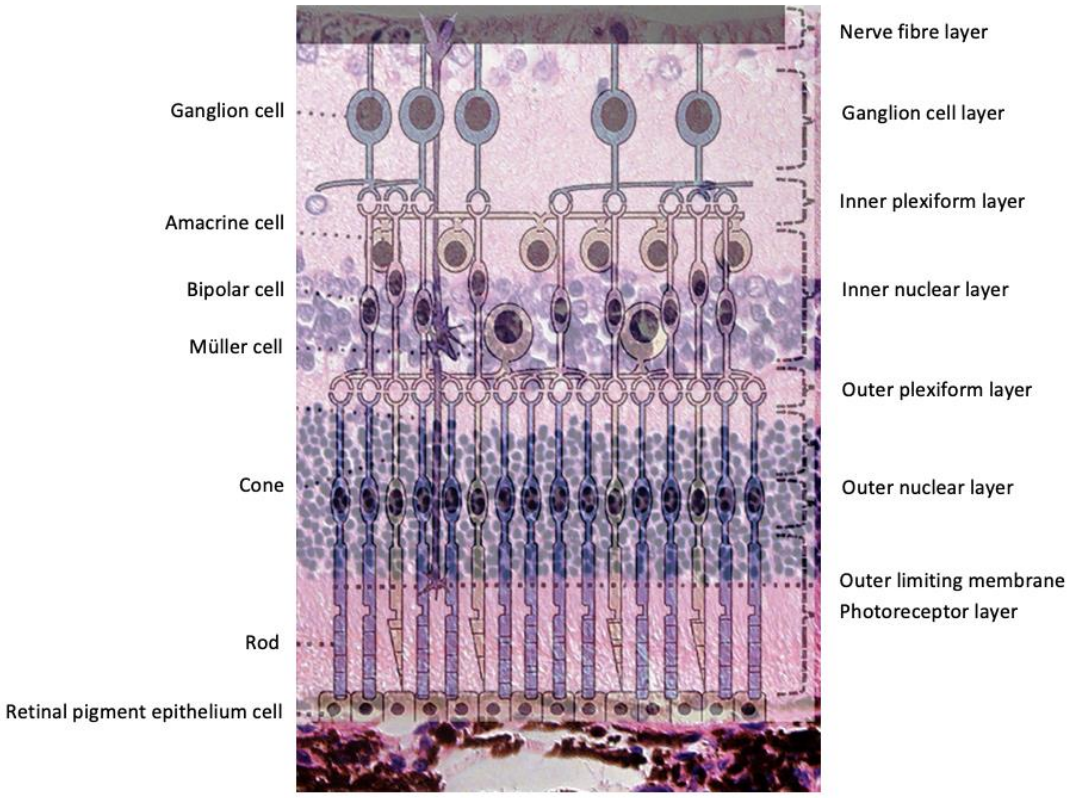

Figure 1.1: Schematic representation of the vertebrate neural retina and retinal pigment epithelium. Modified from Skalicky [10].

1.2 Retinal Vasculature and Barriers: Relevant Cellular and Molecular Aspects

The process of phototransduction and neurotransmission is metabolically demanding, and the photoreceptors have relatively large oxygen demands; however, the fact that blood is a relatively poor transmitter of light has resulted in evolutionary adaptations to blood flow in vertebrate retinas [11-14]. The inner retina receives blood supply from the retinal vessels whilst the outer retina, principally the photoreceptors, is supplied by the choriocapillaris. The retinal capillary system comprises radial peripapillary capillaries, and superficial and deep retinal plexuses. The radial peripapillary capillaries occupy the NFL, whilst the

superficial plexus is situated between the NFL and GCL, and the deep plexus is situated between the INL and OPL [15].

The retina is anatomically an outpouching of the diencephalon and the retinal vessels, as extensions of brain vasculature, exhibit a blood-retinal barrier. Endothelial cell-derived platelet derived growth factor (PDGF) plays a role in establishing and maintaining the blood-retinal barrier, by recruiting pericytes through the PDGF receptor beta (PDGFR-ß) [16, 17]. Pericytes are smooth-muscle-like cells that have an intimate relationship with microvascular endothelial cells. These cells induce vessel quiescence by wrapping around capillaries and extending long cytoplasmic processes which contact with other pericytes and multiple endothelial cells. They are a key player in blood vessel maturation and influence vascular permeability and endothelial cell mitogenesis and migration by liberating opposing factors, vascular endothelial growth factor (VEGF) or angiopoietin-1 (Ang-1), depending on the local oxygen demand of the tissue [18-20].

Angiopoitin-1 is a key factor involved in modulating pathological angiogenesis. It is a well-known anti-permeability factor. It is understood to promote degradation of hypoxia induction factor 1 alpha (HIF-1α), a key upstream induction factor for VEGF-A under hypoxic conditions, and acts as a ligand for endothelial cell-specific tyrosine kinase Tie-2/Tek receptor phosphorylation. It is also an induction factor for tight junction protein expression in microvascular endothelial cells. In this regard, it appears that it directly opposes the pro-permeability and pro-angiogenic effects of VEGF, stabilising the blood-retinal barrier [21-24].

PDGF is liberated by RPE, retinal ganglion cells (RGCs), and amacrine cell as part of normal retinal development, and plays an ongoing role in promoting maturity and stability of the retinal microvasculature to maintain adult retinal homeostasis [25, 26]. The PDGF-BB isomer is a chemoattractant for PDGFR-ß+ pericyte recruitment [27]. It has been observed that blockade of PDGF is associated with impaired pericyte recruitment, and associated aberrant endothelial cell mitogenesis, ultimately resulting in endothelial cell growth arrest and regression of retinal neovascular disease [25, 28]. It is thought that the loss of pericyte-derived VEGF is the specific mechanism underlying this phenomenon [29]. It is postulated that PDGF-blockade makes endothelial cells more suspectable to VEGF-blockage [17, 30]. In the presence of an angiogenic signal, pericytes disengage from the basement membrane shared with endothelial cells through proteolytic degradation mediated by matrix metalloproteinases (MMPs). These tissue factors are involved in extracellular matrix turnover, maintenance of basement membrane integrity, and influence endothelial cell migration and tissue invasion. MMPs liberate endothelial cells from tonic inhibition, allowing them to form new vessels in response to this angiogenic signal [24].

The retinal vascular endothelial cells (VEC) express tight junctions facilitated by their close relationship with pericytes, retinal astrocytes and Müller glial cells, which are separated from the endothelium by a basal lamina; together these form the inner blood retinal barrier (iBRB) [31]. Müller cells are radially oriented glial cells that span the entire depth of the neural retina from the outer limiting membrane (OLM) to the outer limiting membrane (ILM). They form connections with retinal neurons and bridge the various compartments of the retina, allowing for functional exchange of water, ions, neurotransmitters such as gamma-aminobutyric acid (GABA) and glutamate, and

nutrients in the form of glucose and lactate/pyruvate. They also play a role in recycling photopigment constituents, phagocytosis of cellular debris, waste product removal, and modulating the microenvironment especially in regard to potassium homeostasis [4, 32-40]. Müller cells contribute to the iBRB by ensheathing retinal blood vessels, and enhance tight junction expression in, and inhibit proliferation of, VECs by constitutively liberating factors like thrombospondin-1 (TSP-1), and pigment epithelium derived factor (PEDF) [31, 41-45]. These factors selectively cause apoptosis of endothelial cells of new blood vessels without affecting those of established mature blood vessels [46]. This is pertinent in the foveal avascular zone, the central 450-500 μm of the macula, as the maintenance of this avascular zone is thought to be due to a very high expression of PEDF in this region [47]. Müller cells also release VEGF, basic fibroblast growth factor (bFGF/FGF-2) and transforming growth factor beta (TGF-ß), which in combination are fundamental for vasculogenic and angiogenic maintenance of the iBRB [48-51]. Astrocytes make up a relatively minor subset of the macroglial cell population in the retina. In many regards, they behave in a similar manner to Müller cells. Astrocytes contribute to maintenance of the iBRB and modulate pathological angiogenesis in a similar manner through expression of TGF-ß and Ang-1, key factors in modulating pathological angiogenesis, and by extending processes to the ILM at the vitreo-retinal border, intermingling with Müller cell end-feet [24, 31, 34, 52, 53].

Microglia are maintained in a resting-state through tonic inhibition [54, 55]. Under these physiological conditions, microglia appear as horizontally ramified cells located in the NFL, GCL, and IPL. In this ‘resting phenotype’ these cells constantly survey the microenvironment, aided by their arborescent morphology [54-57]. Perivascular

macrophages and microglia play an important role in maintenance of the blood-retinal-barrier to regulate the extracellular milieu and to confer immune privilege by deterring the inflammatory immune response. They appear to have secondary blood-retinal-barrier properties by phagocytosing extravasated proteins to protect the extracellular environment from exogenous fluid [31, 58]. This is especially pertinent in the context of compromised and immature vessels in choroidal neovascular membranes.

The outer retina receives its nutritive supply from the choroidal vessels. The outer blood retinal barrier (oBRB) is 1.4-1.5 μm thick and is formed by tight junctions between adjacent RPE cells, and Bruch's membrane, of which the choriocapillary basement membrane forms the outer layer. It forms an impermeable barrier separating the neural retina from the choroidal blood vessels. Thus, exchange between the vasculature and the retinal microenvironment is strictly controlled [59, 60]. The choriocapillary network receives 65-85% of the total ocular blood supply. It thus has a capacity to supply blood to the retina that exceeds the photoreceptor demand by 20 times [61]. The choroidal VECs have fenestrations to increase permeability of solutes and macromolecules [16]. The photoreceptor population is highly reliant on the RPE and choroid to carefully control the microenvironment. The function and metabolic demand of photoreceptors varies between the macular and peripheral retina. The foveal avascular zone correspondingly has a higher capillary density (7:1 ratio) and larger capillary diameter (34 μm versus 22-28 μm) in the choriocapillary network. Furthermore, the density and morphology of RPE cells also varies from central to peripherally, being less pigmented, more numerous, and more cuboidal at the macular compared to the periphery [62, 63].

The apical processes of the RPE cells inter-digitate with the outer segments of the rod and cones photoreceptors via long microvilli, whilst the basal surface is associated with Bruch's membrane with the aid of basal infoldings to increase the surface area [64, 65]. RPE cells maintain photoreceptor membrane potential, reinforce the attachment of the photoreceptor to the RPE, and regulate nutrient content and homeostasis of the retina via their polarity. This polarity facilitates the directional transport of regenerated photoreceptor visual pigments, metabolic waste products, oxygen, water, ions, and nutrients, such as glucose, amino acids, retinol and fatty acids between the choriocapillaries and the retina via specialised transporters and channels [63, 66]. The RPE cell cytoskeleton maintains the polarity of these cells as well as facilitates phagocytosis of outer segment tips that are shed by the photoreceptor during their constant renewal process and help transport these phagosomes to undergo lysosomal degradation [5, 60, 67-71].

The oBRB, along with immunosuppressive factors liberated by the RPE, confer immune privilege to the retina [59, 60, 72, 73]. Tight junctions are apically located transmembrane proteins that can be considered as an extension of the cell cytoskeleton that effectively forms a fused region between adjacent cell membranes, obliterating the inter-endothelial space, and conferring selective barrier properties to the capillaries. The main constituents are the claudin, occludin, JAM, and ZO protein families, however, cingulin, 7H6, symplekin and cadherin-5 also contribute to the junctional organisation within the cytoplasm [16, 31]. Tight junctions serve a dual barrier and fence function, controlling the flux of solutes, and movement of proteins and lipids from the basolateral (retinal and choroid capillaries) to apical (neural retina) membrane surface [16].

Inflammation and hypoxia results in the liberation of cytokines that trigger a cascade of changes in the BRB. Several key soluble factors are known to facilitate BRB breakdown in neovascular age-related macular degeneration (nAMD). Cytokines such as tumour necrosing factor alpha (TNF-α), interleukin-1-beta (IL-1ß), and VEGF are associated with rapid changes in the endothelial cell, with loss of endothelial cell tight junctions, appearance of vacuoles in endothelial cell membranes, and increased protein transcytosis into the retinal tissue [58]. These factors are upregulated in recruited neutrophil, retinal VECs, and retinal glia under conditions of ischaemia and inflammation [74, 75]. RPE cells are dense with mitochondria, mandated by the metabolically demanding phototransduction cycle that involves continual degradation and resynthesis of photoreceptor outer segments, thus exposing RPE cells to chronic oxidative stress [59, 60, 65, 72, 73]. The RPE cells thus liberate trophic factors such as VEGF, PEDF, PDGF, TGF-β, fibroblast growth factor (FGF), and ciliary neurotropic factor (CNTF), among others in an autocrine capacity. These are essential for maintenance of the adult retina by activating down-stream pathways that influence endothelial cell mitogenesis and migration to regulate choriocapillaris densities, as well as upregulate anti-apoptotic pathways to maintain deoxyribonucleic acid (DNA) integrity, and optimise RPE cellular function, survival and resistance to oxidative stress [60, 63, 69, 70, 76-84].

1.3 Vascular endothelial growth factor

VEGF is the master controller of retinal angiogenesis in health and disease and is the target of the best current available treatment for nAMD [20]. Hypoxia is known to be a potent stimulator of VEGF secretion. Under hypoxic conditions expression of VEGF is particularly upregulated by the RPE, Müller glia and astrocyte cell populations, and to a

lesser extent by perivascular macrophages, RGCs, retinal pericytes, and VECs [48, 49, 85-88]. VEGF belongs to a family of cytokines; VEGF-A, VEGF-B, VEGF-C, VEGF-D, and placental growth factor (PIGF) [89]. These play an important role in angiogenesis and lymphangiogenesis [90].

VEGF-A is the main isoform that regulates angiogenesis and vascular permeability. VEGF-A exerts its influence on VEC mitogenesis, migration, gene expression and vasopermeability through high-affinity endothelial-specific tyrosine kinase receptors, VEGFR-1 (Flt1) and VEGF-2 (Flk/KDR) [89, 91-94]. VEGF-A has an order of magnitude greater affinity for VEGFR-1 than VEGFR-2, but the latter has proportionally enhanced signal amplitude through greater mitogen-activated protein kinase (MAPK) autophosphorylation pathway activity. VEGFR-2 is expressed by endothelial and retinal cells at all stages of ocular development and is considered the chief receptor signal for angiogenesis [95, 96]. The other VEGF isoforms, VEGF-B, VEGF-C, VEGF-D and PIGF bind to the VEGF-1 and VEGFR-2 receptor only weakly, and thus do not have a significant role to play in control of angiogenesis. VEGF-C and VEGF-D, bind avidly to VEGFR-3 on lymphatic endothelial cells to play a critical role in lymphangiogenesis [95]. In the retinal microvasculature, VEGF-A increases paracellular and transcellular permeability by induction of protein kinase C-mediated endocytosis of occludin tight junctions, redistribution of the occludin component of endothelial tight junctions, and increased inducible nitric oxide synthase (iNOS) mediated caveolae formation in VECs. This VEGF-mediated vascular permeability is potent, reportedly being 50,000 times that of histamine.

The VEGF-driven increased vasopermiability of both the iBRB and oBRB contributes to the accumulation of subretinal fluid and macular oedema in nAMD [16, 75, 97-100]. VEGF-A derived isotype $VEGF_{165}$ is the most pertinent in nAMD [93, 94]. Increased understanding of other proliferative retinal diseases, such as proliferative diabetic retinopathy (PDR), has also paved the way for better understanding of nAMD; these neovascular disease of the retina share a common pathogenic mechanism of hypoxia that promotes an imbalance between VEGF/PEDF. Derangement in the PEDF/VEGF ratio is implicated in choroidal neovascularization (CNV) in nAMD [101]. This ultimately leads to neovascularisation and increased vascular permeability, as in healthy subjects, PEDF expression is 10x higher than VEGF, and predominantly localises to RPE cells [102-108]. PEDF, also known as SERPINF1, is a potent anti-angiogenic, and neuroprotective molecule predominantly released from the RPE and Müller glia cells of the retina [109-114]. PEDF is one of the key endogenous inhibitors of angiogenesis in the eye, along with TSP1, endostatin, and angiostatin [12-14, 115]. These pathogenic mechanisms discussed are as a consequence of unrestrained activity of VEGF, as coincident down-regulation of endogenous antiangiogenic peptides create a pro-angiogenic environment, contributing to the development and progression of CNV in nAMD [116-118].

The impairment of the BRB is associated with extravasation of plasma proteins and deposition of a provisional extracellular matrix. Liberation of MMPs, and down-regulation of their antagonists, tissue inhibitor of metalloproteinases (TIMPs) also occur in the presence of VEGF [50]. MMPs are abundantly present in drusen and neovascular membranes of subjects with nAMD and PDR; deficiency of MMPs is associated with reduced neovascular membrane formation [119-123]. TIMPs are known to prevent

neovascularization by inhibiting VEC invasion even in the presence of potent pro-angiogenic factors like bFGF/FGF-2 and VEGF [124-131]. Deficiency of TIMPs is associated with Sorsby Fundus Dystrophy, an autosomal dominant macular dystrophy, characterized by drusen deposition and neovascular membrane formation, analagous to what is seen in AMD. RPE-derived TIMPs are notably absent at the site RPE cell loss and neovascular membrane formation in subjects with nAMD.

If the BRB is disrupted and Müller cells and the RPE pump action is overwhelmed, the transcellular movement of fluid from the inner retinal tissue and subretinal space to the vasculature is disturbed, and an imbalance in influx and efflux of fluid into the retinal spaces occurs [34, 37, 132]. As a result of this imbalance, fluid accumulates in the extracellular space as a result of Starling's law; $flow = L_p[P_{plasma} - P_{tissue} - \sigma(\pi_{plasma} - \pi_{tissue})]$, where L_p is the membrane permeability, P is the hydrostatic pressure, σ is the osmotic reflection coefficient, and π is the protein osmotic pressure. Retinal oedema results in increase retinal extracellular protein and increased tissue compliance, reducing P_{tissue}. Fluid accumulation at the macula results in macular oedema. This process causes neuronal dysfunction and death, ultimately impairing central vision [32, 34, 36-38].

1.4 Neovascular age-related macular degeneration

AMD is the leading cause of blindness in the developed world, and the fourth leading cause of blindness worldwide [133, 134]. It is a disease of the elderly and has a predilection for Caucasian individuals compared to that of other ethnic groups (Asian, African, Hispanic) at every stage of disease. It has a prevalence of 8% and due to the ageing population, is becoming more prevalent at an exponential rate, with an expected global

burden of 300 million by 2040 [135]. It causes damage to the macula, the region of the retina responsible for cone-derived, high-acuity vision. AMD has significant non-visual morbidity associated with it, with close to twice the rate of depression compared to age-matched populations [136, 137].

There are four broad classifications of AMD as defined by the Age-Related Eye Disease Study (AREDS) [138]. Advanced AMD is typically categorized into two key subtypes; dry (atrophic) and wet (neovascular/exudative). The neovascular subtype, also known as exudative AMD, accounts for 10-15% of AMD cases, and 80-90% of AMD-related vision loss [139-141]. Common subtypes are characterised by abnormal blood vessel growth from the choroid into the retinal layer. This phenomenon is called choroidal neovascularisation (CNV). These blood vessels break through Bruch's membrane and the RPE, and grow into the retina, causing exudative and haemorrhagic detachment, and ultimately macular fibrosis. Functionally, this pathology is associated with metamorphopsia and usually a profound degradation of central vision. The chronic fibrotic component, referred to as geographic atrophy, remains essentially untreatable [139-143].

Whilst some factors are linked to the development of AMD, such as aging, smoking, diet, obesity, vascular disease, and heredity, the precise mechanism for its development is still unknown. The current perspective is that the interplay between chronic hypoxia, low-grade inflammation, and complement activation causes RPE cell and glial cell dysfunction [144-148]. It is understood that ageing in-itself is characterised by dysregulation of the immune system, with a shift towards pro-inflammatory and pro-oxidative stress milieu. This is believed to place glial cells in a 'primed' state. Consequently, glial cell

function is altered, leading to excitotoxicity, dysfunctional synaptic activity, downregulated trophic factor production, and ultimately, to apoptotic cellular death. It is speculated that in conditions like AMD oxidative stress and inflammation are amplified, perpetuating this cytotoxic state [34, 54].

1.5 Inflammation in neovascular age-related macular degeneration

Chronic inflammation contributes to the pathogenesis of AMD through glial-glial and cytokine-endothelial interactions. Retinal microglia are a specialized population of resident retinal immunocompetent cells that are intimately involved in retinal inflammation, immune function, and tissue repair, but also fulfil the role of a scavenger cell, phagocytosing cellular debris [54, 149, 150]. They are activated and migrate to the site of retinal injury and are believed to play a role in various retinal degenerative processes. Microglial activation is a pivotal step in the development of CNV in nAMD. This is reflected in AMD maculae, where both microglial cells and perivascular macrophages are noted to relocate to the subretinal space in close contact with drusen deposits and express a higher pro-inflammatory 'M1-phenotype' compared to a reparative 'M2-phenotype' chemokine transcript ratio when compared to normal age-matched eyes [151-153]. In this cytotoxic form, glia down-regulate expression of neurotrophins such as bFGF/FGF-2, TGF-ß, PDGF, epidermal growth factor (EGF), insulin-like growth factor (IGF), nerve growth factor (NGF), and brain-derived neurotrophic factor (BDNF). These factors are known to regulate neuronal growth, modulate gliotic reactivity and be protective against cell death induced by hypoxia, oxidative stress, tissue inflammation, apoptosis, and glutamate excitotoxicity in fundamental retinal cell populations; namely, photoreceptors, ganglion cells and RPE cells [52, 149, 154-167]. These glial–neuron cell interactions in the retina

are important for photoreceptor survival [161, 168-181]. Retinal glial act as a template for neuronal and vascular growth and structural organization of the developing retina and ongoing maintenance of the functional and mechanical integrity of the adult retina [20, 182]. Thus, the loss of glia-derived trophic support to glia and neurons perpetuates retinal degeneration [52, 149, 150, 165-167, 183].

Furthermore, in a cytotoxic state, microglia secrete oxidative products, and pro-inflammatory cytokines; namely, TNF-α, IL-1ß, interleukin-6 (IL-6), and interferon-gamma (IFN-γ), which perpetuates further polarization to the cytotoxic phenotype. There is cross-talk between microglia and Müller cells, thus, microglial activation detrimentally alters the Müller cell response under conditions of stress and injury [56, 184]. This Müller cell phenotype switch towards gliosis is associated with upregulation of the expression of pro-inflammatory cytokines, endothelial cell adhesion molecules, and immune cell chemokines [185]. This in turn leads to blood-retinal barrier breakdown, and the activation and recruitment of additional microglia. This is instigated and perpetuated by the retinal Müller cells, and perivascular macrophages, which are known to be abundantly present in CNV membranes of subjects with AMD, and which in turn release more IL-1ß and TNF-α [87, 88].

Inhibition of immune cell infiltration into retinal tissue is associated with inhibition of CNV development [186-188]. This is likely due to reduced cytokine release. Ultimately, TNF-α is considered the master controller of inflammation. TNF-α is an induction factor for IL-1ß and IL-6 [189]. These factors appear to have synergistic amplifying effects on BRB breakdown [58, 75, 190-195]. TNF-α disrupts retinal VEC tight junctions in the iBRB and oBRB

and is known to upregulate expression of intercellular adhesion molecue 1 (ICAM-1), platelet endothelial cell adhesion molecule 1 (PECAM-1) and vascular cell adhesion protein 1 (VCAN-1) receptor adhesion molecule expression on VEC membranes [74, 75, 195, 196]. Furthermore, it appears to be a signal transduction molecule for VEGF in the RPE [75, 197, 198]. The reduction in serum VEGF levels with blockade of TNF-α by adalimumab adds further weight to the importance it plays in nAMD [199]. IL-1ß directly induces VEGF expression and is a potent chemotactic factor for leukocytes, which induce break down of VEC tight junctions during infiltration across the endothelial barrier. In this regard, it differs from TNF-α, which directly induces tight junctional disruption [58, 75, 190-195].

Pathological activation of the complement cascade is believed to be another key mechanism implicated in the development of AMD [200-207]. Blockade of complement factors C3 and C5, which are the key factors in the formation of membrane attack complexes (MAC), prevents CNV development [208-210]. IL-1ß is an induction factor for the complement cascade, in particular C3 [9]. There are numerous AMD susceptibility genes affecting the alternate complement cascade identified in the literature, however, the complement factor H (CFH) and complement factor B and complement component 2 (CFB/C2) pathogenic gene variants are present in 74% of AMD patients [144, 211-214]. This may explain why complement components C3a and C5a are found in abundance in drusen and noted to be elevated in the serum of AMD subjects [215-219]. This in turn appears to promote aberrant angiogenesis by propagating retinal inflammation and inducing VEGF expression in RPE cells in AMD [210].

1.6 Mitochondrial dysfunction and oxidative stress in neovascular age-related macular degeneration

Several lines of evidence indicate a role for mitochondrial dysfunction and resultant chronic oxidative stress in the pathogenesis of AMD. Mitochondria are the primary source of reactive oxygen species (ROS) in the cell, as part of the normal process of oxidative phosphorylation. Thus, mitochondria are particularly susceptible to oxidative stress. Superoxide dismutase is a key antioxidant in mitochondria and first line of defence against oxidative stress. This system appears to be overwhelmed by chronic oxidative stress during aging. This causes secondary mitochondrial dysfunction such as mitochondrial depolarization, swelling, and release of cytochrome c (cyt c), with resultant dysregulation of the main mitochondrial apoptotic pathway, BAX/BCL-2 ratio, and induction of apoptosis [220-224].

This chronic oxidative stress appears to be mediated by several mechanisms. Age-related basement membrane thickening and capillary drop out in the choriocapillaris, which is exacerbated in AMD, results in diminished lysosomal activity and phagocytosis of the photoreceptor outer segments, and disrupts the transportation of nutrients and cell debris through the RPE to and from the choriocapillaris [225-227]. Evidence suggests that this capillary drop out precedes RPE loss in nAMD [228]. RPE cells secrete VEGF to maintain the choriocapillary bed and their permeability [229]. Coincident loss of RPE results into choriocapllary atrophy, and in particular, reduction in choriocapillary diameter and loss of capillary fenestrations [225, 230]. This is believed to be due to loss of RPE-derived VEGF with RPE degeneration [231, 232]. This promotes a pro-inflammatory and hypoxic environment [228].

Gene and protein analysis of mitochondria in retina and RPE of aged subjects, including subjects with AMD demonstrate that there is accumulation of mitochondrial DNA mutations with age [233]. Teruk et al found that mitochondrial DNA mutations occurred only in the RPE of donors and that the quantity of mutations correlated with AMD severity [234]. An earlier study in AMD subjects, that investigated the whole cell and not just mitochondria, showed similar findings [235]. As with other groups, they demonstrated mutations in genes coding process involved in oxidative phosphorylation, adenosine triphosphate (ATP) production, phagocytic function, and cytoprotective proteins such as heat-shock-proteins (HSPs) [234]. This is supported by evidence demonstrating decreased mitochondrial membrane potential, reduced cytochrome c oxidase (CCO) activity and impaired oxidative phosphorylation in the mitochondrial respiratory chain, and decreased phagocytic activity and survival of RPE cells [220-222, 236]. However, they demonstrated that there was no difference between RPE cells at the macula versus the peripheral retina, which does not correlate to the selective macular degeneration that occurs in AMD [234]. The retina is vulnerable to oxidative injury because it has high energy requirements and oxygen consumption rate. The presence of an avascular zone in the central fovea, being hence dependence on the choroidal circulation, makes the macula particularly susceptible to hypoxic stress. This could explain why mitochondrial mutations and resultant dysfunction have a greater clinical implication at the macula.

RPE cells contain numerous intracellular pigments; melanin, lipofusin and flavins that absorb excess light, which aids vision functionally by reducing glare and protects the retina from photo-oxidative stress [69]. Evidence demonstrates that the mitochondria in RPE cells absorb light in the blue spectrum; life-long exposure to light in the blue-

spectrum results in accumulation of cytotoxic lipofuscin/A2E in the RPE and this in turn triggers production of ROS, causing mitochondrial DNA damage [48, 222]. In RPE cell lines with in-built mitochondrial dysfunction as a model of AMD, the addition of lipofusion/A2E caused cell death but could be reversed with addition of an antioxidant [236]. This same mechanism is believed to also be the pathogenesis for mitochondrial retinal dystrophies; for example, mitochondrial 'maternal inherited' mutation subtypes of retinitis pigmentosa (RP) [233].

Mitochondrial DNA damage is also contributed to by TNF-α-mediated inflammation, which leads to induction of ROS and reactive nitrogen species (RNS), inhibits RPE cell phagocytotic function, increases microvascular permeability and has chemokine properties, promoting immune cell infiltration into the retina [196, 237-239]. It is suggested that TNF-α acts as a transduction molecule for the potent pro-angiogenic factor, VEGF, through these complex mechanisms [197]. Angiogenesis is tightly regulated under physiological conditions. Persistent upregulation of angiogenesis is a common pathological process in several blinding disease, including PDR, branch retinal vein occlusion (BRVO), retinopathy of prematurity (ROP), and nAMD [240]. VEGF is abundantly present in neovascular membranes of individuals with nAMD and there is increased expression of VEGF in the RPE and outer nuclear layer of the macula of individuals affected by AMD compared to controls [241-243].

1.7 Current best practice for treatment of neovascular age-related macular degeneration

Historical treatment for CNV utilised laser photocoagulation to ablate neovascular vessels. However, this treatment modality was only suitable for a small proportion of patients. This was because it could itself cause visual deterioration through nonselective thermal retinal tissue destruction and scar formation, and was associated with an approximate 40-60% disease recurrence rate [244-247]. Photodynamic therapy with photosensitizing compound, verteporfin, is a treatment that was found to reduce severe vision loss through a selective photochemical angio-occlusion mechanism [248]. However, it did not result in clinically significant improvement in visual acuity [249-254]. Furthermore, this treatment is frequently unable to stabilise vision; whilst closure of neovascular vessels temporarily controls disease, it unfortunately triggers local hypoxia-driven VEGF elevation that encourages neovascular vessel formation and exacerbates disease in the long-term [251, 255].

The over-expression of the pro-angiogenic factor, VEGF, is the main molecular effector of the abnormal new vessel growth in nAMD [143]. Its blockade causes CNV regression [256]. Immunological blockade, colloquially referred to as anti-VEGF therapy, has revolutionized modern ophthalmic practice. Anti-VEGF therapy is administered via intravitreal injection into the affected eye(s). The advent of anti-VEGF therapy in 2004, following the VISION trial, radically changed the visual prognosis of nAMD [257]. This success led to a paradigm shift in treatment; consequently, anti-VEGF therapy is now considered current best practice. Photodynamic therapy with verteporfin, however, has a potential use as adjunctive therapy in those patients that do not respond to anti-VEGF

therapy alone, as investigated in the FOCUS and SUMMIT trials [258-262]. Anti-VEGF therapy is also used in other retinal diseases characterised by pathological intraocular neovascularisation, such as BRVO, diabetic macular oedema (DME), and ROP [48].

Currently, five anti-VEGF agents are used in practice for treatment of nAMD; ranibizumab (Lucentis), pagaptanib (Macugen), aflibercept (Eylea), bevacizumab (Avastin), and conbercept (Lumitin) [263-273]. Ranibizumab is a humanized recombinant monoclonal antibody fragment with high affinity for human VEGF-A; thus, binding to this isoform and preventing binding of VEGF-A to its receptors [268, 272, 274]. Two landmark studies, the MARINA and ANCHOR trials, convincingly demonstrated its efficacy in improving and stabilizing visual acuity and inhibiting clinical disease progression in nAMD and its superiority to photodynamic therapy with verteporfin, cementing its use in clinical practice [265, 266]. Bevacizumab is the parent drug of ranibizumab. It was traditionally utilized as adjuvant therapy in the treatment of cancer. It has been proven to be non-inferior to ranibizumab for nAMD in the CATT and IVAN trials; it is now widely used off-label [275-278]. The novel agent, aflibercept, also known as VEGF-Trap, is a receptor decoy that contains VEGF-binding elements for the extracellular domains of VEGFR1 and VEGFR2, thus binding and 'trapping' all VEGF-A isoforms and PGF with high affinity. It has also been found to be non-inferior to ranibizumab in the VIEW trials [270, 277-279]. The receptor actions of conbercept are similar to aflibercept, and thus has high affinity for all isoforms of VEGF-A and PGF. The AURORA and PHEONIX clinical trials demonstrated clinical safety and efficacy, but non-inferiority studies have yet to be conducted. However, a metanalysis comparing conbercept and ranibizumab suggested superiority of the former regarding number of injections required to achieve disease remission. This may be explained by the extra binding domain for VEGFR-2 that

conbercept possesses, which is thought to allow it to bind more avidly [280-283]. Pagaptanib is considered inferior to these newer agents and is now utilised as second-line therapy. However, amongst the newer agents, switching anti-VEGF therapy has been investigated, and does not appear to have a clinically significant benefit [284, 285]. However, halting progression early is imperative, as the evidence strongly indicates that there is a ceiling to optimal BCVA achievable with anti-VEGF therapy with delays in treatment initiation [266, 286-288].

The invasive nature of anti-VEGF administration comes with potentially sight-threatening complications, such as choroidal detachment and haemorrhage, endophthalmitis, uveitis, retinal tears and retinal detachment [289]. Extensive clinical trials have been performed with the primary aim of identifying the minimum effective dose regimen in hopes of offering the potential to reduce the burden of monitoring and the risk of the sight-threatening adverse event outlined above with the established monthly intravitreal injection regimen. However, fixed quarterly and pro re nata (PRN) dosing regimens, as adopted in the SUSTAIN, EXCITE, HORIZON, PIER and SAILOR clinical trials, were associated with inferior visual outcomes and thus are considered suboptimal when compared to the strict monthly treatment regimens adopted in the MERINA and ANCHOR trials [287, 290-294]. Thus, it is still considered best practice to administer 1-3 monthly injection for the patient's lifetime [295, 296]. A treat and extend regimen has evolved as common practice. This strategy aims to reduce the treatment burden on individuals, the health system, and the economy whilst maintaining efficacy. The protocol begins with 3 monthly injections, monitors visual acuity and macula fluid on optical coherence tomography (OCT) and titrates these variables, aiming to keep the macula dry and vision stable whilst extending the duration between injections, although generally no further

than 3 months. However, important data from the Australian Fight Retinal Blindness! (AFB!) Registry has demonstrated that a greater number of injections leads to better visual outcomes [297]. Additionally, despite best current practice, a third of individuals show resistance to anti-VEGF, exhibiting persistent oedema and progression of disease, and a tenth exhibit tachyphylaxis over the long-term, resulting in vision loss and compromised quality of life [298-301]. A goal of evolving therapeutics is to reduce the injection burden. Potential therapeutic targets include the up-stream hypoxic and pro-inflammatory drivers behind this disease [24, 276, 302-307].

1.8 The role that light plays in the treatment of retinal disease

The publication of the diabetic retinopathy study (DRS) and the early treatment of diabetic retinopathy study (ETDRS), demonstrating an improved visual prognosis with argon blue-green laser photocoagulation in subjects with PDR, and advanced non-proliferative diabetic disease with clinically significant macular oedema, respectively, cemented laser photocoagulation as a standard therapy for diabetic maculopathy [308, 309]. Whilst laser photocoagulation is still routinely used to treat pre-PDR, and PDR, anti-VEGF therapy has a proven superiority for treatment of DME and can replace pan-retinal photocoagulation (PRP) provided ongoing treatment is possible [310, 311]. Laser photocoagulation remains the standard therapy for ROP, as alternate treatment modalities, such as anti-VEGF, have insufficient evidence in support of superiority or long-term side effect profile in this population to urge a change in current best practice [312, 313]. Laser photocoagulation was also considered as a possible intervention to treat drusen in early-stage AMD in an attempt to slow progression to advanced disease, as characterised by CNV and geographic atrophy (GA). However, whilst a Cochrane

Review in 2009, and again in 2015, found that there was a reduction in drusen, no clinically significant reduction in progression to advanced disease was proven, which dampened interest in this particular avenue of inquiry [314, 315].

Conventional photocoagulation is performed using continuous wave (CW) laser irradiation, whereby approximately 50% of the incident laser energy is absorbed by the melanin pigment in the RPE cells and is converted to thermal energy [316-318]. The irradiation time exceeds the thermal relaxation time of the RPE cells, which approximately equals 10μs, and results in heat dissipation out of the RPE during and after the laser treatment, causing thermal damage to the adjacent choroidal and photoreceptor cells [319-323]. Traditional theories regarding the mechanism of action of PRP have been, firstly, the notion that PRP destroys photoreceptors and reduces oxygen demand; and secondly, that PRP creates chorio-retinal shunts delivering oxygen to the retina [324]. The mechanism of action of focal photocoagulation targeting leaky microaneurysms is clear but its mechanism on diffuse macular oedema is less well understood.

Possible mechanisms of low power photocoagulation laser include altered gene expression, increased extracellular matrix turnover and liberation of cell viability factor mediated by the wound-healing response of RPE cells that receive a sublethal thermal injury around the laser burn [81, 325-327]. Histological studies have shown that in proliferating RPE cells surrounding laser photocoagulation lesions, there is up-regulation of cell viability factors, increased extracellular matrix turnover, and a shift in VEGF and PEDF expression ratio to favour an anti-angiogenic microenvironment [327-332]. It also appears that short-pulse laser can influence RPE expression of MMPs and their antagonists,

TIMPs. It is postulated that this process removes drusen and other toxic waste products that contribute to RPE dysfunction in nAMD [120, 123, 333-335]. With this new perspective, there is a drive to develop laser therapies that selectively target the effector cells, the RPE, and to further investigate the molecular response of the RPE in this model of conditioning injury. This is particularly important as there is ongoing concern around treating disease near the macula due to an increased frequency of CNV from injury to Bruch's membrane with laser photocoagulation treatment, and visual impairment from thermal injury to the photoreceptors and inner nuclear layer, firstly from the initial treatment, and secondarily from 'atrophic creep'. These clinical issues have stimulated investigation of minimum intensity laser therapy for the treatment of macular disease [317, 336-342].

1.9 Photobiomodulation laser

The application of light in the far red and near-infrared range (600-100 nm) for therapeutic purposes is referred to by several terms; low-level light therapy (LLLT), photobiomodulation (PBM), low-level laser therapy, low-power laser irradiation, and red/near-infrared light therapy (R/NIR) [343]. In this thesis, I will refer to this therapy as PBM. The medical applications of light therapy date back to antiquity and were re-introduced by Finsen, in studies for which he received a Nobel Prize in Medicine in 1903 [344]. In the 1960's, working with an early low energy ruby laser, Mester observed the wound healing effects of PBM [345]. As a principle of photobiology, the biological effects of PBM are mediated through a 'photo-acceptor', which is defined as a molecule in a cell that when exposed to a certain light frequency, activates cellular processes that promote cellular repair or regeneration.

The concept of an action spectrum is important when attempting to understand the biological response of tissue to different wavelengths of light. Under ideal conditions, the wavelength of light used should be analogous to the absorption spectrum of the photo-acceptor molecule intended to absorb this light and within which the photochemical reaction causes the intended effect [346]. It is suggested that CCO is the photoacceptor in the eye and brain [62, 63, 347-349]. CCO is composed of 4 redox active metal centers: dinuclear CuA, CuB, heme a and heme a3. These preferentially absorb red to near-infrared light [349]. It is the rate-limiting enzyme in terminal phosphorylation in the mitochondrial respiration electron transport chain [350]. PBM is postulated to counteract hypoxia and modulate cellular survival by increasing expression of, and up-regulating activity of CCO [351-353]. It is believed to do so by causing dissociation of nitric oxide (NO) from CCO, with oxygen preferentially binding, and thus improving mitochondrial oxidative phosphorylation and increasing mitochondrial membrane potential, with resultant reduction in ROS production, and promoting recovery from mitochondrial respiratory chain blockade under hypoxic conditions [354-356]. The observed biological effects of increased CCO activity are increased ribonucleic acid (RNA) and DNA synthesis rates, increased ATP production, cellular migration, increased blood flow, improved oxygen binding, and reduced oxidative stress and inflammation [346, 347, 357].

The visible to near-infrared light used for PBM ranges from 500-1000 nm but the wavelengths at which it exerts its major biological effects are in the range of 600-860 nm, with peak absorption spectra at 613.5-623.5 nm, 667.5-683.7 nm, 750.7-772.3 nm, and 812.5-846.0 nm [346]. There are a growing number of medical conditions amenable to PBM at energy densities (fluence) between 2-10 J/cm^2, with a wide diversity of application,

from neuropathic pain management, brain and spinal cord injury and wound healing, to more recent applications in retinal diseases [358-361].

PBM has been demonstrated to be a safe, non-invasive therapy in a number of case studies and animal models for ROP, amblyopia, PDR, light-induced retinal injury, methanol-induced retinal injury, and RP [362-369]. The evidence for the clinical benefit for PBM in AMD so far is mainly limited to LED based photobiomodulation application in dry age-related macular degeneration (dAMD), with LIGHTSITE I clinical trial investigators demonstrating improvement in drusen burden and BCVA in subjects with dAMD [370-373]. However, this improvement in BCVA was transient, suggesting repeated, maintenance treatment is required for ongoing benefit. Furthermore, the majority of clinically significant improvement occurs in subjects without evidence of geographic atrophy, an observation also made in the subsequent LIGHTSITE II trial; this reaffirms the notion that a viable retina-RPE complex must be present to reap benefit from PBM treatment [374]. The investigators were unable to comment on disease progression; however, the reduction in drusen burden suggests that there is potential to modulate the natural history in treated subjects. The application of PBM in dAMD with the TORPA clinical trial provided more insight into the potential role PBM has in the treatment of AMD. Investigators demonstrated that treatment with PBM in 18 subjects with dAMD was associated with a statistically significant improvement in visual acuity and contrast sensitivity immediately, with benefits maintained at statistical significance at 4, 6, and 12 months follow up [370, 371].

Ivandic et al conducted a case series in AMD that presented pooled data that included subjects with nAMD. The authors reported that there was clinical improvement in oedema and bleeding in this subgroup, although, these features were not specifically measured in a quantitative manner, nor specifically discussed [372]. Preliminary data from a case series conducted by Tang et al in subjects with DME demonstrated PBM treatment reduced central retinal thickness in treated eyes [365]. The NIRD clinical trial added weight to these findings by demonstrating a reduction in central macular thickness, and improvement in BCVA in subject with DME that had received treatment with PBM laser; further to this, no treatment related adverse events were reported [375]. This limited but promising clinical evidence provide more insight into the role of PBM treatment in neovascular retinal disease. However, a mechanistic understanding of how photobiomodulation may impact on the specific aspect of neovascularization and vascular permeability in nAMD are still lacking.

Derangement in the balance between anti-angiogenic and pro-angiogenic tissue factors is implicated in CNV formation in nAMD due to altered gene expression in the context of hypoxic drive. This is further supported by the correction of this balance when mitochondrial antioxidants are introduced [101, 376]. There is a suggestion that PBM treatment can shift the ratio of key players in retinal angiogenic balance, VEGF/PEDF, towards an anti-angiogenic cytokine profile [377]. Certainly, PBM treatment has been demonstrated to modulate VEGF expression in Müller cell exposed to light-stress, reduce neovascularization in a mouse model of ROP, reduce VEGF expression in a rabbit model of oral mucositis, and reduce central macular thickness in subjects with DME and nAMD [362, 365, 372, 378-380].

PBM has pleotropic effects and thus there are a number of possible mechanisms. It is clear that within an hour of application, gene expression involved in cellular proliferation, antioxidant production, anti-apoptosis, mitochondrial energy function, membrane potential and ion-channel activation, DNA synthesis and repair, and immunomodulation are upregulated [381, 382]. Of particular interest is that PBM is known to down-regulate the expression of TNF-α, the master controller of inflammation that is implicated in a number of pathogenic pathways involved in nAMD development; this modulation is noted in the retina under hypoxic conditions, in an aged-mouse model of AMD, and in light-induced retinopathy, as well as in the spine in autoimmune encephalitis [350, 383, 384]. PBM is also known to downregulate C3 expression in a CFH-deficient mouse model of AMD [363, 383, 385]. PBM has further anti-inflammatory actions by reducing the number of activated, M1-polarised, pro-inflammatory state, microglial cells in animal models of ROP, and AMD [367, 383]. Furthermore, PBM treatment is associated with reduced Müller cell activation, and leukocyte activation and infiltration [350, 366, 386].

PBM has been shown to activate the main anti-apoptotic pathway factor, BCL-2, and is associated with modulation of expression of expression of neurotrophic factors such as bFGF and CNTF in a light-damage rat model of AMD, is consistently associated with improved photoreceptor survival in animal studies, and is associated with improvement in ERG responses and best corrected visual acuity in patients with amblyopia, DME, and both dAMD and nAMD as an indicator of improved photoreceptors function [362, 364, 365, 367, 371, 372, 378, 379, 387, 388]. Of particular interest is the feasibility of this application in nAMD

as the biological effects of PBM appear to target multiple key pathogenic mechanisms believed to cause nAMD.

1.10 The laser induced choroidal neovascularisation model in animal

Following the establishment of a straightforward effective laser CNV model in primates by Ryan et al [389], several research groups then replicated and modified the technique to produce rodent models. Laser-induced CNV in rat is now a well-established model utilized for therapeutic applications, which shares many pathogenic mechanisms common to CNV in nAMD [368, 390-392]. When used at high-energy levels, the thermal burn from continuous wave laser can rupture Bruch's membrane, leading to the growth of new choroidal vessels into the subretinal space, mimicking the choroidal neovascularization seen in human nAMD [392]. Review of the literature revealed that investigators typically used red or green laser to induce CNV lesions. The solid-state frequency-doubled neodymium: yttrium aluminium garnet (fd Nd:YAG) laser produces green light of 532 nm wavelength by way of second harmonic generation; the 1064 nm radiation emitted from the Nd:YAG crystal is then passed through a potassium titinyl phosphate (KTP) crystal, which is a non-linear compound, causing the pump radiation to double in frequency as it passes through, producing 532 nm radiation. The fd Nd:YAG laser causes tissue effects through a thermal reaction in the pigment of cells that have a corresponding wavelength absorption spectrum as the laser light; in the case of melanin in RPE and choroid it has a broad absorption spectrum, whilst haemoglobin optimally absorbs light in the blue-green spectrum [393, 394]. Whilst there is much variability in the laser settings used to produce CNV lesions, in studies that utilised 532 nm laser, the laser settings were typically between 50-100 ms, 50-100 µm, and 100-200 mW [395-400].

It appears that an inflammatory milieu is propagated following laser induction. The complement cascade and resultant formation and deposition of membrane attack complexes (MAC), the end-product of the complement cascade, between 24-72 hours after induction is a trigger for CNV formation in laser-induced CNV models [208-210]. Macrophage cell infiltration of the site of laser injury is another suggested inflammatory mechanism for CNV induction in this model, with infiltration occurring as early as 24 hours, peaking at 48-72 hours and normalising by 7 days. Further to this, it appears that macrophage infiltration is closely correlated to the quantity of VEGF expression and CNV lesions volumes [187, 188, 401]. The resultant inflammatory milieu appears to stimulate the release of a number of viability factors that play an important role in angiogenesis, including VEGF, aFGF, bFGF, and TGF-β. However, VEGF is thought to be the key pro-angiogenic factor in laser-induced CNV development, as it is in clinical nAMD, as VEGF blockade causes CNV regression [187, 208, 402, 403]. It appears that VEGF-C and VEGFR-3 are in particular implicated in laser-induced CNV membrane formation, with Müller cells being an important source [404]. As there are multiple common pathogenic mechanisms between laser induced CNV model and nAMD development, the use of this model of CNV can aid in studying the modulation of CNV with new therapies in nAMD.

1.11 Rationale for the study

There is a growing evidence base for the anti-inflammatory effects of PBM treatment in neuronal tissues. Our understanding is that chronic retinal inflammation plays a core role in instigating and perpetuating choroidal neovascularization in clinical nAMD. Replicating this fundamental pathogenic process in an accelerated model of nAMD, as will be done with the laser-induced CNV model, will allow investigation into the role of

PBM laser treatment in modulating retinal inflammation and pathological neovascularization.

1.12 Hypothesis

It is hypothesized that retinal photobiomodulation laser treatment will modulate the retinal stress response in a laser-induced choroidal neovascularization model. This modulation of inflammation is hypothesized to reduce associated expression of the key pro-angiogenic factor, vascular endothelial growth factor, and consequently limit choroidal neovascular membrane formation and the accompanying vasopermeability.

1.13 Study aims

1. Establish a laser-induced CNV model in rat eye
2. Ascertain the safety profile of PBM-laser treatment in the rat eye
3. Ascertain the effects of PBM-laser treatment on the outcomes of this laser-induced CNV model
4. Ascertain if these effects involve inflammatory and/or angiogenic pathways in the eye

Chapter 2:

Materials and Methods

2.1 Animal ethics and handling

Permission to use animals was obtained from the Central Adelaide Local Health Network Animal Ethics Committee. The work undertaken conformed with both the Australian Code of Practice for the Care and Use of Animals for Scientific Purposes, 2013, and to the ARVO statement for the Use of Animals in Ophthalmic and Vision Research (Ethics number: M-2017-084; M-2019-073). Female Brown Norway rats (average weight, 150 $\pm$ 100g) were utilised for all experiments described below. Pigmented rats were used as the melanin pigment in RPE optimally absorbs laser energy in the green wavelength and responds reliably to laser applications to the eye [394]. Animals were obtained from the University of Adelaide, Adelaide, South Australia. They were housed in temperature- and humidity-regulated rooms with 12 hour light and 12 hour dark cycles. Food and water were provided ad libitum. Prior to procedures, animals underwent general anaesthesia with an intraperitoneal injection of a mixture of 100mg/kg Ketamine and 10mg/kg Xylazine at 0.4-0.6mL/100g of body weight. At the conclusion of the experiment, animals were humanely killed with transcardial perfusion of physiological (0.9%) saline under general anaesthesia.

2.2 Induction of choroidal neovascularization with laser

Animals underwent general anaesthesia with an intraperitoneal injection of a mixture of 100mg/kg ketamine and 10mg/kg xylazine at 0.4mL/100g of body weight. Pupils were dilated with topical application of 1% Tropicamide, and anaesthetized with topical application of 0.4% Oxybuprocaine. Once deep anesthesia was confirmed, animals were

then placed on a specially designed rodent holder by the researcher at the slit lamp laser delivery system. Lubricating eye gel was applied to prevent the dehydration of the cornea during laser treatment. A glass slide was used as a surrogate contact lens to focus the light beam onto the retina. A frequency-doubled neodymium: yttrium-aluminium-garnet (fd Nd:YAG) laser with 532-nm wavelength was used to place 4 laser spots at approximately the 12 o'clock, 3 o'clock, 6 o'clock and 9 o'clock positions between each main retinal vessel, approximately 1-2 disc diameters from the optic disc. Laser setting B (100 ms pulse duration, 100 μm spot size, 100 mW power) was utilised for all PBM laser experiments. Breakage of Bruch's membrane was confirmed by bubble formation with or without choroidal haemorrhage and used as an end point for treatment. Lesions with severe haemorrhage or without bubble formation were excluded from further study. This methodology was modified from a protocol outlined by Lambert et al [405].

2.3 Fundus fluorescein angiography

Animals underwent general anaesthesia with an intraperitoneal injection of a mixture of 100mg/kg Ketamine and 10mg/kg Xylazine at 0.5mL/100g of body weight. Pupils were dilated with topical application of 1% w/v Tropicamide, and anaesthetized with topical application of 0.4% w/v Oxybuprocaine. Lubricating eye gel was applied to prevent dehydration of the cornea during imaging. A fundus laser contact lens was used to focus the light beam onto the retina. The retinal fundi of rats were viewed and photographed with a Spectralis HRA+OCT device (Heidelberg Engineering, Heidelberg, Germany). All images were collected by using the specialty Spectralis HRA+OCT software. Following an intraperitoneal injection of 0.5 mL 10% Fluorescein Sodium (Alcon Laboratories, Inc.,

Fort Worth, TX), fundus fluorescein angiographs (FFA) were viewed and captured with a green filter attached to the Spectralis HRA+OCT camera at 5 minutely intervals for 20 minutes post fluorescein injection. Images were exported as tagged image files (.tif). Lesions were scored on a grade scale based on the spatial and temporal evolution of fluorescein leakage on FFA following a documented standard as described previously by Liu et al [400]: (0) no leakage, faint hyperfluorescence, or speckled fluorescence without leakage; (1) questionable leakage, hyperfluorescent lesion without advancing increase in size or intensity; (2) leaky, hyperfluorescence increasing in intensity but not significantly in size without definite leakage; (3) pathologically significant leakage, hyperfluorescence increasing in intensity and in size with definite leakage. The presence or absence of a halo of fluorescence around perfused vessels was used to assess their permeability. During establishment of the laser CNV model, CNV lesions were quantified as a function of area from regions of fluorescence leakage using the thresholding function in ImageJ, (https://imagej.nih.gov; provided in the public domain by the National Institutes of Health, Bethesda, MD, USA), as previously described by Guthrie et al [406] (Figure 2.1).

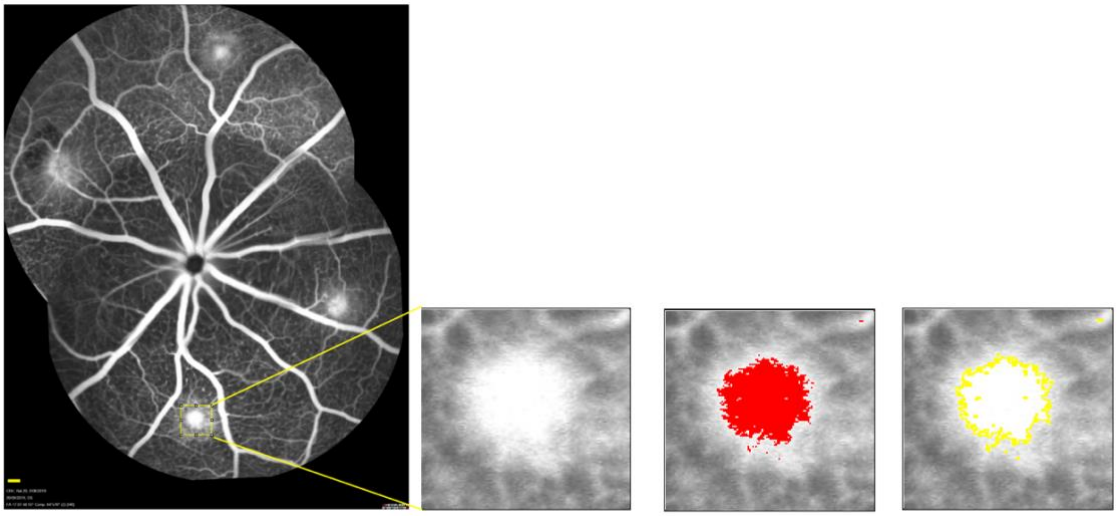

Figure 2.1: Area calculations of CNV lesions from digital images of late-phase FFA using the thresholding tool in imageJ. Scale bar: 200 μm. CNV, choroidal neovascularisation.

2.4 Spectral domain optical coherence tomography

Spectral domain optical coherence tomography (SD-OCT) is an established, non-invasive, high-resolution, medical imaging technique utilized to measure CNV status [286]. Animals were anaesthetized with an intraperitoneal injection of a mixture of 100mg/kg Ketamine and 10mg/kg Xylazine at 0.5mL/100g of body weight. Pupils were dilated with topical application of 1% w/v Tropicamide, and anaesthetized with topical application of 0.4% w/v Oxybuprocaine. Once anesthesia was confirmed, a series of radial B-scan SD-OCT images were captured at the mid-peripheral 12 o'clock, 3 o'clock, 6 o'clock and 9 o'clock laser positions. The volume of the CNV was calculated by inputting the width, length and depth measurements taken from the SD-OCT B-scan images using measuring tool in ImageJ software into an ellipsoid volume formula, as described by Sulaiman et al

[407]. (Figure 2.2)

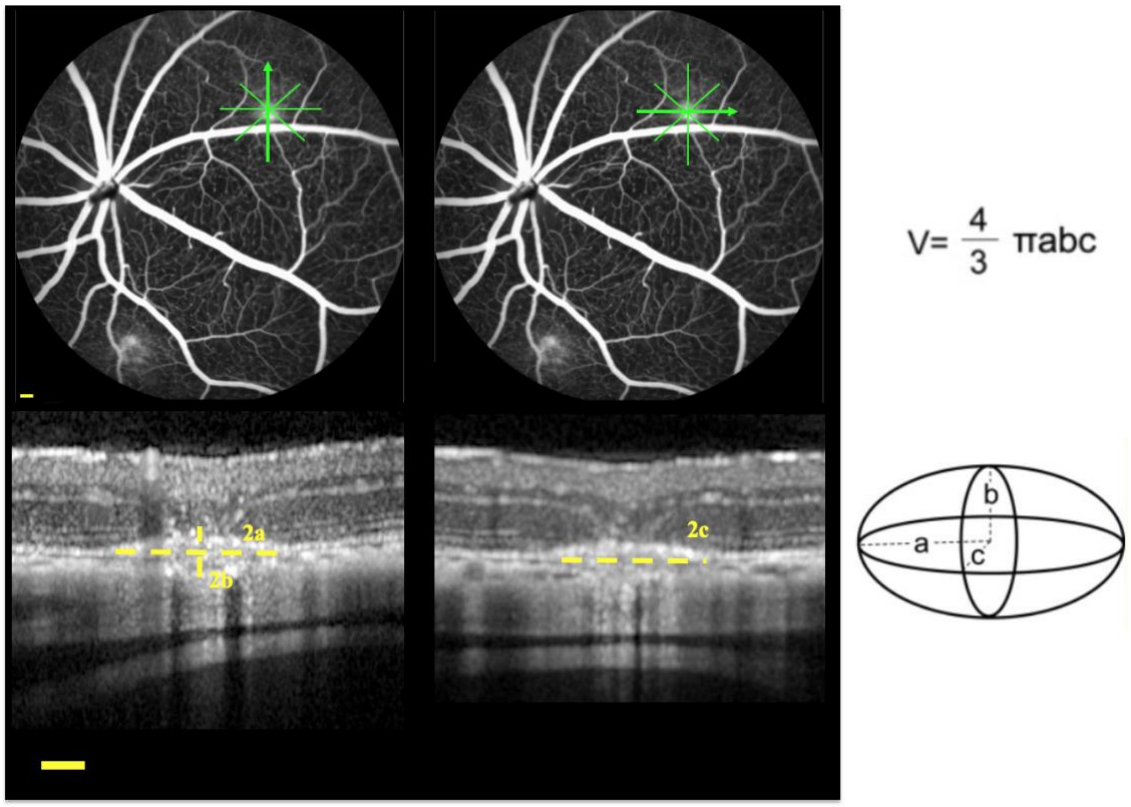

Figure 2.2: CNV lesion volume calculation from width, length and depth measurements taken from SD-OCT images using the measurement tool in imageJ software. Scale bar: 200 μm.

2.5 Wholemount preparation

Animals were killed by intraperitoneal injection of a mixture of 100mg/kg Ketamine and 10mg/kg Xylazine at 1mL/100g of body weight, followed by transcardial perfusion with 0.9% saline. The eyes were immediately enucleated, and the globes with optic nerve attached were then carefully dissected (Figure 2.3a). The superior aspect of the conjunctiva was marked with a dye for the purpose of orientation to facilitate direct comparison of each lesion between SD-OCT (in vivo), FFA (in vivo) and wholemount

(WM)(ex vivo). Eyes were subsequently fixed by immersion in 30mL of 10% buffered formalin at room temperature (10% v/v from formalin 40% w/v pH 7 ± 0.2 at 25°C). After 6 hours the eyes were washed in PBS. Eyes were then bisected equatorially, and optic nerve cut way at the papilla, and the anterior halves and vitreous discarded (Figure 2.3b). 4-8 incisions were made into each of the posterior eyecups (Figure 2.3c). The retina of each eye was carefully pealed from the underlying retinal pigment epithelium (Figure 2.6d). RPE WM (Figure 2.3e) and retinal WM (Figure 2.3f) were then prepared for immunohistochemistry.

RPE WM were washed in phosphate buffered saline (PBS). Following washing with PBS, WM were incubated in 1% (v/v) Triton in PBS (PBS-T) for 1 hour at room temperature to make cell membranes permeable and subsequently blocked for 1 hour at room temperature in horse serum dilution buffer (NHS-T), 3% (v/v) normal horse serum, 1% (v/v) Triton in PBS. Isolectin-B4 (IB4) is a protein isolated from the seed of the African legume, *Griffonia simplicifolia*. It is known to bind to endothelial cells, and as such was utilised in this study as an endothelial cell marker to identify neovascular membranes [408]. IB4 (1:100 dilution, Sigma-Aldrich, St Louis, MO, USA) was applied for 24 hours at 4°C. WM were counterstained with IBA-1 (1:4000, Novus Biologicals, CO, USA) as a marker of pro-inflammatory microglial cell infiltration. WM were washed in PBST 1% at room temperature for 1 hour and incubated for 3 hours at room temperature in AlexaFluor-488 and AlexaFluor-594 conjugated secondary antibodies (1:250; Invitrogen, Carlsbad, CA) in NHS-T. WM were washed in PBST at room temperature for 1 hour and incubated for 5 minutes at room temperature in 4', 6'-Diamidino-2-phenylindole (DAPI) (1:2000 dilution in PBST; Sigma-Aldrich, Castle Hill, NSW, Australia). Omission of

primary antibody constituted control immunolabelling. WM were washed in PBS at room temperature for 5 minutes, mounted on a slide with antifade medium (Dako Australia Pty Ltd, Victoria, Australia) and a cover slip. Slides were allowed to seal for 24 hours before being visualised under fluorescent microscope and images digitally captured using a ColourView camera on an Olympus BX61 fluorescent microscope at 10x magnification (Olympus Australia Pty Ltd, Victoria, Australia). Retinal WM were washed in PBS. Following washing with PBS, WM were incubated in 1% (v/v) PBS-T for 1 hour at room temperature to make cell membranes permeable and blocked for 1 hour at room temperature in 3% (v/v) NHS-T. Nestin (1:50 dilution, DHSB, Iowa, IA, USA) was applied for 48 hours at 4°C. Retinal WM were counterstained with IBA-1 (1:4000, Novus Biologicals, CO, USA) as a marker of pro-inflammatory microglial cell infiltration. WM were washed in 1% (v/v) PBST at room temperature for 1 hour and incubated for 24 hours at 4°C in AlexaFluor-488 and AlexaFluor-594 conjugated secondary antibodies (1:500; Invitrogen, Carlsbad, CA) in NHS-T. WM were washed in PBS for 90 minutes, mounted on a slide with antifade medium (Dako Australia Pty Ltd, Victoria, Australia) and a cover slip. Slides were allowed to seal for 24 hours before being visualised under fluorescent microscope and images digitally captured using a ColourView camera on an Olympus BX61 fluorescent microscope at 10x magnification (Olympus Australia Pty Ltd, Victoria, Australia). CNV lesions were quantified as a function of area from regions of fluorescence using the thresholding function in ImageJ, URL; provided in the public domain by the National Institutes of Health, Bethesda, MD, USA), as previously described by Guthrie et al [406] (Figure 2.4).

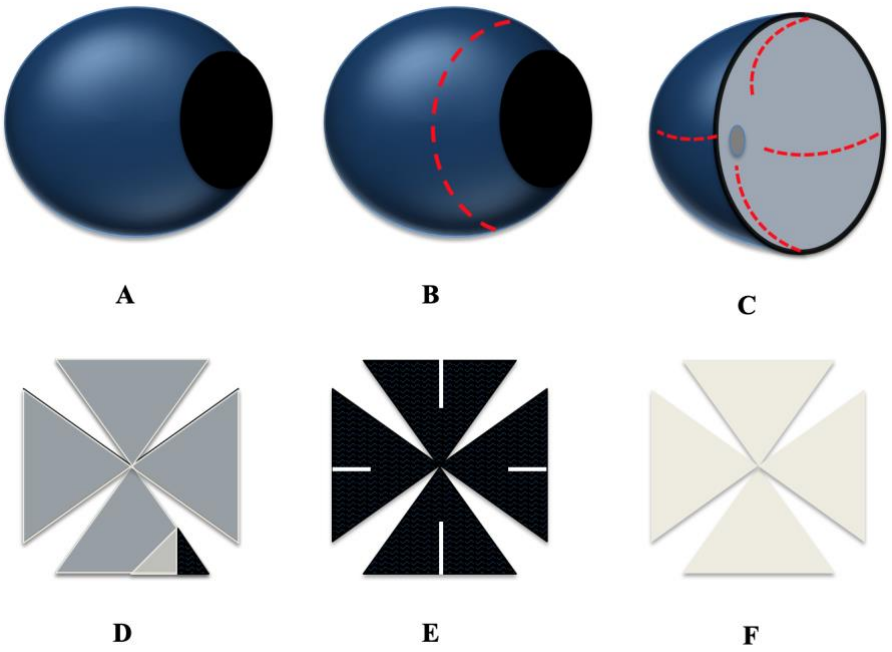

Figure 2.3: Schematic depicting the procedure for preparing rat retinal and RPE WM. Under a dissection microscope the eyes, (A), were bisected equatorially and optic nerve cut away at the papilla, (B), and the vitreous and anterior segments of the eye including the cornea, iris and lens were discarded, and 4 radial incisions were made into each of the posterior eyecups, (C). The retina of each eye was carefully pealed from the underlying RPE, (D), leaving the posterior eyecup, with a further 4 radial incisions made, (E), and the retina, (F). The RPE and retinal WM were then processed for immunohistochemistry. RPE, retinal pigment epithelium. WM: wholemount.

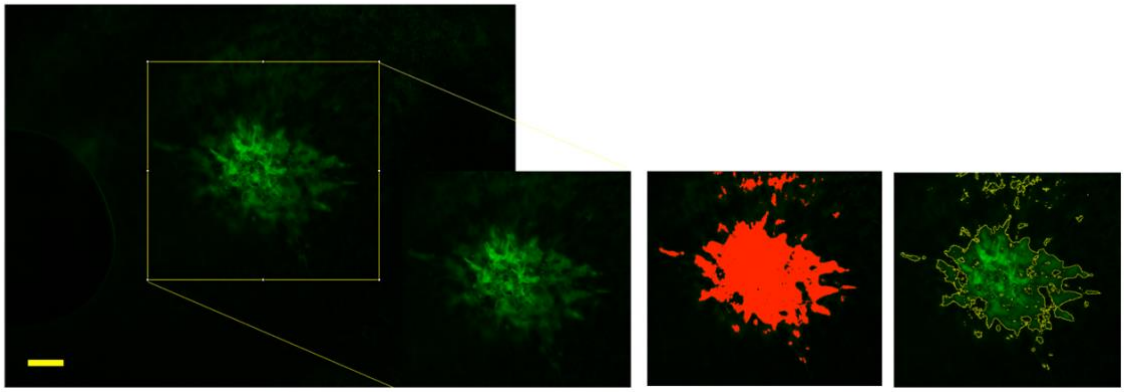

Figure 2.4: Area calculations of CNV lesions from images taken of immunofluorescent WM treated with Alexa-488 for IB4 using colour thresholding tool in imageJ. Scale bar: 100 μm. CNV, choroidal neovascularisation. WM: wholemount.

2.6 Photobiomodulation laser system and experimental procedure

The PBM laser device used in the present study was mounted on a slit-lamp with a similar arrangement to current lasers utilised in ophthalmic clinics (Figure 2.5a). The system comprised a slit-lamp (Ellex Medical Lasers, Adelaide, South Australia, Australia) with an in-build laser that emits a 670 nm laser. The beam was 4.5 mm in diameter with a flat-top profile. Depending on the treatment group, the power setting was adjusted according to a reference table created by Ellex Medical Lasers that took into consideration the animal's maximum dilated pupil size to produce the intended irradiance at the retina. A nose cone was used to deliver inhaled Isoflurane to the animals, which were then placed on a specially designed rodent holder by the researcher at the slit lamp laser delivery system. Pupils were dilated with 1% w/v Tropicamide, and anaesthetized with topical application of 0.4% w/v Oxybuprocaine. Once anesthesia was confirmed, the retina was

visualized, and then exposed to laser delivered photobiomodulation (PBM) or to sham treatment for ninety seconds (Figure 2.5b). The high-dose photobiomodulation (HPBM) laser group received 100 mW/cm^2 for 90 seconds per eye, and the low-dose photobiomodulation (LPBM) laser group received 32 mW/cm^2 for 90 seconds per eye. The sham-control group received aiming beam only for 90 seconds per eye. The laser fluence delivered with the HPBM and LPBM laser settings were equivalent to 9 J/cm^2 and 2.88 J/cm^2, respectively. Animals were then allowed to recover, which typically took several minutes.

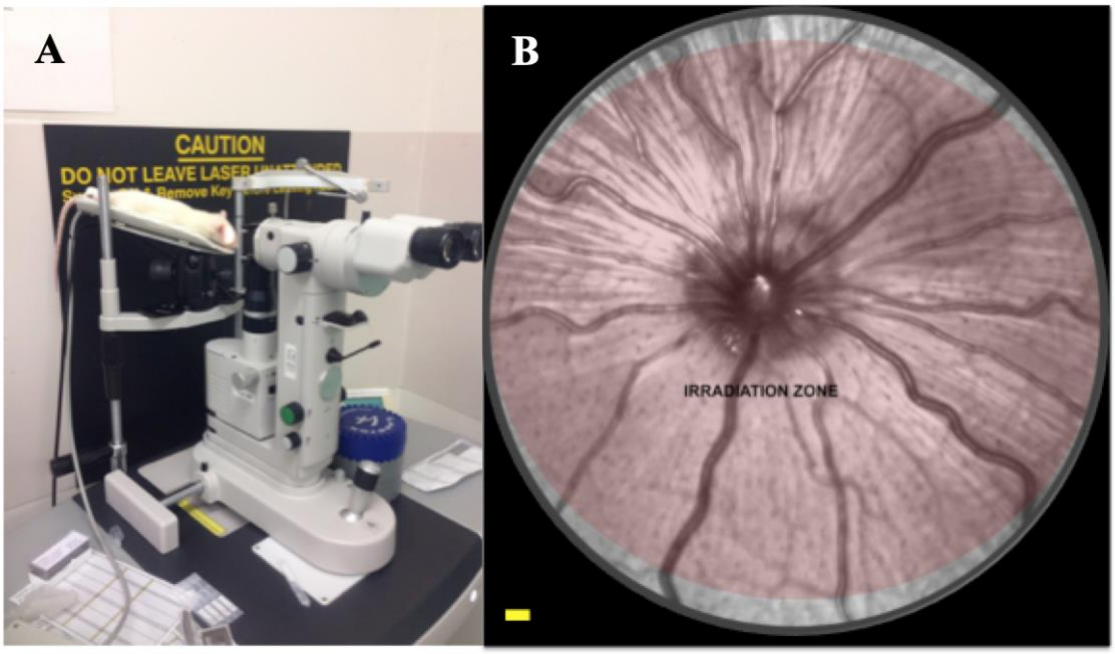

Figure 2.5: (A) Laser equipment set-up. The anaesthetised animal is placed onto a custom-designed platform attached to a slit lamp. The irradiance dose was produced by adjusting the power setting with reference to a setting conversion table. (B) Confocal scanning laser ophthalmoscopy fundus photo with depicted irradiation zone. During the laser procedure, the fundus was visualized with a microscope coverslip lubricated with methylcellulose applied to the cornea. Scale bar: 200 μm.

2.7 Retinal and RPE-choroid complex tissue protein extraction for enzyme-linked immunosorbent assay

Animals were killed at 3 days following induction of CNV by laser, as this was deemed to be optimal time frame for maximal cytokine release [187, 404]. Immediately following enucleating the right eye of each rat, the globes with optic nerve attached were then carefully dissected (Figure 2.6a). The eyes were bisected equatorially, optic nerve cut way at the papilla to aid separation of the retina, and the anterior halves and vitreous were discarded (Figure 2.6b). 4 small incisions were made to relax the globe. A 5mm punch around the optic nerve was then taken (Figure 2.6c). The retina was carefully pealed from the underlying retinal pigment epithelium and placed in 175μL of lysis buffer for protein isolation (RayBio; RayBiotech, Norcross, GA, USA) (Figure 2.6d). The posterior eyecup remained. The RPE-choroid complex was scraped from the sclera using a slit angled ophthalmic knife and placed in 175μL of lysis buffer for protein isolation (RayBio; RayBiotech, Norcross, GA, USA) (Figure 2.6e). The RPE-choroid complex and the retina were sonicated in lysis buffer on ice for 15 seconds. After homogenization, the lysate was centrifuged to remove cell/tissue debris from 5 min at 10,000 x g and the supernatant was saved and stored at -80°C, until enzyme-linked immunosorbent assay (ELISA) was performed. VEGF protein levels in the supernatant were determined with duplicate measurement using a sandwich ELISA kit as per the manufacturer's instruction (threshold of detection 2 pg/mL; RayBio; RayBiotech, Norcross, GA, USA) that recognizes all splice variants, at 450 nm with an absorption spectrometer, and normalized to total protein. The procedure was as follows. All reagents and samples were brought to room temperature before use. As per the manufacturer's instructions, standards and samples

were run in duplicate. Firstly, a dilution series was prepared, with VEGF standards concentrations as follows; 200 pg/ml, 80 pg/ml, 32 pg/ml, 12.8 pg/ml, 5.12 pg/ml, 2.05 pg/ml, 0.82 pg/ml, and 0 pg/ml. 100 µL of each standard and sample were added to appropriate wells in duplicates. Wells were covered and allowed to incubate for 2.5 hours at room temperature with gentle shaking. The solutions were discarded, and wells washed four times with 300 µL of wash buffer and finally inverted and blotted against clean paper towel. 100 µL of biotinylated antibody was added to each well and incubated for 1 hour at room temperature with gentle shaking. The solutions were discarded and well washed four times with 300 µL of wash buffer and finally inverted and blotted against clean paper towel. 100 µL of streptavidin solution was added to each well and incubated for 45 minutes at room temperature with gentle shaking. The solutions were discarded and well washed four times with 300 µL of wash buffer and finally inverted and blotted against clean paper towel. 100 µL of TMB substrate reagent was added to each well and incubated for 30 minutes at room temperature in the dark with gentle shaking. Finally, 50 µL of stop solution was added to each well and plate absorbance immediately read at 450 nm with an absorbance spectrometer. Duplicate measurements were performed. A bicinchroninic acid protein assay (BCA) was performed as per the manufacturer's instructions to determine protein quantity in each sample (Sigma-Aldrich, St Louis, MO, USA). This was utilized to standardize samples for pg/mg of protein following the ELISA assay.

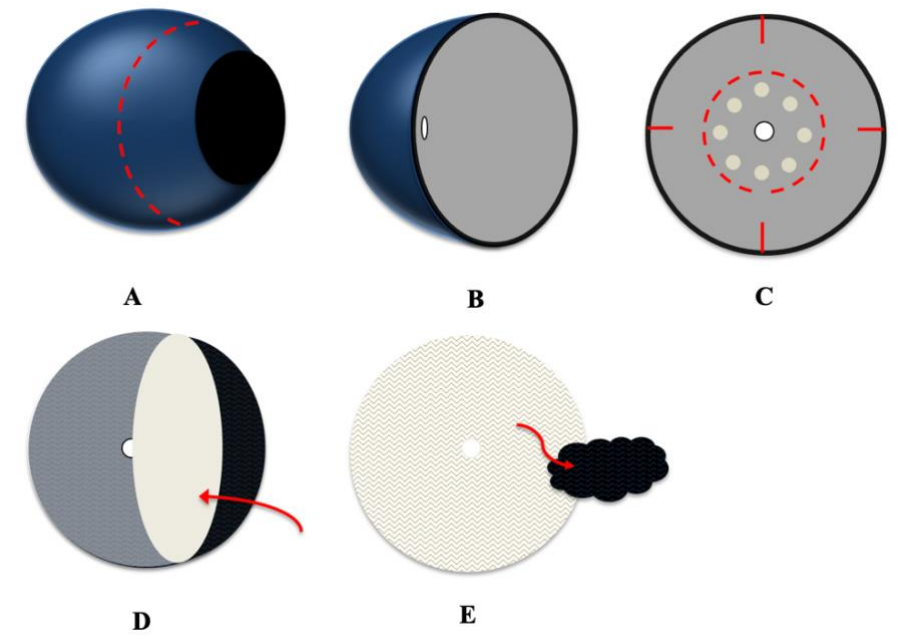

Figure 2.6: Schematic depicting the procedure for extracting rat retinal and RPE-choroid tissue for ELISA. Under a dissection microscope the eyes, (A), were bisected equatorially and optic nerve cut away at the papilla to aid separation of the retina, and the vitreous and anterior segments of the eye including the cornea, iris and lens were discarded, leaving the posterior eyecups, (B). A 5 mm punch was made around the optic nerve to produce a punch biopsy (C). The retina of each punch biopsy was carefully pealed from the underlying RPE, (D), and placed in an Eppendorf tube for protein extraction, and the exposed RPE-choroid of each punch biopsy was scrapped from the sclera, (E), and placed in a separate Eppendorf tube for protein extraction. The retinal and RPE-choroid tissue lysates were then processed using a sandwich ELISA for Rat VEGF as per the manufacturer's instructions and protein quantified on a colorimetric scale, which was expressed as pg of VEGF protein per mg of retinal tissue. RPE; retinal pigment epithelium. ELISA; enzyme-linked immunosorbent assay.

2.8 Retinal cross-sections

Eyes were fixed, processed, embedded, and sectioned in paraffin for histologic and immunohistochemical analysis as per a previously described method [409]. The left eye of each animal was enucleated and marked on the superior aspect with ink for future orientation. The eyes were then immersion-fixed in Davidsons solution (2-parts formaldehyde (37%), 3-parts 100% ethanol, 1-part glacial acetic acid, and 3-parts distilled water) for 24 hours. Eyes were then immersed in 70% ethanol until tissue processing. At the time of tissue processing eyes were immersed in 70% ethanol for 60 minutes, followed by 100% ethanol 3 times for 60 minutes each, then in 100% xylene twice for 60 minutes each, then in 50% xylene/50% wax for 60 minutes at 62°C, and finally in wax twice for 60 minutes each at 62°C. Globes were subsequently embed sagittally and 4-μm sections were cut using a rotary microtome. Sections were captured on SuperFrost Ultra Plus slides. Slides were stored at room temperature in the dark until immunohistochemical processing. In preparation for immunohistochemical analysis, sections were deparaffinized by heating at 70°C for 15 minutes, followed by immersion in xylene 2 times for 5 minutes. Sections were then rinsed in 100% ethanol, and immersed in 0.5% (v/v) H_2O_2 in absolute methanol for 20 minutes to block endogenous peroxidase activity before being washed in PBS. For antigen-retrieval, sections were microwaved for 10 minutes at 95–100°C in 10mM citrate buffer (pH 6.0), or in the case of immunostaining for bFGF, 1 mM EDTA buffer (pH 8.0). Following antigen retrieval, tissue sections were then blocked in PBS containing 3% (v/v) normal horse serum (NHS) for 30 minutes and then incubated with primary antibody in PBS containing 3% (v/v) NHS for 24 hours at room temperature (Table 2.1). Omission of primary antibody constituted control

immunolabelling (Figure 2.7). Tissue sections, with the exception of sections immunostained for IB4, were subsequently washed and incubated in streptavidin-peroxidase conjugate secondary antibody 1:250 for 1 hour at room temperature and given colour through incubation with a DAB substrate kit for 3-5 minutes. All tissue sections were counterstained with hemotoxylin (purple) for visualisation of cell nuclei. Stained transverse tissue sections were visualised under and photomicrographs captured under a light microscope (BX-51; Olympus, Mount Waverly, VIC, Australia). All images presented in this thesis were captured within two disc-diameters of the optic nerve head.

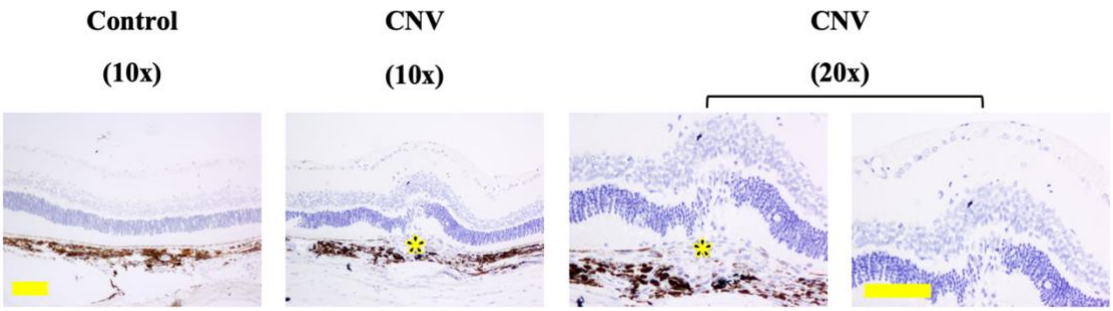

Figure 2.7: Representative image of primary antibody control for immunohistochemistry on retinal paraffin cross-sections from control eye and CNV eyes. CNV membranes are highlighted by a yellow asterisk in the present and all subsequent cross section figures. Scale bar: 100 µm. CNV: choroidal neovascularization.

Target	Host	Clone/Cat No.	Dilution	Source
FGF-2/bFGF	**Mouse**	**bFM-2**	**1:1,000***	**Millipore, NSW, AUS**
CNTF	**Goat**	**AD 557-NA**	**1:1,000***	**R&D Systems, Abingdon, UK**
CD3	**Rabbit**	**A0452**	**1:2,000***	**Dako, NSW, AUS**
HSP32/HO-1	**Rabbit**	**SPA-895**	**1:2,000***	**Enzo life sciences, NY, USA**
IBA-1	**Rabbit**	**019-19741**	**1:4,000†**	**Novus, CO, USA**
PCNA	**Mouse**	**PC10**	**1: 20,000***	**Dako, NSW, AUS**
GS	**Mouse**	**610517**	**1:10,000***	**Transduction laboratories,**
RPE65	**Mouse**	**SC-53489**	**1:2,000***	**Santa Cruz Biotechnology, Texas, USA**
MPO	**Rabbit**	**A 0398**	**1:45,000***	**Dako, NSW, AUS**
IB4	**Biotinylated**	**L2140-1 MG**	**1:100† 1:300***	**Sigma-Aldrich, MO, USA**
Nestin	**Rat**	**AB 2235915**	**1: 100†**	**DSHB, IA, USA**

Table 2.1: Antibodies used for immunofluorescence staining of retinal and RPE wholemount (†), and immunoperoxidase staining of paraffin cross-sections (*) in this study.

2.9 Mitochondrial energy metabolism

Superoxide is a ROS that is produced as a by-product of incomplete oxidation of oxygen during mitochondrial respiration. The MitoSOX Red live cell assay is a well-established method of ascertaining mitochondrial superoxide generation based on relative fluorescence emission at 580 nm of DNA-bound mito-hydroethidiuin when specifically oxidised by superoxide. The assay was used as a measure of mitochondrial oxygen metabolism in retinal-RPE and RPE-only WM. This assay is particularly useful in the retina, due to the mitochondrial density of this highly metabolically active tissue. Tissue preparation was as follows. Rats were humanely killed by transcardial perfusion with 0.9% saline under general anaesthesia and the eyes were enucleated and dissected into posterior eyecups. The neurosensory retina of each eye was either left in place or carefully detached from the underlying retinal pigment epithelium (RPE) yielding ‘retina-RPE’, or

‘RPE-only’ WM. These were then placed on an upturned small petri-dish lid on a 0.4 micrometer pore-size nitrocellulose filter paper (13 mm diameter) in a drop of Hank's Balanced Salt Solution (HBSS). One leaf was then treated with 100 mW/cm^2 PBM for 90 seconds. WM were then bathed in MEM medium (1% v/v penicillin/streptomycin, 5mM glucose, no FBS) for 45 minutes. WM were incubated for 15 minutes in MitoSOX Red dye and live-cell nuclear binding dye Hoechst 33342 at a final concentration of 5 microM, and 1 microgram/ml, respectively. WM were again washed with MEM medium and mounted on a slide and coverslipped. WM were examined under a fluorescence microscope (BX-61; Olympus, Mount Waverly, Australia) equipped with a scientific grade, cooled CCD camera at 20x magnification.

Chapter 3:

Establishing a rat model of laser-induced choroidal neovascularization

3.1 Introduction

It is widely accepted that nAMD results from an intimate relationship between chronic tissue hypoxia, low-grade inflammation and activation of the complement cascade. This induces a stress response in the RPE and retinal glia [145-148]. This consequently leads to down-regulation of endogenous anti-angiogenic peptides, and upregulation of pro-angiogenic peptides, which creates a pro-angiogenic environment, contributing to the development and progression of CNV in nAMD [116-118]. For a long time there was a prevailing belief that retinal photocoagulation was effective in treating proliferative eye disease by eliminating photoreceptors, and consequently reducing the associated oxygen demand, and thus reducing hypoxia-driven retinal oedema and neovascularisation [324]. However, it was observed that laser photocoagulation in the treatment of DME, sickle cell disease and proliferative diabetic retinopathy was associated with upregulation of pro-angiogenic factors in susceptible subjects [410]. The general consensus is that there is an increased frequency of CNV in eyes treated with laser photocoagulation secondary to injury to Bruch's membrane and the disruption of the retinal-RPE-choroid complex, which encourages the growth of new choroidal vessels into the sub-RPE and sub-retinal space, mimicking CNV membranes observed in clinical nAMD [338-340, 392, 410].

Extrapolating from this observation, Ryan et al established a laser CNV model in primates [389]. This was subsequently adapted and modified to rodent models, and is now widely accepted as a reliable and reproducible animal model for CNV [390-392, 405]. Rupture of Bruch's membrane is the fundamental clinical end point for laser CNV induction. From the literature, investigators have utilised a broad range of laser energy settings to induce

Bruch's membrane rupture to successfully induce CNV. It appears that a minimum laser power of 60 mW is required to successfully rupture Bruch's membrane [411]. However, with energy setting greater than 130 mW, there are increased incidences of choroidal haemorrhage, which is undesirable. This model mimics the complex pathogenic mechanisms involved in clinical nAMD. It appears that an inflammatory milieu is propagated following laser induction, with upregulation of inflammatory cytokines, retinal glial cell activation, macrophage infiltration, and activation of the complement cascade and resultant formation of membrane attack complexes [187, 392, 396, 400, 404, 412]. These features are interactive and perpetuate further inflammation and are associated with upregulation of pro-angiogenic factors; VEGF is one of the most pertinent and of particular interest in the study of treatments for nAMD [187, 208, 402, 404]. This factor ultimately triggers CNV formation in laser-induced CNV models [210]. Further to this, when measures are taken to inhibit this inflammatory processes, CNV regression occurs [187, 208, 392]. It is understood that the inflammatory cascade induced by laser rupture of Bruch's membrane is initiated as early as 1 day after photocoagulation and peaks at 3 days after photocoagulation, returning to baseline levels after 7 days [187]. However, it appears that VEGF expression appears to remains upregulated for at least 30 days after CNV induction, although it begins to trend downwards after 18 days [186, 192, 407, 419]. It is well described in the literature, that CNV lesions peak at 7 days, and begin to regress from 14-21 days, in parallel with the natural history of tissue inflammation and VEGF expression [396, 400, 404]. By 14 days CNV membranes are mature and VEGF levels begin to decline, with ongoing exudative retinal detachment but the RPE layer is re-established. For this reason, from the literature, it is common for investigators to select 14 days as the experimental end point in the laser-induced CNV model [392]. There are a variety of animal

models of CNV [392] [411]. This particular laser-induced rodent model of CNV described by Lambert et al [405], upon which this study was modelled after, is a validated model to use to screen potential nAMD therapies. The laser-induced CNV model was considered ideal for the purposes of this thesis as it is a technically reproducible method and encompasses the key pathogenic features of clinical nAMD; Bruch's membrane disruption, elevated VEGF expression, and propagation of inflammation. Due to the variability in laser settings utilised for CNV induction in the literature, it was deemed prudent to initially characterise the laser settings to optimise this model for application of the experimental PBM laser.

3.2 Study aims

The primary aim of this study was to establish a laser-induced CNV model in rat. The secondary aim was to determine the reliability of FFA, SD-OCT and WM fluorescence immunohistochemistry as quantitative measures of CNV size and permeability.

3.3 Study design

Animals were randomized during the experiments. Animals received 4 distinct laser spots to each eye 1-2 disc diameters from the optic nerve head with either laser setting A, B, or C. The following laser settings were utilised:

A. 100 ms pulse duration, 50 μm spot size, 200 mW power
B. 100 ms pulse duration, 100 μm spot size, 100 mW power
C. 100 ms pulse duration, 100 μm spot size, 200 mW power

CNV membranes were imaged with fundus fluorescein angiography (FFA) and spectral domain optical coherence tomography (SD-OCT) at 7 days (n = 36 spots per laser setting), 14 days (n = 20 spots per laser setting), and 18 days (n = 14 spots per laser setting). Some animals were imaged at multiple time-points. 24 hours after the final FFA and SD-OCT analysis, animals were humanely killed at either 8 days (n = 5 animals per laser setting), 15 days (n = 20 animals per laser setting) or 18 days (n = 15 animals per laser setting) after CNV induction, and eyes enucleated and processed for WM tissue analysis (Figure 3.1). Rupture of Bruch's membrane, evidenced by formation of a vaporisation bubble, was considered a 'successful' laser spot. Each laser spot was treated as n = 1 for all analyses of FFA, SD-OCT, and WM data. Results were confirmed by a second investigator blinded to group allocation during the outcome analyses. A contingency analysis on qualitative data was conducted utilizing Chi-Square Test of Independence. Variance in quantitative data was analyzed utilizing F-test of equality of variance. Statistical significance was set at the 0.05 level.

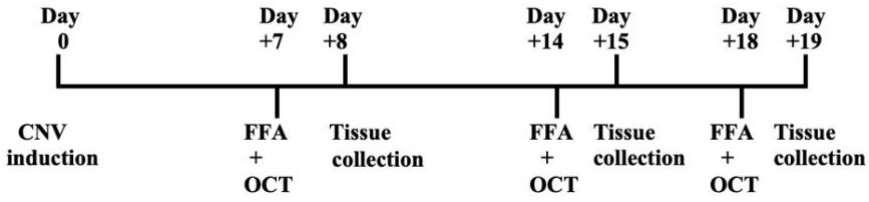

Figure 3.1: Pictorial timeline of CNV membrane analyses following laser induction.

3.4 Results

Laser induction of choroidal neovascularization

Rupture of Bruch's membrane, evidenced by formation of a vaporisation bubble, is considered the clinical end point for laser CNV induction. Of the three laser settings, laser setting A was more frequently associated with undesirable choroidal haemorrhage. This frequency did not reach statistical significance ($p = 0.29$; Figure 3.2). Furthermore, there was no statistically significant difference in the frequency of successful Bruch's membrane rupture between the laser settings ($p = 0.53$; Figure 3.2).

This reference standard was then utilised to scrutinise whether successful bubble formation translated in practice to a measurable CNV lesion on FFA, SD-OCT and WM analysis. When this comparison was performed utilising Chi-Square Test of Independence, no statistically significant difference was found between the reference standard and FFA ($p = 0.77$), SD-OCT ($p = 0.053$), or WM ($p = 0.62$; Figure 3.3).

To determine the reliability of FFA, WM and SD-OCT for identifying CNV membranes, sensitivity, specificity, positive predictive value (PPV), and negative predictive value (NPV) analyses were conducted on the available data, defining bubble formation as the reference standard. There was no statistically significant difference in the sensitivity ($p = 0.14$) and specificity ($p = 0.69$) of these three modalities. FFA has 97.5% sensitivity and 70.0% specificity, WM has 92.9% sensitivity and 72.4% specificity, and SD-OCT has 95.1% sensitivity and 74.1% specificity for identifying CNV membranes. When

considering the practical utility for these three modalities, it was noted that no statistically significant difference in positive predictive value existed between the modalities (p = 0.14), which were of high quality; FFA has 97.5% positive predictive value, WM has 94.8% positive predictive value, and SD-OCT has 95.1% positive predictive value for identifying CNV membranes. However, there was a statistically significant difference in the negative predictive value between modalities when Chi-Square Test of Independence was applied with Bonferroni Correction (p = 0.017). Both FFA and SD-OCT have reasonable negative predictive value for identifying CNV membranes, achieving 80.8% for FFA and 74.1% for SD-OCT (p = 0.06). However, WM has a poor negative predictive value of 65.6%, and this reached statistical significance when compared to FFA (p = 0.001) and SD-OCT analyses (p = 0.03; Figure 3.4).

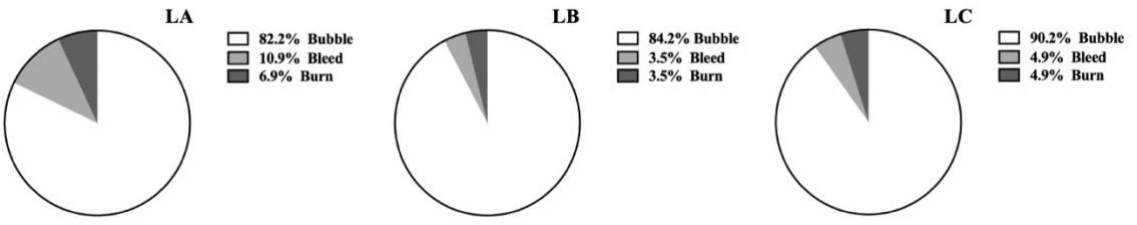

Figure 3.2: Pie chart depicting proportion of 532 nm CW Nd:YAG laser spots that resulted in Bruch's membrane rupture, choroidal haemorrhage or burn in rat eyes with laser setting LA (n = 73), LB (n = 61), and LC (n = 41). No statistically significant difference in outcomes between laser settings (p > 0.05), by Chi-Square Test of Independence. LA: laser set at 100 ms, 50 μm, and 200 mW. LB: laser set at 100 ms, 100 μm, 100 mW. LC: laser set at 100 ms, 100 μm, 200 mW. Scale bar: 1000 μm. CW: continuous wave.

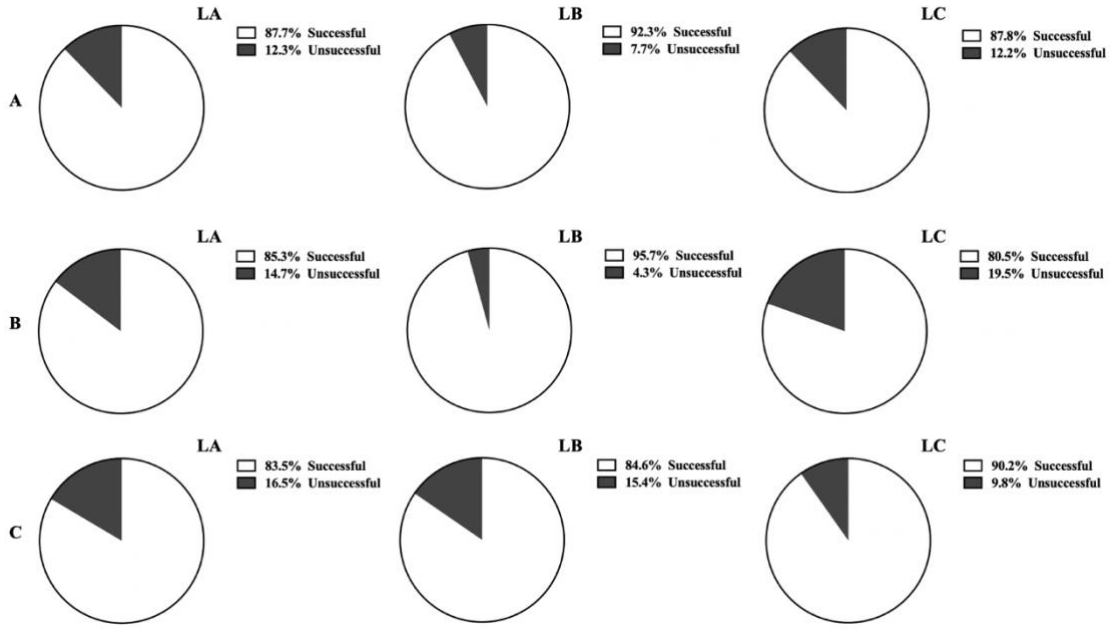

Figure 3.3: (A) Pie chart depicting proportion of 532 nm CW Nd:YAG laser spots that resulted in CNV membrane formation as determined from FFA for laser setting LA (n = 73), LB (n = 57), and LC (n = 41). (B) Pie chart depicting proportion of 532 nm CW Nd:YAG laser spots that resulted in CNV membrane formation as determined from SD-OCT B-scan for laser setting LA (n = 73), LB (n = 57), and LC (n = 41). (C) Pie chart depicting proportion of 532 nm CW Nd:YAG laser spots that resulted in CNV membrane formation as determined from WM analysis via immunohistochemistry with vascular endothelial cell marker IB4 for laser setting LA (n = 73), LB (n = 57), and LC (n = 41). No statistically significant difference (p > 0.05) by Chi-Square Test of Independence. LA: Laser set at 100 ms, 50 μm, and 200 mW. LB: Laser set at 100 ms, 100 μm, 100 mW. LC: Laser set at 100 ms, 100 μm, 200 mW. CW: continuous wave. FFA: fundus fluorescein angiography. SD-OCT: Spectral-Domain Optical Coherence Tomography. WM: wholemount. IB4: isolectin-B4.

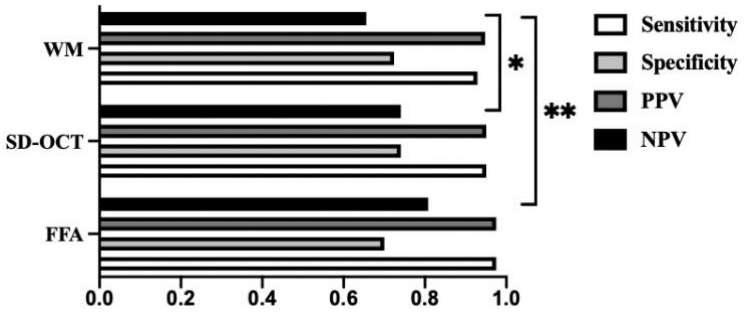

Figure 3.4: (A) Bar graph depicting sensitivity, specificity, PPV and NPV of FFA, SD-OCT, and WM analysis for detecting CNV membranes. Analyses conducted on pooled data from LA, LB, LC (n = 171). * Statistically significant difference (p < 0.05) by Chi-Square Test of Independence with Bonferroni correction, and post-hoc Fisher's Exact Correlational Test. ** Statistically significant difference (p < 0.01), by Chi-Square Test of Independence with Bonferroni correction, and post-hoc Fisher's Exact Correlational Test. FFA: fundus fluorescein angiography. SD-OCT: Spectral-Domain Optical Coherence Tomography. WM: wholemount. PPV: positive predictive value. NPV: negative predictive value/

The natural history of choroidal neovascular membranes varied between laser settings on late-phase fundus fluorescein angiography

An intact blood-retinal barrier is impermeable to fluorescein. Thus, the presence or absence of a halo of fluorescein around perfused vessels was utilised to assess the permeability of CNV lesions. Lesions were scored on a grade scale based on the spatial and temporal evolution of fluorescein leakage following a documented standard as described previously by Liu et al [400]: (0) no leakage, faint hyperfluorescence, or speckled fluorescence without leakage; (1) questionable leakage, hyperfluorescent lesion without

advancing increase in size or intensity; (2) leaky, hyperfluorescence increasing in intensity but not significantly in size without definite leakage; (3) pathologically significant leakage, hyperfluorescence increasing in intensity and in size with definite leakage.

The temporal evolution of the CNV membrane hyperfluorescence and leakage was pronounced at day 7 for all three laser settings, and remained stable at 14 days for CNV lesions induced by laser settings B and C. However, the CNV membranes induced by laser setting A appear to regress by 14 days with minimal hyperfluorescence and fluorescein leakage, which remained stable at 18 days. CNV membranes induced by laser setting B and C had persistent hyperfluorescence and leakage even at 18 days (Figure 3.5). CNV membrane size was objective quantified from hyperfluorescent regions on late-phase FFA images using the thresholding tool on imageJ software. An F-test was applied to the data. Laser settings A and C showed no statistically significant variance in CNV membrane size at 7 days 14 days, and 18 days ($p > 0.05$). However, laser setting B was associated with significantly less variance in CNV membrane size when compared to laser settings A at 7 days ($p = 0.0008$) and 18 days ($p = 0.00007$). This was also the case for laser B and C at 7 days ($p = 0.00002$) and 18 days ($p = 0.00009$). There was no statistically significant difference ($p > 0.05$) in the variance of CNV lesions size between the three laser settings at 14 days (Figure 3.5).

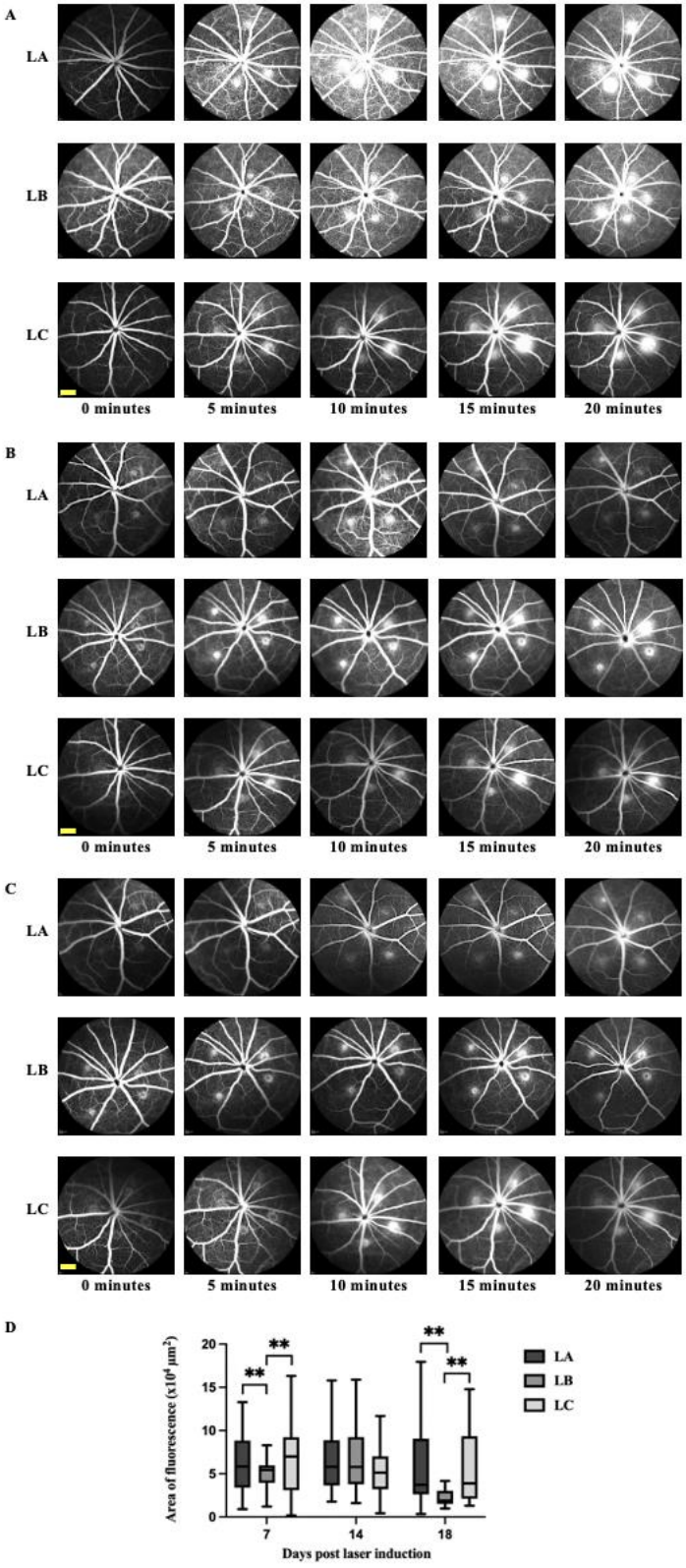

Figure 3.5: (A) Representative images of timelapse FFAs at 7 days after laser induction of CNV with 532 nm CW Nd:YAG laser. (B) Representative images of

timelapse FFAs at 14 days after laser induction of CNV with 532 nm CW Nd:YAG laser. (C) Representative images of timelapse FFA at 18 days after laser induction of CNV with 532 nm CW Nd:YAG laser. Scale bar: 1000 μm. (D) Box plots depicting distribution of CNV membrane area measured from fluorescein leakage on late-phase FFA images at 7 days (LA (n = 27), LB (n = 23), LC (n = 30)); 14 days (LA (n = 19), LB (n = 31), LC (n = 20)); and 18 days (LA (n = 13), LB (n = 12), LC (n = 12)) after laser induction of CNV with 532 nm CW Nd:YAG laser. **Statistically significant difference ($p < 0.01$) when applied to F test of variance. LA: laser set at 100 ms, 50 μm, and 200 mW. LB: laser set at 100 ms, 100 μm, 100 mW. LC: laser set at 100 ms, 100 μm, 200 mW. FFA: fundus fluorescein angiography. CNV: choroidal neovascularization. CW: continuous wave.

The natural history of choroidal neovascular membranes did not vary between laser settings on spectral-domain optical coherence tomography

On spectral-domain optical coherence tomography (SD-OCT) B-scan, CNV membranes appear as ellipsoid densities arising from the choroid into the subretinal space (Figure 3.5A). CNV membrane volumes were measured using SD-OCT B-scans and expressed as a function of volume in μm^3, as previously described by Sulaiman et al [407]. Applying a F-test to the data, there was no statistically significant difference in the variance in SD-OCT membrane volume data between the three laser settings, at all measured time points ($p > 0.05$; Figure 3.5B).

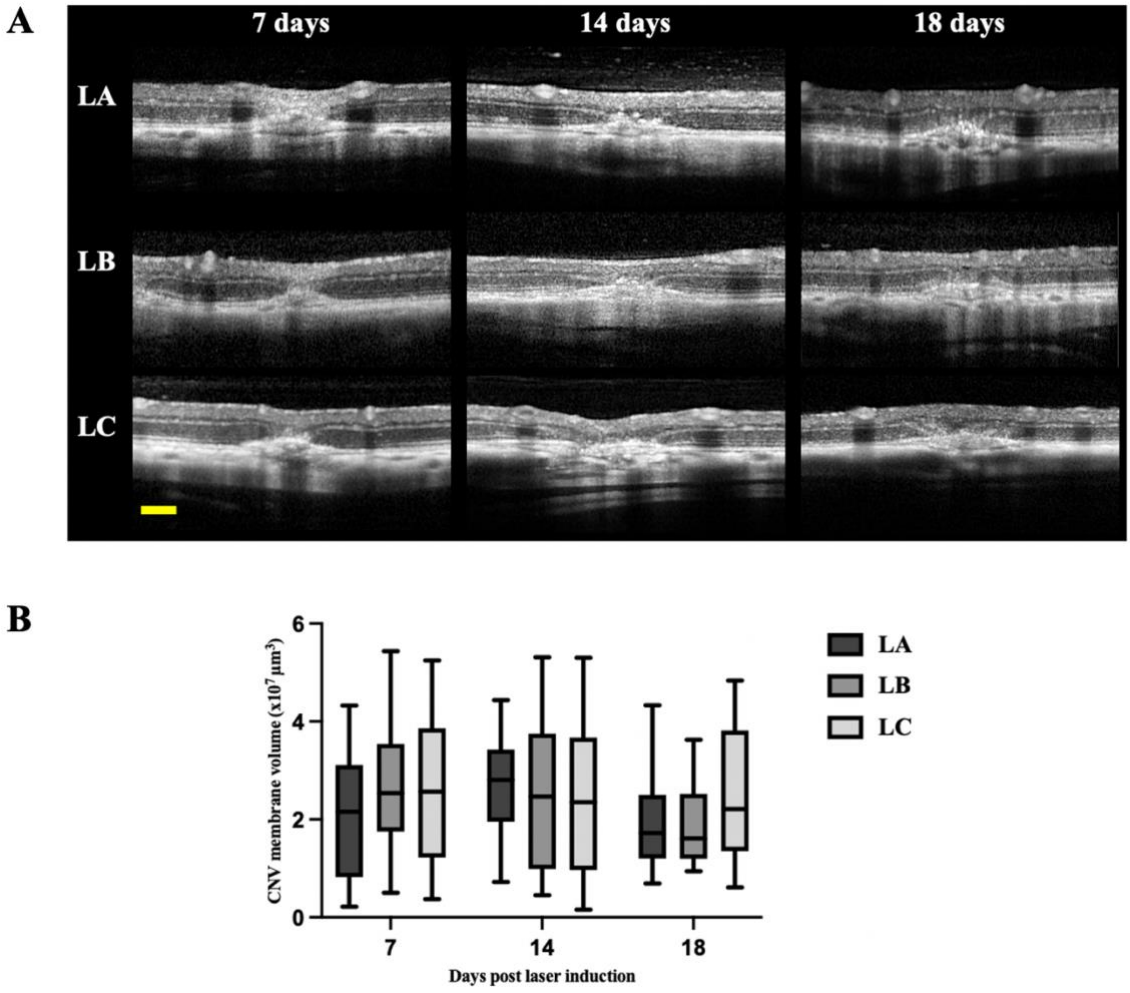

Figure 3.5: (A) Representative SD-OCT B-scans of CNV lesions at 7 days, 14 days, or 18 days after laser induction with 532 nm Nd:YAG CW laser. CNV lesions are characterised by ellipsoid mass emerging from the RPE-choroid complex. Scale bar: 200 µm. (B) Box plots depicting distribution of CNV membrane volume as determined from inputting width, length and depth measurements into an ellipsoid volume formula taken from retinal SD-OCT B-scans captured at 7 days (LA (n = 27), LB (n = 23), LC (n = 30)); 14 days (LA (n = 19), LB (n = 31), LC (n = 20)); and 18 days (LA (n = 13), LB (n = 12), LC (n = 12)) following laser induction. No statistically significant difference ($p > 0.05$) exists between laser settings when applied to F test of variance. LA: laser set at 100 ms, 50 µm, and 200 mW. LB: laser

set at 100 ms, 100 μm, 100 mW. LC: laser set at 100 ms, 100 μm, 200 mW. SD-OCT: Spectral-Domain Optical Coherence Tomograph. CNV: choroidal neovascularization. CW: continuous wave.

The natural history of choroidal neovascular membranes varied between laser settings on wholemount immunohistochemistry

IB4 selectively binds to endothelial cells and was used to immunolabel CNV membranes in RPE WM to allow quantification of CNV membranes area (Figure 3.6A). The size of the CNV membranes was then measured using the colour thresholding tool in ImageJ software on images taken of IB4 immunostained WM, and expressed as a function of area in μm^2. The variance in CNV membrane area with each laser setting was then calculated utilising F test. Laser setting C was associated with significantly greater variance in CNV membrane size as compared to laser setting B at 7 days ($p = 0.01$), and 18 days ($p = 0.002$), and as compared to laser setting A at 18 days ($p = 0.036$). There was no significant difference in the variance of data between the three laser settings at 14 days after induction with laser ($p > 0.05$; Figure 3.6B).

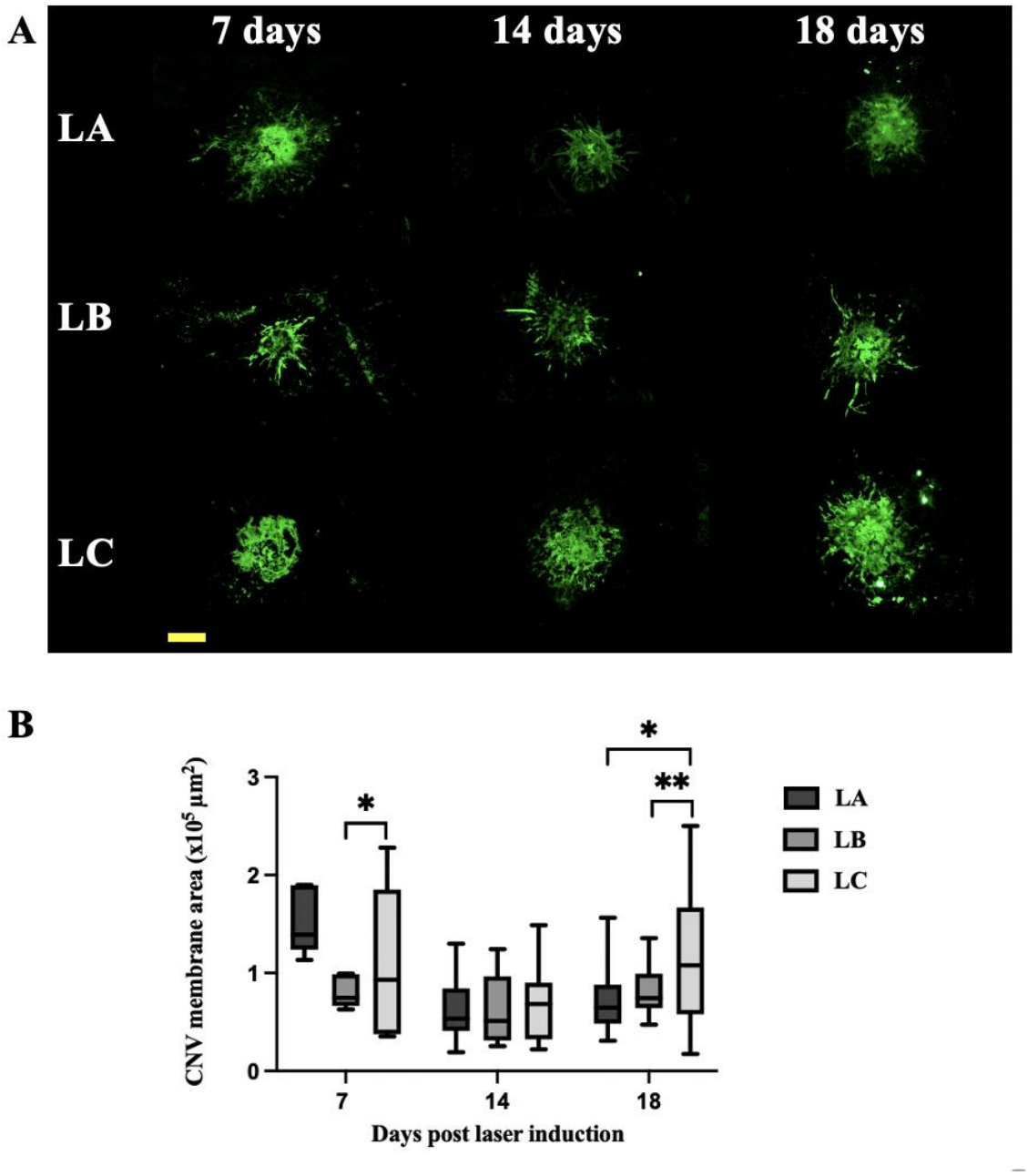

Figure 3.6: (A) Expression of endothelial cell marker IB4, in rat RPE WM, as shown by green fluorescence, at 7, 14 and 18 days following laser-induction of CNV with 532 nm CW Nd:YAG laser. Scale bar: 200 µm. (B) Box plots depicting distribution of CNV membrane area, as measured by expression of IB4 within RPE WM. *Statistically significant difference ($p < 0.05$) when applied to F test of variance. **Statistically significant difference ($p < 0.01$) when applied to F test of variance.

LA: Laser set at 100 ms, 50 μm, and 200 mW. LB: Laser set at 100 ms, 100 μm, 100 mW. LC: Laser set at 100 ms, 100 μm, 200 mW. Scale bar: 200 μm. IB4: Isolectin-B4. WM: wholemount. RPE; retinal pigment epithelium. CNV: choroidal neovascularization. CW: continuous wave.

An inflammatory cell response was associated with choroidal neovascular membranes on wholemount immunohistochemistry

Ionized calcium binding adaptor molecule 1 (IBA-1) is expressed by macrophage-lineage cells, and thus can be used as a microglial and macrophage marker; it is expressed in resting cells and is upregulated when these cells are activated. In RPE WM, double labelling immunofluorescence was employed to identify macrophage-lineage cells at the site of CNV lesions. Specifically, IB4 was utilised to identify CNV membranes, while IBA-1 demarcated microglia/macrophages. An inflammatory cell response in retinal microglia and macrophage-lineage cells was noted on RPE WM, as evidence by IBA-1+ cells. This aggregation of macrophage-lineage cells was localised to the site of the CNV membranes, as determined by colocalization of IBA-1+ macrophage-lineage cells to the site of IB4-marked CNV membranes (Figure 3.7). This was important to highlight as inflammation is a key pathogenic mechanism for CNV formation in this model and in clinical nAMD, and one of the potential pathways targeted in this study.

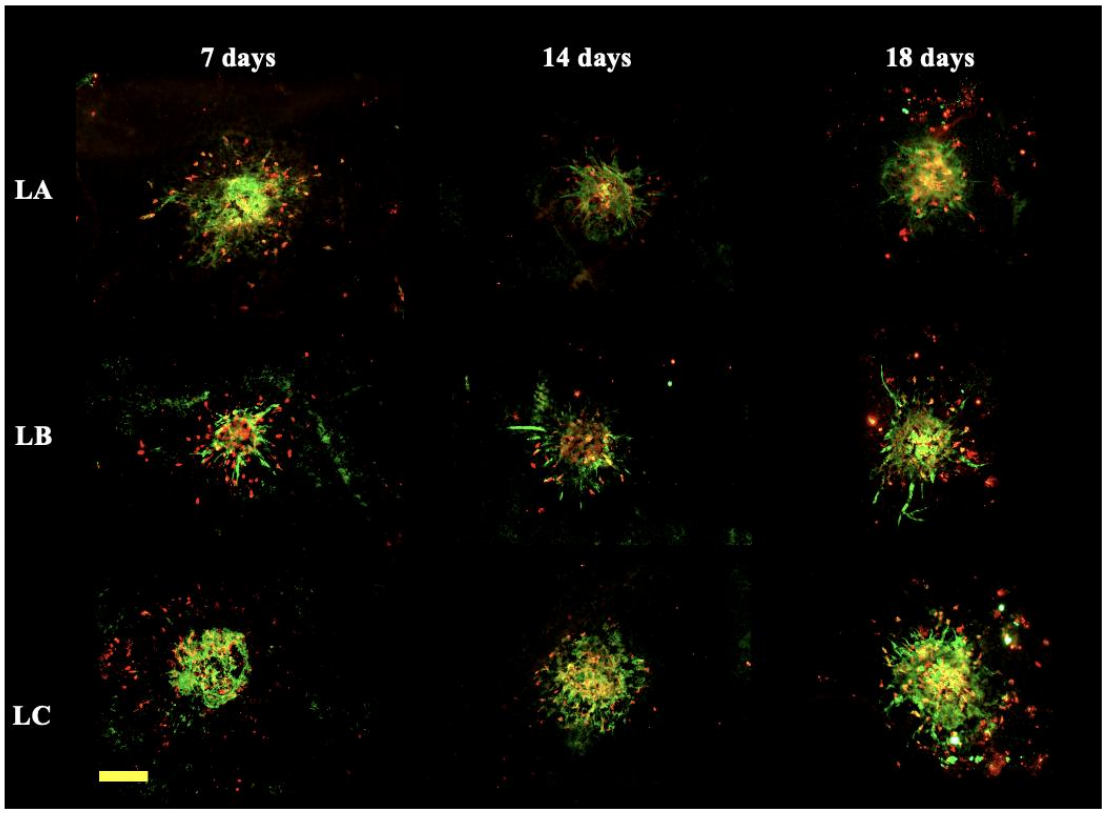

Figure 3.7: Expression of macrophage-lineage marker IBA-1 (red) co-localisation with IB4 immunostaining (green) in rat RPE WM, at 7, 14 and 18 days following laser-induction of CNV with 532 nm CW Nd:YAG laser. Scale bar: 200 µm. IB4: Isolectin-B4. IBA-1; ionized calcium-binding adapter molecule 1. RPE; retinal pigment epithelium. WM: wholemount. CNV: choroidal neovascularization. CW: continuous wave.

3.5 Discussion

The laser-induced CNV model is a well-established and reliable model for therapeutic applications that mimics many of the pathogenic pathways involved in clinical nAMD [187, 396, 400, 404]. Rupture of Bruch's membrane is considered an important clinical end point for laser CNV induction [392, 405]. There was a learning curve associated with developing the

laser CNV model, with more consistent results occurring with refinement of the procedure. It was noted that adequate pupil dilation, a clear cornea and vitreous medium, as well as careful focusing onto the nerve fibre layer was imperative for successful Bruch's membrane rupture. If these conditions were not met, failure to rupture Bruch's membrane would quite predictably occur, with a resultant burn occurring instead, and failure of CNV induction. As previously established by Lui [400], on fluorescein angiography, CNV is defined as being present if there is early hyperfluorescence with late leakage at the site of the induced laser injury. For this reason, lesions that showed no leakage were excluded from analysis. There was a clear correlation between Bruch's membrane rupture and successful CNV membrane induction in our laser model, as evidenced from the FFA, WM and SD-OCT analyses, with no statistically significant difference in successful CNV membrane induction between the laser settings. The rate of successful CNV induction was higher than that quoted in the literature [411]. Dobi *et al* described that often a small haemorrhage was associated with Bruch's membrane rupture and did not negatively impact on CNV development, whilst, a large haemorrhage that obscured the view of the fundus was an unwanted adverse event, which precluded further analysis of the affected eye [390]. Certainly laser setting A, which has the highest energy per cm^2 of the three laser settings, was more frequently associated with unwanted choroidal haemorrhage with laser induction, an observation seen with use of energy laser settings greater than 130 mW [411].

A qualitative assessment of temporal evolution of CNV membrane leakage on time-lapse FFA, with allocation of a numerical grading from 0-3, demonstrated a general trend towards membrane regression at 18 days. Our findings with laser settings B and C were

in line with previous observations that CNV lesions peak at 7 days, stabilise at 14 days and begin to regress at 18 days [396, 400, 404], whilst laser setting A demonstrated early trend towards regression at 14 days. The development of CNV in this model closely correlates to reports that VEGF levels peak at 3 days but trend downwards after 18 days [187, 404]. The inflammatory cascade that is triggered following laser induction is an important mechanism as leukocyte infiltration is maximal in the first 7 days and the macroglia are the main source of VEGF in this model [187]. The close relationship between microglial cell activation and CNV membranes on fluorescence immunohistochemistry of WM in this study supports Zhao *et al* findings and validates the pro-inflammatory arm of VEGF elevation underlying CNV formation in clinical and experiment CNV [404]. For this reason, PBM treatment was implemented within the early critical phase of CNV membrane formation and the experimental end point of 14 days was selected.

Multiple quantitative measures of CNV lesions size were also done; CNV membrane volume calculated from SD-OCT images, CNV membrane area from fluorescence in late-phase FFA, and CNV membrane area on immunohistochemical staining of RPE WM. It appears from comparative analysis of FFA, WM and SD-OCT, that FFA fared better overall, however, it had poorer specificity comparatively to SD-OCT and WM [413]. It is expected that FFA will have a lower specificity, as fluorescein leakage is an indirect measure of CNV membrane presence, and leakage can occur with Bruch's membrane disruption without a CNV membrane being present and inversely, a mature CNV membrane may not leak, as previously postulated [411]. Several investigators countered this issue with the use of perfusion with high-molecular-weight fluorescein-labelled dextrans, as was well described in mice by D'Amato *et al* [414], and later applied in rats by Edelman

and Castro [391]. These do not leak from vessels, and allows for post-mortem imaging of CNV lesions under fluorescence microscopy. Thus, this practice has been successfully adopted by investigators using the laser-induced CNV model [415]. This is reflected in clinical practice, with FFA and SD-OCT analysis used as gold standard for identifying and monitoring of clinical nAMD, although the former will likely be superseded by OCT-angiography, an evolving *in vivo* flow-based interferometric imaging modality with resolution to the microcirculation, due to its comparative non-inferiority, speed of analysis, and non-invasive nature [416-420]. The suboptimal reliability of WM analysis in regard to negative predictive value is influenced by a number of factors, including the sensitivity and specificity of primary and secondary antibodies used in the analysis, and, further, CNV membranes can be disrupted in the process of peeling the retina from the RPE-choroid-scleral WM. SD-OCT analysis is mainly limited by image resolution [421]. The difficulty that lies with the laser-induced CNV model is that there is variability in the tissue response between laser spots [422]. Thus, in this study, the FFA, SD-OCT and fluorescent immunohistochemical results were controlled for by identifying laser spots at induction and linking them throughout repeat FFA and SD-OCT and finally in WM analysis.

The natural history of the CNV lesions and the variability in the size of the CNV membrane induced by the three different laser settings were the factor that influenced the decision regarding the most suitable laser setting to use to induce CNV lesions in future experiments. Statistically, it was demonstrated that laser setting B (100 ms, 100 mW, 100 µm) was associated with less variance compared to both laser setting A and C on FFA analysis at two time points, and with less variance compared to laser setting C on WM at

two time points. The natural history of the laser induced CNV lesions was determined by measuring the CNV membranes at multiple time points to determine the optimal treatment times points. It was noted that laser setting A was associated with a higher rate of CNV formation secondary to haemorrhage, and an earlier CNV membrane regression then the other laser settings. Thus, overall, laser setting B was considered the most suitable laser setting for the CNV model.

Chapter 4:

Affirming the safety profile of photobiomodulation laser in the retina

4.1 Introduction

Quite consistently, investigators have affirmed the safety of PBM in biological tissues through in vitro and in vivo animal studies [362, 367, 387, 423, 424]. There have been a wide array of treatment regimens utilized by investigators, making it difficult to ascertain the ideal therapeutic dose. There are 8 variables that need to be reported for the PBM laser setting to allow for reproducibility; center wavelength (nm), spectral bandwidth (nm), operating mode frequency (Hz), pulse on off duration/duty cycle (sec/%), energy per pulse (J), peak radiant power (mW), average radiant power (mW), polarization, aperture diameter (cm), irradiance at aperture (mW/cm^2), beam divergence (rad), beam shape, and beam profile [425]. The doses must be reported in J/cm^2, with duration and frequency included as the former allows for reproducibility and the latter allows from total energy calculation [425]. The evidence in support of PBM is largely founded on LED-based PBM therapy, however, there is a suggestion that laser-PBM has comparable safety and efficacy [375, 380, 426]. Laser-delivered PBM have three main advantages over LED-delivered PBM due to the foundation principle of light amplification by stimulation emission of radiation. Firstly, as photons are emitted at the same phase, they are coherent, secondly, they emit monochromatic light as the wavelength of light emitted is of a narrow range, and thirdly, the light source is well collimated making it possible to tightly aim and focus the beam [427]. Previous published work in the host laboratory has demonstrated the safety profile of the selected PBM laser fluence settings, and additionally presented evidence to suggested a neuroprotective effect in photoreceptor degenerative disease [428]. In the eye and brain, the biological effects of PBM are believed to be mediated through upregulation of the activity of mitochondrial respiratory chain molecule, CCO, which has pleotropic effects

in biological tissues, up-regulating gene expression involved in cellular proliferation, RNA synthesis and DNA repair, anti-apoptosis, membrane potential and ion-channel activation, mitochondrial oxygen metabolism and ATP production, antioxidant production, and immunomodulation [62, 63, 346-349, 353, 357, 381]. Much of the evidence for the biological effects of PBM treatment in the eye have been applied to pathological cellular processes [362-369]. However, there is a general belief that PBM only targets pathological cellular processes and otherwise does not alter physiological cellular function [367, 375, 426]. The confidence in the safety of PBM has led to clinical trials in the treatment of retinitis pigmentosa, dry AMD, and DME [371-375, 388, 428, 429]. Enquiry into how PBM laser treatment influences the specific aspects of retinal glial cell behaviour and retinal endothelial proliferation and permeability is an important step to better understand the role this treatment modality has in the prevention of aberrant vascular tissue growth in neovascular disease of the eye.

4.2 Study aim

The primary aim of this study was to determine the safety profile of two PBM-laser settings by analysing the tissue effects of these treatment doses on healthy retinae.

4.3 Study design

For cross-section analysis, animals received treatment to both eyes with either LPBM (n = 8), HPBM (n = 8), or sham (n = 8) at 6 days, 3 days, and immediately prior to induction of CNV by CW laser. Animals were randomized during group allocation for the

experiment. Animals were humanely killed at 3 days following laser CNV induction. Eyes were immediately enucleated. All left eyes were prepared for immunoperoxidase staining of retinal tissue cross-sections (Figure 4.1). Control animals were also used for comparative analysis. All analysis of cross-section data was performed on sections taken through the center of the CNV membrane; each eye was treated as n = 1. The primary investigator was not blinded to the group allocation during the outcome analyses. Results were confirmed by a second investigator blinded to group allocation during the outcome analyses. Quantitative immunostaining data were reported as means. Means were compared between experimental groups using One-way ANOVA with post-hoc Tukey's HSD Test performed for multiple comparisons. Statistical significance was determined at the 0.05 level.

For FFA, SD-OCT and wholemount analysis animals received treatment to both eyes with either LPBM (n = 9), HPBM (n = 9), or sham (n = 9) every 3 days from 6 days prior to CNV laser induction, until 12 days after laser CNV induction. Animals were randomized during the experiments. CNV was only induced in the left eye of each animal, whilst the right eye acted as a treatment control analysis. Animals were randomized during group allocation for the experiment. FFA and SD-OCT analysis was conducted at 7 days and 14 days following CNV induction. Animals were humanely killed at 15 days after CNV induction and eyes enucleated and processed for wholemount tissue analysis 24 hours after the final FFA and SD-OCT analysis (Figure 4.2). All analysis of FFA, SD-OCT, and wholemount data was performed on pooled averages of successful laser spots in each eye; each eye was treated as n = 1. The primary investigator was not blinded to the group allocation during the outcome analyses. Results were confirmed by a second

investigator blinded to group allocation during the outcome analyses. Quantitative data are reported as means. Means were compared between experimental groups using One-way ANOVA with post-hoc Tukey's HSD Test performed for multiple comparisons. Statistical significance was determined at the 0.05 level.

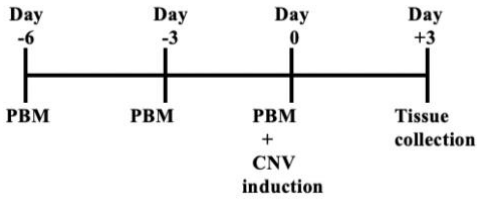

Figure 4.1: Pictorial timeline of PBM experimental treatment regimen and timeline of tissue collection for retinal tissue cross-section.

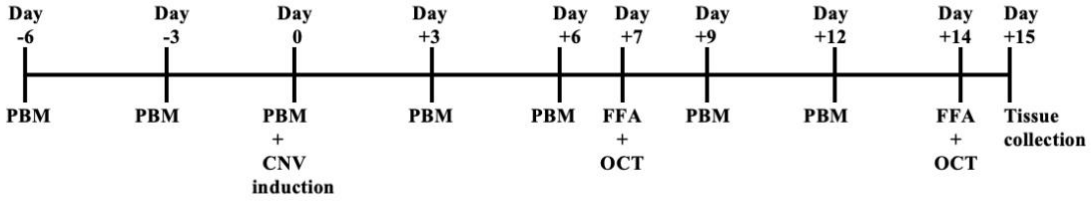

Figure 4.2: Pictorial timeline of PBM experimental treatment regimen treatment and CNV membrane analyses following laser induction.

4.4 Results

Photobiomodulation laser treatment does not change retinal histomorphology

Hematoxylin and eosin immunolabelling was utilized to visualise the retinal histomorphology in control eyes treated with HPBM-laser, LPBM-laser and sham. The retinal histomorphology was not observably different in retinas treated with either setting

of PBM laser when compared to sham retinas. The highly organised, laminar structure of the retina was maintained, and the RPE layer remains intact in all treatment groups (Figure 4.3).

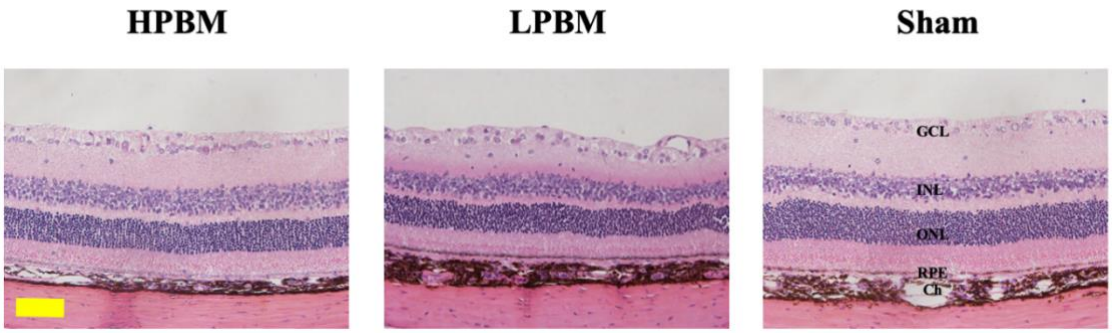

Figure 4.3: Representative images of H&E immunostaining of retinal cross-sections of eyes treated with HPBM laser, LPBM laser, and sham. Comparatively, PBM-treated eyes have normal histomorphology. Scale bar: 100 µm. H&E: hematoxylin and eosin. HPBM: high-dose photobiomodulation. LPBM: low-dose photobiomodulation. GCL: ganglion cell layer. INL: inner nuclear layer. ONL: outer nuclear layer. RPE: retinal pigment epithelium. Ch: choroid.

Photobiomodulation laser treatment does not change retinal thickness

SD-OCT imaging is useful for visualising the retina in cross section in detail in vivo. This tool was particularly useful in assessment whether any retinal phototoxicity occurs after PBM treatment. SD-OCT B scans of retinas of PBM treated control eyes were compared to those of retinas of sham-treated control eyes to ascertain whether PBM has any adverse effects on the healthy retina (Figure 4.4A). A one-way ANOVA was performed to compare the effect of PBM on retinal thickness. This revealed that there was not a

statistically significant difference in retinal thickness between treatment groups (F = 0.14, p = 0.87, Figure 4.4B).

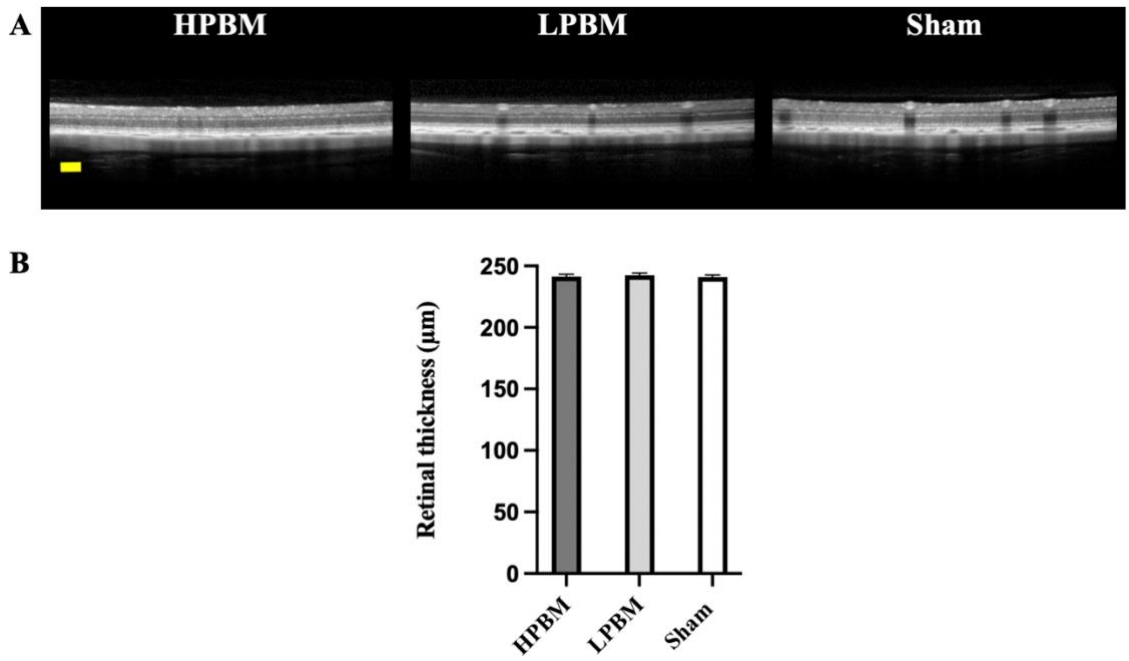

Figure 4.4: (A) Representative SD-OCT B-scans of the retina in control eyes at completion of treatment with HPBM, LPBM, and sham. Scale bar: 200 µm. (B) Bar graph depicting retinal thickness measured from SD-OCT B-scans captured from control eyes at completion of treatment with HPBM laser (n = 9), LPBM laser (n = 9), and sham (n = 9). Data are presented as mean ± SEM. There was no statistically significant difference (p > 0.05) between the treatment groups, as per one-way ANOVA. SD-OCT: Spectral-Domain Optical Coherence Tomography. HPBM: high-dose photobiomodulation. LPBM: low-dose photobiomodulation.

Photobiomodulation laser treatment does not induce neovascularization

Time-lapse FFA in control eyes treated with either HPBM, LPBM, or sham was performed at the mid-point, and at the completion of the treatment. Appropriate filling of retinal vessels and the choroidal capillary network was visible in all treatment groups. No pathological vascular networks, nor fluorescein leakage was observed in any of the treatment groups. These results indicated that PBM laser does not in itself induce neovascularization or disruption of the blood-retina-barrier in the healthy eye (Figure 4.5).

Weak nestin immunolabelling was observed in the retinal vasculature, as is expected with a mature vascular network in retinal tissue. No focal upregulation of nestin or aberrant vascular networks, indicative of pathological neovascularization, were visualised in any group. Furthermore, no Nestin+ Müller cells were observed in any group, suggesting that no glial cell activation occurred. This normal pattern of expression was observed in retinas treated with HPBM-laser, LPBM-laser, and sham. This supports the evidence provided by FFA that PBM laser treatment does not incite an inflammatory glial response, nor promote the development of pathological neovascularization in the healthy retina (Figure 4.6).

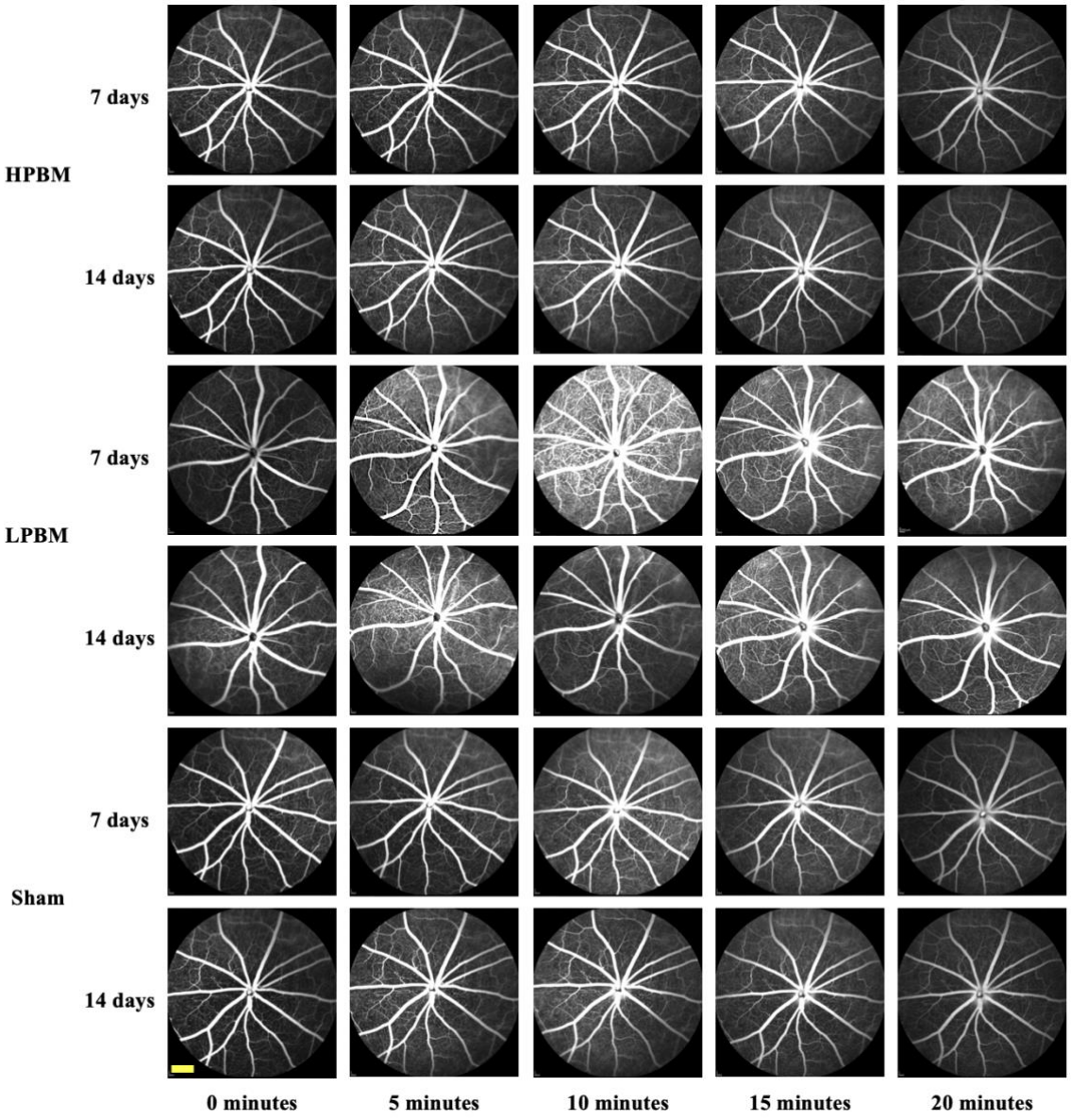

Figure 4.5: Representative images of time-lapse FFA of control eyes at completion of treatment with HPBM laser, LPBM laser, and sham. No pathological hyperfluorescence or leakage is evident in any of the treatment groups. Scale bar: 1000 μm. FFA: fundus fluorescein angiography. CNV: choroidal neovascularization. HPBM: high-dose photobiomodulation. LPBM: low-dose photobiomodulation.

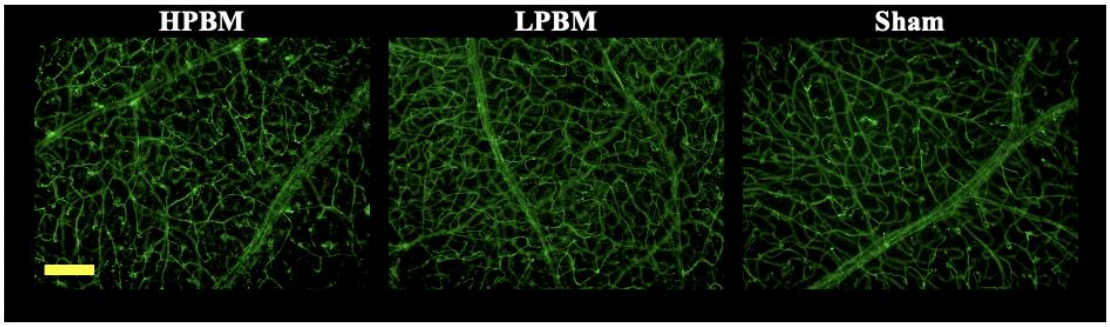

Figure 4.6: Expression of Nestin in retinal WM from eyes treatment with HPBM, LPBM, or sham. Normal retinal vascular networks are observed in all treatment groups. Scale bar: 200 µm. WM: wholemount. HPBM: high-dose photobiomodulation. LPBM: low-dose photobiomodulation.

Photobiomodulation laser treatment does not induce an inflammatory glial cell response

In retinal WM from control eyes treatment with HPBM laser, LPBM laser, and sham, scattered IBA-1-positive microglial cells were noted in a pattern that did not differ between treatment groups. These cells possessed the characteristic arborescent morphology of resting-state cells (Figure 4.7A). In control retinal cross-sections from HPBM-laser, LPBM-laser, and sham treatment groups, similarly a few IBA-1-positive microglial cells were appropriately observed in the GCL and IPL as is typical for these retinal glia. However, the characteristic arborescent morphology of resting microglia was not fully appreciated in these thin tissue cross sections (Figure 4.7B). In control RPE WM, microglial cells were not observed. Since microglia are resident cells of the retina, and are not indigenous to the RPE, this finding is also expected (data not shown).

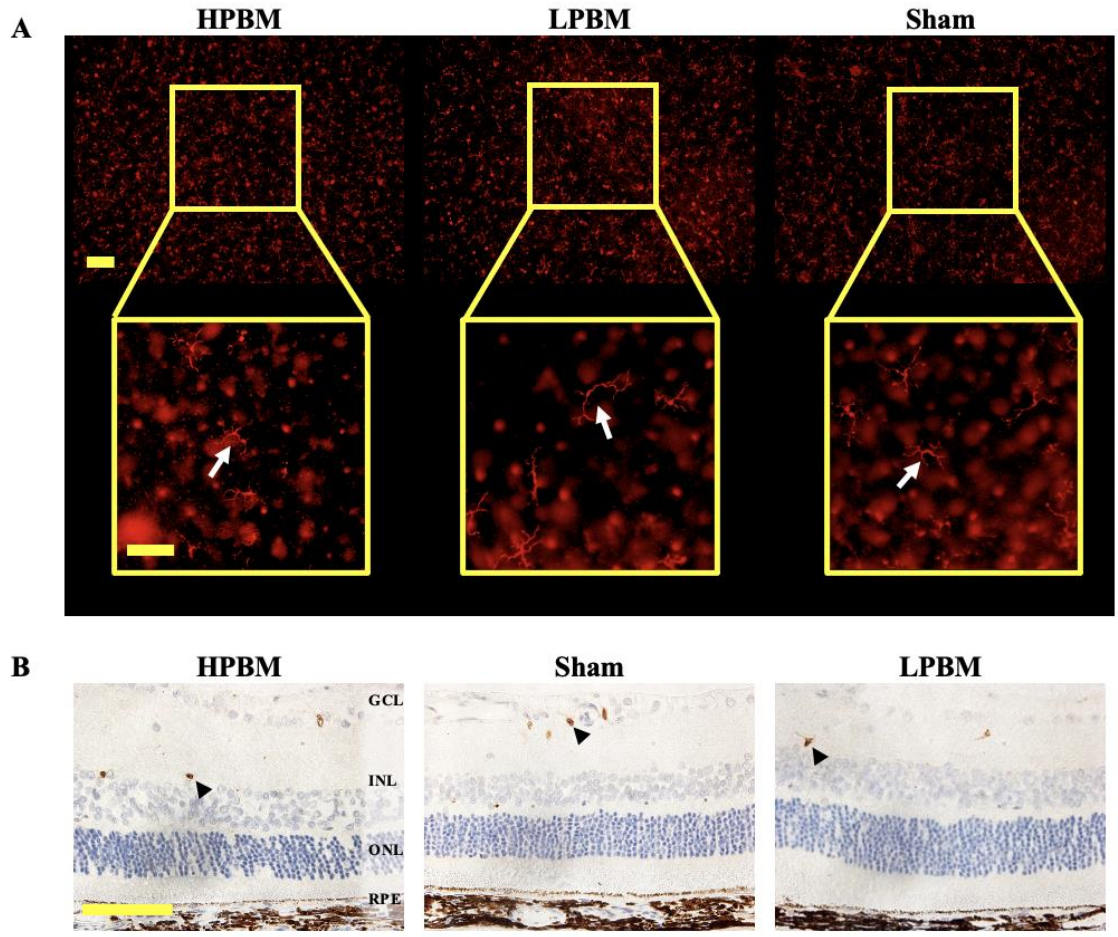

Figure 4.7: (A) Expression of IBA-1 resident microglial cells as determined by fluorescence immunohistochemistry of retinal WM from eyes at completion of the treatment period with HPBM laser, LPBM laser, and sham. Scale bar: 100 µm. White arrow: microglial cell. (B) Expression of IBA-1 resident microglial cells (black arrowhead) as determined by immunolabelling of retinal paraffin cross-sections from eyes at completion of the treatment period with HPBM laser, LPBM laser, and sham. Scale bar: 100 µm. IBA-1: ionized calcium-binding adapter molecule 1. WM: wholemount. GCL: ganglion cell layer. INL: inner nuclear layer. ONL: outer nuclear layer. RPE: retinal pigment epithelium. HPBM: high-dose photobiomodulation. LPBM: low-dose photobiomodulation.

In healthy retinas, GS labelled all parts of the Müller cell, from the vitreal end-feet, the main processes spanning the retina, to the scleral end processes and the lateral side branches. Examination of GS expression in retinal cross-sections from eyes treatment with HPBM laser, LPBM laser or sham revealed no discernable difference in the pattern of immunolabelling. This observation suggests that PBM laser does not induce morphological changes in the Müller cell that would suggest gliotic reactivity (Figure 4.8).

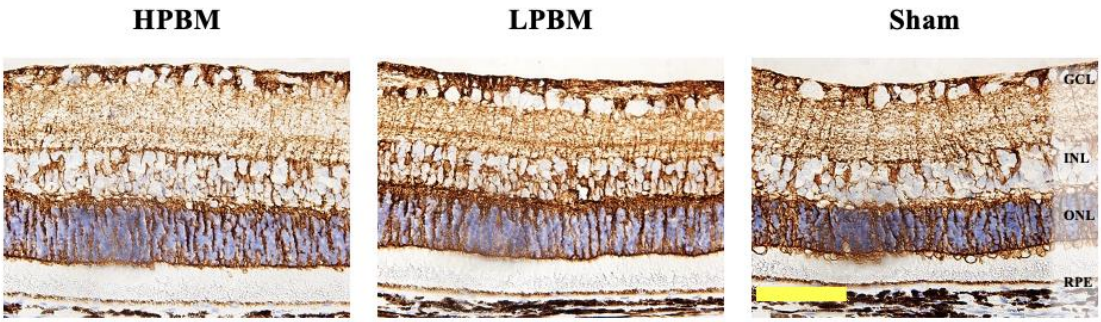

Figure 4.8: Representative images of glutamine synthetase staining of Müller cells in cross-sections from eyes at completion of the treatment period with HPBM laser, LPBM laser, and sham. Müller cells appear histomorphologically normal in all treatment groups. Scale bar: 100 µm. GCL: ganglion cell layer. INL: inner nuclear layer. ONL: outer nuclear layer. RPE: retinal pigment epithelium. HPBM: high-dose photobiomodulation. LPBM: low-dose photobiomodulation.

4.5 Discussion

In the field of ophthalmology, there a complex relationship with light. Hormesis, originally described by the Arndt-Schulz Law, describes the biphasic response of biological tissue to differing concentrations of certain substances, whereby exposure to low levels of a substance, which would otherwise be harmful at a higher dose, leads to positive effects in biological tissues [345, 430, 431]. This process is exemplified in ocular tissue when exposed to laser treatment. Ocular tissues have a variable response to exposure to light. Low levels of light exposure can have advantageous consequences, but elevated levels of light exposure can pass the tissue threshold and consequently being detrimental to tissue function. Retinal phototoxicity is a well-documented process. The dense melanin pigment of the RPE and choroid absorbs incident laser energy that is then converted to thermal energy [316-318]. When the irradiation time exceeds the thermal relaxation time of the RPE cells, which approximately equals 10μs, heat dissipation out of the RPE during and after the laser treatment and causes thermal damage to the adjacent choroidal and photoreceptor cells [319]. This is a rapidly evolving area of inquiry; it is the basis for subthreshold laser therapy in degenerative and proliferative retinal disease. It is suggested that at the right laser fluence there is up-regulation of the expression of cell viability factors, increased extracellular matrix turnover, and a shift in vascular endothelial growth factor (VEGF) and pigment epithelium factor (PEDF) expression ratio to favour an anti-angiogenic microenvironment, and resultant involution of retinal neovascularization [327-332, 432-434].

Glutamine synthase (GS) is a functional protein constitutively expression by Müller cells of developmentally-mature healthy retinas. Müller cells constitutively express GS as part of their role in the uptake, metabolism, and inactivation of glutamate, the major excitatory neurotransmitter in the retina. GS is a marker of health and is utilized to assess Müller cell phenotypic status in retinal cross-sections by highlighting any morphological and functional changes that occur in response to Müller cell stress. Conversely, Nestin is a class VI intermediate filament protein that is expressed at low levels in quiescent vascular endothelium, and not at all in terminally differentiated Müller cells in the health adult retina. Nestin is utilised as a marker of proliferation in vascular endothelial cells and Müller cells as it is upregulated in these population during angiogenesis and gliosis [435-442]. GFAP is another maker of gliosis, as it is expressed in terminally differentiated glia. And is upregulated as part of the glial stress response [413, 443]. Although attempts were made to facilitate optimal morphology in retinal cross-sections with utilization of Davidson's fixative to circumvent artefactual retinal detachment, attempts to stain with glial stress marker GFAP, did not produce cross-section that could be reliably used for analysis and representation in this thesis. In clinical practice, FFA and SD-OCT analysis is considered gold standard for identifying and monitoring of clinical nAMD; these were thus confidently utilised as reliable outcome measures of retinal morphological and vasopermiability following PBM laser treatment [416-420]. The evidence presented here is indicative that PBM laser at the selected laser fluences utilised in this study does not cause phototoxicity, induce an inflammatory retinal glial stress response, nor stimulate growth of aberrant vascular tissue or cause disruption of the blood-retinal-barrier in otherwise healthy retinae.

These findings reaffirm the safety profile of PBM-laser at the selected laser fluences. It is suggested that PBM at the fluences utilized in this study do not detrimentally altering biochemical processes in healthy tissue [367, 375]. This is not unexpected, considering that the safety of the laser settings utilised in this study have been previously validated. These findings mirror the laser fluence range utilised in numerous studies that have demonstrated neuroprotection and immunomodulation [358-369, 371, 388, 444]. It is of particular interest to determine the retinal glial cell response to PBM, for which the evidence has thus far swayed towards an immunomodulatory effect [228, 379, 383, 384, 445]. This is especially pertinent as members of this cell population have a strong influence on the retinal response under conditions of stress and are a strong driver of pathological neovascularization in the retina under conditions of unrestrained inflammation [160, 446, 447]. This is pertinent when considering how PBM will influence angiogenic pathways, because PBM appears to have variable effects on these pathways depending on the tissue conditions [448, 449].

Chapter 5:

Ascertaining if photobiomodulation laser influences neovascular membrane size and permeability in the choroidal neovascularization model

5.1 Introduction

A dense vascular supply is fundamental to meet the requirements of the photoreceptor population to facilitate the metabolically demanding phototransduction cascade. The pathogenesis of nAMD is characterised by a multitude of factors including chronic hypoxia and neuroinflammation. A major downstream consequence is unrestrained expression of the pro-angiogenic factor VEGF. This leads to growth and infiltration of the subretinal space by new vessels that lack barrier properties. Photoreceptors are highly reliant on an intact blood-retinal barrier to carefully control the microenvironment and confer immune privilege [16, 60-62, 73]. Disruption of the blood-retinal barrier results in an imbalance in the influx and efflux of fluid between the vasculature and the retinal space and invites immune cell infiltration, leading to further barrier disruption. This results in exudative retinal detachment and corruption of the retinal phototransduction process acutely, as well as apoptosis and atrophic scaring of the retinal tissue in the protracted phase, with consequential irreversible visual impairment [34, 37, 132]. Based on the shared belief that VEGF is the master control of angiogenesis, the goal of evolving therapeutics is to target upstream pathogenic mechanisms that lead to upregulation of VEGF with the intention to abort retinal neovascularisation and consequently prevent retinal degeneration [143, 450].

5.2 Study aim

The aim of this study was to determine the effects of treatment with two PBM-laser settings on the size and permeability of CNV in this laser-induced CNV model

5.3 Study design

For FFA, SD-OCT and WM analysis, animals received treatment to both eyes with either HPBM (n = 9), LPBM (n = 9), or sham (n = 9) every 3 days from 6 days prior to CNV induction, until 12 days after CNV induction. Animals were randomized during group allocation for the experiment. CNV was only induced in the left eye of each animal, whilst the right eye acted for treatment control analysis. FFA and SD-OCT analysis was conducted at 7 days and 14 days following CNV induction. Animals were humanely killed at 15 days after CNV induction, and eyes enucleated and processed for WM tissue analysis 24 hours after the final FFA and SD-OCT analysis (Figure 5.1). All analysis of SD-OCT and WM data was performed on pooled averages of laser spots in each eye; each eye was treated as n = 1. The primary investigator was not blinded to the group allocation during the outcome analyses. Results were confirmed by a second investigator blinded to group allocation during the outcome analyses. Quantitative data are reported as means. Means were compared between experimental groups using One-way ANOVA with post-hoc Tukey's HSD Test performed for multiple comparisons. Statistical significance was determined at the 0.05 level. All semi-quantitative analysis of FFA data was performed on individual laser spots in each eye; each laser spot was treated as n = 1. Data are reported as categorical data. Chi-Square Test of Independence was applied to this data with Bonferroni Correction and post-hoc Fisher's Exact Contingency Test performed for multiple comparisons.

For cross-section analysis, animals received treatment to both eyes with either HPBM (n = 8), LPBM (n = 8), or sham (n = 8) at 6 days, 3 days, and immediately prior to induction

of CNV by CW laser (Figure 5.2). Animals were randomized during group allocation for the experiment. To allow analysis of CNV lesions during the peak period of inflammation, animals were humanely killed at 3 days following CNV induction. Eyes were immediately enucleated. All left eyes were prepared for immunoperoxidase staining of retinal tissue cross-sections. Control animals were also used for comparative analysis. All analysis of cross-section data was performed on pooled averages of successful laser spots in each eye; each eye was treated as n = 1. The primary investigator was not blinded to the group allocation during the outcome analyses. Results were confirmed by a second investigator blinded to group allocation during the outcome analyses. Quantitative immunostaining data are reported as means. Means were compared between experimental groups using One-way ANOVA with post-hoc Tukey's HSD Test performed for multiple comparisons. Statistical significance was determined at the 0.05 level.

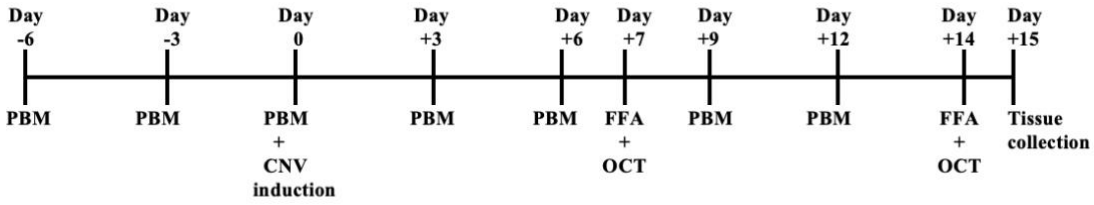

Figure 5.1: Pictorial timeline of PBM experimental treatment regimen treatment and CNV membrane analyses following laser induction.

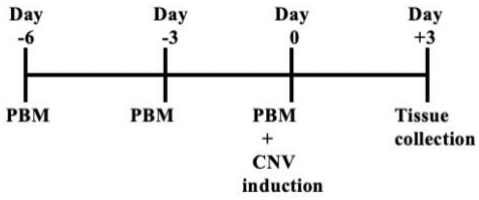

Figure 5.2: Pictorial timeline of PBM experimental treatment regimen and timeline of tissue collection for retinal tissue cross-section.

5.4 Results

Choroidal neovascular membrane histomorphology

At the site of laser induction, a CNV membrane is seen as an ellipsoid mass arising from the choroid and infiltrate into the subretinal space. Disruption of the overlying retinal morphology and loss of photoreceptors is observed secondary to the thermal insult to the retina in the process of rupturing Bruch's membrane. This is highlighted when comparing normal retinal histomorphology to CNV lesions (Figure 5.3).

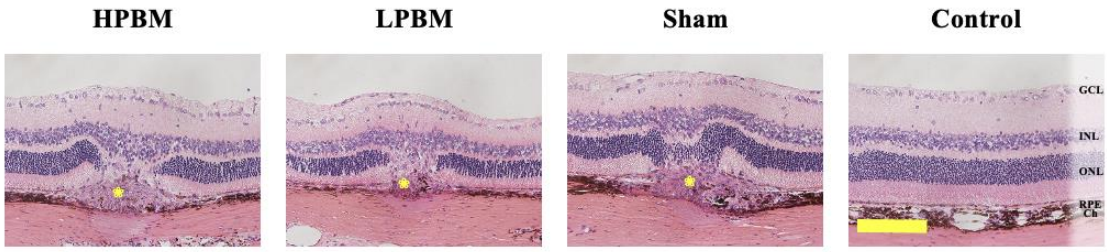

Figure 5.3: Representative images of H&E stained retinal cross-sections 3 days after CNV induction in eyes treated with HPBM, LPBM, or sham. CNV membranes are marked by yellow asterisks. Representative image of a control eye has been included to demonstrate normal histomorphology of the retina. Scale bar: 100 µm. H&E: hematoxylin and eosin. CNV: choroidal neovascularization. HPBM: high-dose

photobiomodulation. LPBM: low-dose photobiomodulation. GCL: ganglion cell layer. INL: inner nuclear layer. ONL: outer nuclear layer. RPE: retinal pigment epithelium. Ch: choroid.

Photobiomodulation laser influences choroidal neovascular membrane growth

Laser-induced CNV membranes were visualised in RPE wholemounts by immunostaining with IB4, which localised to the endothelial cell cytoplasm. IB4 also appeared to weakly localise to RPE cell tight junctions in control RPE wholemounts (data not shown). CNV membranes were characterised by a nest of neovascular vessels (Figure 5.4A). CNV membrane area was quantified utilizing a colour-thresholding tool on IB4 immunofluorescence images. A one-way ANOVA was performed to compare the effect of PBM on CNV membrane size at the completion of the treatment period. This revealed that there was a statistically significant difference in CNV membrane size between at least two treatment groups ($F = 5.93$, $p = 0.008$). Tukey's HSD Test for multiple comparisons found that the mean value of CNV membranes size in sham eyes were significantly larger than that of HPBM ($p = 0.01$, 95% C.I. [$3.95x10^4$, $6.15x10^4$]) and LPBM ($p = 0.02$, 95% C.I. [$4.28x10^4$, $6.15x10^4$]) treated eyes. No statistically significant difference ($p = 0.89$) in CNV membrane size was observed between LPBM and HPBM treated eyes (Figure 5.4B).

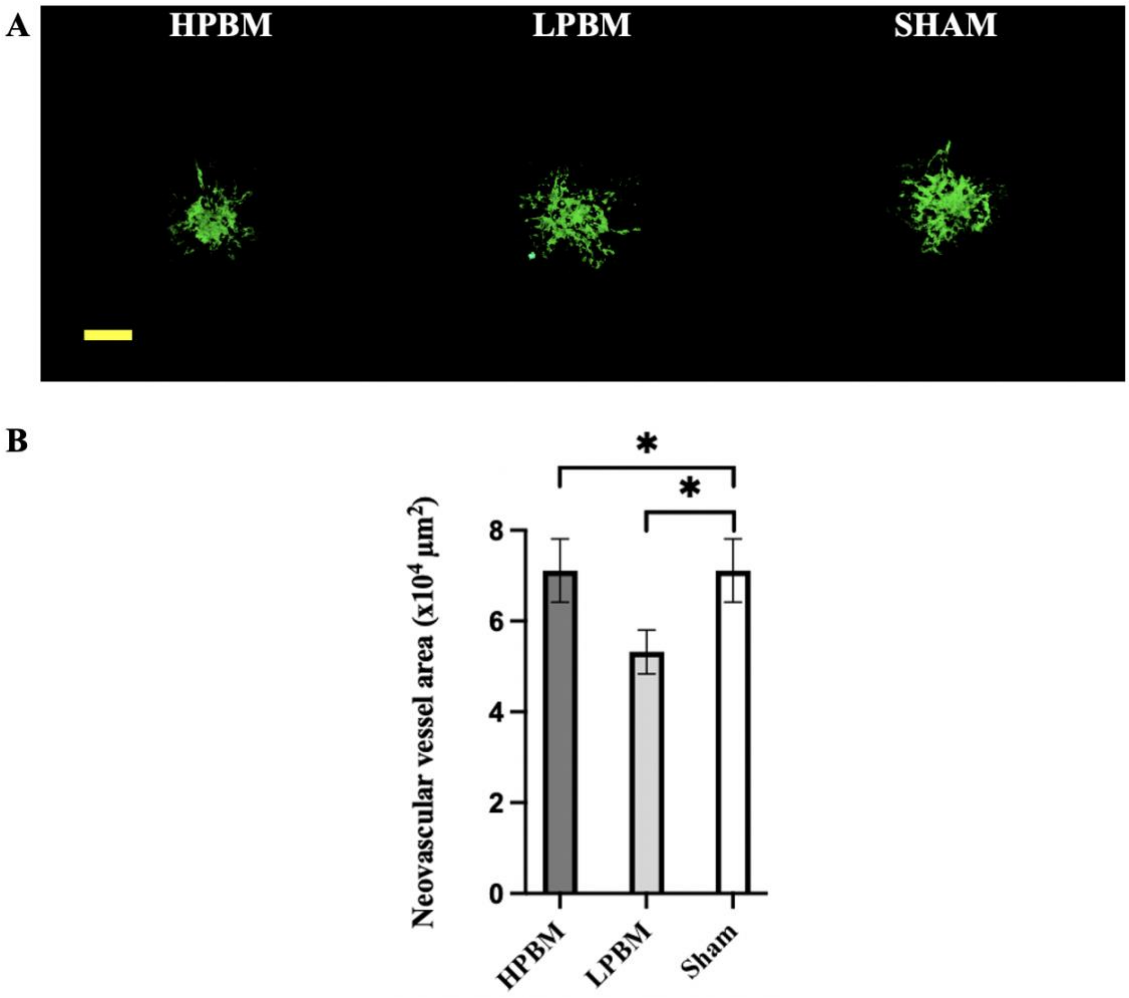

Figure 5.4: (A) Representative images of laser-induced CNV membranes marked by expression of IB4 in rat RPE WM at 14 days after induction with CW laser in eyes treated with HPBM laser, LPBM laser, or sham. Scale bar: 200 µm. (B) Bar graph depicting CNV membrane size as determined by colour-thresholding of images of IB4 immunofluorescence in RPE WM from eyes treated with HPBM laser (n = 9), LPBM laser (n = 9), or sham (n = 9). Data are presented as mean ± SEM. * Statistically significant difference ($p < 0.05$), by one-way ANOVA with a Tukey's HSD post-hoc test. CNV: choroidal neovascularization. WM: wholemount. IB4: isolectin-B4. RPE, retinal pigment epithelium. HPBM: high-dose photobiomodulation. LPBM: low-dose photobiomodulation.

Retinal cross-sections were immunolabelled with IB4 to highlight VECs in the CNV membranes. CNV membranes could be clearly defined as an ellipsoid mass projecting from the choroid into the subretinal space. IB4 immunoreactivity was also associated with retinal microglial and infiltrating macrophages that are observed in and overlying the CNV membrane. In control retinas, there was immunoreactivity to IB4 in vascular structures and to scattered retinal microglia as is considered typical for these retinal glia (Figure 5.5A). A one-way ANOVA was performed to compare the effect of PBM on CNV membrane size determined from area calculations taken from retinal cross-sections. This revealed that there was a statistically significant difference in CNV membrane cross-sectional size between at least two treatment groups ($F = 5.43$, $p = 0.025$). Tukey's HSD Test for multiple comparisons found that the mean value of CNV membrane area was significantly different between HPBM ($p = 0.042$, 95% C.I. [5.14×10^4, 8.86×10^4]) and LPBM ($p = 0.048$, 95% C.I. [6.02×10^4, 8.18×10^4]) treated eyes as compared to sham eyes. No statistically significant difference ($p = 0.89$) in CNV membrane size was found between LPBM and HPBM treated eyes (Figure 5.5B).

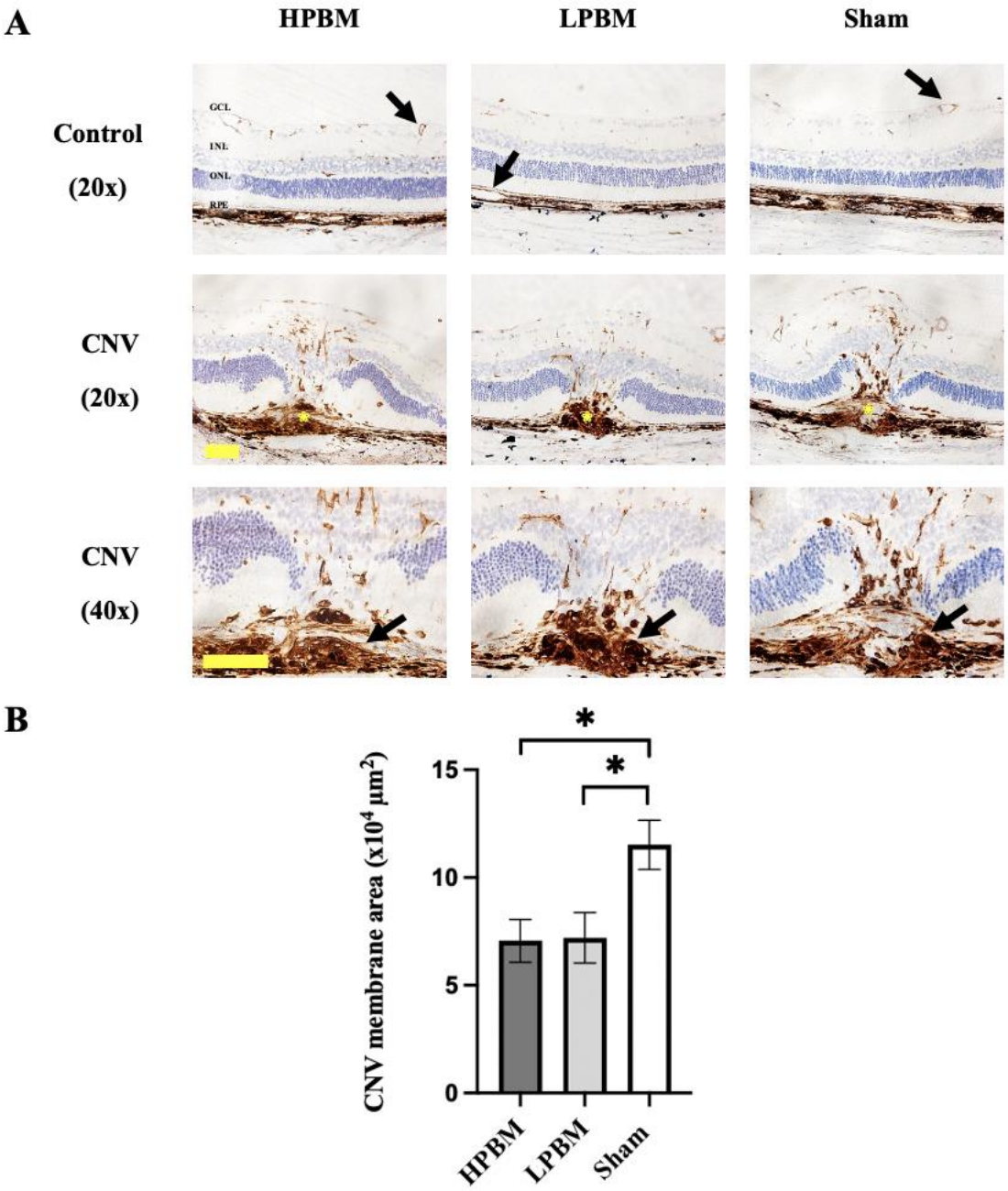

Figure 5.5: (A) Representative images of IB4 immunolabelling in cross-sections 3 days after CNV induction. In control retinas, IB4 localizes to blood vessel walls (arrow). CNV membranes are clearly defines as an ellipsoid mass projecting from the choroid into the subretinal space. CNV membranes are marked by yellow asterisks. IB4 immunoreactivity is associated with a dense nest of vascular endothelial cells (arrow). Scale bar: 100 µm. (B) Bar graph depicting CNV

membrane area in eyes treated with HPBM laser (n = 4), LPBM laser (n = 4), or sham (n = 5), as determined from inputting height and width measurements taken from retinal cross-sections immunostained with IB4 into an ellipsoid area formula. Data are presented as mean ± SEM. * Statistically significant difference ($p < 0.05$), by one-way ANOVA with a Tukey's HSD post-hoc test. IB4: Isolectin-B4. CNV: choroidal neovascularization. HPBM: high-dose photobiomodulation. LPBM: low-dose photobiomodulation.

SD-OCT was further utilised to visualise and quantify CNV membrane volume 14 days after induction (Figure 5.6A). A one-way ANOVA was performed to compare the effect of PBM treatment on CNV membrane volume utilising measurement of membrane height, and two measurements of width in perpendicular planes from SD-OCT B scans. This revealed that there was a statistically significant difference between treatment groups ($F = 7.26$, $p = 0.003$). Tukey's HSD Test for multiple comparisons found that there was no statistically significant difference between PBM treatment groups ($p= 0.89$). It was noted that the mean size of CNV membranes in eyes treated with PBM laser were smaller than membranes in sham-treated eyes. This reached statistical significance for both HPBM ($p = 0.01$, 95% C.I. [$3.35x10^6$, $4.65x10^6$]), and LPBM ($p = 0.006$, 95% C.I. [$3.37x10^6$, $4.41x10^6$]) treatment groups (Figure 5.6B).

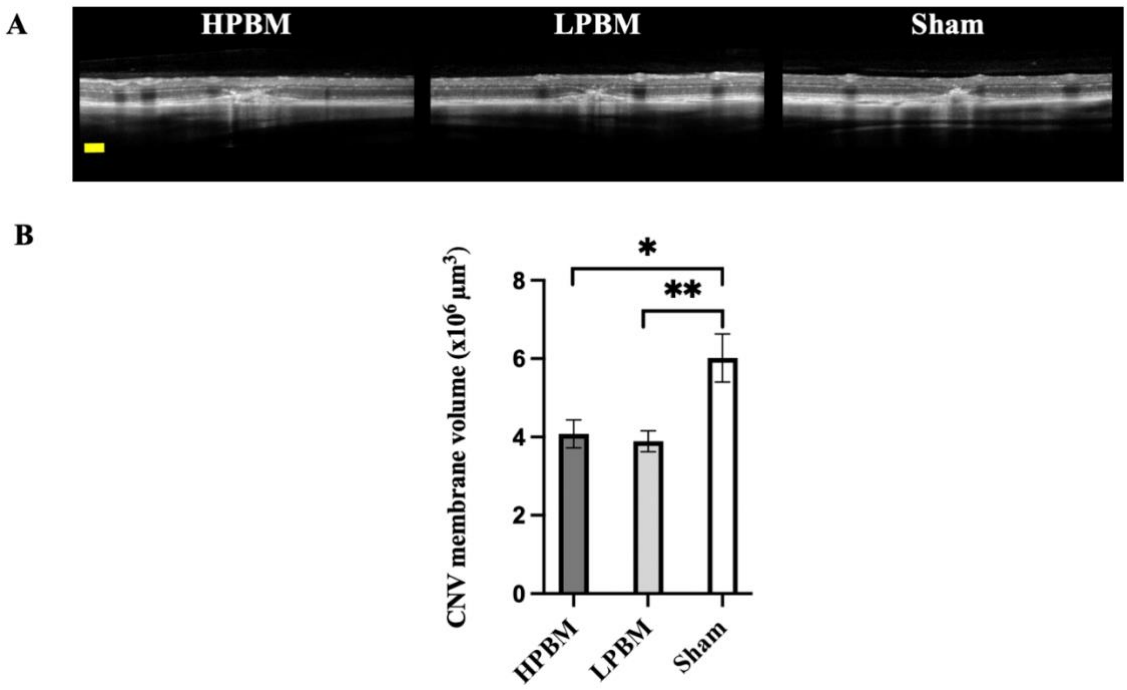

Figure 5.6: (A) SD-OCT B-scan of CNV membranes at 14 days after induction with CW laser in eyes treated with LPBM laser, HPBM laser, or sham. CNV lesions are characterised by ellipsoid mass in the subretinal space. Scale bar: 200 µm. (B) Bar graph depicting CNV membrane volume measured from SD-OCT B-scans captured in retinas treated with HPBM laser (n = 9), LPBM laser (n = 9), or sham (n = 9). Data are presented as mean ± SEM. * Statistically significant difference ($p < 0.05$), ** Statistically significant difference ($p < 0.01$), by one-way ANOVA with a Tukey's HSD post-hoc test. SD-OCT: spectral-domain optical coherence tomograph. CNV: choroidal neovascularization. CW: continuous wave. HPBM: high-dose photobiomodulation. LPBM: low-dose photobiomodulation.

Photobiomodulation laser influences choroidal neovascular membrane permeability

Time-lapse FFA was utilized to identify leaky choroidal neovascular membranes induced by Bruch's membrane rupture with laser photocoagulation. Lesions were analyzed on a grade scale based on the spatial and temporal evolution of fluorescein leakage following a documented standard (see Chapter 2, Materials and Methodology).

It was noted from this semi-quantitative analysis that CNV membranes displayed persistent pathological leakiness at completion of the 14-day treatment period in 36.4% of HPBM-treated eyes, 26.5% of LPBM-treated eyes, and 50% of sham-treated eyes (Figure 5.7A). A Chi-Square test of independence was applied to compare the effect of PBM on vascular permeability at the completion of the treatment period and found a statistically significant difference between at leave two groups even after a Bonferroni Correction was applied ($p = 0.013$). Post-hoc Fisher's Exact Test revealed that there was a statistically significant difference in vascular permeability between the LPBM ($p = 0.006$) and HPBM ($p = 0.013$) treatment groups when compared to the sham treatment group. There was no statistically significant difference ($p = 0.78$) between PBM treatment groups (Figure 5.7B).

Evaluations were made from time-lapse photographs of FFA at 7 and 14 days following CNV induction. CNV membranes in eyes treated with HPBM laser or LPBM laser did not worsen at 14 days compared to 7 days, whilst 35.3% of CNV membranes in sham eyes had worsening of pathological leakage at 14 days when compared to 7 days. A Chi-Square Test of Independence was applied to compare the effect of PBM on the natural

history of CNV membrane vascular permeability. This revealed that there was a statistically significant difference between at least two groups even after a Bonferroni Correction was applied (p = 0.0003). Post-hoc Fisher's Exact Correlational Test revealed a statistically significant improvement in vascular permeability of CNV membranes between HPBM (p = 0.00001) and LPBM (p = 0.02) treatment groups when compared to the sham group. There was no statistically significant difference (p = 0.14) between PBM treatment groups (Figure 5.8).

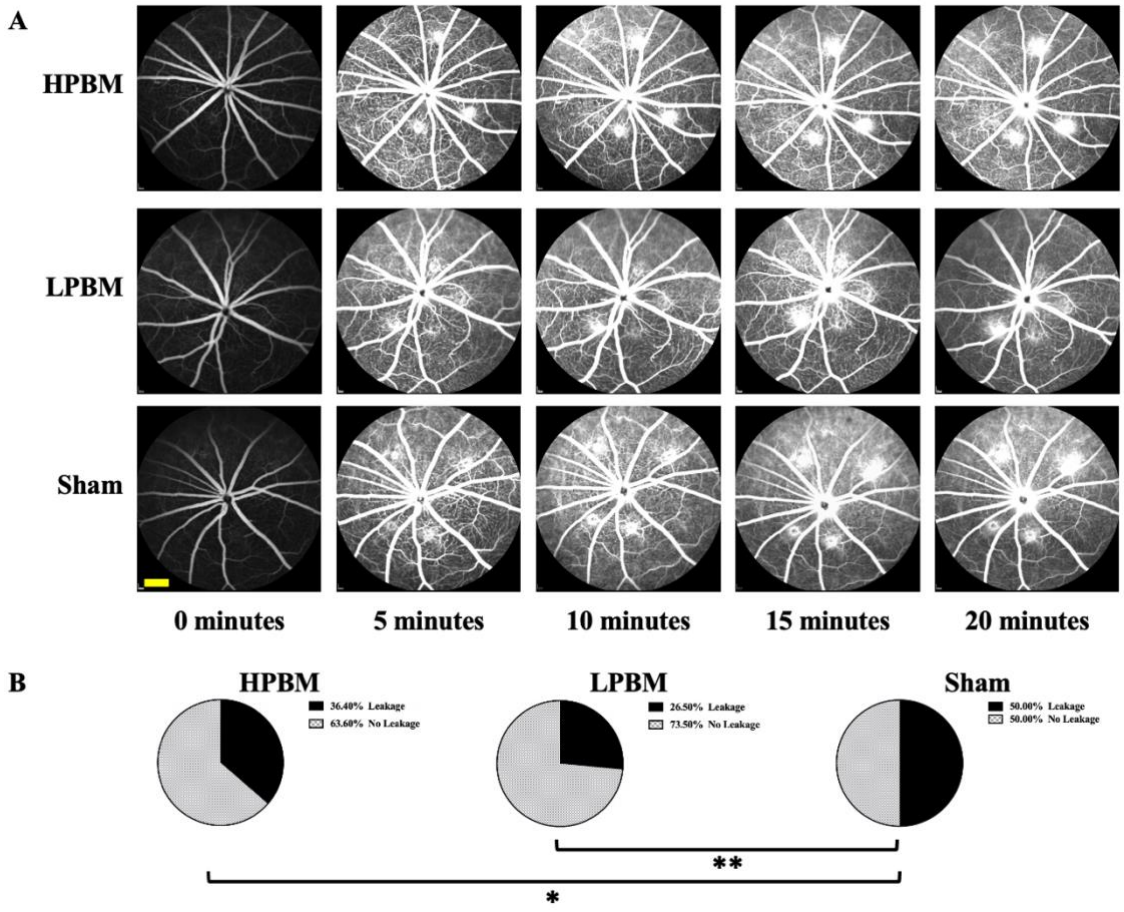

Figure 5.7: (A) Time-lapse FFA at completion of treatment with HPBM laser, LPBM laser, or sham 14 days after induction of CNV. Scale bar: 1000 μm. (B) Pie graph depicting proportion of CNV membranes with persistent vascular leakage

based on FFA grading at 14 days following laser induction in eyes treated with HPBM laser (n = 33), LPBM laser (n = 34), or sham (n = 34). * Statistically significant difference (p < 0.05), by Chi-Square Test of Independence with Bonferroni correction, and post-hoc Fisher's Exact Correlational Test for multiple comparisons. ** Statistically significant difference (p < 0.01), by Chi-Square Test of Independence with Bonferroni correction, and post-hoc Fisher's Exact Correlational Test for multiple comparisons. FFA: fundus fluorescein angiography. CNV: choroidal neovascularization. HPBM: high-dose photobiomodulation. LPBM: low-dose photobiomodulation.

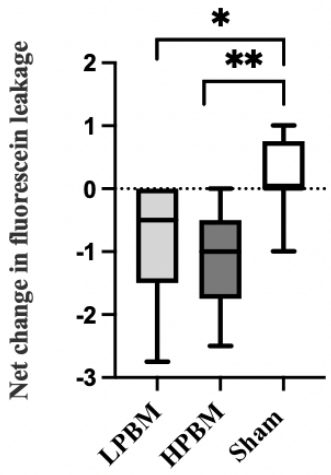

Figure 5.8: Box plot depicting average net change in CNV membrane activity based on FFA grading at 7 to 14 days following laser induction in eyes treated with HPBM laser (n = 33), LPBM laser (n = 34), or sham (n = 34). A value of 0 represent no net change. A positive value represents worsening fluorescein leakage. A negative value represents reduced fluorescein leakage. * Statistically significant difference (p < 0.05), by Chi-Square Test of Independence with Bonferroni correction, and post-hoc Fisher's Exact Correlational Test for multiple comparisons. ** Statistically

significant difference ($p < 0.01$), by Chi-Square Test of Independence with Bonferroni correction, and post-hoc Fisher's Exact Correlational Test for multiple comparisons. FFA: fundus fluorescein angiography. CNV: choroidal neovascularization. HPBM: high-dose photobiomodulation. LPBM: low-dose photobiomodulation.

Photobiomodulation laser influences repair of the outer blood retinal barrier

RPE-65 is a phototransduction molecule that is constitutively expressed in adult RPE cells. Cross-sections were immunolabelled with RPE-65 to ascertain RPE cell integrity at the site of CNV lesions. Disruption of the oBRB and invasion of the subretinal space by CNV tissue was observed. RPE cells were seen traversing the CNV membrane in all treatment groups; however, in both HPBM- and LPBM-treated eyes, RPE cell migration and closure of the defect was more advanced than in the sham group. A cross-section of a control retina serves to demonstrate the appearance of an intact outer blood-retinal barrier, of which the RPE constitutes the inner layer (Figure 5.9).

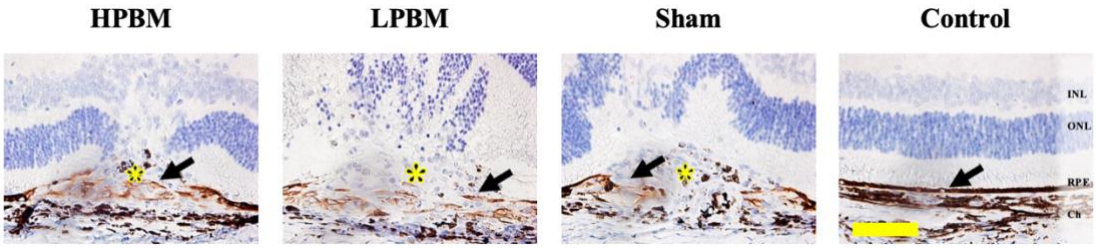

Figure 5.9: Representative images of RPE-65 immunolabelling in retinal cross-sections at 3 days after CNV induction. Disruption of the outer blood-retinal barrier is seen at the site of CNV membrane in all eyes. CNV membranes are marked by

yellow asterisks. RPE cells (arrows) are seen traversing the defect in HPBM laser, LPBM laser, and sham-treated retinas. Representative image of a control eye demonstrates normal histomorphology of an intact blood-retinal barrier. Scale bar: 100 µm. RPE-65: Retinal pigment epithelium-specific 65 kDa protein. CNV: choroidal neovascularization. HPBM: high-dose photobiomodulation. LPBM: low-dose photobiomodulation. INL: inner nuclear layer. ONL: outer nuclear layer. RPE: retinal pigment epithelium. Ch: choroid.

5.5 Discussion

There is published evidence that PBM may have beneficial effects that are of clinical relevance in retinal neovascular diseases. A case series conducted by Ivandic *et al* demonstrated clinical improvement in oedema and bleeding in PBM-treated subjects with nAMD [372]. Similarly, Tang *et al* conducted a case series in subjects with DME and demonstrated that PBM reduced central retinal thickness in treated eyes [365]. The NIRD clinical trial further added weight to this case series. This study demonstrated that treatment with PBM laser in subjects with DME resulted in a reduction in central macular thickness and improvement in BCVA without any related adverse events [375]. It is recognised that chronic hypoxia and inflammation, with recruitment of retinal and vascular inflammatory cells, are important pathogenic mechanisms for the propagation of CNV in nAMD [225, 230, 451-453]. This process occurs potentially via vascular endothelial proliferation, migration, and impaired barrier function by direct and indirect influences on VEGF and VEGF-adjacent proangiogenic pathways through cytokine and chemokine signaling from the RPE and retinal glia [48, 56, 102, 197, 241-243, 454-465]. It has been hypothesised

that PBM modulates these pathogenic pathways by rectifying mitochondrial respiratory chain dysfunction, polarising retinal glia to their dormant phenotypes, modulating immune cell recruitment and influencing multiple pro-inflammatory pathways by down-regulating expression of proinflammatory and pro-angiogenic cytokines such as NO, ICAM-1, CCL2, IFN- γ, IL-6, IL-1 β, TNF-α, and C3 [228, 354, 355, 363, 366, 383-386, 466-468]. In this study, CNV membranes were analysed in two main domains: size and permeability. The CNV membrane areas and volumes were in-line with previous reported values in the laser-induced CNV model [406, 407]. Of importance, PBM treatment partially restrained the extent and pathology of neovascularisation. PBM treatment was consistently associated with smaller and less permeable CNV membranes. It seems that in the laser-induced model of CNV, maximal cellular inflammation and cytokine release occurs early in the course. [193]. Previous studies with immunohistochemistry on paraffin cross-sections at various time points after induction have demonstrated that in the laser-induced CNV model early choroidal vessels are present at 3 days following induction, but it isn't until 7 days that RPE cell recruitment to the site of exudative retinal detachment is noted, and it takes a further 7-14 days before the RPE has enclosed the CNV membrane [469]. This period coincides with peak leukocyte infiltration and tissue inflammation. It could be speculated that early RPE cell recruitment and closure of the defect in the oBRB could curb leukocyte infiltration and tissue inflammation, contributing to the smaller and less permeable CNV membranes that were observed in PBM treated eyes [187, 404]. Of note, PBM treatment has been shown to be associated with upregulation of neurotrophins and improved RPE cell phagocytic function under conditions of retinal stress and hypoxia [367, 378, 379, 424]. Although the evidence supporting the clinical benefit for PBM is still limited,

this preliminary evidence presented here supports further enquiry into the application of PBM treatment to clinical nAMD.

Chapter 6:

Ascertaining how photobiomodulation laser influences neovascular membrane size and permeability in the choroidal neovascularization model

6.1 Introduction

Kadiu and colleagues very accurately referred to immunological cells as the Dr Jekyll and Mr Hyde of the central nervous system when considering chronic degenerative disease [446]. Chronic inflammation is a key pathogenic mechanism in nAMD. Retinal ischaemia and mitochondrial respiratory chain dysfunction may be a driving force for this inflammation in nAMD [192, 233, 470]. This mechanism is a leading theory behind the pathogenesis of nAMD [150, 183, 190]. Astrocytes and Müller cells, the two neuron-supporting macroglia of the retina, and microglia, the resident macrophages of the retina, constitute the key glial cell population of the retina [34, 182]. The retinal glial population are active participants in retinal vascular disorders [471, 472].

Histopathological evidence reveals that microglia migrate to, differentiate, and proliferate at the site of inflammation [54, 149, 473, 474]. Microglia and perivascular macrophages are found in abundance in CNV membranes of subjects with nAMD [87, 88, 451, 452, 454, 455]. The activation profile is consistent with a cytotoxic 'M1' phenotype profile for microglia and macrophages [167, 466]. In this cytotoxic state, these cells liberate cytokines and chemokines, most notably TNF-α, IFN-γ, IL-1, and IL-6, thus creating an inflammatory milieu [150, 183, 190]. These factors propagate neuroinflammatory signals within the retina and signal peripheral immune cells recruitment. This inflammatory milieu is believed to be a key component of the early evolving neurodegeneration that occurs in nAMD, as they are potent chemokines for vascular leukocytes and inducers of VEGF in the retina and are implicated in the BRB disruption and macular oedema observed in nAMD [9, 194, 475-477].

This glial–neuronal cell interaction in the retina is important for photoreceptor survival as the retinal glial system possesses valuable trophic effects [161, 168-181]. Under conditions of hypoxic and inflammation, RPE cells and retinal macroglia upregulate expression of neurotrophins to protect against apoptosis. These retinal cells are known to release factors like CNTF, bFGF, NGF, PDGF, EGF, BDNF, and TGF-ß. However, to add insult to injury, microglial neurotrophic factor expression can be downregulated when in a cytotoxic state [160, 447]. These factors are known to regulate neuronal growth, modulate gliotic reactivity, and be protective against cell death induced by hypoxia, oxidative stress, tissue inflammation, apoptosis, and glutamate excitotoxicity in fundamental retinal cell populations, namely, photoreceptors, ganglion cells and RPE cells [52, 154-164]. Many of the pathways that are involved in cellular survival also influence angiogenic pathways in the retina, as these pathways play a core role in tissue repair. These aforementioned survival factors are also known pro-angiogenic factors, degrading endothelial cell tight junctions, and promoting VEC proliferation and vascular tissue infiltration [48-50]. The RPE cells, and retina macroglia are the key subset of retinal cells that liberate VEGF under conditions of hypoxia, contributing to neovascularisation, and thus these cell populations are considered important in the pathogenesis of nAMD [102, 241-243, 459, 460, 478].

PBM treatment is consistently associated with improved photoreceptor survival in animal studies and improved best corrected visual acuity in patients with amblyopia, DME, and both dAMD and nAMD [362, 364, 365, 368, 371, 372, 382, 387, 388]. Modulation of the glial response is one of the foci of therapeutics; to reap the rewards whilst mitigating the cytotoxic and reactive gliotic component of the immune and inflammatory system to improve therapeutic outcomes in degenerative diseases such as nAMD.

6.2 Study aim

The aim of this study was to determine if treatment with two PBM-laser settings influenced inflammatory and/or angiogenic pathways in the eye.

6.3 Study Design

For ELISA and cross-section analysis, animals received treatment to both eyes with either LPBM (n = 8), HPBM (n = 8), or sham (n = 8) at 6 days, 3 days, and immediately prior to induction of CNV by CW laser. Animals were randomized during group allocation for the experiment. It is thus suggested that the point of peak retinal inflammation and cellular tissue remodeling in the laser-induced CNV model is at day 3 post-induction [187, 404]. For this reason, to allow characterization of the cellular inflammatory and angiogenesis response to PBM treatment in this critical period, animals were humanely killed at 3 days following laser CNV induction (Figure 6.1). Eyes were immediately enucleated. All right eyes were dissected, and relevant tissues harvested for ELISA. All analysis of ELISA data was performed on pooled averages of laser spots in each eye; each eye was treated as n = 1. Quantitative VEGF protein data are reported as means. Means were compared between experimental groups using One-way ANOVA with a post-hoc Tukey's HSD Test performed for multiple comparisons. Statistical significance was determined at the 0.05 level. All left eyes were prepared for immunoperoxidase staining of retinal tissue cross-sections. Control animals were also used for comparative analysis. All analysis of cross-section data was performed on sections taken through the center of the CNV membrane; each eye was treated as n = 1. The primary investigator was not blinded to the

group allocation during the outcome analyses. Results were confirmed by a second investigator blinded to group allocation during the outcome analyses. Quantitative immunostaining data are reported as means. Means were compared between experimental groups using One-way ANOVA with post-hoc Tukey's HSD Test performed for multiple comparisons. Statistical significance was determined at the 0.05 level.

For FFA, SD-OCT and WM analysis animals received treatment to both eyes with either LPBM (n = 9), HPBM (n = 9), or sham (n = 9) every 3 days from 6 days prior to CNV laser induction, until 12 days after laser CNV induction. CNV was only induced in the left eye of each animal, whilst the right eye acted as a treatment control analysis. Animals were randomized during group allocation for the experiment. FFA and SD-OCT analysis was conducted at 7 days and 14 days following CNV induction. Animals were humanely killed at 15 days after CNV induction, and eyes enucleated and processed for WM tissue analysis 24 hours after the final FFA and SD-OCT analysis (Figure 6.2). All analysis of FFA, SD-OCT, and WM data was performed on pooled averages of laser spots in each eye; each eye was treated as n = 1. The primary investigator was not blinded to the group allocation during the outcome analyses. Results were confirmed by a second investigator blinded to group allocation during the outcome analyses. Quantitative data are reported as means. Means were compared between experimental groups using One-way ANOVA with post-hoc Tukey's HSD Test performed for multiple comparisons. Statistical significance was determined at the 0.05 level.

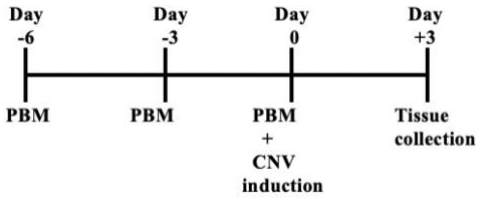

Figure 6.1: Pictorial timeline of PBM experimental treatment regimen and timeline of tissue collection for ELISA and retinal tissue cross-section.

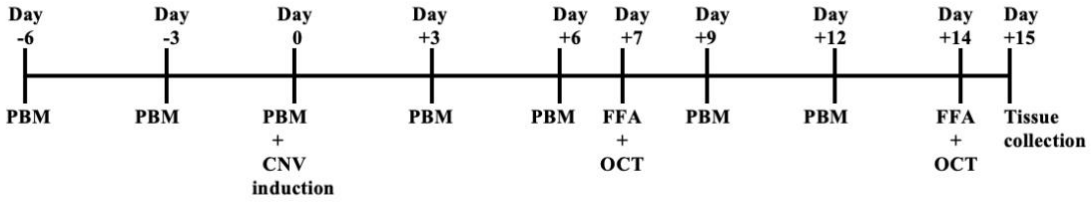

Figure 6.2: Pictorial timeline of PBM experimental treatment regimen treatment and CNV membrane analyses following laser induction.

6.4 Results:

Photobiomodulation laser treatment modulates retinal and retinal pigment epithelium mitochondrial respiratory chain activity

RPE and retinal explants from healthy rat eyes were treated with HPBM. There was an observable increase in mitochondrial respiratory chain activity within the treatment zone versus outside of the treatment zone, indicated by increased mitochondrial superoxide production as a by-product of increased mitochondrial oxygen metabolism (Figure 6.3).

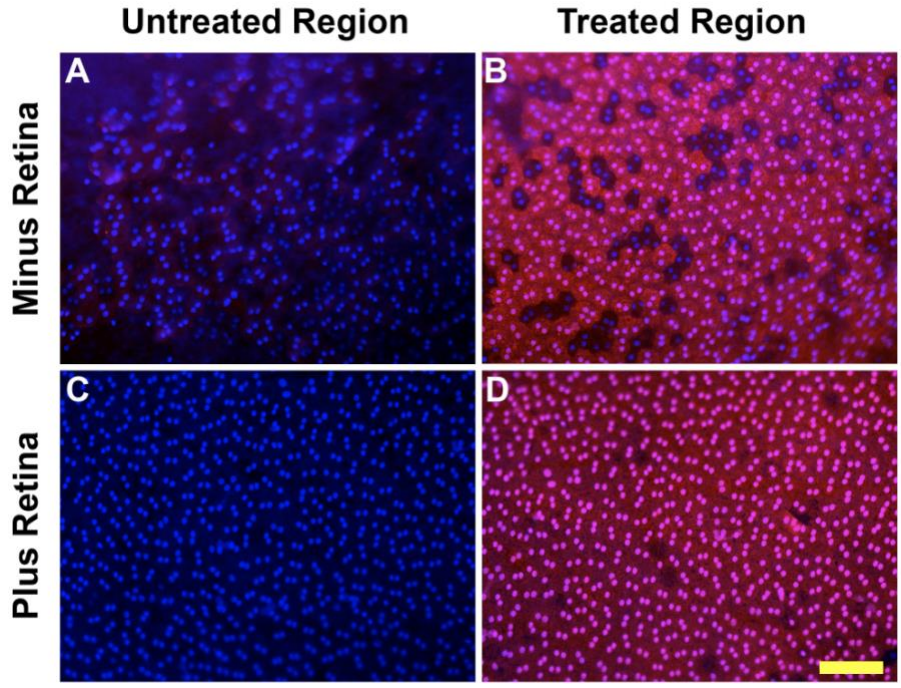

Figure 6.3. Representative images of mitochondrial superoxide concentration in control versus HPBM-treated rat RPE explants, without (A, B), and with (C, D) retina attached. Blue fluorescence denotes cell nuclei. Red fluorescence denotes increased cellular mitochondrial oxygen metabolism. Scale bar: 200 µm. RPE, retinal pigment epithelium; PBM, photobiomodulation.

Effect of photobiomodulation laser treatment on vascular endothelial growth factor levels

Sandwich ELISAs for all splice variants of VEGF were performed on retinal and RPE-choroid tissue harvested from eyes 3 days after laser induction of CNV. There was no statistically significant difference in VEGF levels between treatment groups in either the retinal ($F = 3.26$, $p = 0.069$; Figure 6.4B) or RPE-choroid tissue ($F = 0.13$, $p = 0.88$; Figure 6.4C). The results of the retinal VEGF quantification need to be considered with

the caveat that it was not possible to separate retinal from vitreous tissues with absolute certainty. This has an implication for analysis as control rat vitreous samples possessed a mean VEGF levels of 217.18 pg/mg. In an analogous fashion, separation of retina from RPE-choroid tissue was technically difficult; however, if retinal and RPE-choroid values were considered within a combined analysis, this did not result in a statistically significant difference in means between treatment groups (data not shown). It should also be noted that VEGF levels in some retinal samples were close to the lower end of detection sensitivity for the ELISA kit, which has a threshold of detection of 2 pg/mL.

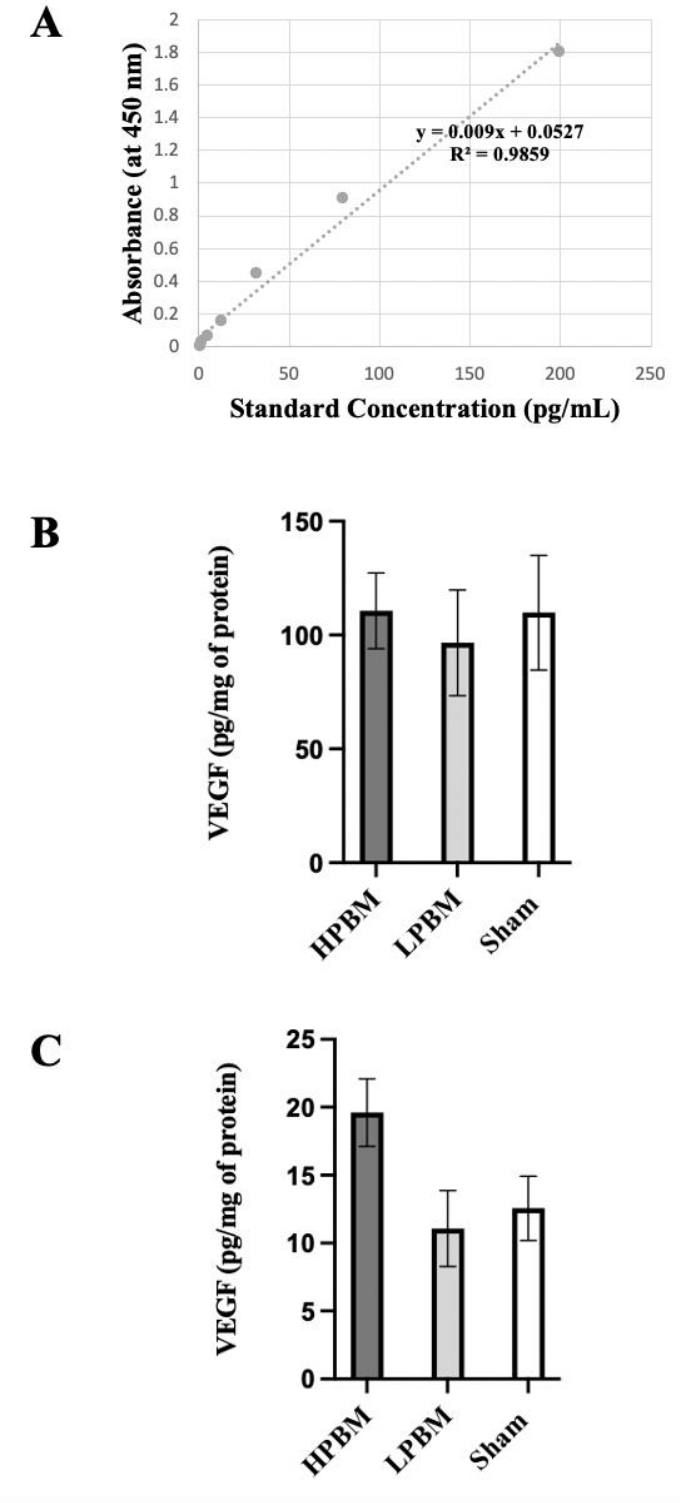

Figure 6.4: VEGF levels in that rat retina and RPE-choroid complex at 3 days after CNV induction, as determined by sandwich ELISA. (A) VEGF standard concentration curve. (B) VEGF concentration expressed as pg/mg of protein in

RPE-choroid tissue harvested from HPBM laser (n = 8), LPBM laser (n = 8), and sham treated eyes (n = 8). There was no statistically significant difference (p > 0.05) in VEGF levels, by one-way ANOVA. (C) VEGF concentration expressed as pg/mg of protein in retinal tissue harvested from HPBM laser (n = 7), LPBM laser (n = 5), and sham treated eyes (n = 6). There was no statistically significant difference (p > 0.05) in VEGF levels, by one-way ANOVA. VEGF: vascular endothelial growth factor. CNV: choroidal neovascularisation. ELISA: enzyme-linked immunosorbent assay. RPE: retinal pigment epithelium. LPBM: low-dose photobiomodulation. HPBM: high-dose photobiomodulation.

Effect of photobiomodulation laser treatment on cell proliferation

In cross-sections of control retinas, PCNA weakly localises to a scattered number of cell nuclei in the inner nuclear layer, presumably Müller cells. In cross-sections of CNV retinas, PCNA was associated with Müller cell soma that had adopted the characteristic gliotic morphology and migrated to the CNV lesion site. Qualitative assessment of tissue sections revealed there to be fewer $PCNA^{+}$ Müller cells observed overlying CNV membrane in the PBM treatment groups, particularly the LPBM group, as compared to the sham group. PCNA also localized to proliferating endothelial cells within the CNV membranes in both groups (Figure 6.5).

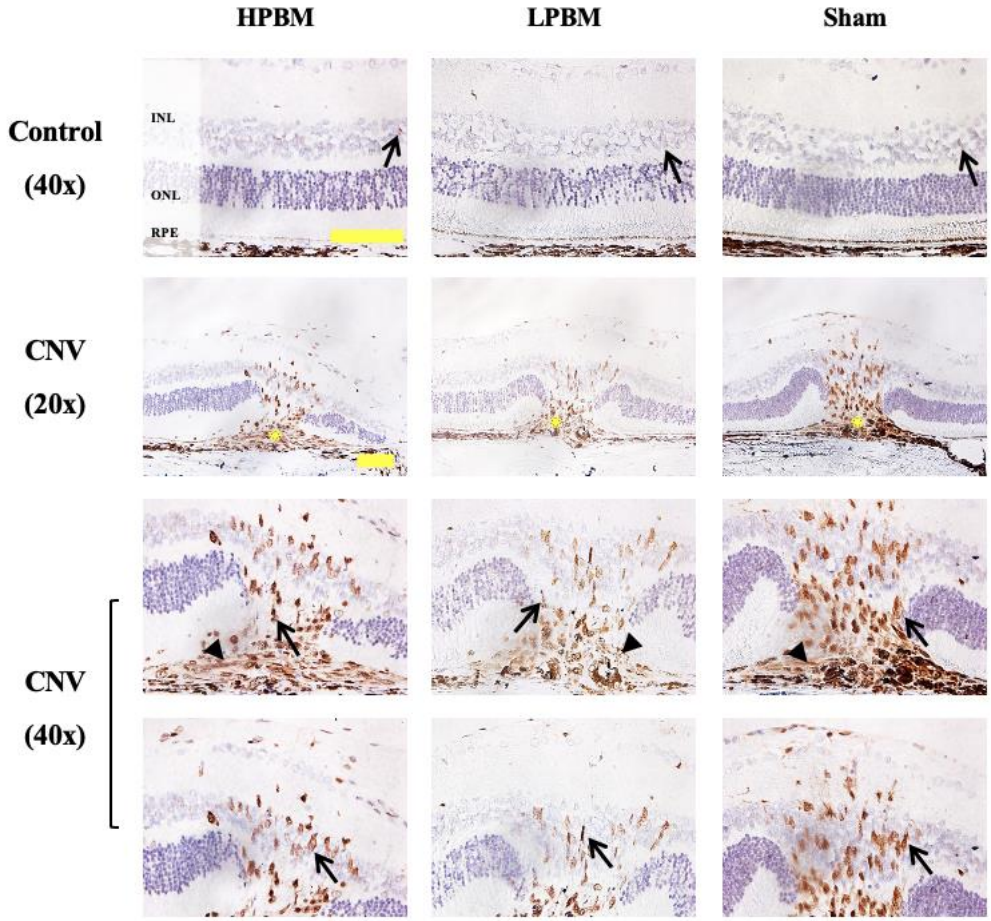

Figure 6.5: Representative images of PCNA immunolabelling in retinal cross-sections of control eyes, and eyes 3 days after CNV induction. A few weakly labelled PCNA cells (arrows) are seen in control eyes. $PCNA^{+}$ cells are observed in (arrowheads) and around (arrows) the CNV membrane in HPBM laser, LPBM laser and sham-treated retinas. CNV membranes are marked by yellow asterisks. Scale bar: 100 µm. PCNA: proliferation cell nuclear antigen CNV: choroidal neovascularization. INL: inner nuclear layer. ONL: outer nuclear layer. RPE: retinal pigment epithelium. HPBM: high-dose photobiomodulation. LPBM: low-dose photobiomodulation.

Effect of photobiomodulation laser treatment on haemoxygenase-1 expression

Retinal cross sections were immunostained for HO-1. As expected, HO-1 was not expressed in control eyes. Within CNV eyes, HO-1^{+} glial cells and putative RPE cells were observed within the retina and subretinal space. These cells appear to have migrated to the site of CNV membranes around the laser induction zone. Qualitative assessment of tissue sections revealed there to be more robust HO-1 expression in PBM-treated retinas than sham retinas (Figure 6.6).

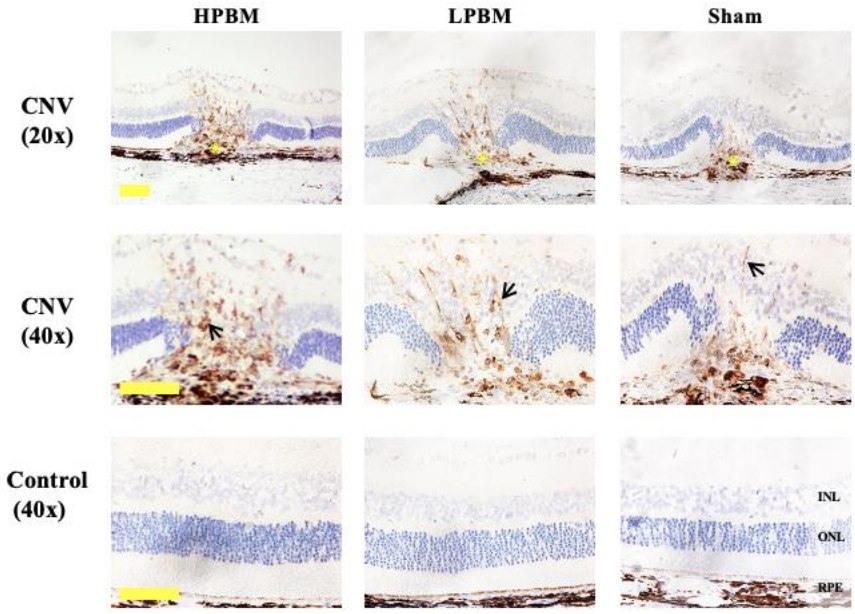

Figure 6.6: Representative images of HO-1 immunolabelling in retinal cross-sections of control eyes, and eyes 3 days after CNV induction. In CNV eyes, HO-1 expression is seen in reactive retinal glia (open arrow) within and surrounding the CNV membrane in all three treatment groups. CNV membranes are marked by yellow asterisks. No discernable HO-1 expression is seen in control eyes. Scale bar: 100 µm. HO-1: haemoxygenase-1. CNV: choroidal neovascularization. INL: inner nuclear

layer. ONL: outer nuclear layer. RPE: retinal pigment epithelium. HPBM: high-dose photobiomodulation. LPBM: low-dose photobiomodulation.

Effect of photobiomodulation laser treatment on expression of cell survival factors

In control retinas, weak CNTF expression was observed within astrocytes and Müller cell end-feet, soma and processes (Figure 6.7). In CNV eyes from all treatment groups, there was abundant expression of CNTF around CNV membranes in all treatment groups. CNTF expression was seen most prominently in the dense gliotic scar at the CNV membrane formed by Müller cells, but expression encompassed reactive astrocytes and migrating RPE cells. Reactive morphological changes in these cells are also seen. Upregulation of CNTF expression was essentially limited to CNV membranes and the overlying retina. CNTF expression was also observed in a radial pattern through the retinal layers, presumed to be Müller cell processes. Expression was also seen in the RPE cell layer. Qualitative assessment of tissue sections revealed similar abundance of CNTF in all three treatment groups (Figure 6.7).

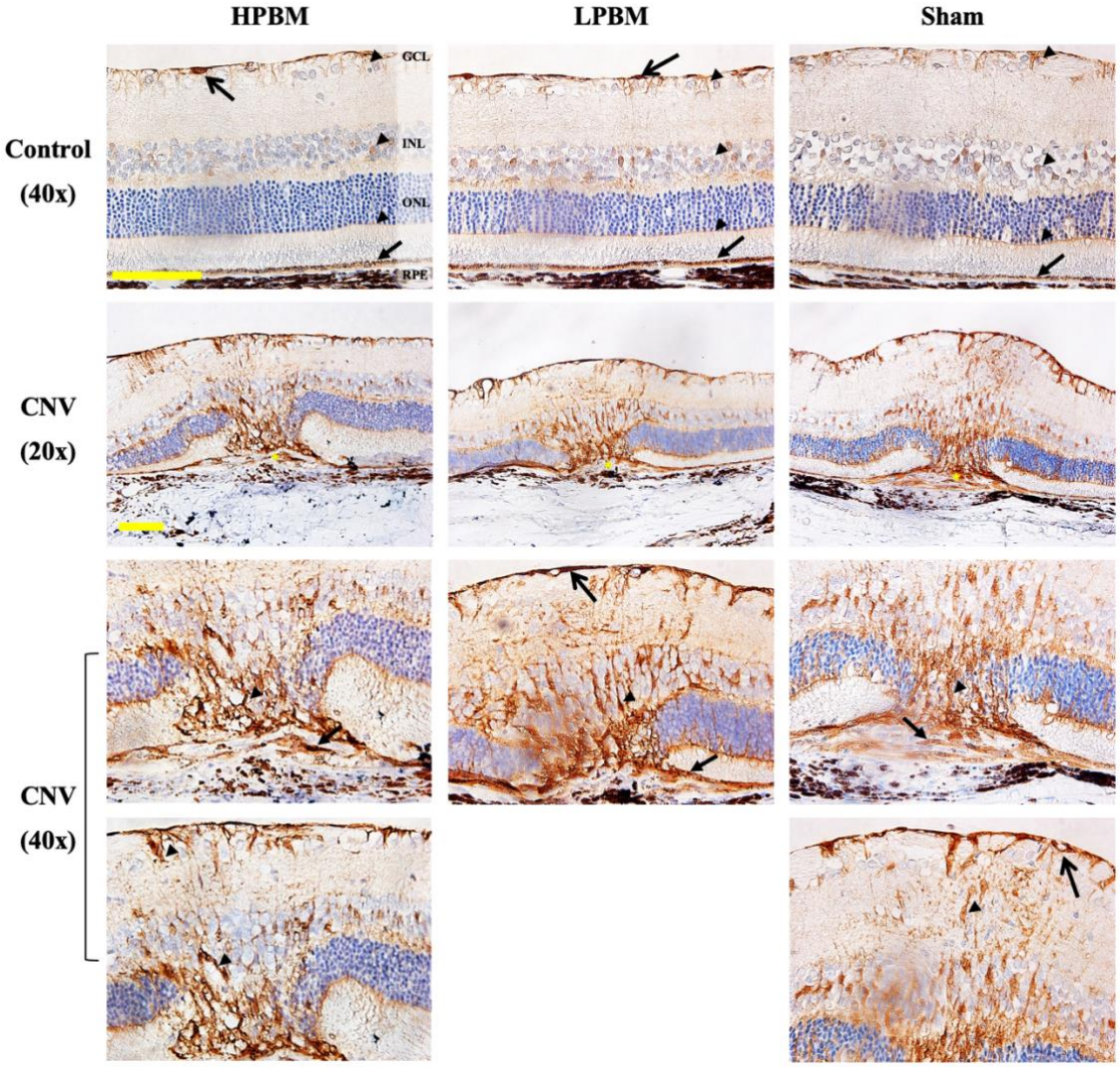

Figure 6.7: Representative images of CNTF immunolabelling in retinal cross-sections of control eyes, and 3 days after CNV induction. Weak labelling of astrocytes (open arrows), and Müller cells (arrowheads) is seen in control eyes. Upregulated expression of CNTF is evident in astrocytes, Müller cells, and RPE (filled arrow) overlying the CNV membrane in HPBM laser, LPBM laser and sham-treated CNV eyes. CNV membranes are marked by yellow asterisks. Scale bar: 100 µm. CNV: choroidal neovascularization. GCL: ganglion cell layer. INL: inner nuclear layer. ONL: outer nuclear layer. RPE: retinal pigment epithelium. HPBM: high-dose photobiomodulation. LPBM: low-dose photobiomodulation.

The expression of bFGF was upregulated in Müller soma around CNV membranes in retinas of all treatment groups. Qualitative assessment of tissue sections revealed that the density of expression of bFGF in the glial scar overlying CNV membranes formed by Müller cells in PBM retinas was not dramatically different between treatment groups. Outside of the induction zone, it was also noted that bFGF expression was globally upregulated in retinas of HPBM, LPBM, and sham-treated eyes when compared to control retinas. In control retinas bFGF expression was localized to ganglion cell nuclei, Müller soma, and RPE cells. This pattern of expression was seen in all retinas (Figure 6.8).

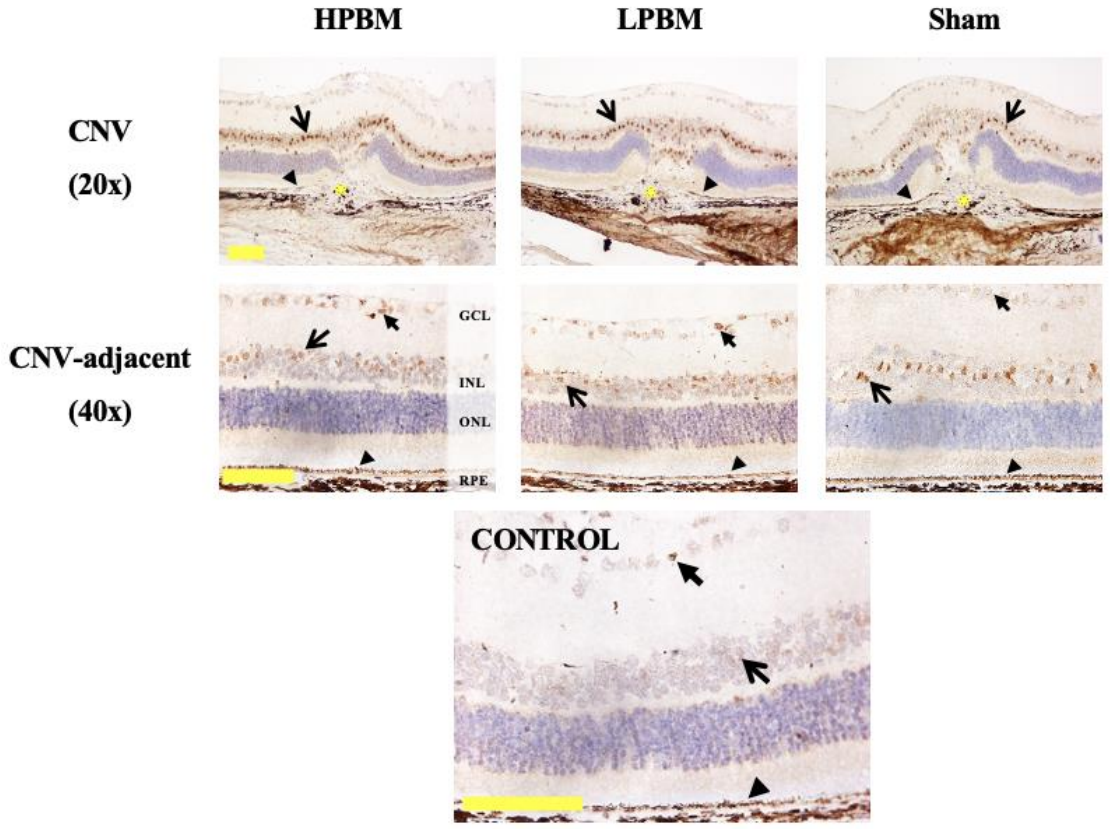

Figure 6.8: Representative images of bFGF immunolabelling of retinal cross-sections of control eyes, and eyes 3 days after induction of CNV in HPBM laser, LPBM laser, and sham-treated eyes. Upregulated expression of bFGF is evident in ganglion cells (filled arrow), Müller cells (open arrow) and RPE cells (arrowhead)

around CNV membranes in HPBM laser, LPBM laser and sham-treated CNV eyes. CNV membranes are marked by yellow asterisks. Scale bar: 100 µm. bFGF: basic fibroblast growth factor. CNV: choroidal neovascularization. GCL: ganglion cell layer. INL: inner nuclear layer. ONL: outer nuclear layer. RPE: retinal pigment epithelium. HPBM: high-dose photobiomodulation. LPBM: Low-dose photobiomodulation.

Effect of photobiomodulation laser on microglia/macrophages

In RPE WM from CNV eyes, there was a localised aggregation of IBA-1^+ cells at the site of CNV membranes in all treatment groups. These cells had the amoeboid morphology that characterises M1-polarised microglial cells. IBA-1^+ cells were scarcely seen outside of the CNV membrane area (Figure 6.9A). In control RPE WM, IBA-1^+ microglial cells were scarcely seen (data not shown). Colour-thresholding was utilised to measure the area of IBA-1 expression as a function of microglial cell recruitment. A one-way ANOVA was performed to compare the effect of PBM on microglial recruitment. There was statistically significant difference between at least two groups ($F = 10.7$, $p = 0.0005$). The median area of microglial recruitment in RPE WM was statistically similar between HPBM, and LPBM treated eyes on Tukey's HSD Test for multiple comparisons ($p = 0.2$; Figure 6.9B). The median area of microglial activation was smaller in both PBM treatment groups compared to the sham group. This reached statistical significance for both HPBM ($p = 0.02$, 95% C.I. [$3.87x10^4$, $5.19 x10^4$]), and LPBM ($p = 0.001$, 95% C.I. [$2.60x10^4$, $4.38x10^4$]) treatment regimens (Figure 6.9B).

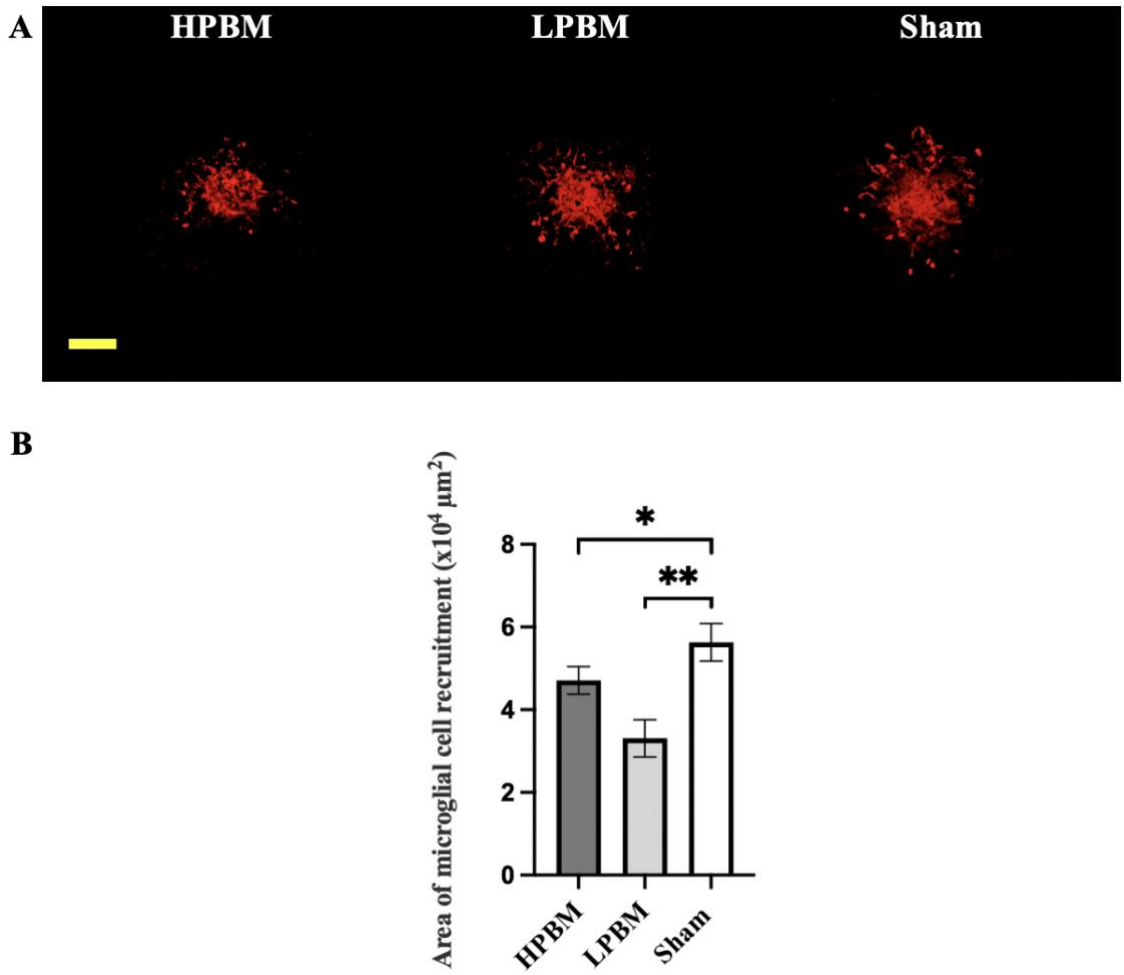

Figure 6.9: (A) Representative images of fluorescent IBA-1 immunolabelling in RPE WM at 14 days after CNV induction in eyes treated with HPBM laser, LPBM laser, or sham. Scale bar: 200 µm. (B) Bar graph depicting amount of reactive IBA-1^{+} cells infiltrating the CNV lesion, as determined by the colour-thresholding function in imageJ applied to images of RPE WM treated with HPBM laser (n = 9), LPBM laser (n = 9), or sham (n = 9). Data are presented as mean ± SEM. * Statistically significant difference ($p < 0.05$), by one-way ANOVA with a Tukey's HSD post-hoc test. ** Statistically significant difference ($p < 0.01$), by one-way ANOVA with a Tukey's HSD post-hoc test. IBA-1: ionized calcium-binding adapter molecule 1. RPE: retinal pigment epithelium. WM: wholemount. CNV: choroidal

neovascularization. HPBM: high-dose photobiomodulation. LPBM: low-dose photobiomodulation.

In retinal WM from sham and PBM control eyes, scattered IBA-1^+ microglial cells were seen. These cells however possessed the arborescent morphology that characterises resting state cells (see Chapter 4, Figure 4.7). In retinal WM from CNV eyes, there was localised aggregation of amoeboid-shaped IBA-1^+ cells at the lesion site consistent with the morphology of reactive microglia (Figure 6.10A). A one-way ANOVA was performed to compare the effect of PBM on microglial recruitment. Comparison between treatment groups revealed that there was a statistically significant difference between at least two groups ($F = 7.53$, $p = 0.004$). Tukey's HSD Test for multiple comparisons found no statistically significant difference in microglial cell abundance between the HPBM and LPBM treatment groups ($p = 0.9$). There was, however, a significant difference in IBA-1^+ cell abundance between the sham group and both HPBM ($p = 0.007$, 95% C.I. [$6.11x10^3$, $10.6x10^3$]), and LPBM ($p = 0.02$, 95% C.I. [$5.98x10^3$, $10.7x10^3$,]) treatment groups (Figure 6.10B).

The migration and congregation of microglia/macrophages to the CNV lesion that was observed in WM analyses was mirrored when retinal cross-section analysis was conducted. In control retinas of all treatment groups, IBA1 immunoreactivity comprised scattered ramified microglia, a pattern consistent with resting-state microglia (see Chapter 4, Figure 4.7). In CNV retinas, the pattern of microglial reactivity is highlighted, with engorged, amoeboid-shaped IBA-1+ cell evident in all treatment groups, and at all levels of the retina overlying the site of CNV membranes: a morphology consistent with reactive microglia. Within the CNV membrane, mononuclear pigmented cells were seen in all

treatment groups, consistent with infiltrating vascular-derived macrophage (Figure 6.11A). A one-way ANOVA was performed to compare the effect of PBM on microglial recruitment. Comparison between treatment groups revealed that there was a statistically significant difference in microglial cell abundance between at last two groups ($F = 10.3$, $p = 0.005$). Tukey's HSD Test for multiple comparisons found no statistically significant difference in microglial cell abundance between the PBM treatment groups ($p = 0.26$). However, there was a statistically significant difference in IBA-1^{+} cell abundance between both HPBM ($p = 0.049$, 95% C.I. [25.6, 31.4]), and LPBM ($p = 0.004$, 95% C.I. [24.2, 32.8]) treatment groups when compared to sham (Figure 6.11B).

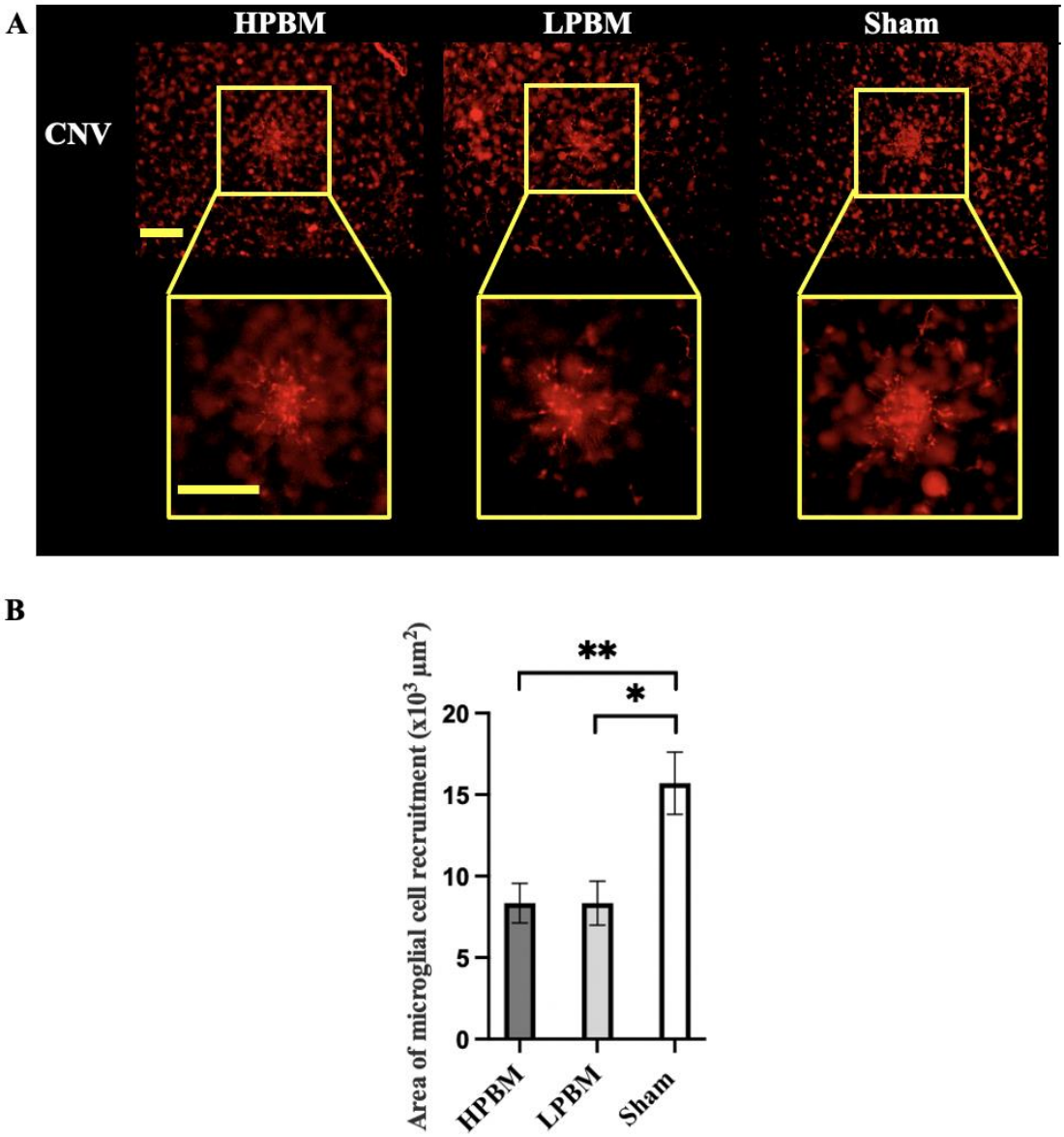

Figure 6.10: (A) Representative images of fluorescent IBA-1 immunolabelling in retinal WM at 14 days after CNV induction in eyes treated with HPBM laser, LPBM laser, or sham. At the site of CNV membranes there is marked increase in density of reactive IBA-1$^+$ cells. Scale bar: 200 µm. (B) Bar graph depicting amount of IBA-1$^+$ cells infiltrating the site of laser-CNV induction, as determined by the colour-thresholding function in imageJ applied to images of retinal WM treated with HPBM (n = 8), LPBM (n = 5), or sham (n = 9). Data are presented as mean ± SEM.

*** Statistically significant difference (p < 0.05), by one-way ANOVA with a Tukey's HSD post-hoc test. ** Statistically significant difference (p < 0.01), by one-way ANOVA with a Tukey's HSD post-hoc test. IBA-1: ionized calcium-binding adapter molecule 1. WM: wholemount. HPBM: high-dose photobiomodulation. LPBM: low-dose photobiomodulation. CNV: choroidal neovascularization.**

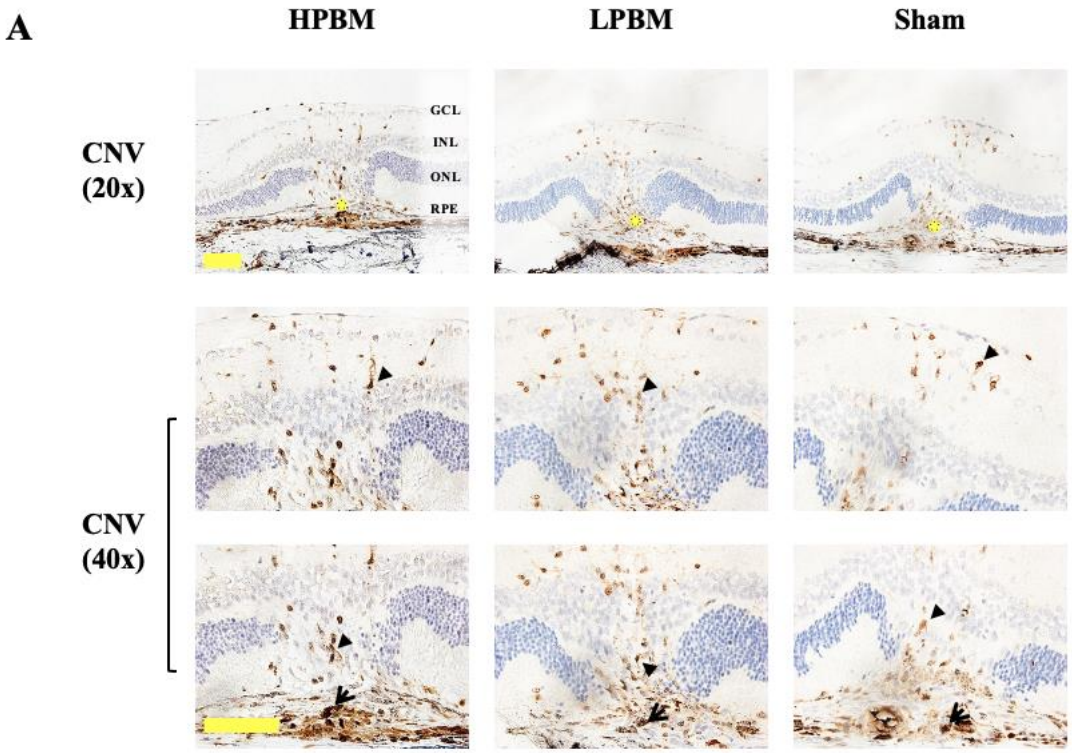

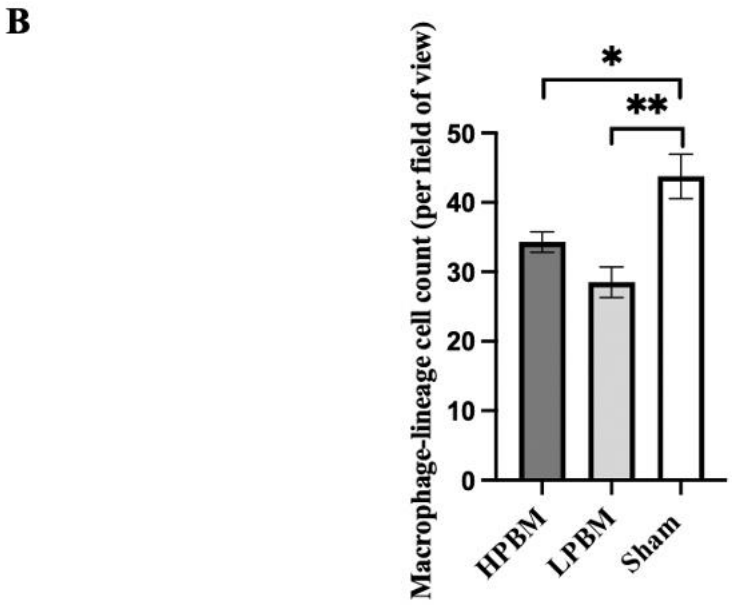

Figure 6.11: (A) Representative images of IBA-1+ cells in retinal cross-sections from control eyes, and eyes 3 days after CNV induction. In CNV retinas, retinal microglia (arrowhead) and macrophages (open arrow) are seen in and overlying CNV membranes in all treatment groups. CNV membranes are marked by yellow asterisks. Scale bar: 100 µm. (B) Bar graph depicting macrophage-lineage cell count in and around CNV membranes in eye treated with HPBM (n = 4), LPBM (n = 4), and sham (n = 4) using the cell count tool in imageJ. Data are presented as mean ± SEM. * Statistically significant difference ($p < 0.05$), by one-way ANOVA with a Tukey's HSD post-hoc test. ** Statistically significant difference ($p < 0.01$), by one-way ANOVA with a Tukey's HSD post-hoc test. IBA-1: ionized calcium-binding adapter molecule 1. CNV: choroidal neovascularization. CW: continuous wave photocoagulation laser. HPBM: high-dose photobiomodulation. LPBM: low-dose photobiomodulation. GCL: ganglion cell layer. INL: inner nuclear layer. ONL: outer nuclear layer. RPE: retinal pigment epithelium.

Effect of photobiomodulation laser on Müller cells

The highly organised laminar structure of the Müller cell that is typically seen in health retinae (see Chapter 4; Figure 4.8) was disrupted in CNV retinae. There is an observable reduction of GS immunostaining in the retina overlying CNV membranes in all treatment groups, with a coincident increase in GS immunolabelling in a nest of Müller cell adjacent to CNV membranes. This is consistent with Müller cells that have migrated and form a glial scar around CNV membranes. Qualitative assessment revealed that the patterns of GS immunoreactivity appeared similar in all three treatment groups (Figure 6.12).

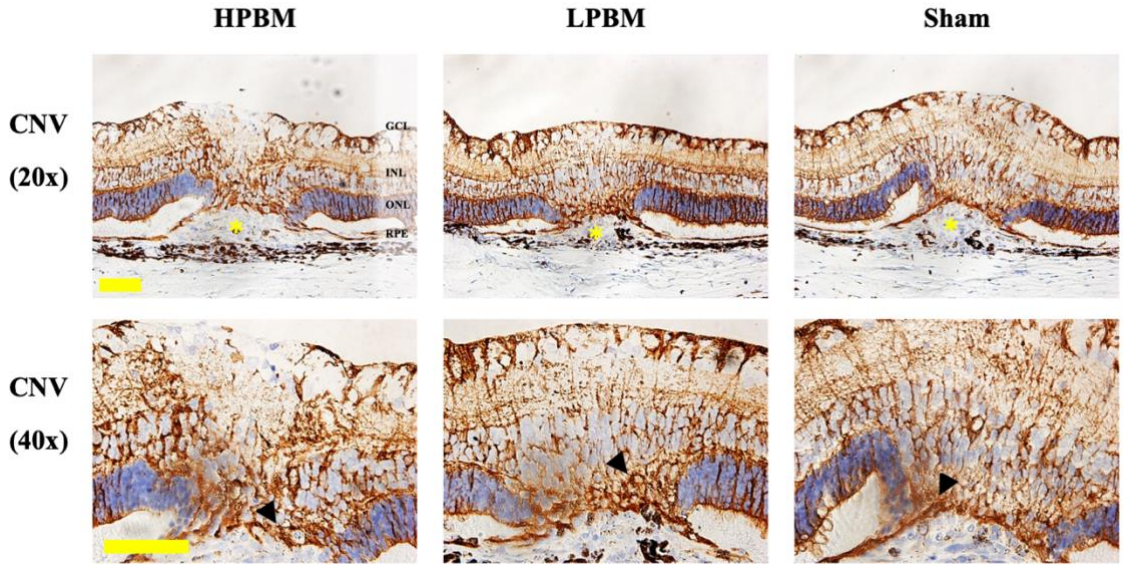

Figure 6.12: Representative images of GS immunostaining of Müller cells in cross-sections 3 days after CNV induction. Müller are seen to have migrated and formed a glial scar (arrowheads) around CNV membranes in retinas from all three treatment groups. CNV membranes are marked by yellow asterisks. Scale bar: 100 µm. GS: glutamine synthetase. CNV: choroidal neovascularization. HPBM: high-dose photobiomodulation. LPBM: low-dose photobiomodulation.

To shed further light on Müller cell responses to CNV, retinal WM were immunolabelled with nestin. In healthy retinal WM, nestin weaky labelled the retinal vasculature (see Chapter 4; Figure 4.6). In CNV eyes, nestin strongly localised to dense collections of elongated spindle-shaped cells, oriented perpendicular to the retinal cell layers in a pattern indicative of Müller cells that have undergone gliotic transformation overlying the site of laser-CNV induction (Figure 6.13A). Colour-thresholding was utilised to measure the area of nestin expression overlying the site of CNV membranes as a surrogate marker of Müller cell gliosis. Comparison between treatment groups using one-way ANOVA revealed that there was significant difference between at least two treatment groups (F =

11.4, p = 0.0005). Tukey's HSD Test for multiple comparisons found no significant difference in nestin immunoreactivity between the PBM treatment groups (p = 0.36). However, there a statistically significant difference in nestin immunoreactivity in the HPBM ((p = 0.014, 95% C.I. [$5.40x10^3$, $6.59x10^3$]), and the LPBM (p = 0.001, 95% C.I. [$3.85x10^3$, $5.74x10^3$]) treatment groups when compared to the sham group (Figure 6.13B).

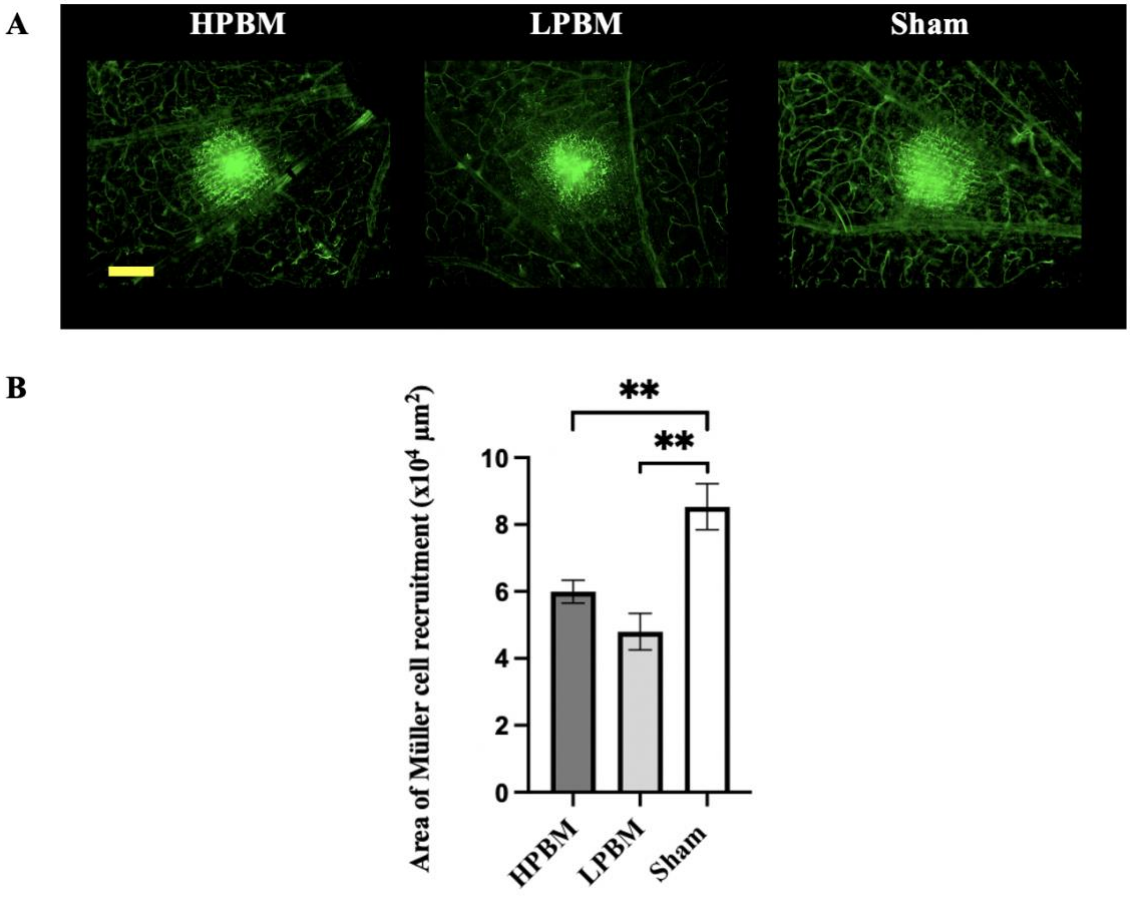

Figure 6.13: (A) Representative images of fluorescent nestin immunolabelling in retinal WM from CNV eyes at completion of the treatment period. At the site of CNV membranes there is marked increased density of reactive nestin$^+$ Müller cells. Scale bar: 200 µm. (B) Bar graph depicting amount of nestin$^+$ Müller cells overlying

the CNV lesion, as determined by the colour-thresholding function in imageJ applied to images of retinal WM of eyes treated with HPBM (n = 7), LPBM (n = 7), and sham (n = 9). Data are presented as mean ± SEM. ** Statistically significant difference ($p < 0.01$), by one-way ANOVA with a Tukey's HSD post-hoc test. WM: wholemount. CNV: choroidal neovascularization. HPBM: high-dose photobiomodulation. LPBM: low-dose photobiomodulation.

Effect of photobiomodulation laser on neutrophils

Myeloperoxidase (MPO) is a marker of cells of myeloid origin and is used to identify infiltrating neutrophils. In control retinas, no MPO^+ cells were observed (data not shown). MPO immunoreactivity was conducted in the different treatment groups. Extensive infiltration of MPO^+ cells, within and overlying the CNV lesion, was observed in sham retinas. A few MPO^+ neutrophils were seen in retinas from both PBM treatment groups (Figure 6.14).

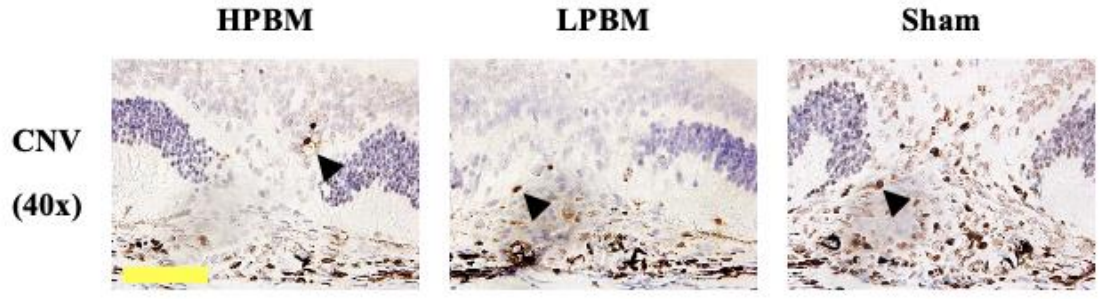

Figure 6.14: Representative images of MPO+ cells in retinal cross-sections 3 days after CNV induction with CW laser. MPO+ neutrophils (arrowheads) are seen infiltrating CNV membranes. Scale bar: 100 µm. MPO: myeloperoxidase. CNV:

choroidal neovascularization. HPBM: high-dose photobiomodulation. LPBM: low-dose photobiomodulation.

Effect of photobiomodulation laser on T-lymphocytes

CD3 is a pan-T-cell marker. In control retinas, no $CD3^+$ cells were observed (data not shown). Sham retinas featured numerous $CD3^+$ lymphocytes in and around the CNV membrane; these cells were seen in retinal tissue well beyond the CNV lesions. Whilst $CD3^+$ cells were observed at the site of CNV membranes in HPBM retinas, these are largely restricted to the CNV lesion. No $CD3^+$ cells are observed in LPBM retinas (Figure 6.15).

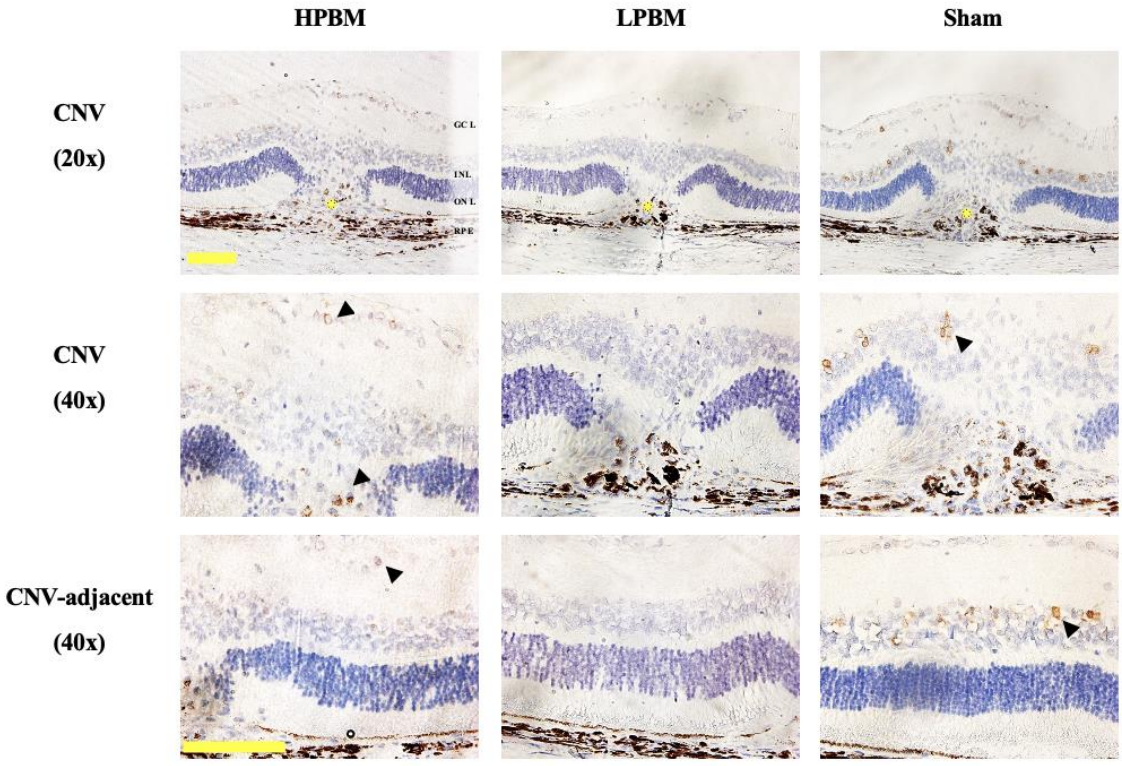

Figure 6.15: Representative images of CD3+ cells in cross-sections 3 days after CNV induction with CW laser. CD3+ T-cell (arrowhead) are seen to infiltrate in and

around the CNV membranes in HPBM, and sham retinas, although this is more extensive in the former. CNV membranes are marked by yellow asterisks. No CD3+ cells are observed in LPBM retinas. Scale bar: 100 µm. CD3: cluster of differentiation 3. CNV: choroidal neovascularization. HPBM: high-dose photobiomodulation. LPBM: low-dose photobiomodulation.

Effect of photobiomodulation laser on expression of pro-inflammatory cytokines

Immunostaining of retinal cross-sections at 3 days after CNV induction was also performed for the pro-inflammatory cytokines TNF-α, iNOS, IL-1β, and IL-6 because of their well-recognized role in nAMD. In archival positive control retinas from eyes injected with the bacterial toxin lipopolysaccharide, expression of all four cytokines was observed in microglia (data not shown). However, no expression of TNF-α, iNOS, IL-1β, and IL-6 was discernible in CNV eyes (data not shown). The most likely explanation for the lack of expression of these cytokines is that the time point of analysis, 3 days after laser-induced CNV induction, is too, past the peak period of expression of these cytokines.

6.5 Discussion:

PBM is postulated to counteract hypoxia and modulate cellular survival by increasing expression of, and activity of CCO [351-353]. It does so by causing dissociation of nitric oxide (NO) from CCO, with oxygen preferentially binding instead. This improves mitochondrial oxidative phosphorylation, increases mitochondrial membrane potential,

with resultant reduction in ROS production, and aids recovery from mitochondrial respiratory chain blockade under hypoxic conditions; this leads to increased available energy in target cells [347, 354-357, 479]. We affirmed that PBM increases mitochondrial respiratory chain activity in retinal tissue under normoxic conditions. It would be of interest to ascertain how this would translate to hypoxic tissue as it is known that under such conditions, scavenger molecule, superoxide dismutase, can become overwhelmed, leading to oxidative stress within the tissue. PBM is known to overcome oxidative stress in target tissues by normalise expression of the superoxide dismutase within 30-120 minutes of treatment [220, 222, 352, 366, 480351-353, 382]. Supplementary analysis of superoxide dismutase expression to follow on from this study would be prudent to ascertain the net oxidative status of the target tissues. We postulated that if PBM can improve mitochondrial function, and increase scavenger activity, it may therefore reduce VEGF-driven CNV development.

Hypoxia and inflammation are potent induction factors for VEGF expression [48, 232, 481-483]. In the laser-induced CNV model of AMD, investigators have demonstrated that VEGF levels peak at 3 days following induction and begin decreasing after 18 days, but can remain elevated for at least 30 days [187, 404]. Whilst the results in this study did not affirm the hypothesis that PBM reduces VEGF levels, the earlier presented WM and cross-section analysis supports down-regulation of pathogenic proangiogenic mechanisms. Whilst ELISA is a high-quality method for protein quantification, in samples of minute amount, such as is suggested in this study, alternative methodology may be useful, such as polymerase chain reaction (PCR) [484, 485]. The angiogenic pathways in the retina are complex. There are several tissue mediators of VEGF expression and

blood-retinal barrier disruption in nAMD, and these factors are interactive. Thus, the effects of PBM laser cannot be attributed to VEGF levels alone. For example, PBM may influence VEGF tissue interactions indirectly by influencing the relative half-life of VEGF in tissue or VEGF receptors expression on target tissues, as it is known that under hypoxic conditions, VEGF has a prolonged half-life, lasting 2-3 times longer in tissue when compared to normoxic conditions [48]. However, it is understood that the tissue response to VEGF is also dependent on the relative counteractivity of local antiangiogenic factors.

There is suggested that PBM treatment can shift the VEGF/PEDF ratio towards an anti-angiogenic profile [377]. PEDF is one of the key endogenous inhibitors of angiogenesis in the eye, along with TSP1, endostatin, and angiostatin [12-14, 115]. PEDF is a potent anti-angiogenic factor secreted from the apical aspect of RPE cells [76]. It is typically present at an order of magnitude higher level in retinal tissue compared to VEGF. It exerts its effects by inhibiting the expression and binding of VEGF to VEGFR-2 [102, 486, 487]. Reduced RPE production of, and hence reduced levels of the antiangiogenic factors PEDF, TSP1, endostatin and angiostatin in Bruch's membrane and the choriocapillaris potentially contributes to the development of CNV and perpetuation of nAMD [12-14, 115, 118, 488, 489]. Thus, derangement in the ratio of VEGF in relation to these factors is implicated in CNV formation in nAMD [27, 101, 104, 105, 143, 197, 198, 232, 454, 481-483, 490]. In turn, application of mitochondrial antioxidants preferentially shifts the ratio back towards normal [376, 486]. The consideration that PBM could upregulate counteractive antiangiogenic tissue factors is an avenue of further enquiry, as upregulation of these peptides is associated with attenuation of retinal vascular development and neovascularization [24, 46, 491-495].

In the literature, the tissue effects of PBM have been attributed to its ability to combat tissue inflammation and oxidative stress. The modulating effect on neovascularisation that has been earlier presented is most likely dependent upon an interaction of multiple factors and its influence on VEGF-independent proangiogenic pathways. For example, the anti-angiogenic effects of PEDF are not selective for VEGF. This factor also inhibits endothelial cell migration and proliferation by down-regulating angiogenic and chemotactic signals from TGF-ß, aFGF, bFGF, TNF-α, ICAM-1, MCP-1 and CTGF, as well as playing an important role in physiological vascular pruning in late retinal vascularization by selectively causing apoptosis of endothelial cells of new blood vessels without affecting those of established mature blood vessels through the Fas/FasL pathway; the aforementioned retinal antiangiogenic factors are known to also act through this pathway [24, 46, 491, 496-498]. Exogenous administration of these factors is associated with suppression of experimental CNV and has garnered enough interest to be extended into clinical trials in AMD [12, 499-502]. Furthermore, PEDF has inhibitory effects on macrophage, microglia, and astrocyte proliferation, suggesting a role for immunomodulatory effects in the eye and brain [503, 504]. PEDF expression is upregulated in stromal cells in the retina, which is thought to be as part of the Müller cell neuroprotective response [102, 108, 111]. PEDF exerts neurotrophic effects in the retina directly through the PEDFR, which is strongly expressed in RPE, and photoreceptor inner segments, but also weakly expressed in the inner nuclear, and retinal ganglion cell layers [505, 506]. PEDFR activation is associated with upregulation of bcl-2 expression, which protects against photoreceptor apoptosis through bcl-2 mediated inhibition of nuclear translocation of apoptosis-inducing factor, in a caspase-independent manner [177, 507]. However, neuroprotection may also be indirectly through PEDF-mediated upregulation of other neurotrophic factors, such as BDNF,

GDNF, NT-3, and NGF [508]. The presented evidence suggests PBM treatment modulates vascular proliferation and permeability through VEGF-adjacent pathways. Consequently, the specific anti-angiogenic pathways targeted by PBM will require further elucidating. Identification and definitive qualification of the tissue factors involved in mitigating angiogenesis with an ELISA angiogenesis panel would be illuminating.

PBM has pleotropic effects on cellular survival. It is suggested that it may do so through activation of the main cellular anti-apoptotic pathway protein, bcl-2 [382, 509]. Müller cells may be one of the retinal cells targeted by PBM. Müller cells retain progenitor cell characteristics, having the capacity to migrate to the site of injury and differentiate into new neurons [35, 36, 435, 510-512]. Nestin is a marker de-dedifferentiated Müller cells that have adopted neuronal progenitor cells characteristics, as it is upregulated in the process of Müller cells as part of the process of proliferation, migration and dedifferentiation during gliosis [435-442]. Proliferation cell nuclear antigen (PCNA) is an essential nuclear protein required for DNA synthesis that is maximally expressed during the G1/S phase of the cell cycle. PCNA expression is often employed as a marker of cell proliferation because cells remain for a longer time in the G1/S phase when proliferating. Like nestin, PCNA is expressed at low levels in the normal adult retina; it is considered a marker of cellular proliferation [512-516]. It is believed that the expression of PCNA in Müller cells may play a role in the resistance of this cell type to ischaemic insult through its role in DNA mismatch repair [517, 518]. Many of the stimuli that promote apoptosis, such as heat shock or oxidative stress, also induce the synthesis of heat shock proteins (HSP). HPSs are molecular chaperones that participate in synthesis, folding, assembly, transportation, and degradation of proteins. Under physiological conditions, HSPs are weakly expressed in

cells; however, expression is increased in conditions of cellular stress [519, 520]. Under conditions of retinal stress, HSPs have pleotropic effects; they play a protective role in the retinal stress response by influencing mitochondrial calcium balance, anti-apoptotic gene expression, and mitochondrial oxidative phosphorylation by inhibiting the mitochondrial cyt c-mediated apoptotic cascade [521]. Furthermore, HSPs induce phenotype switching of microglia to their 'M2' anti-inflammatory phenotype and downregulate leukocyte adhesion; this in turn is associated with liberation of neurotrophic factors, and modulation of retinal inflammation [149, 165-167, 233, 235, 522, 523]. Heme Oxygenase-1 (HO-1/HSP32) is a HSP and molecular chaperone of interest in the central nervous system and neuroretina [524-526]. It is upregulated as part of the retinal stress response; it is involved in conferring cellular resistance to apoptosis. It appears to be upregulated by, and contribute to, the observed anti-inflammatory and anti-apoptotic effects PBM treatment exerts in neovascular disease of the retina [366, 386]. In this study, as is reflective in the literature, PBM appears to modulate the gliotic reactivity of retinal glia, without a detrimental effect on retinal survival mechanisms.

PBM has also been shown to upregulate the expression of neurotrophic factor CNTF in a light-damage rat model of AMD, with associated improvement in ERG responses as an indicator of improved photoreceptors survival [367]. CNTF is considered a 'lesion factor'; it is expressed at low levels in the healthy retina but is upregulated by RPE and macroglia in stressed retina. It is thought that it indirectly exerts its survival effects by binding to the CNTFRα expressed on cell membranes of retinal macroglia and microglia resulting in a switch to a neuroprotective phenotype [168, 170, 171, 183]. It is also known to down-regulate the expression of VEGF by the RPE and increase fluid absorption across the outer blood-

retina-barrier by upregulating CNTFR chloride channels at the basolateral RPE cell membrane, mediated by JAK2/STAT3 signalling. Whilst PBM treatment has been shown to modulate the expression of this neurotrophin under conditions of retinal stress, it does not seem to influence expression of CNTF in otherwise healthy tissue [170, 171, 527]. Our findings confirmed that PBM treatment itself does not appear to cause upregulation of CNTF expression in otherwise healthy retinas when compared to sham retinas. CNTF expression was upregulated around the CNV membrane in the laser-induction zone in all treatment groups, but not discernable different between sham, and PBM treated retinas was observed. However, definitive protein and receptor quantification with ELISA would be illuminating.

It is well established that VEGF is the master controller of angiogenesis in the retina but there are a number of key molecules of particular interest that influence barrier function and angiogenesis in the retina [20]. The FGF family of proteins and their receptors control a wide range of biological functions in the retina. The physiological role that bFGF plays in the retina should not be underestimated. It is a key neurotrophin in the retina, playing an especially important role as a survival factor in the stressed retina [154, 155]. RPE cells and macroglia secrete bFGF in an autocrine capacity, which is important for maintaining vascular integrity, but upregulate expression under hypoxic conditions, contributing to neovascularisation [232, 453, 528-530]. FGFs directly induce angiogenesis by promoting endothelial cell mitogenesis and motogenesis, independent of VEGF [24, 531]. Furthermore, there is evidence to suggest that VEGFR blockade may upregulate the FGF family pro-angiogenic pathways, and this has implications for the recurrence and the aggressiveness of neovascularization in the face of VEGFR blockade under hypoxic conditions. This

may also explain the loss of efficacy and development of tolerance to ranibizumab and bevacizumab that is observed over time with repeated intravitreal administration of anti-VEGF therapy [299, 532, 533]. Overexpression of FGF ligands and their receptors are associated with neovascular disease of the retina and neoplastic disease [367, 531]. Furthermore, when looking at models of overexpression of the FGFR family of tyrosine kinase receptor, blockade of the FGFR is associated with inhibition of pathogenic vascular behaviour, such as neovascularisation, cell migration and tissue invasion [24, 102, 367, 453, 459-461, 464, 534-537]. Müller cell population appears to be a key source of chemokines, and pro-angiogenic factors like bFGF under conditions of retinal stress. It is known that bFGF expression is elevated in this laser-induced model of CNV [402]. The effects of PBM on Müller cell expression of bFGF under conditions of stress have been demonstrated by other investigators [378, 379]. Of note, the expression of bFGF appears to be upregulation in the region of retinas treatment with PBM laser when compared to control, affirming that PBM laser does not down-regulate the expression of this survival factor below control level in otherwise healthy retinal tissue. Thus, the modulation of bFGF expression may be one of the pathways through which PBM exerts its retinal survival effects without inducing exacerbation of CNV membrane growth in this study. The role of alternative angiogenic pathways mediated by bFGF, is one avenue of investigation to follow when considering neovascular tissue development in clinical nAMD. PBM laser does not appear to influence this particular pathway in this study [367, 379, 538, 539]. However definitive protein and receptor quantification with ELISA would be illuminating.

Further investigation in to the role of other neurotrophic factors that influence angiogenesis in the retina would be of interest. TGF-ß is one such factor. TGF-ß is of

particular interest as there is a duality to the role that TGF-ß plays in angiogenesis; its role is conditional. RPE cells secrete TGF-β in an autocrine capacity. Under these conditions, TGF-β indirectly promoted angiogenesis through endothelial-cell-derived MMP-mediated remodelling of the extracellular matrix. However, when upregulated in retinal hypoxia and inflammation by microglia, Müller cells, perivascular macrophages and infiltrating leukocytes, TGF-β largely plays a modulatory role. It modulates inflammation in the retinal wound-healing response, suppressing TNF-α, IL-1 and IL-6 expression, inhibiting cytokine-induced endothelial adhesion and polarising microglia to the 'M2', reparative phenotype [54, 195, 540-544]. It also mitigates pathological angiogenesis by inhibiting VEC migration, proliferation, and invasion across the extracellular matrix both directly, and indirectly, through secondary inhibition of bFGF-mediated pro-angiogenesis [24, 83, 192, 470, 545-549]. Furthermore, TGF-ß is known to modulate gliotic reactivity and is protective against neuronal cell death induced by hypoxia, oxidative stress, apoptosis, and glutamate excitotoxicity [52, 156-159]. The modulating effects of PBM in inflammation and neovascularisation are most likely dependent upon an interaction of multiple factors, which require further exploration. Identification and definitive qualification of the tissue factors involved in control of angiogenesis with an ELISA angiogenesis panel would be illuminating.

Penfold *et al* suggested from data attained from staining AMD and age-matched healthy human eye WM for microglial activity that in AMD eyes there is increased microglial activity, especially around vessels and that this immunologic responses in neural retinal microglia and vasculature appear to be related to early pathogenetic changes in RPE pigmentation and drusen formation [550]. Microglial steady-state maintenance is mediated

by photoreceptor-derived neurotrophic factor cell-cell interactions. Thus, photoreceptor degeneration, and with it, a loss of soluble and membrane-bound neurotrophic factors, releases microglia from tonic inhibition, resulting in a phenotype switch to a pro-inflammatory, 'activated' M1 microglial cell population [54, 55]. In this activated form, microglia secrete ROS, and RNS, as well as pro-inflammatory cytokines such as TNF-α, IL-1ß, and IFN-γ, which perpetuates further polarization of the microglial population to the cytotoxic phenotype [150, 167, 183]. The coincident loss of microglia-derived trophic support to glial and neuronal cells exacerbates retinal degeneration. This pro-inflammatory state is associated with a phenotype switch in Müller cells towards gliosis. In acute retinal stress, the typical features of Müller cell gliosis involve cellular hypertrophy, proliferation, and migration. The process of epithelial-mesenchymal transition results in a functional change in this cell population [438-441, 511, 512, 551]. In this study, less marked gliotic transformation in the Müller cells population in the PBM-treatment groups may result in a less potent cytokine soup, as the phenotype switch to a cytotoxic state is associated with upregulation of expression of inflammatory cytokine like TNF-α, IL-1ß, IL-6, and iNOS, and cell adhesion molecules like VCAM-1 and ICAM-1, and chemokines like CCL2 and CCL3 in Müller cells [185]. It seems that in the laser-induced model of CNV, maximal cellular inflammation and cytokine release occurs early in the course. Leukocyte recruitment and infiltration into retinal tissue following activation of this inflammatory cascade tends to peak at 48-72 hours but subsequently persists, perpetuating ongoing inflammation for up to 5-7 days [193, 469]. This cellular response is considered an important pathogenic mechanism in nAMD, as investigators have demonstrated that leukocyte depletion directly inhibits CNV development [186-188]. Further analysis at various time-points and quantification would be useful to ascertain the

natural history of lymphocyte infiltration. Identification and definitive qualification of the tissue factors involved in retinal inflammation with an ELISA inflammation panel would be illuminating.

Microglia and Müller cell activation, and infiltration of leukocytes are associated with tissue upregulation of the expression of inflammatory cytokine like TNF-α, IL-1ß, IL-6, IFN-γ and iNOS [150, 167, 183, 185]. These cytokines are induction factors for activation of structural and functional changes in VECs that have implications for BRB dysfunction, retinal inflammation and loss of immune privilege of retinal tissue in nAMD [56, 102, 197, 241-243, 404, 456-465]. TNF-α is considered to be one of the master controllers of inflammation and is a strong induction factor for expression of VEGF. TNF-α contributes to mitochondrial DNA damage and acts as a chemokine, increasing microvascular permeability and promoting immune cell infiltration into the retina [196-198, 238, 239, 454]. It is thus a factor of interest as it has a well-recognized role in the pathogenesis of nAMD. Its blockade has the potential to inhibit CNV formation and cause regression in existing membranes. PBM treatment could potentiate this, as it is known to downregulate expression in Müller cells following treatment [228, 552]. However, there was no noticeable expression of this factor in any of the retinas in the present study. This is not all to together unexpected as this factor is known to be upregulated early following laser induction. It is presumed that this factor, whilst an important markers of retinal inflammation, and cellular oxidative stress, is expressed early in this process, and may no longer be expressed at a detectable level by the day-3 analysis time point. Compatibility of TNF-α antibody immunolabelling with Davidson's fixed retinal tissue has been confirmed previously, so technical issues are an unlikely explanation for poor immunolabelling with this antibody [409]. TNF-α-mediated

inflammation induces production of potent pro-inflammatory ROS and RNS in RPE, macrophages, Müller cells and microglial cells [196, 238, 239]. Immunostaining for nitric oxide synthase (iNOS), the enzyme responsible for NO production, was attempted. However, no discernible immunostaining for iNOS was noted in retinal tissues in the present study. This factor is expressed early in the retinal stress response, and like TNF-α may have no longer been expressed at a detectable level at the day-3 analysis time point [196, 239]. However, immunostaining for iNOS is known to be suboptimal with Davidson's formula fixed tissue [409].

TNF-α is also an induction factor for IL-1ß [189]. These two factors appear to have synergistic amplifying effects on BRB breakdown [58, 75, 190-195]. It is understood that within 3-6 hours of exposure to these factors, polymorphonuclear cell and macrophage recruitment and infiltration, activation of perivascular monocytes and Müller cells, and blood-retinal-barrier break down with resultant oedema and haemorrhage occurs [58]. As IL-1β is known to be involved in early inflammatory process, it is possible that like the aforementioned cytokines, levels may have been expressed below detectable levels for immunohistochemical at the day-3 time point of analysis. TNF-α is also an induction factor for IL-6 [189]. IL-6 is another factor of interest as it is also upregulated in retinal glia under conditions of hypoxia and inflammation. It is an important chemotactic factor, and thus mediates BRB disruption in retinal endothelial cells indirectly. Its blockade normalises retinal endothelial barrier function [190, 194, 476, 477]. However, no discernable immunostaining of these cytokines was noted in any of the study eyes. The conclusion from the lack of success with immunostaining for TNF-α, IL-1ß, IL-6, and iNOS was to

conduct analysis of these factors at an earlier time point following laser-induction. In support of this deduction, previous work from our laboratory has found upregulated expression of proinflammatory cytokines in a time window of 6 to 24 hours after continuous wave photocoagulation injury of the retina [553]. Several key cytokines were selected for this study, as discussed, however, further investigation of the role of other factors, such as IFN-γ is warranted as it is another key cytokine involved in BRB disruption and cellular inflammation in the retina [167, 183, 470]. It is a factor known to be involved in activation of the complement cascade and in priming macrophages to M1 cytotoxic phenotype [466-468]. These pro-inflammatory mediators are important factors in perpetuation of gliosis and vascular permeability, which in turn perpetuates neovascularisation and neuronal cell death, ultimately interfering with visual function factors.

These pro-inflammatory tissue factors are produced in retinal stress and injury by Müller cells to activate and recruit more microglia, and are strong induction factors for leukocyte recruitment, adhesion and transendothelial migration into retinal tissues. There is resultant disruption of the BRB due to break down of VEC tight junctions during leukocyte infiltration across the endothelial barrier [9, 34, 36-38, 58, 74, 75, 190-198, 475]. Neutrophils are involved in early aspects of the wound healing response of the retina. There were less neutrophils seen in PBM-treated retinas when compared to sham retinas, implying that PBM may modulate the early inflammatory response in tissue and thus mitigate a prolonged, or exaggerated response from immunological cells. PBM treatment down-regulates expression of TNF-α and endothelial adhesion molecule expression in autoimmune encephalopathy [383, 384]. This is reflected in the observation that there was less

T lymphocytes recruitment in PBM retinas when compared to sham retinas in this study. It is also known to polarise activated microglial cells to their dormant, anti-inflammatory phenotype and is associated with reduced macrophage cell tissue infiltration and in a mouse model of ROP, and aged-mouse model of AMD [367, 383]. This was reflected in the present study by notably fewer microglial cell and macrophage recruitment in PBM treated groups. It was also observed that there was a negligible microglial cell population in RPE WM outside of the laser induction zone. As microglia are resident cells of the retina, and thus, are not native to the RPE, this observation confirms that the injurious response from retinal microglia is localised and that treatment with PBM laser does not induce microglial activation. Furthermore, PBM treatment is associated with reduced Müller cell activation in vitro, and in a mouse model of light-induced retinopathy, and leukocyte activation and infiltration in a rodent model of diabetic retinopathy [228, 350, 366, 379, 386, 445]. In this way, PBM is believed to modulate tissue inflammation. Along this vein, if PBM imparts immunomodulatory effects, it may also influence microglial cells to favour an immunomodulatory phenotype. This phenotype profile is associated with liberation of neurotrophins, such as CNTF, bFGF, NGF, PDGF, EGF, BDNF, and TGF-ß that shift retinal glial cells toward a more neuroprotective phenotype [52, 149, 165-167]. [160, 446, 447].

Müller are an important source of and express receptors for neurotrophic factors in acute retinal stress, and through glial-glial interactions, in turn, they liberate neurotrophins to support retinal glia and neuronal cells. In this way, the response of the Müller cell population under conditions of stress and injury can be protective to the retina by favouring a neuroprotective phenotype [160, 446, 447]. This cell population has the capacity to

adopt progenitor cell characteristics, as part of the retinal wound-healing response process, with potential, moreover, to differentiate into new neurons [35, 36, 510]. Thus, further phenotypic characterisation of the retinal macroglial stress response would assist to determine whether PBM treatment influences these cells to preferentially express an immunomodulating versus cytotoxic phenotype [413, 443]. Microglia share phenotype markers with macrophages, and thus, there are no microglia specific antigen markers; all macrophage-like cells have Fc receptors for immunoglobulin, C3 receptors to bind complement, binding of IBA-1, and antigenicity for F4/80, and CD68/ED1 monoclonal antibodies [8, 9, 554-557]. However, labelling does not differentiate between microglial cell phenotypes. Whether PBM treatment is associated with less M1-polarised microglial cell recruitment is yet to be answered. Further investigations need to be performed to clarify if PBM influences microglial phenotypes by immunolabelling for 'M1' cytotoxic markers such as CD14, CD16, CD32, CD 40, CD86, and MHCII, and immunolabelling for 'M2' immunomodulatory markers such as CD163 and CD206 [558, 559].

Chapter 7:

Final words

7.1 Study conclusions

The primary outcome measure of this study was to determine whether PBM treatment influences the development of CNV in an animal model in terms of membrane size and vascular permeability. PBM treatment was found to be associated with smaller and less permeable CNV membranes. However, the levels of the key pro-angiogenic factor, VEGF, were not statistically different between treatment groups. This suggests that whilst PBM induced early regression of CNV membranes in this study, it appears to modulate VEC growth, migration and vascular barrier function through VEGF-independent or VEGF-adjacent proangiogenic pathways. PBM treatment was associated with less retinal glial cell recruitment. Tissue inflammation is a potent driver for angiogenesis and disruption of the BRB. Thus, modulation of retinal tissue inflammation is a potential pathway through which PBM treatment has achieved the primary outcome measured in this study. The secondary outcome measure was that PBM laser treatment did not have adverse tissue effects on retinal tissue. No evidence of photoreceptor degeneration, glial cell reactivity, nor aberrant neovascular tissue development was noted upon treatment of control retinal tissues with PBM laser. Thus, the conclusions drawn from this study were that the PBM laser is both safe to use in retinal tissue, and that it has the potential to modulate neovascular tissue development in nAMD through targeting of retinal tissue inflammation and VEGF-adjacent angiogenic pathways. This study provides more insight into the role that the PBM laser could play in management of neovascular disease of the retina. There have been reports of retinal tissue effects in untreated fellow eyes in studies utilising retinal laser treatment; a caveat to consider in this current study and in future animal and human studies investigating retinal laser treatment [560-563].

7.2 Future directions

Evidence from long-term follow-up of subjects receiving intravitreal anti-VEGF suggests that despite best current practice, a third of individuals show resistance to anti-VEGF treatment, exhibiting persistent oedema and progression of disease, resulting in vision loss and compromised quality of life [298]. The inability to induce complete disease regression may be attributable to that fact that anti-VEGF therapy does not target the up-stream hypoxic and pro-inflammatory drive behind this disease [24, 276, 302-307]. The goal of evolving treatment strategies is to achieve the therapeutic effects of anti-VEGF therapy, which is the current best practice, whilst reducing or avoiding the invasiveness of intravitreal drug delivery. The pleotropic nature of VEGF in the eye is well established. VEGF is an important factor for endothelial, neuronal and glial cell function and survival, especially under disease conditions [48, 232, 564-566]. Understandably, there is a concern amongst trial investigators from extended observations in subjects that receive anti-VEGF therapy, that this may have adverse long-term effects on the RPE. There is also a suggestion that anti-VEGF therapy may contribute to geographic atrophy with long-term treatment in nAMD subjects. We know that VEGF blockade interferes with ocular development, RPE cell survival, RPE phagocytic function and microvilli morphology, as well as RPE cell survival under oxidative stress [48, 232, 564-567]. This confounds the validity of anti-VEGF strategies, particularly under chronic disease conditions as discussed in a review by Zarbin [568]. Furthermore, it is suggested that intravitreal anti-VEGF administration is plausibly associated with an increased incidence of arteriothrombotic events, although the precise mechanism appears to not be directly attributable to a VEGF-lowering effect. With our growing understanding of the pathogenic mechanism

predisposing to CNV development, of which the leading theories have focused on chronic hypoxia and low-grade inflammation, there is increasing interest in generation of a therapeutic approach that targets these underlying mechanisms [450]. PBM treatment is a potential untapped therapeutic modality, as there is an ever-growing evidence base in support of its effects on the key pathogenic processes of chronic hypoxia and inflammation that instigate CNV formation in nAMD, and this treatment may therefore, prove to be successful in combating the development and progression of nAMD [62, 63, 346-349, 353, 357, 381].

Chapter 8:

List of references

1. Reh T, A. . The development of the retina In: Schachat A, P., Wilkinson C, P. , Hinton D, R. , et al. (eds) *Ryan's retina* 7 ed.: Elsevier inc. , 2018, pp.375-386.
2. Chen J and Sampath AP. Structure and function of rod and cone photoreceptors. In: Schachat A, P., Wilkinson C, P. , Hinton D, R. , et al. (eds) *Ryan's retina* 7th ed.: Elsevier inc. , 2018, pp.421-442.
3. Gregg R, G., Singer J, Kamermans M, et al. Function and anatomy of the mammalian retina. In: Schachat A, P., Wilkinson C, P. , Hinton D, R. , et al. (eds) *Ryan's retina* 7ed.: Elsevier inc. , 2018, pp.378-420.
4. Bringmann A and Wiedemann P. Glial cells of the fovea. In: Schachat A, P., Wilkinson C, P. , Hinton D, R. , et al. (eds) *Ryan's retina* 7ed.: Elsevier inc. , 2018, pp.458-475.
5. Rattner A, Sun H and Nathans J. Molecular genetics of human retinal disease. *Annu Rev Genet* 1999; 33: 89-131. 2000/02/26. DOI: 10.1146/annurev.genet.33.1.89.
6. Clarke G, Heon E and McInnes RR. Recent advances in the molecular basis of inherited photoreceptor degeneration. *Clinical genetics* 2000; 57: 313-329. 2000/06/14.
7. Cepko C. Intrinsically different retinal progenitor cells produce specific types of progeny. *Nature Reviews Neuroscience* 2014; 15: 615-627. DOI: 10.1038/nrn3767.
8. Stoll G, Trapp BD and Griffin JW. Macrophage function during Wallerian degeneration of rat optic nerve: clearance of degenerating myelin and Ia expression. *J Neurosci* 1989; 9: 2327-2335. 1989/07/01. DOI: 10.1523/jneurosci.09-07-02327.1989.
9. Benveniste EN. Inflammatory cytokines within the central nervous system: sources, function, and mechanism of action. *The American journal of physiology* 1992; 263: C1-16. 1992/07/01. DOI: 10.1152/ajpcell.1992.263.1.C1.
10. Skalicky SE. *Ocular and Visual Physiology: Clinical Application*. Singapore: Springer Singapore Pte. Limited, 2015.
11. Goldberg MA and Schneider TJ. Similarities between the oxygen-sensing mechanisms regulating the expression of vascular endothelial growth factor and erythropoietin. *The Journal of biological chemistry* 1994; 269: 4355-4359. 1994/02/11.
12. O'Reilly MS, Boehm T, Shing Y, et al. Endostatin: an endogenous inhibitor of angiogenesis and tumor growth. *Cell* 1997; 88: 277-285. 1997/01/24.
13. Dawson DW, Volpert OV, Gillis P, et al. Pigment epithelium-derived factor: a potent inhibitor of angiogenesis. *Science (New York, NY)* 1999; 285: 245-248. 1999/07/10.
14. Sheibani N, Sorenson CM, Cornelius LA, et al. Thrombospondin-1, a Natural Inhibitor of Angiogenesis, Is Present in Vitreous and Aqueous Humor and Is Modulated by Hyperglycemia. *Biochemical and biophysical research communications* 2000; 267: 257-261. DOI: https://doi.org/10.1006/bbrc.1999.1903.
15. Henkind P. Symposium on glaucoma: joint meeting with the National Society for the Prevention of Blindness. New observations on the radial peripapillary capillaries. *Invest Ophthalmol* 1967; 6: 103-108. 1967/04/01.
16. Runkle EA and Antonetti DA. The blood-retinal barrier: structure and functional significance. *Methods in molecular biology (Clifton, NJ)* 2011; 686: 133-148. 2010/11/18. DOI: 10.1007/978-1-60761-938-3_5.
17. Bergers G, Song S, Meyer-Morse N, et al. Benefits of targeting both pericytes and endothelial cells in the tumor vasculature with kinase inhibitors. *The Journal of clinical investigation* 2003; 111: 1287-1295. DOI: 10.1172/JCI17929.
18. Bergers G and Song S. The role of pericytes in blood-vessel formation and maintenance. *Neuro Oncol* 2005; 7: 452-464. DOI: 10.1215/S1152851705000232.

19. Hellberg C, Ostman A and Heldin CH. PDGF and vessel maturation. *Recent Results Cancer Res* 2010; 180: 103-114. 2009/12/25. DOI: 10.1007/978-3-540-78281-0_7.
20. Stone J and Maslim J. Mechanisms of retinal angiogenesis. *Progress in Retinal and Eye Research* 1997; 16: 157-181. DOI: https://doi.org/10.1016/S1350-9462(96)00019-5.
21. Knuckey NW, Finch P, Palm DE, et al. Differential neuronal and astrocytic expression of transforming growth factor beta isoforms in rat hippocampus following transient forebrain ischemia. *Brain research Molecular brain research* 1996; 40: 1-14. 1996/08/01. DOI: 10.1016/0169-328x(96)00016-2.
22. Kalaria RN, Cohen DL, Premkumar DR, et al. Vascular endothelial growth factor in Alzheimer's disease and experimental cerebral ischemia. *Brain research Molecular brain research* 1998; 62: 101-105. 1998/10/31. DOI: 10.1016/s0169-328x(98)00190-9.
23. Choi YK, Kim JH, Kim WJ, et al. AKAP12 regulates human blood-retinal barrier formation by downregulation of hypoxia-inducible factor-1alpha. *J Neurosci* 2007; 27: 4472-4481. 2007/04/20. DOI: 10.1523/jneurosci.5368-06.2007.
24. Bussolino F, Mantovani A and Persico G. Molecular mechanisms of blood vessel formation. *Trends in biochemical sciences* 1997; 22: 251-256. 1997/07/01.
25. Carmeliet P and Jain RK. Molecular mechanisms and clinical applications of angiogenesis. *Nature* 2011; 473: 298-307. 2011/05/20. DOI: 10.1038/nature10144.
26. Mudhar HS, Pollock RA, Wang C, et al. PDGF and its receptors in the developing rodent retina and optic nerve. *Development (Cambridge, England)* 1993; 118: 539-552. 1993/06/01. DOI: 10.1242/dev.118.2.539.
27. Lindahl P, Johansson BR, Levéen P, et al. Pericyte loss and microaneurysm formation in PDGF-B-deficient mice. *Science (New York, NY)* 1997; 277: 242-245. 1997/07/11. DOI: 10.1126/science.277.5323.242.
28. Hellström M, Gerhardt H, Kalén M, et al. Lack of pericytes leads to endothelial hyperplasia and abnormal vascular morphogenesis. *The Journal of cell biology* 2001; 153: 543-553. DOI: 10.1083/jcb.153.3.543.
29. Sennino B, Kuhnert F, Tabruyn SP, et al. Cellular source and amount of vascular endothelial growth factor and platelet-derived growth factor in tumors determine response to angiogenesis inhibitors. *Cancer research* 2009; 69: 4527-4536. 2009/04/28. DOI: 10.1158/0008-5472.CAN-08-3779.
30. Sadiq MA, Hanout M, Sarwar S, et al. Platelet-Derived Growth Factor Inhibitors: A Potential Therapeutic Approach for Ocular Neovascularization. *Developments in ophthalmology* 2016; 55: 310-316. 2015/10/27. DOI: 10.1159/000438953.
31. Kaur C, Foulds WS and Ling EA. Blood-retinal barrier in hypoxic ischaemic conditions: basic concepts, clinical features and management. *Prog Retin Eye Res* 2008; 27: 622-647. 2008/10/23. DOI: 10.1016/j.preteyeres.2008.09.003.
32. Wang M, Ma W, Zhao L, et al. Adaptive Müller cell responses to microglial activation mediate neuroprotection and coordinate inflammation in the retina. *Journal of neuroinflammation* 2011; 8: 173-173. DOI: 10.1186/1742-2094-8-173.
33. Newman EA. Voltage-dependent calcium and potassium channels in retinal glial cells. *Nature* 1985; 317: 809-811. DOI: 10.1038/317809a0.

34. Bringmann A, Pannicke T, Grosche J, et al. Müller cells in the healthy and diseased retina. *Prog Retin Eye Res* 2006; 25: 397-424. 2006/07/15. DOI: 10.1016/j.preteyeres.2006.05.003.
35. Ooto S, Akagi T, Kageyama R, et al. Potential for neural regeneration after neurotoxic injury in the adult mammalian retina. *Proc Natl Acad Sci U S A* 2004; 101: 13654-13659. 2004/09/09. DOI: 10.1073/pnas.0402129101.
36. Fischer AJ and Reh TA. Müller glia are a potential source of neural regeneration in the postnatal chicken retina. *Nature neuroscience* 2001; 4: 247-252. DOI: 10.1038/85090.
37. Vecino E, Rodriguez FD, Ruzafa N, et al. Glia-neuron interactions in the mammalian retina. *Prog Retin Eye Res* 2016; 51: 1-40. 2015/06/27. DOI: 10.1016/j.preteyeres.2015.06.003.
38. Bringmann A, Grosche A, Pannicke T, et al. GABA and Glutamate Uptake and Metabolism in Retinal Glial (Müller) Cells. *Front Endocrinol (Lausanne)* 2013; 4: 48-48. DOI: 10.3389/fendo.2013.00048.
39. Poitry-Yamate CL, Poitry S and Tsacopoulos M. Lactate released by Müller glial cells is metabolized by photoreceptors from mammalian retina. *J Neurosci* 1995; 15: 5179-5191. 1995/07/01. DOI: 10.1523/jneurosci.15-07-05179.1995.
40. Bailey TJ, Fossum SL, Fimbel SM, et al. The inhibitor of phagocytosis, O-phospho-L-serine, suppresses Müller glia proliferation and cone cell regeneration in the light-damaged zebrafish retina. *Exp Eye Res* 2010; 91: 601-612. 2010/08/11. DOI: 10.1016/j.exer.2010.07.017.
41. Tout S, Chan-Ling T, Holländer H, et al. The role of Müller cells in the formation of the blood-retinal barrier. *Neuroscience* 1993; 55: 291-301. 1993/07/01. DOI: 10.1016/0306-4522(93)90473-s.
42. Ikeda T, Homma Y, Nisida K, et al. Expression of transforming growth factor-beta s and their receptors by human retinal glial cells. *Curr Eye Res* 1998; 17: 546-550. 1998/06/09. DOI: 10.1076/ceyr.17.5.546.5197.
43. Eichler W, Yafai Y, Wiedemann P, et al. Angiogenesis-related factors derived from retinal glial (Müller) cells in hypoxia. *Neuroreport* 2004; 15: 1633-1637. 2004/07/03. DOI: 10.1097/01.wnr.0000133071.00786.a4.
44. Eichler W, Yafai Y, Kuhrt H, et al. Hypoxia: modulation of endothelial cell proliferation by soluble factors released by retinal cells. *NeuroReport* 2001; 12.
45. Yafai Y, Iandiev I, Lange J, et al. Müller glial cells inhibit proliferation of retinal endothelial cells via TGF-β2 and Smad signaling. *Glia* 2014; 62: 1476-1485. 2014/05/20. DOI: 10.1002/glia.22694.
46. Volpert OV, Zaichuk T, Zhou W, et al. Inducer-stimulated Fas targets activated endothelium for destruction by anti-angiogenic thrombospondin-1 and pigment epithelium-derived factor. *Nature medicine* 2002; 8: 349-357. 2002/04/03. DOI: 10.1038/nm0402-349.
47. Kociok N and Joussen AM. Varied expression of functionally important genes of RPE and choroid in the macula and in the periphery of normal human eyes. *Graefe's archive for clinical and experimental ophthalmology = Albrecht von Graefes Archiv fur klinische und experimentelle Ophthalmologie* 2007; 245: 101-113. 2006/04/07. DOI: 10.1007/s00417-006-0266-x.
48. Penn JS, Madan A, Caldwell RB, et al. Vascular endothelial growth factor in eye disease. *Prog Retin Eye Res* 2008; 27: 331-371. 2008/07/26. DOI: 10.1016/j.preteyeres.2008.05.001.

49. Pierce EA, Avery RL, Foley ED, et al. Vascular endothelial growth factor/vascular permeability factor expression in a mouse model of retinal neovascularization. *Proc Natl Acad Sci U S A* 1995; 92: 905-909. 1995/01/31. DOI: 10.1073/pnas.92.3.905.
50. Lamoreaux WJ, Fitzgerald MEC, Reiner A, et al. Vascular Endothelial Growth Factor Increases Release of Gelatinase A and Decreases Release of Tissue Inhibitor of Metalloproteinases by Microvascular Endothelial Cellsin Vitro. *Microvascular research* 1998; 55: 29-42. DOI: https://doi.org/10.1006/mvre.1997.2056.
51. Eichler W, Yafai Y, Wiedemann P, et al. Angiogenesis-related factors derived from retinal glial (Müller) cells in hypoxia. *NeuroReport* 2004; 15: 1633-1637. DOI: 10.1097/01.wnr.0000133071.00786.a4.
52. Lindholm D, Castrén E, Kiefer R, et al. Transforming growth factor-beta 1 in the rat brain: increase after injury and inhibition of astrocyte proliferation. *J Cell Biol* 1992; 117: 395-400. 1992/04/01. DOI: 10.1083/jcb.117.2.395.
53. Duan LJ and Fong GH. Developmental vascular pruning in neonatal mouse retinas is programmed by the astrocytic oxygen-sensing mechanism. *Development (Cambridge, England)* 2019; 146 2019/03/27. DOI: 10.1242/dev.175117.
54. Perry VH and Teeling J. Microglia and macrophages of the central nervous system: the contribution of microglia priming and systemic inflammation to chronic neurodegeneration. *Seminars in immunopathology* 2013; 35: 601-612. 2013/06/05. DOI: 10.1007/s00281-013-0382-8.
55. Harada T, Harada C, Kohsaka S, et al. Microglia-Muller glia cell interactions control neurotrophic factor production during light-induced retinal degeneration. *J Neurosci* 2002; 22: 9228-9236. 2002/11/06.
56. Wang M and Wong WT. Microglia-Muller cell interactions in the retina. *Adv Exp Med Biol* 2014; 801: 333-338. 2014/03/26. DOI: 10.1007/978-1-4614-3209-8_42.
57. Lee JE, Liang KJ, Fariss RN, et al. Ex vivo dynamic imaging of retinal microglia using time-lapse confocal microscopy. *Investigative ophthalmology & visual science* 2008; 49: 4169-4176. 2008/05/16. DOI: 10.1167/iovs.08-2076.
58. Claudio L, Martiney JA and Brosnan CF. Ultrastructural studies of the blood-retina barrier after exposure to interleukin-1 beta or tumor necrosis factor-alpha. *Laboratory investigation; a journal of technical methods and pathology* 1994; 70: 850-861. 1994/06/01.
59. Holtkamp GM, Kijlstra A, Peek R, et al. Retinal pigment epithelium-immune system interactions: cytokine production and cytokine-induced changes. *Progress in retinal and eye research* 2001; 20: 29-48. 2000/11/09.
60. Thumann G, Dou G, Wang Y, et al. Retina. In: Ryan S, J. (ed) *Retina*. 3rd ed.: Saunders, 2013, pp.401-414.
61. Snell R, S. and Lemp M, A. *Clinical anatomy of the eye* 2nd ed. Oxford Blackwell science 1998.
62. Zhang HR. Scanning electron-microscopic study of corrosion casts on retinal and choroidal angioarchitecture in man and animals. *Prog Retin Eye Res* 1994; 13: 243-270.
63. Strauss O. The retinal pigment epithelium in visual function. *Physiological reviews* 2005; 85: 845-881. 2005/07/01. DOI: 10.1152/physrev.00021.2004.
64. Bonilha VL. Retinal pigment epithelium (RPE) cytoskeleton in vivo and in vitro. *Experimental eye research* 2014; 126: 38-45. 2013/10/05. DOI: 10.1016/j.exer.2013.09.015.

65. Steinberg RH, Wood I and Hogan MJ. Pigment epithelial ensheathment and phagocytosis of extrafoveal cones in human retina. *Philosophical transactions of the Royal Society of London Series B, Biological sciences* 1977; 277: 459-474. 1977/03/28. DOI: 10.1098/rstb.1977.0028.
66. Marmorstein AD. The polarity of the retinal pigment epithelium. *Traffic (Copenhagen, Denmark)* 2001; 2: 867-872. 2001/12/12.
67. Smith RL, Sivaprasad S and Chong V. Retinal Biochemistry, Physiology and Cell Biology. *Developments in ophthalmology* 2016; 55: 18-27. 2015/10/27. DOI: 10.1159/000431118.
68. Delyfer MN, Leveillard T, Mohand-Said S, et al. Inherited retinal degenerations: therapeutic prospects. *Biology of the cell / under the auspices of the European Cell Biology Organization* 2004; 96: 261-269. 2004/05/18. DOI: 10.1016/j.biolcel.2004.01.006.
69. Plafker SM, O'Mealey GB and Szweda LI. Mechanisms for countering oxidative stress and damage in retinal pigment epithelium. *Int Rev Cell Mol Biol* 2012; 298: 135-177. 2012/08/11. DOI: 10.1016/b978-0-12-394309-5.00004-3.
70. Cook B, Lewis GP, Fisher SK, et al. Apoptotic photoreceptor degeneration in experimental retinal detachment. *Investigative ophthalmology & visual science* 1995; 36: 990-996. 1995/05/01.
71. Mullen RJ and LaVail MM. Inherited retinal dystrophy: primary defect in pigment epithelium determined with experimental rat chimeras. *Science (New York, NY)* 1976; 192: 799-801. 1976/05/21.
72. Ishida K, Panjwani N, Cao Z, et al. Participation of pigment epithelium in ocular immune privilege. 3. Epithelia cultured from iris, ciliary body, and retina suppress T-cell activation by partially non-overlapping mechanisms. *Ocular immunology and inflammation* 2003; 11: 91-105. 2003/10/09.
73. Liversidge J, McKay D, Mullen G, et al. Retinal pigment epithelial cells modulate lymphocyte function at the blood-retina barrier by autocrine PGE2 and membrane-bound mechanisms. *Cellular immunology* 1993; 149: 315-330. 1993/07/01. DOI: 10.1006/cimm.1993.1158.
74. *Macular Edema: Conference Proceedings of the 2nd International Symposium on Macular Edema, Lausanne, 23–25 April 1998*. 1 ed. Netherlands: Springer, 2000.
75. Luna JD, Chan CC, Derevjanik NL, et al. Blood-retinal barrier (BRB) breakdown in experimental autoimmune uveoretinitis: comparison with vascular endothelial growth factor, tumor necrosis factor alpha, and interleukin-1beta-mediated breakdown. *Journal of neuroscience research* 1997; 49: 268-280. 1997/08/01. DOI: 10.1002/(sici)1097-4547(19970801)49:3<268::aid-jnr2>3.0.co;2-a.
76. Maminishkis A, Chen S, Jalickee S, et al. Confluent monolayers of cultured human fetal retinal pigment epithelium exhibit morphology and physiology of native tissue. *Investigative ophthalmology & visual science* 2006; 47: 3612-3624. 2006/08/01. DOI: 10.1167/iovs.05-1622.
77. Dawson D, Volpert O, Gillis P, et al. Pigment epithelium-derived factor: a potent inhibitor of angiogenesis. *Science* 1999; 285: 245-248. DOI: 10.1126/science.285.5425.245
78. Li R, Wen R, Banzon T, et al. CNTF mediates neurotrophic factor secretion and fluid absorption in human retinal pigment epithelium. *PLoS One* 2011; 6: e23148. 2011/09/14. DOI: 10.1371/journal.pone.0023148.

79. Lavail MM. Survival factors for treatment of retinal degenerative disorders: preclinical gains and issues for translation into clinical studies. *Retina* 2005; 25: S25-S26. 2005/12/24.
80. Sheedlo HJ, Nelson TH, Lin N, et al. RPE secreted proteins and antibody influence photoreceptor cell survival and maturation. *Brain Res Dev Brain Res* 1998; 107: 57-69. 1998/05/29.
81. Xiao M, McLeod D, Cranley J, et al. Growth factor staining patterns in the pig retina following retinal laser photocoagulation. *The British journal of ophthalmology* 1999; 83: 728-736. 1999/05/26.
82. Ming M, Li X, Fan X, et al. Retinal pigment epithelial cells secrete neurotrophic factors and synthesize dopamine: possible contribution to therapeutic effects of RPE cell transplantation in Parkinson's disease. *Journal of translational medicine* 2009; 7: 53. 2009/06/30. DOI: 10.1186/1479-5876-7-53.
83. Matsumoto M, Yoshimura N and Honda Y. Increased production of transforming growth factor-beta 2 from cultured human retinal pigment epithelial cells by photocoagulation. *Invest Ophthalmol Vis Sci* 1994; 35: 4245-4252. 1994/12/01.
84. Campochiaro PA, Sugg R, Grotendorst G, et al. Retinal pigment epithelial cells produce PDGF-like proteins and secrete them into their media. *Exp Eye Res* 1989; 49: 217-227. 1989/08/01. DOI: 10.1016/0014-4835(89)90092-4.
85. Takagi H, King GL, Robinson GS, et al. Adenosine mediates hypoxic induction of vascular endothelial growth factor in retinal pericytes and endothelial cells. *Invest Ophthalmol Vis Sci* 1996; 37: 2165-2176. 1996/10/01.
86. Aiello LP, Northrup JM, Keyt BA, et al. Hypoxic Regulation of Vascular Endothelial Growth Factor in Retinal Cells. *Archives of ophthalmology* 1995; 113: 1538-1544. DOI: 10.1001/archopht.1995.01100120068012.
87. Otani A, Takagi H, Oh H, et al. Expressions of angiopoietins and Tie2 in human choroidal neovascular membranes. *Investigative ophthalmology & visual science* 1999; 40: 1912-1920. 1999/08/10.
88. Oh H, Takagi H, Takagi C, et al. The potential angiogenic role of macrophages in the formation of choroidal neovascular membranes. *Investigative ophthalmology & visual science* 1999; 40: 1891-1898. 1999/08/10.
89. Shibuya M. Vascular Endothelial Growth Factor (VEGF) and Its Receptor (VEGFR) Signaling in Angiogenesis: A Crucial Target for Anti- and Pro-Angiogenic Therapies. *Genes Cancer* 2011; 2: 1097-1105. 2012/08/07. DOI: 10.1177/1947601911423031.
90. Jussila L, Valtola R, Partanen TA, et al. Lymphatic endothelium and Kaposi's sarcoma spindle cells detected by antibodies against the vascular endothelial growth factor receptor-3. *Cancer research* 1998; 58: 1599-1604. 1998/05/01.
91. Lutty GA, Mathews MK, Merges C, et al. Adenosine stimulates canine retinal microvascular endothelial cell migration and tube formation. *Curr Eye Res* 1998; 17: 594-607. 1998/07/15.
92. Lee S, Chen TT, Barber CL, et al. Autocrine VEGF signaling is required for vascular homeostasis. *Cell* 2007; 130: 691-703. 2007/08/28. DOI: 10.1016/j.cell.2007.06.054.
93. Keyt BA, Berleau LT, Nguyen HV, et al. The carboxyl-terminal domain (111-165) of vascular endothelial growth factor is critical for its mitogenic potency. *The Journal of biological chemistry* 1996; 271: 7788-7795. 1996/03/29. DOI: 10.1074/jbc.271.13.7788.

94. Saint-Geniez M, Maldonado AE and D'Amore PA. VEGF expression and receptor activation in the choroid during development and in the adult. *Invest Ophthalmol Vis Sci* 2006; 47: 3135-3142. 2006/06/27. DOI: 10.1167/iovs.05-1229.
95. Shibuya M. Vascular endothelial growth factor and its receptor system: physiological functions in angiogenesis and pathological roles in various diseases. *J Biochem* 2013; 153: 13-19. 2012/11/23. DOI: 10.1093/jb/mvs136.
96. Millauer B, Wizigmann-Voos S, Schnurch H, et al. High affinity VEGF binding and developmental expression suggest Flk-1 as a major regulator of vasculogenesis and angiogenesis. *Cell* 1993; 72: 835-846. 1993/03/26. DOI: 10.1016/0092-8674(93)90573-9.
97. Feng Y, Venema VJ, Venema RC, et al. VEGF-induced permeability increase is mediated by caveolae. *Invest Ophthalmol Vis Sci* 1999; 40: 157-167. 1999/01/15.
98. Sundstrom JM, Tash BR, Murakami T, et al. Identification and analysis of occludin phosphosites: a combined mass spectrometry and bioinformatics approach. *Journal of proteome research* 2009; 8: 808-817. DOI: 10.1021/pr7007913.
99. Suzuki T, Elias BC, Seth A, et al. PKC eta regulates occludin phosphorylation and epithelial tight junction integrity. *Proceedings of the National Academy of Sciences of the United States of America* 2009; 106: 61-66. 2008/12/31. DOI: 10.1073/pnas.0802741106.
100. Senger DR, Connolly DT, Van De Water L, et al. Purification and NH2-terminal amino acid sequence of guinea pig tumor-secreted vascular permeability factor. *Cancer research* 1990; 50: 1774-1778.
101. Bhutto IA, McLeod DS, Hasegawa T, et al. Pigment epithelium-derived factor (PEDF) and vascular endothelial growth factor (VEGF) in aged human choroid and eyes with age-related macular degeneration. *Experimental eye research* 2006; 82: 99-110. 2005/07/16. DOI: 10.1016/j.exer.2005.05.007.
102. Martin G, Schlunck G, Hansen LL, et al. Differential expression of angioregulatory factors in normal and CNV-derived human retinal pigment epithelium. *Graefe's archive for clinical and experimental ophthalmology = Albrecht von Graefes Archiv fur klinische und experimentelle Ophthalmologie* 2004; 242: 321-326. 2004/01/15. DOI: 10.1007/s00417-003-0838-y.
103. Tang J and Kern TS. Inflammation in diabetic retinopathy. *Progress in retinal and eye research* 2011; 30: 343-358. 2011/06/04. DOI: 10.1016/j.preteyeres.2011.05.002.
104. Ohno-Matsui K, Morita I, Tombran-Tink J, et al. Novel mechanism for age-related macular degeneration: an equilibrium shift between the angiogenesis factors VEGF and PEDF. *Journal of cellular physiology* 2001; 189: 323-333. 2001/12/19. DOI: 10.1002/jcp.10026.
105. Notari L, Miller A, Martinez A, et al. Pigment epithelium-derived factor is a substrate for matrix metalloproteinase type 2 and type 9: implications for downregulation in hypoxia. *Investigative ophthalmology & visual science* 2005; 46: 2736-2747. 2005/07/27. DOI: 10.1167/iovs.04-1489.
106. Gao G, Li Y, Zhang D, et al. Unbalanced expression of VEGF and PEDF in ischemia-induced retinal neovascularization. *FEBS letters* 2001; 489: 270-276. 2001/02/13. DOI: 10.1016/s0014-5793(01)02110-x.
107. Spranger J, Osterhoff M, Reimann M, et al. Loss of the Antiangiogenic Pigment Epithelium-Derived Factor in Patients With Angiogenic Eye Disease. *Diabetes* 2001; 50: 2641-2645. DOI: 10.2337/diabetes.50.12.2641.

108. King GL and Suzuma K. Pigment-epithelium-derived factor--a key coordinator of retinal neuronal and vascular functions. *The New England journal of medicine* 2000; 342: 349-351. 2000/02/03. DOI: 10.1056/nejm200002033420511.
109. Becerra SP. Structure-function studies on PEDF. A noninhibitory serpin with neurotrophic activity. *Adv Exp Med Biol* 1997; 425: 223-237. 1997/01/01.
110. Tombran-Tink J, Chader GG and Johnson LV. PEDF: a pigment epithelium-derived factor with potent neuronal differentiative activity. *Exp Eye Res* 1991; 53: 411-414. 1991/09/01. DOI: 10.1016/0014-4835(91)90248-d.
111. Yafai Y, Lange J, Wiedemann P, et al. Pigment epithelium-derived factor acts as an opponent of growth-stimulatory factors in retinal glial-endothelial cell interactions. *Glia* 2007; 55: 642-651. 2007/02/20. DOI: 10.1002/glia.20495.
112. SERPINF1 serpin family F member 1 [Homo sapiens]. *National Centre Biotechnology Information*. Genebank: National Library of Medicine., 2016.
113. Taniwaki T, Hirashima N, Becerra SP, et al. Pigment epithelium-derived factor protects cultured cerebellar granule cells against glutamate-induced neurotoxicity. *J Neurochem* 1997; 68: 26-32. 1997/01/01. DOI: 10.1046/j.1471-4159.1997.68010026.x.
114. Steele FR, Chader GJ, Johnson LV, et al. Pigment epithelium-derived factor: neurotrophic activity and identification as a member of the serine protease inhibitor gene family. *Proc Natl Acad Sci U S A* 1993; 90: 1526-1530. 1993/02/15. DOI: 10.1073/pnas.90.4.1526.
115. Carmeliet P and Jain RK. Angiogenesis in cancer and other diseases. *Nature* 2000; 407: 249-257. 2000/09/23. DOI: 10.1038/35025220.
116. Zhang SX and Ma JX. Ocular neovascularization: Implication of endogenous angiogenic inhibitors and potential therapy. *Progress in retinal and eye research* 2007; 26: 1-37. 2006/11/01. DOI: 10.1016/j.preteyeres.2006.09.002.
117. Witmer AN, Vrensen GF, Van Noorden CJ, et al. Vascular endothelial growth factors and angiogenesis in eye disease. *Progress in retinal and eye research* 2003; 22: 1-29. 2003/02/25.
118. Bhutto I and Lutty G. Understanding age-related macular degeneration (AMD): relationships between the photoreceptor/retinal pigment epithelium/Bruch's membrane/choriocapillaris complex. *Molecular aspects of medicine* 2012; 33: 295-317. 2012/05/01. DOI: 10.1016/j.mam.2012.04.005.
119. Das A, McGuire P, Eriqat C, et al. Human diabetic neovascular membranes contain high levels of urokinase and metalloproteinase enzymes. *Invest Ophthalmol Vis Sci* 1999; 40: 809-813. 1999/03. DOI: https://doi.org/.
120. Matrisian LM. Metalloproteinases and their inhibitors in matrix remodeling. *Trends in genetics : TIG* 1990; 6: 121-125. 1990/04/01.
121. Sethi CS, Bailey TA, Luthert PJ, et al. Matrix metalloproteinase biology applied to vitreoretinal disorders. *The British journal of ophthalmology* 2000; 84: 654-666. 2000/06/06. DOI: 10.1136/bjo.84.6.654.
122. Steen B, Sejersen S, Berglin L, et al. Matrix metalloproteinases and metalloproteinase inhibitors in choroidal neovascular membranes. *Investigative ophthalmology & visual science* 1998; 39: 2194-2200. 1998/10/07.
123. Berglin L, Sarman S, van der Ploeg I, et al. Reduced choroidal neovascular membrane formation in matrix metalloproteinase-2-deficient mice. *Investigative ophthalmology & visual science* 2003; 44: 403-408. 2002/12/31. DOI: 10.1167/iovs.02-0180.

124. Murphy AN, Unsworth EJ and Stetler-Stevenson WG. Tissue inhibitor of metalloproteinases-2 inhibits bFGF-induced human microvascular endothelial cell proliferation. *Journal of cellular physiology* 1993; 157: 351-358. 1993/11/01. DOI: 10.1002/jcp.1041570219.
125. Anand-Apte B, Pepper MS, Voest E, et al. Inhibition of angiogenesis by tissue inhibitor of metalloproteinase-3. *Investigative ophthalmology & visual science* 1997; 38: 817-823. 1997/04/01.
126. Qi JH, Ebrahem Q, Ali M, et al. Tissue inhibitor of metalloproteinases-3 peptides inhibit angiogenesis and choroidal neovascularization in mice. *PLoS One* 2013; 8: e55667. 2013/03/08. DOI: 10.1371/journal.pone.0055667.
127. Christensen DRG, Brown FE, Cree AJ, et al. Sorsby fundus dystrophy - A review of pathology and disease mechanisms. *Exp Eye Res* 2017; 165: 35-46. 2017/08/30. DOI: 10.1016/j.exer.2017.08.014.
128. Qi JH, Ebrahem Q, Moore N, et al. A novel function for tissue inhibitor of metalloproteinases-3 (TIMP3): inhibition of angiogenesis by blockage of VEGF binding to VEGF receptor-2. *Nature medicine* 2003; 9: 407-415. DOI: 10.1038/nm846.
129. Della NG, Campochiaro PA and Zack DJ. Localization of TIMP-3 mRNA expression to the retinal pigment epithelium. *Invest Ophthalmol Vis Sci* 1996; 37: 1921-1924. 1996/08/01.
130. Ruiz A, Brett P and Bok D. TIMP-3 is expressed in the human retinal pigment epithelium. *Biochemical and biophysical research communications* 1996; 226: 467-474. 1996/09/13. DOI: 10.1006/bbrc.1996.1379.
131. Kamei M and Hollyfield JG. TIMP-3 in Bruch's Membrane: Changes during Aging and in Age-Related Macular Degeneration. *Investigative Ophthalmology & Visual Science* 1999; 40: 2367-2375.
132. Bringmann A, Reichenbach A and Wiedemann P. Pathomechanisms of Cystoid Macular Edema. *Ophthalmic Research* 2004; 36: 241-249.
133. Causes of blindness and vision impairment in 2020 and trends over 30 years, and prevalence of avoidable blindness in relation to VISION 2020: the Right to Sight: an analysis for the Global Burden of Disease Study. *The Lancet Global health* 2021; 9: e144-e160. 2020/12/05. DOI: 10.1016/s2214-109x(20)30489-7.
134. Resnikoff S, Pascolini D, Etya'ale D, et al. Global data on visual impairment in the year 2002. *Bulletin of the World Health Organization* 2004; 82: 844-851. 2005/01/11. DOI: /S0042-96862004001100009.
135. Wong WL, Su X, Li X, et al. Global prevalence of age-related macular degeneration and disease burden projection for 2020 and 2040: a systematic review and meta-analysis. *The Lancet Global health* 2014; 2: e106-116. 2014/08/12. DOI: 10.1016/s2214-109x(13)70145-1.
136. Brody BL, Gamst AC, Williams RA, et al. Depression, visual acuity, comorbidity, and disability associated with age-related macular degeneration. *Ophthalmology* 2001; 108: 1893-1900; discussion 1900-1891. 2001/10/03.
137. Casten RJ and Rovner BW. Update on depression and age-related macular degeneration. *Current opinion in ophthalmology* 2013; 24: 239-243. 2013/02/23. DOI: 10.1097/ICU.0b013e32835f8e55.
138. The Age-Related Eye Disease Study (AREDS): design implications. AREDS report no. 1. *Controlled clinical trials* 1999; 20: 573-600. 1999/12/10.

139. Fine SL, Berger JW, Maguire MG, et al. Age-related macular degeneration. *The New England journal of medicine* 2000; 342: 483-492. 2000/02/17. DOI: 10.1056/nejm200002173420707.
140. McConnell V and Silvestri G. Age-related macular degeneration. *The Ulster medical journal* 2005; 74: 82-92. 2005/10/21.
141. Bressler NM, Bressler SB and Fine SL. Age-related macular degeneration. *Survey of ophthalmology* 1988; 32: 375-413. 1988/05/01.
142. Chew EY, Clemons TE, Agron E, et al. Ten-year follow-up of age-related macular degeneration in the age-related eye disease study: AREDS report no. 36. *JAMA ophthalmology* 2014; 132: 272-277. 2014/01/05. DOI: 10.1001/jamaophthalmol.2013.6636.
143. Nowak JZ. AMD--the retinal disease with an unprecised etiopathogenesis: in search of effective therapeutics. *Acta poloniae pharmaceutica* 2014; 71: 900-916. 2015/03/10.
144. Mitchell P, Liew G, Gopinath B, et al. Age-related macular degeneration. *Lancet (London, England)* 2018; 392: 1147-1159. 2018/10/12. DOI: 10.1016/s0140-6736(18)31550-2.
145. Celkova L, Doyle SL and Campbell M. NLRP3 Inflammasome and Pathobiology in AMD. *Journal of clinical medicine* 2015; 4: 172-192. 2015/08/04. DOI: 10.3390/jcm4010172.
146. Kaneko H, Dridi S, Tarallo V, et al. DICER1 deficit induces Alu RNA toxicity in age-related macular degeneration. *Nature* 2011; 471: 325-330. 2011/02/08. DOI: 10.1038/nature09830.
147. Campochiaro PA. Molecular pathogenesis of retinal and choroidal vascular diseases. *Progress in retinal and eye research* 2015; 49: 67-81. 2015/06/27. DOI: 10.1016/j.preteyeres.2015.06.002.
148. Whitmore SS, Sohn EH, Chirco KR, et al. Complement activation and choriocapillaris loss in early AMD: implications for pathophysiology and therapy. *Progress in retinal and eye research* 2015; 45: 1-29. 2014/12/09. DOI: 10.1016/j.preteyeres.2014.11.005.
149. Chao CC, Hu S and Peterson PK. Glia, cytokines, and neurotoxicity. *Crit Rev Neurobiol* 1995; 9: 189-205. 1995/01/01.
150. Kim SU and de Vellis J. Microglia in health and disease. *Journal of neuroscience research* 2005; 81: 302-313. 2005/06/15. DOI: 10.1002/jnr.20562.
151. Ma W, Zhao L, Fontainhas AM, et al. Microglia in the mouse retina alter the structure and function of retinal pigmented epithelial cells: a potential cellular interaction relevant to AMD. *PloS one* 2009; 4: e7945-e7945. DOI: 10.1371/journal.pone.0007945.
152. Gupta N, Brown KE and Milam AH. Activated microglia in human retinitis pigmentosa, late-onset retinal degeneration, and age-related macular degeneration. *Experimental Eye Research* 2003; 76: 463-471. DOI: https://doi.org/10.1016/S0014-4835(02)00332-9.
153. Cao X, Shen D, Patel MM, et al. Macrophage polarization in the maculae of age-related macular degeneration: a pilot study. *Pathology international* 2011; 61: 528-535. 2011/09/03. DOI: 10.1111/j.1440-1827.2011.02695.x.
154. Mattson MP, Dou P and Kater SB. Outgrowth-regulating actions of glutamate in isolated hippocampal pyramidal neurons. *J Neurosci* 1988; 8: 2087-2100. 1988/06/01. DOI: 10.1523/jneurosci.08-06-02087.1988.

155. Mattson MP, Kumar KN, Wang H, et al. Basic FGF regulates the expression of a functional 71 kDa NMDA receptor protein that mediates calcium influx and neurotoxicity in hippocampal neurons. *The Journal of neuroscience : the official journal of the Society for Neuroscience* 1993; 13: 4575-4588. DOI: 10.1523/JNEUROSCI.13-11-04575.1993.
156. Qian L, Wei SJ, Zhang D, et al. Potent anti-inflammatory and neuroprotective effects of TGF-beta1 are mediated through the inhibition of ERK and p47phox-Ser345 phosphorylation and translocation in microglia. *Journal of immunology (Baltimore, Md : 1950)* 2008; 181: 660-668. 2008/06/21. DOI: 10.4049/jimmunol.181.1.660.
157. Zhu Y, Yang G-Y, Ahlemeyer B, et al. Transforming growth factor-beta 1 increases bad phosphorylation and protects neurons against damage. *The Journal of neuroscience : the official journal of the Society for Neuroscience* 2002; 22: 3898-3909. DOI: 10.1523/JNEUROSCI.22-10-03898.2002.
158. Ruocco A, Nicole O, Docagne F, et al. A transforming growth factor-beta antagonist unmasks the neuroprotective role of this endogenous cytokine in excitotoxic and ischemic brain injury. *Journal of cerebral blood flow and metabolism : official journal of the International Society of Cerebral Blood Flow and Metabolism* 1999; 19: 1345-1353. 1999/12/22. DOI: 10.1097/00004647-199912000-00008.
159. Prehn JH, Bindokas VP, Marcuccilli CJ, et al. Regulation of neuronal Bcl2 protein expression and calcium homeostasis by transforming growth factor type beta confers wide-ranging protection on rat hippocampal neurons. *Proc Natl Acad Sci U S A* 1994; 91: 12599-12603. 1994/12/20. DOI: 10.1073/pnas.91.26.12599.
160. Vecino E, Caminos E, Ugarte M, et al. Immunohistochemical Distribution of Neurotrophins and their Receptors in the Rat Retina and the Effects of Ischemia and Reperfusion*. *General Pharmacology: The Vascular System* 1998; 30: 305-314. DOI: https://doi.org/10.1016/S0306-3623(97)00361-3.
161. LaVail MM, Unoki K, Yasumura D, et al. Multiple growth factors, cytokines, and neurotrophins rescue photoreceptors from the damaging effects of constant light. *Proc Natl Acad Sci U S A* 1992; 89: 11249-11253. 1992/12/01.
162. Wang Y, Abu-Asab MS, Yu CR, et al. Platelet-derived growth factor (PDGF)-C inhibits neuroretinal apoptosis in a murine model of focal retinal degeneration. *Laboratory investigation; a journal of technical methods and pathology* 2014; 94: 674-682. 2014/04/09. DOI: 10.1038/labinvest.2014.60.
163. Tang Z, Arjunan P, Lee C, et al. Survival effect of PDGF-CC rescues neurons from apoptosis in both brain and retina by regulating GSK3beta phosphorylation. *The Journal of experimental medicine* 2010; 207: 867-880. 2010/03/15. DOI: 10.1084/jem.20091704.
164. Siliprandi R, Canella R and Carmignoto G. Nerve growth factor promotes functional recovery of retinal ganglion cells after ischemia. *Invest Ophthalmol Vis Sci* 1993; 34: 3232-3245. 1993/11/01.
165. Elkabes S, DiCicco-Bloom EM and Black IB. Brain microglia/macrophages express neurotrophins that selectively regulate microglial proliferation and function. *J Neurosci* 1996; 16: 2508-2521. 1996/04/15. DOI: 10.1523/jneurosci.16-08-02508.1996.
166. Shimojo M, Nakajima K, Takei N, et al. Production of basic fibroblast growth factor in cultured rat brain microglia. *Neuroscience Letters* 1991; 123: 229-231. DOI: https://doi.org/10.1016/0304-3940(91)90937-O.

167. Mantovani A, Sica A, Sozzani S, et al. The chemokine system in diverse forms of macrophage activation and polarization. *Trends Immunol* 2004; 25: 677-686. 2004/11/09. DOI: 10.1016/j.it.2004.09.015.
168. Steinberg RH. Survival factors in retinal degenerations. *Current opinion in neurobiology* 1994; 4: 515-524. 1994/08/01.
169. LaVail MM, Yasumura D, Matthes MT, et al. Protection of mouse photoreceptors by survival factors in retinal degenerations. *Investigative ophthalmology & visual science* 1998; 39: 592-602. 1998/03/21.
170. Wahlin KJ, Campochiaro PA, Zack DJ, et al. Neurotrophic Factors Cause Activation of Intracellular Signaling Pathways in Müller Cells and Other Cells of the Inner Retina, but Not Photoreceptors. *Investigative Ophthalmology & Visual Science* 2000; 41: 927-936.
171. Kirsch M, Lee MY, Meyer V, et al. Evidence for multiple, local functions of ciliary neurotrophic factor (CNTF) in retinal development: expression of CNTF and its receptors and in vitro effects on target cells. *J Neurochem* 1997; 68: 979-990. 1997/03/01. DOI: 10.1046/j.1471-4159.1997.68030979.x.
172. Tian C, Weng CC and Yin ZQ. BDNF improves the efficacy ERG amplitude maintenance by transplantation of retinal stem cells in RCS rats. *Advances in experimental medicine and biology* 2010; 664: 375-384. 2010/03/20. DOI: 10.1007/978-1-4419-1399-9_43.
173. Weber AJ, Viswanathan S, Ramanathan C, et al. Combined application of BDNF to the eye and brain enhances ganglion cell survival and function in the cat after optic nerve injury. *Investigative ophthalmology & visual science* 2010; 51: 327-334. 2009/08/28. DOI: 10.1167/iovs.09-3740.
174. Ren R, Li Y, Liu Z, et al. Long-term rescue of rat retinal ganglion cells and visual function by AAV-mediated BDNF expression after acute elevation of intraocular pressure. *Investigative ophthalmology & visual science* 2012; 53: 1003-1011. 2012/01/17. DOI: 10.1167/iovs.11-8484.
175. Frasson M, Picaud S, Leveillard T, et al. Glial cell line-derived neurotrophic factor induces histologic and functional protection of rod photoreceptors in the rd/rd mouse. *Investigative ophthalmology & visual science* 1999; 40: 2724-2734. 1999/10/06.
176. Liu C, Peng M, Laties AM, et al. Preconditioning with bright light evokes a protective response against light damage in the rat retina. *The Journal of neuroscience : the official journal of the Society for Neuroscience* 1998; 18: 1337-1344. 1998/03/14.
177. Murakami Y, Ikeda Y, Yonemitsu Y, et al. Inhibition of nuclear translocation of apoptosis-inducing factor is an essential mechanism of the neuroprotective activity of pigment epithelium-derived factor in a rat model of retinal degeneration. *Am J Pathol* 2008; 173: 1326-1338. 2008/10/11. DOI: 10.2353/ajpath.2008.080466.
178. Cao W, Tombran-Tink J, Elias R, et al. In vivo protection of photoreceptors from light damage by pigment epithelium-derived factor. *Investigative ophthalmology & visual science* 2001; 42: 1646-1652. 2001/05/31.
179. Cao W, Tombran-Tink J, Chen W, et al. Pigment epithelium-derived factor protects cultured retinal neurons against hydrogen peroxide-induced cell death. *Journal of neuroscience research* 1999; 57: 789-800. 1999/09/01.
180. Huang PC, Gaitan AE, Hao Y, et al. Cellular interactions implicated in the mechanism of photoreceptor degeneration in transgenic mice expressing a mutant rhodopsin gene. *Proc Natl Acad Sci U S A* 1993; 90: 8484-8488. 1993/09/15. DOI: 10.1073/pnas.90.18.8484.

181. Harada T, Harada C, Nakayama N, et al. Modification of Glial–Neuronal Cell Interactions Prevents Photoreceptor Apoptosis during Light-Induced Retinal Degeneration. *Neuron* 2000; 26: 533-541. DOI: https://doi.org/10.1016/S0896-6273(00)81185-X.
182. de Hoz R, Rojas B, Ramírez AI, et al. Retinal Macroglial Responses in Health and Disease. *BioMed research international* 2016; 2016: 2954721-2954721. 2016/05/18. DOI: 10.1155/2016/2954721.
183. Lee YB, Nagai A and Kim SU. Cytokines, chemokines, and cytokine receptors in human microglia. *Journal of neuroscience research* 2002; 69: 94-103. DOI: https://doi.org/10.1002/jnr.10253.
184. Conedera FM, Pousa AMQ, Mercader N, et al. Retinal microglia signaling affects Müller cell behavior in the zebrafish following laser injury induction. *Glia* 2019; 67: 1150-1166. 2019/02/23. DOI: 10.1002/glia.23601.
185. Wang M, Ma W, Zhao L, et al. Adaptive Müller cell responses to microglial activation mediate neuroprotection and coordinate inflammation in the retina. *Journal of neuroinflammation* 2011; 8: 173. DOI: 10.1186/1742-2094-8-173.
186. Luhmann UF, Robbie S, Munro PM, et al. The drusenlike phenotype in aging Ccl2-knockout mice is caused by an accelerated accumulation of swollen autofluorescent subretinal macrophages. *Investigative ophthalmology & visual science* 2009; 50: 5934-5943. 2009/07/07. DOI: 10.1167/iovs.09-3462.
187. Sakurai E, Anand A, Ambati BK, et al. Macrophage depletion inhibits experimental choroidal neovascularization. *Investigative ophthalmology & visual science* 2003; 44: 3578-3585. 2003/07/29. DOI: 10.1167/iovs.03-0097.
188. Tsutsumi C, Sonoda KH, Egashira K, et al. The critical role of ocular-infiltrating macrophages in the development of choroidal neovascularization. *Journal of leukocyte biology* 2003; 74: 25-32. 2003/07/02. DOI: 10.1189/jlb.0902436.
189. Fong Y, Tracey KJ, Moldawer LL, et al. Antibodies to cachectin/tumor necrosis factor reduce interleukin 1 beta and interleukin 6 appearance during lethal bacteremia. *The Journal of experimental medicine* 1989; 170: 1627-1633. 1989/11/01. DOI: 10.1084/jem.170.5.1627.
190. Bamforth SD, Lightman S and Greenwood J. The effect of TNF-alpha and IL-6 on the permeability of the rat blood-retinal barrier in vivo. *Acta Neuropathol* 1996; 91: 624-632. 1996/01/01. DOI: 10.1007/s004010050476.
191. de Vries HE, Blom-Roosemalen MC, van Oosten M, et al. The influence of cytokines on the integrity of the blood-brain barrier in vitro. *Journal of neuroimmunology* 1996; 64: 37-43. 1996/01/01. DOI: 10.1016/0165-5728(95)00148-4.
192. Hangai M, Yoshimura N, Yoshida M, et al. Interleukin-1 gene expression in transient retinal ischemia in the rat. *Invest Ophthalmol Vis Sci* 1995; 36: 571-578. 1995/03/01.
193. Bamforth SD, Lightman SL and Greenwood J. Ultrastructural analysis of interleukin-1 beta-induced leukocyte recruitment to the rat retina. *Invest Ophthalmol Vis Sci* 1997; 38: 25-35. 1997/01/01.
194. Burke-Gaffeyy A and Keenan AK. Modulation of human endothelial cell permeability by combinations of the cytokines interleukin-1 α/β, tumor necrosis factor-α and interferon-γ. *Immunopharmacology* 1993; 25: 1-9. DOI: https://doi.org/10.1016/0162-3109(93)90025-L.

195. Cotran RS and Pober JS. Cytokine-endothelial interactions in inflammation, immunity, and vascular injury. *J Am Soc Nephrol* 1990; 1: 225-235. 1990/09/01. DOI: 10.1681/asn.V13225.
196. Cotinet A, Goureau O, Hicks D, et al. Tumor necrosis factor and nitric oxide production by retinal Muller glial cells from rats exhibiting inherited retinal dystrophy. *Glia* 1997; 20: 59-69. 1997/05/01.
197. Yoshida S, Ono M, Shono T, et al. Involvement of interleukin-8, vascular endothelial growth factor, and basic fibroblast growth factor in tumor necrosis factor alpha-dependent angiogenesis. *Molecular and cellular biology* 1997; 17: 4015-4023. 1997/07/01. DOI: 10.1128/mcb.17.7.4015.
198. Giraudo E, Primo L, Audero E, et al. Tumor necrosis factor-alpha regulates expression of vascular endothelial growth factor receptor-2 and of its co-receptor neuropilin-1 in human vascular endothelial cells. *The Journal of biological chemistry* 1998; 273: 22128-22135. 1998/08/15. DOI: 10.1074/jbc.273.34.22128.
199. Calleja S, Cordero-Coma M, Rodriguez E, et al. Adalimumab specifically induces CD3(+) CD4(+) CD25(high) Foxp3(+) CD127(-) T-regulatory cells and decreases vascular endothelial growth factor plasma levels in refractory immuno-mediated uveitis: a non-randomized pilot intervention study. *Eye (London, England)* 2012; 26: 468-477. 2012/01/10. DOI: 10.1038/eye.2011.320.
200. Boyer DS, Schmidt-Erfurth U, van Lookeren Campagne M, et al. The pathophysiology of geographic atrophy secondary to age-related macular degeneration and the complement pathway as a therapeutic target. *Retina (Philadelphia, Pa)* 2017; 37: 819-835. 2016/12/03. DOI: 10.1097/iae.0000000000001392.
201. Jensen EG, Jakobsen TS, Thiel S, et al. Associations between the Complement System and Choroidal Neovascularization in Wet Age-Related Macular Degeneration. *International journal of molecular sciences* 2020; 21: 9752. DOI: 10.3390/ijms21249752.
202. Kaushal S, Grossi F, Francois C, et al. Complement C3 inhibitor POT-4: Clinical Safety of Intravitreal Administration. *Investigative Ophthalmology & Visual Science* 2009; 50: 5010-5010.
203. Grossi F. Assessment of Safety, Tolerability and Pharmacokinetics of Intravitreal Pegcetacoplan (APL-2) for Patients With Wet AMD (ASAP II), https://clinicaltrials.gov/ct2/show/study/NCT02461771 (2020).
204. Grossi F. Study of Pegcetacoplan (APL-2) Therapy in Patients With Geographic Atrophy (FILLY), https://clinicaltrials.gov/ct2/show/NCT02503332 (2020).
205. Hosseini M. A Multicenter, Proof-Of-Concept Study Of Intravitreal AL-78898A In Patients With Geographic Atrophy (GA) Associated With Age-Related Macular Degeneration (AMD), https://clinicaltrials.gov/ct2/show/NCT01603043 (2014).
206. Grossi F. Pegcetacoplan (APL-2) in Neovascular AMD, https://clinicaltrials.gov/ct2/show/NCT03465709 (2020).
207. (U.S.) NLoM. A Study to Compare the Efficacy and Safety of Intravitreal APL-2 Therapy With Sham Injections in Patients With Geographic Atrophy (GA) Secondary to Age-Related Macular Degeneration, https://clinicaltrials.gov/ct2/show/NCT03525613 (2022).
208. Bora PS, Sohn JH, Cruz JM, et al. Role of complement and complement membrane attack complex in laser-induced choroidal neovascularization. *Journal of immunology (Baltimore, Md : 1950)* 2005; 174: 491-497. 2004/12/22. DOI: 10.4049/jimmunol.174.1.491.

209. Bora NS, Kaliappan S, Jha P, et al. Complement activation via alternative pathway is critical in the development of laser-induced choroidal neovascularization: role of factor B and factor H. *Journal of immunology (Baltimore, Md : 1950)* 2006; 177: 1872-1878. 2006/07/20.
210. Nozaki M, Raisler BJ, Sakurai E, et al. Drusen complement components C3a and C5a promote choroidal neovascularization. *Proceedings of the National Academy of Sciences of the United States of America* 2006; 103: 2328-2333. 2006/02/03. DOI: 10.1073/pnas.0408835103.
211. Gold B, Merriam JE, Zernant J, et al. Variation in factor B (BF) and complement component 2 (C2) genes is associated with age-related macular degeneration. *Nature genetics* 2006; 38: 458-462. 2006/03/07. DOI: 10.1038/ng1750.
212. Yu JJ, Agron E, Clemons TE, et al. Natural History of Drusenoid Pigment Epithelial Detachment Associated with Age-Related Macular Degeneration: Age-Related Eye Disease Study 2 Report No. 17. *Ophthalmology* 2019; 126: 261-273. 2018/08/25. DOI: 10.1016/j.ophtha.2018.08.017.
213. Lorés-Motta L, Paun CC, Corominas J, et al. Genome-Wide Association Study Reveals Variants in CFH and CFHR4 Associated with Systemic Complement Activation: Implications in Age-Related Macular Degeneration. *Ophthalmology* 2018; 125: 1064-1074. 2018/02/06. DOI: 10.1016/j.ophtha.2017.12.023.
214. Scholl HP, Charbel Issa P, Walier M, et al. Systemic complement activation in age-related macular degeneration. *PLoS One* 2008; 3: e2593. 2008/07/04. DOI: 10.1371/journal.pone.0002593.
215. Smailhodzic D, Klaver CCW, Klevering BJ, et al. Risk Alleles in CFH and ARMS2 Are Independently Associated with Systemic Complement Activation in Age-related Macular Degeneration. *Ophthalmology* 2012; 119: 339-346. DOI: 10.1016/j.ophtha.2011.07.056.
216. Ristau T, Paun C, Ersoy L, et al. Impact of the common genetic associations of age-related macular degeneration upon systemic complement component C3d levels. *PloS one* 2014; 9: e93459-e93459. DOI: 10.1371/journal.pone.0093459.
217. Lechner J, Chen M, Hogg RE, et al. Higher plasma levels of complement C3a, C4a and C5a increase the risk of subretinal fibrosis in neovascular age-related macular degeneration: Complement activation in AMD. *Immunity & ageing : I & A* 2016; 13: 4. 2016/02/18. DOI: 10.1186/s12979-016-0060-5.
218. Reynolds R, Hartnett ME, Atkinson JP, et al. Plasma complement components and activation fragments: associations with age-related macular degeneration genotypes and phenotypes. *Invest Ophthalmol Vis Sci* 2009; 50: 5818-5827. 2009/08/08. DOI: 10.1167/iovs.09-3928.
219. Sivaprasad S, Adewoyin T, Bailey TA, et al. Estimation of Systemic Complement C3 Activity in Age-Related Macular Degeneration. *Archives of ophthalmology* 2007; 125: 515-519. DOI: 10.1001/archopht.125.4.515.
220. Ballinger SW, Van Houten B, Jin GF, et al. Hydrogen peroxide causes significant mitochondrial DNA damage in human RPE cells. *Experimental eye research* 1999; 68: 765-772. 1999/06/22. DOI: 10.1006/exer.1998.0661.
221. King A, Gottlieb E, Brooks DG, et al. Mitochondria-derived reactive oxygen species mediate blue light-induced death of retinal pigment epithelial cells. *Photochemistry and photobiology* 2004; 79: 470-475. 2004/06/12.

222. Godley BF, Shamsi FA, Liang FQ, et al. Blue light induces mitochondrial DNA damage and free radical production in epithelial cells. *The Journal of biological chemistry* 2005; 280: 21061-21066. 2005/03/31. DOI: 10.1074/jbc.M502194200.
223. Chen Y and Chen C. Corilagin prevents tert-butyl hydroperoxide-induced oxidative stress injury in cultured N9 murine microglia cells. *Neurochemistry International* 2011; 59: 290-296. DOI: https://doi.org/10.1016/j.neuint.2011.05.020.
224. Gille JJP and Joenje H. Cell culture models for oxidative stress: superoxide and hydrogen peroxide versus normobaric hyperoxia. *Mutation Research/DNAging* 1992; 275: 405-414. DOI: https://doi.org/10.1016/0921-8734(92)90043-O.
225. Sarks SH. Ageing and degeneration in the macular region: a clinico-pathological study. *The British journal of ophthalmology* 1976; 60: 324-341. 1976/05/01. DOI: 10.1136/bjo.60.5.324.
226. Moore DJ and Clover GM. The effect of age on the macromolecular permeability of human Bruch's membrane. *Investigative ophthalmology & visual science* 2001; 42: 2970-2975. 2001/11/01.
227. Grunwald JE, Metelitsina TI, Dupont JC, et al. Reduced foveolar choroidal blood flow in eyes with increasing AMD severity. *Investigative ophthalmology & visual science* 2005; 46: 1033-1038. 2005/02/25. DOI: 10.1167/iovs.04-1050.
228. Seddon JM, McLeod DS, Bhutto IA, et al. Histopathological Insights Into Choroidal Vascular Loss in Clinically Documented Cases of Age-Related Macular Degeneration. *JAMA ophthalmology* 2016; 134: 1272-1280. 2016/09/23. DOI: 10.1001/jamaophthalmol.2016.3519.
229. Blaauwgeers HG, Holtkamp GM, Rutten H, et al. Polarized vascular endothelial growth factor secretion by human retinal pigment epithelium and localization of vascular endothelial growth factor receptors on the inner choriocapillaris. Evidence for a trophic paracrine relation. *The American journal of pathology* 1999; 155: 421-428. 1999/08/06. DOI: 10.1016/s0002-9440(10)65138-3.
230. Korte GE, Reppucci V and Henkind P. RPE destruction causes choriocapillary atrophy. *Investigative ophthalmology & visual science* 1984; 25: 1135-1145. 1984/10/01.
231. Saint-Geniez M, Kurihara T, Sekiyama E, et al. An essential role for RPE-derived soluble VEGF in the maintenance of the choriocapillaris. *Proceedings of the National Academy of Sciences of the United States of America* 2009; 106: 18751-18756. 2009/10/21. DOI: 10.1073/pnas.0905010106.
232. Marneros AG, Fan J, Yokoyama Y, et al. Vascular endothelial growth factor expression in the retinal pigment epithelium is essential for choriocapillaris development and visual function. *The American journal of pathology* 2005; 167: 1451-1459. 2005/10/28. DOI: 10.1016/s0002-9440(10)61231-x.
233. Nordgaard CL, Karunadharma PP, Feng X, et al. Mitochondrial proteomics of the retinal pigment epithelium at progressive stages of age-related macular degeneration. *Invest Ophthalmol Vis Sci* 2008; 49: 2848-2855. 2008/03/18. DOI: 10.1167/iovs.07-1352.
234. Terluk MR, Kapphahn RJ, Soukup LM, et al. Investigating mitochondria as a target for treating age-related macular degeneration. *The Journal of neuroscience : the official journal of the Society for Neuroscience* 2015; 35: 7304-7311. 2015/05/08. DOI: 10.1523/jneurosci.0190-15.2015.
235. Nordgaard CL, Berg KM, Kapphahn RJ, et al. Proteomics of the retinal pigment epithelium reveals altered protein expression at progressive stages of age-related

macular degeneration. *Investigative ophthalmology & visual science* 2006; 47: 815-822. 2006/03/01. DOI: 10.1167/iovs.05-0976.
236. Vives-Bauza C, Anand M, Shiraz AK, et al. The age lipid A2E and mitochondrial dysfunction synergistically impair phagocytosis by retinal pigment epithelial cells. *The Journal of biological chemistry* 2008; 283: 24770-24780. 2008/07/16. DOI: 10.1074/jbc.M800706200.
237. Becquet F, Courtois Y and Goureau O. Nitric oxide decreases in vitro phagocytosis of photoreceptor outer segments by bovine retinal pigmented epithelial cells. *Journal of cellular physiology* 1994; 159: 256-262. 1994/05/01. DOI: 10.1002/jcp.1041590209.
238. Suematsu N, Tsutsui H, Wen J, et al. Oxidative stress mediates tumor necrosis factor-alpha-induced mitochondrial DNA damage and dysfunction in cardiac myocytes. *Circulation* 2003; 107: 1418-1423. 2003/03/19. DOI: 10.1161/01.cir.0000055318.09997.1f.
239. Goureau O, Lepoivre M and Courtois Y. Lipopolysaccharide and cytokines induce a macrophage-type of nitric oxide synthase in bovine retinal pigmented epithelial cells. *Biochemical and biophysical research communications* 1992; 186: 854-859. 1992/07/31. DOI: 10.1016/0006-291x(92)90824-5.
240. Aiello LP, Avery RL, Arrigg PG, et al. Vascular endothelial growth factor in ocular fluid of patients with diabetic retinopathy and other retinal disorders. *The New England journal of medicine* 1994; 331: 1480-1487. 1994/12/01. DOI: 10.1056/nejm199412013312203.
241. Kliffen M, Sharma HS, Mooy CM, et al. Increased expression of angiogenic growth factors in age-related maculopathy. *The British journal of ophthalmology* 1997; 81: 154-162. 1997/02/01. DOI: 10.1136/bjo.81.2.154.
242. Lopez PF, Sippy BD, Lambert HM, et al. Transdifferentiated retinal pigment epithelial cells are immunoreactive for vascular endothelial growth factor in surgically excised age-related macular degeneration-related choroidal neovascular membranes. *Investigative ophthalmology & visual science* 1996; 37: 855-868. 1996/04/01.
243. Otani A, Takagi H, Oh H, et al. Vascular endothelial growth factor family and receptor expression in human choroidal neovascular membranes. *Microvascular research* 2002; 64: 162-169. 2002/06/21. DOI: 10.1006/mvre.2002.2407.
244. Recurrent choroidal neovascularization after argon laser photocoagulation for neovascular maculopathy. Macular Photocoagulation Study Group. *Archives of ophthalmology* 1986; 104: 503-512. 1986/04/01. DOI: 10.1001/archopht.1986.01050160059012.
245. Persistent and recurrent neovascularization after krypton laser photocoagulation for neovascular lesions of age-related macular degeneration. Macular Photocoagulation Study Group. *Archives of ophthalmology* 1990; 108: 825-831. 1990/06/01. DOI: 10.1001/archopht.1990.01070080067037.
246. Sorenson JA, Yannuzzi LA and Shakin JL. Recurrent subretinal neovascularization. *Ophthalmology* 1985; 92: 1059-1074. 1985/08/01.
247. Subfoveal neovascular lesions in age-related macular degeneration. Guidelines for evaluation and treatment in the macular photocoagulation study. Macular Photocoagulation Study Group. *Archives of ophthalmology* 1991; 109: 1242-1257. 1991/09/01.

248. Schmidt-Erfurth U and Hasan T. Mechanisms of action of photodynamic therapy with verteporfin for the treatment of age-related macular degeneration. *Survey of ophthalmology* 2000; 45: 195-214. 2000/11/30.
249. Verteporfin therapy of subfoveal choroidal neovascularization in age-related macular degeneration: two-year results of a randomized clinical trial including lesions with occult with no classic choroidal neovascularization—verteporfin in photodynamic therapy report 2. *American journal of ophthalmology* 2001; 131: 541-560. DOI: https://doi.org/10.1016/S0002-9394(01)00967-9.
250. Blinder KJ, Blumenkranz MS, Bressler NM, et al. Verteporfin therapy of subfoveal choroidal neovascularization in pathologic myopia: 2-year results of a randomized clinical trial--VIP report no. 3. *Ophthalmology* 2003; 110: 667-673. 2003/04/12. DOI: 10.1016/s0161-6420(02)01998-x.
251. Kaiser PK. Verteporfin therapy of subfoveal choroidal neovascularization in age-related macular degeneration: 5-year results of two randomized clinical trials with an open-label extension: TAP report no. 8. *Graefe's archive for clinical and experimental ophthalmology = Albrecht von Graefes Archiv fur klinische und experimentelle Ophthalmologie* 2006; 244: 1132-1142. 2006/03/16. DOI: 10.1007/s00417-005-0199-9.
252. Bressler NM. Photodynamic therapy of subfoveal choroidal neovascularization in age-related macular degeneration with verteporfin: two-year results of 2 randomized clinical trials-tap report 2. *Archives of ophthalmology* 2001; 119: 198-207. 2001/02/15.
253. Photodynamic therapy of subfoveal choroidal neovascularization in age-related macular degeneration with verteporfin: one-year results of 2 randomized clinical trials--TAP report. Treatment of age-related macular degeneration with photodynamic therapy (TAP) Study Group. *Archives of ophthalmology* 1999; 117: 1329-1345. 1999/10/26.
254. Guidelines for using verteporfin (visudyne) in photodynamic therapy to treat choroidal neovascularization due to age-related macular degeneration and other causes. *Retina (Philadelphia, Pa)* 2002; 22: 6-18. 2002/03/09.
255. Verteporfin therapy of subfoveal choroidal neovascularization in pathologic myopia: 2-year results of a randomized clinical trial—VIP report no. 3. *Ophthalmology* 2003; 110: 667-673. DOI: https://doi.org/10.1016/S0161-6420(02)01998-X.
256. Kwak N, Okamoto N, Wood JM, et al. VEGF is major stimulator in model of choroidal neovascularization. *Investigative ophthalmology & visual science* 2000; 41: 3158-3164. 2000/09/01.
257. Gragoudas ES, Adamis AP, Cunningham ET, Jr., et al. Pegaptanib for neovascular age-related macular degeneration. *The New England journal of medicine* 2004; 351: 2805-2816. 2004/12/31. DOI: 10.1056/NEJMoa042760.
258. Kaiser PK, Boyer DS, Cruess AF, et al. Verteporfin plus ranibizumab for choroidal neovascularization in age-related macular degeneration: twelve-month results of the DENALI study. *Ophthalmology* 2012; 119: 1001-1010. 2012/03/27. DOI: 10.1016/j.ophtha.2012.02.003.
259. Larsen M, Schmidt-Erfurth U, Lanzetta P, et al. Verteporfin plus ranibizumab for choroidal neovascularization in age-related macular degeneration: twelve-month MONT BLANC study results. *Ophthalmology* 2012; 119: 992-1000. 2012/03/20. DOI: 10.1016/j.ophtha.2012.02.002.
260. Schmidt-Erfurth U and Wolf S. Same-day administration of verteporfin and ranibizumab 0.5 mg in patients with choroidal neovascularisation due to age-related

macular degeneration. *The British journal of ophthalmology* 2008; 92: 1628-1635. 2008/09/06. DOI: 10.1136/bjo.2007.135277.
261. Heier JS, Brown D, Ciulla T, et al. Ranibizumab for choroidal neovascularization secondary to causes other than age-related macular degeneration: a phase I clinical trial. *Ophthalmology* 2011; 118: 111-118. 2010/08/04. DOI: 10.1016/j.ophtha.2010.04.016.
262. Heier JS, Boyer DS, Ciulla TA, et al. Ranibizumab combined with verteporfin photodynamic therapy in neovascular age-related macular degeneration: year 1 results of the FOCUS Study. *Archives of ophthalmology* 2006; 124: 1532-1542. 2006/11/15. DOI: 10.1001/archopht.124.11.1532.
263. Tufail A, Patel PJ, Egan C, et al. Bevacizumab for neovascular age related macular degeneration (ABC Trial): multicentre randomised double masked study. *BMJ (Clinical research ed)* 2010; 340: c2459. 2010/06/12. DOI: 10.1136/bmj.c2459.
264. Menon G, Chandran M, Sivaprasad S, et al. Is it necessary to use three mandatory loading doses when commencing therapy for neovascular age-related macular degeneration using bevacizumab? (BeMOc Trial). *Eye (London, England)* 2013; 27: 959-963. 2013/06/08. DOI: 10.1038/eye.2013.93.
265. Rosenfeld PJ, Brown DM, Heier JS, et al. Ranibizumab for neovascular age-related macular degeneration. *The New England journal of medicine* 2006; 355: 1419-1431. 2006/10/06. DOI: 10.1056/NEJMoa054481.
266. Brown DM, Michels M, Kaiser PK, et al. Ranibizumab versus verteporfin photodynamic therapy for neovascular age-related macular degeneration: Two-year results of the ANCHOR study. *Ophthalmology* 2009; 116: 57-65 e55. 2009/01/03. DOI: 10.1016/j.ophtha.2008.10.018.
267. Schmidt-Erfurth U, Kaiser PK, Korobelnik JF, et al. Intravitreal aflibercept injection for neovascular age-related macular degeneration: ninety-six-week results of the VIEW studies. *Ophthalmology* 2014; 121: 193-201. 2013/10/03. DOI: 10.1016/j.ophtha.2013.08.011.
268. administration Tg. Australian public assessment report for ranibizumab. In: administration Tg, (ed.). Woden, ACT: Australian Government Department of Health and Aging, 2011, p. 121.
269. Zampros I, Praidou A, Brazitikos P, et al. Antivascular endothelial growth factor agents for neovascular age-related macular degeneration. *Journal of ophthalmology* 2012; 2012: 319728. 2011/12/17. DOI: 10.1155/2012/319728.
270. Heier JS, Brown DM, Chong V, et al. Intravitreal Aflibercept (VEGF Trap-Eye) in Wet Age-related Macular Degeneration. *Ophthalmology* 2012; 119: 2537-2548. DOI: 10.1016/j.ophtha.2012.09.006.
271. Grisanti S and Ziemssen F. Bevacizumab: off-label use in ophthalmology. *Indian journal of ophthalmology* 2007; 55: 417-420. DOI: 10.4103/0301-4738.36474.
272. Administration TD. Australian Public Assessment Report for Bevacizumab (recombinant humanised). In: Ageing DoHa, (ed.). Canberra, Australia2013.
273. Administration TD. Australian Public Assessment Report for Aflibercept. In: Ageing DoHa, (ed.). Canberra, Australia2015.
274. Ferrara N, Hillan KJ and Novotny W. Bevacizumab (Avastin), a humanized anti-VEGF monoclonal antibody for cancer therapy. *Biochemical and biophysical research communications* 2005; 333: 328-335. DOI: https://doi.org/10.1016/j.bbrc.2005.05.132.

275. Martin DF, Maguire MG, Fine SL, et al. Ranibizumab and bevacizumab for treatment of neovascular age-related macular degeneration: two-year results. *Ophthalmology* 2012; 119: 1388-1398. 2012/05/05. DOI: 10.1016/j.ophtha.2012.03.053.
276. Martin DF, Maguire MG, Ying GS, et al. Ranibizumab and bevacizumab for neovascular age-related macular degeneration. *The New England journal of medicine* 2011; 364: 1897-1908. 2011/04/30. DOI: 10.1056/NEJMoa1102673.
277. Chakravarthy U, Harding SP, Rogers CA, et al. Alternative treatments to inhibit VEGF in age-related choroidal neovascularisation: 2-year findings of the IVAN randomised controlled trial. *Lancet* 2013; 382: 1258-1267. 2013/07/23. DOI: 10.1016/s0140-6736(13)61501-9.
278. Chakravarthy U, Harding SP, Rogers CA, et al. Ranibizumab versus bevacizumab to treat neovascular age-related macular degeneration: one-year findings from the IVAN randomized trial. *Ophthalmology* 2012; 119: 1399-1411. 2012/05/15. DOI: 10.1016/j.ophtha.2012.04.015.
279. Balaratnasingam C, Dhrami-Gavazi E, McCann JT, et al. Aflibercept: a review of its use in the treatment of choroidal neovascularization due to age-related macular degeneration. *Clinical ophthalmology (Auckland, NZ)* 2015; 9: 2355-2371. DOI: 10.2147/OPTH.S80040.
280. Li X, Xu G, Wang Y, et al. Safety and efficacy of conbercept in neovascular age-related macular degeneration: results from a 12-month randomized phase 2 study: AURORA study. *Ophthalmology* 2014; 121: 1740-1747. 2014/05/06. DOI: 10.1016/j.ophtha.2014.03.026.
281. Liu K, Song Y, Xu G, et al. Conbercept for Treatment of Neovascular Age-related Macular Degeneration: Results of the Randomized Phase 3 PHOENIX Study. *American journal of ophthalmology* 2019; 197: 156-167. 2018/08/28. DOI: 10.1016/j.ajo.2018.08.026.
282. Lu X and Sun X. Profile of conbercept in the treatment of neovascular age-related macular degeneration. *Drug design, development and therapy* 2015; 9: 2311-2320. 2015/05/12. DOI: 10.2147/dddt.S67536.
283. Wang L, Zhang C and Hua R. Clinical effectiveness of ranibizumab and conbercept for neovascular age-related macular degeneration: a meta-analysis. *Drug design, development and therapy* 2018; 12: 3625-3633. 2018/11/23. DOI: 10.2147/dddt.S176021.
284. Mehta H, Tufail A, Daien V, et al. Real-world outcomes in patients with neovascular age-related macular degeneration treated with intravitreal vascular endothelial growth factor inhibitors. *Progress in retinal and eye research* 2018; 65: 127-146. 2018/01/07. DOI: 10.1016/j.preteyeres.2017.12.002.
285. Zarbin M, Tsuboi M, Hill LF, et al. Simulating an Anti-Vascular Endothelial Growth Factor Switch in Neovascular Age-Related Macular Degeneration: A HARBOR Subanalysis. *Ophthalmology* 2019 2019/01/15. DOI: 10.1016/j.ophtha.2019.01.003.
286. Volz C, Grassmann F, Greslechner R, et al. Spectral Domain Optical Coherence Tomography Allows the Unification of Clinical Decision Making for the Evaluation of Choroidal Neovascularization Activity. *Ophthalmologica Journal international d'ophtalmologie International journal of ophthalmology Zeitschrift fur Augenheilkunde* 2019; 241: 32-37. 2018/06/22. DOI: 10.1159/000489344.
287. Abraham P, Yue H and Wilson L. Randomized, double-masked, sham-controlled trial of ranibizumab for neovascular age-related macular degeneration: PIER

study year 2. *American journal of ophthalmology* 2010; 150: 315-324 e311. 2010/07/06. DOI: 10.1016/j.ajo.2010.04.011.
288. Boyer DS, Antoszyk AN, Awh CC, et al. Subgroup analysis of the MARINA study of ranibizumab in neovascular age-related macular degeneration. *Ophthalmology* 2007; 114: 246-252. 2007/02/03. DOI: 10.1016/j.ophtha.2006.10.045.
289. Ghasemi Falavarjani K and Nguyen QD. Adverse events and complications associated with intravitreal injection of anti-VEGF agents: a review of literature. *Eye (London, England)* 2013; 27: 787-794. Jul, 2013.
290. Singer MA, Awh CC, Sadda S, et al. HORIZON: an open-label extension trial of ranibizumab for choroidal neovascularization secondary to age-related macular degeneration. *Ophthalmology* 2012; 119: 1175-1183. 2012/02/07. DOI: 10.1016/j.ophtha.2011.12.016.
291. Holz FG, Amoaku W, Donate J, et al. Safety and efficacy of a flexible dosing regimen of ranibizumab in neovascular age-related macular degeneration: the SUSTAIN study. *Ophthalmology* 2011; 118: 663-671. 2011/04/05. DOI: 10.1016/j.ophtha.2010.12.019.
292. Boyer DS, Heier JS, Brown DM, et al. A Phase IIIb study to evaluate the safety of ranibizumab in subjects with neovascular age-related macular degeneration. *Ophthalmology* 2009; 116: 1731-1739. 2009/08/01. DOI: 10.1016/j.ophtha.2009.05.024.
293. Schmidt-Erfurth U, Eldem B, Guymer R, et al. Efficacy and safety of monthly versus quarterly ranibizumab treatment in neovascular age-related macular degeneration: the EXCITE study. *Ophthalmology* 2011; 118: 831-839. 2010/12/15. DOI: 10.1016/j.ophtha.2010.09.004.
294. Regillo CD, Brown DM, Abraham P, et al. Randomized, double-masked, sham-controlled trial of ranibizumab for neovascular age-related macular degeneration: PIER Study year 1. *American journal of ophthalmology* 2008; 145: 239-248. 2008/01/29. DOI: 10.1016/j.ajo.2007.10.004.
295. Wykoff CC, Ou WC, Brown DM, et al. Randomized Trial of Treat-and-Extend versus Monthly Dosing for Neovascular Age-Related Macular Degeneration: 2-Year Results of the TREX-AMD Study. *Ophthalmology Retina* 2017; 1: 314-321. 2017/01/01. DOI: 10.1016/j.oret.2016.12.004.
296. Agarwal A, Aggarwal K and Gupta V. Management of Neovascular Age-related Macular Degeneration: A Review on Landmark Randomized Controlled Trials. *Middle East African journal of ophthalmology* 2016; 23: 27-37. DOI: 10.4103/0974-9233.173133.
297. Gillies MC, Campain A, Barthelmes D, et al. Long-Term Outcomes of Treatment of Neovascular Age-Related Macular Degeneration: Data from an Observational Study. *Ophthalmology* 2015; 122: 1837-1845. 2015/06/23. DOI: 10.1016/j.ophtha.2015.05.010.
298. Rofagha S, Bhisitkul RB, Boyer DS, et al. Seven-year outcomes in ranibizumab-treated patients in ANCHOR, MARINA, and HORIZON: a multicenter cohort study (SEVEN-UP). *Ophthalmology* 2013; 120: 2292-2299. 2013/05/07. DOI: 10.1016/j.ophtha.2013.03.046.
299. Schaal S, Kaplan HJ and Tezel TH. Is there tachyphylaxis to intravitreal anti-vascular endothelial growth factor pharmacotherapy in age-related macular degeneration? *Ophthalmology* 2008; 115: 2199-2205. 2008/10/22. DOI: 10.1016/j.ophtha.2008.07.007.

300. Forooghian F, Cukras C, Meyerle CB, et al. Tachyphylaxis after intravitreal bevacizumab for exudative age-related macular degeneration. *Retina* 2009; 29: 723-731. 2009/06/12. DOI: 10.1097/IAE.0b013e3181a2c1c3.
301. Eghøj MS and Sørensen TL. Tachyphylaxis during treatment of exudative age-related macular degeneration with ranibizumab. *The British journal of ophthalmology* 2012; 96: 21-23. 2011/07/08. DOI: 10.1136/bjo.2011.203893.
302. Rezar-Dreindl S, Sacu S, Eibenberger K, et al. The Intraocular Cytokine Profile and Therapeutic Response in Persistent Neovascular Age-Related Macular Degeneration. *Investigative ophthalmology & visual science* 2016; 57: 4144-4150. 2016/08/19. DOI: 10.1167/iovs.16-19772.
303. Maguire MG, Martin DF, Ying GS, et al. Five-Year Outcomes with Anti-Vascular Endothelial Growth Factor Treatment of Neovascular Age-Related Macular Degeneration: The Comparison of Age-Related Macular Degeneration Treatments Trials. *Ophthalmology* 2016; 123: 1751-1761. 2016/05/10. DOI: 10.1016/j.ophtha.2016.03.045.
304. Yang S, Zhao J and Sun X. Resistance to anti-VEGF therapy in neovascular age-related macular degeneration: a comprehensive review. *Drug design, development and therapy* 2016; 10: 1857-1867. 2016/06/23. DOI: 10.2147/dddt.s97653.
305. Framme C, Panagakis G and Birngruber R. Effects on choroidal neovascularization after anti-VEGF Upload using intravitreal ranibizumab, as determined by spectral domain-optical coherence tomography. *Investigative ophthalmology & visual science* 2010; 51: 1671-1676. 2009/10/31. DOI: 10.1167/iovs.09-4496.
306. Rush RB, Rush SW, Aragon AV, 2nd, et al. Evaluation of choroidal neovascularization with indocyanine green angiography in neovascular age-related macular degeneration subjects undergoing intravitreal bevacizumab therapy. *American journal of ophthalmology* 2014; 158: 337-344. 2014/05/23. DOI: 10.1016/j.ajo.2014.05.007.
307. Yamashiro K, Tomita K, Tsujikawa A, et al. Factors associated with the response of age-related macular degeneration to intravitreal ranibizumab treatment. *American journal of ophthalmology* 2012; 154: 125-136. 2012/04/03. DOI: 10.1016/j.ajo.2012.01.010.
308. Photocoagulation for diabetic macular edema. Early Treatment Diabetic Retinopathy Study report number 1. Early Treatment Diabetic Retinopathy Study research group. *Archives of ophthalmology* 1985; 103: 1796-1806. 1985/12/01.
309. Photocoagulation treatment of proliferative diabetic retinopathy: the second report of diabetic retinopathy study findings. *Ophthalmology* 1978; 85: 82-106. 1978/01/01. DOI: 10.1016/s0161-6420(78)35693-1.
310. Elman MJ, Aiello LP, Beck RW, et al. Randomized trial evaluating ranibizumab plus prompt or deferred laser or triamcinolone plus prompt laser for diabetic macular edema. *Ophthalmology* 2010; 117: 1064-1077.e1035. 2010/04/30. DOI: 10.1016/j.ophtha.2010.02.031.
311. Flaxel CJ, Adelman RA, Bailey ST, et al. Diabetic Retinopathy Preferred Practice Pattern(R). *Ophthalmology* 2020; 127: P66-p145. 2019/11/24. DOI: 10.1016/j.ophtha.2019.09.025.
312. Andersen CC and Phelps DL. Peripheral retinal ablation for threshold retinopathy of prematurity in preterm infants. *The Cochrane database of systematic reviews* 2000: Cd001693. 2000/05/05. DOI: 10.1002/14651858.Cd001693.

313. Sankar MJ, Sankar J and Chandra P. Anti-vascular endothelial growth factor (VEGF) drugs for treatment of retinopathy of prematurity. *The Cochrane database of systematic reviews* 2018; 1: Cd009734. 2018/01/09. DOI: 10.1002/14651858.CD009734.pub3.
314. Parodi MB, Virgili G and Evans JR. Laser treatment of drusen to prevent progression to advanced age-related macular degeneration. *The Cochrane database of systematic reviews* 2009: CD006537. 2009/07/10. DOI: 10.1002/14651858.CD006537.pub2.
315. Virgili G, Michelessi M, Parodi MB, et al. Laser treatment of drusen to prevent progression to advanced age-related macular degeneration. *The Cochrane database of systematic reviews* 2015: CD006537. 2015/10/24. DOI: 10.1002/14651858.CD006537.pub3.
316. Graham CE, Binz N, Shen WY, et al. Laser photocoagulation: ocular research and therapy in diabetic retinopathy. *Advances in experimental medicine and biology* 2006; 572: 195-200. 2007/01/26. DOI: 10.1007/0-387-32442-9_29.
317. Dorin G. Evolution of retinal laser therapy: minimum intensity photocoagulation (MIP). Can the laser heal the retina without harming it? *Seminars in ophthalmology* 2004; 19: 62-68. 2004/12/14. DOI: 10.1080/08820530490884173.
318. Vogel A and Birngruber R. Temperature profiles in human retina and choid during laser coagulation with different wavelengths ranging from 514 to 810 nm. *Laser Light Ophthalmol* 1992; 5: 9-16. 1992.
319. Anderson RR and Parrish JA. Selective photothermolysis: precise microsurgery by selective absorption of pulsed radiation. *Science (New York, NY)* 1983; 220: 524-527. 1983/04/29.
320. Parrish JA, Anderson RR, Harrist T, et al. Selective thermal effects with pulsed irradiation from lasers: from organ to organelle. *The Journal of investigative dermatology* 1983; 80: 75s-80s. 1983/06/01. DOI: 10.1038/jid.1983.19.
321. Brinkmann R, Roider J and Birngruber R. Selective retina therapy (SRT): a review on methods, techniques, preclinical and first clinical results. *Bulletin de la Societe belge d'ophtalmologie* 2006: 51-69. 2007/02/03.
322. Marshall J. Thermal and mechanical mechanisms in laser damage to the retina. *Investigative ophthalmology* 1970; 9: 97-115. 1970/02/01.
323. Xiao M, Sastry SM, Li ZY, et al. Effects of retinal laser photocoagulation on photoreceptor basic fibroblast growth factor and survival. *Investigative ophthalmology & visual science* 1998; 39: 618-630. 1998/03/21.
324. Stefansson E. The therapeutic effects of retinal laser treatment and vitrectomy. A theory based on oxygen and vascular physiology. *Acta ophthalmologica Scandinavica* 2001; 79: 435-440. 2001/10/12. DOI: 10.1034/j.1600-0420.2001.790502.x.
325. Shah AM, Bressler NM and Jampol LM. Does laser still have a role in the management of retinal vascular and neovascular diseases? *American journal of ophthalmology* 2011; 152: 332-339 e331. 2011/07/12. DOI: 10.1016/j.ajo.2011.04.015.
326. Luttrull JK, Musch DC and Mainster MA. Subthreshold diode micropulse photocoagulation for the treatment of clinically significant diabetic macular oedema. *The British journal of ophthalmology* 2005; 89: 74-80. 2004/12/24. DOI: 10.1136/bjo.2004.051540.
327. Wilson AS, Hobbs BG, Shen WY, et al. Argon laser photocoagulation-induced modification of gene expression in the retina. *Investigative ophthalmology & visual science* 2003; 44: 1426-1434. 2003/03/27.

328. Roider J, Michaud NA, Flotte TJ, et al. Response of the retinal pigment epithelium to selective photocoagulation. *Archives of ophthalmology* 1992; 110: 1786-1792. 1992/12/01.
329. Chu Y, Humphrey MF, Alder VV, et al. Immunocytochemical localization of basic fibroblast growth factor and glial fibrillary acidic protein after laser photocoagulation in the Royal College of Surgeons rat. *Australian and New Zealand journal of ophthalmology* 1998; 26: 87-96. 1998/04/02.
330. Ogata N, Wada M, Otsuji T, et al. Expression of pigment epithelium-derived factor in normal adult rat eye and experimental choroidal neovascularization. *Investigative ophthalmology & visual science* 2002; 43: 1168-1175. 2002/03/30.
331. Ogata N, Tombran-Tink J, Jo N, et al. Upregulation of pigment epithelium-derived factor after laser photocoagulation. *American journal of ophthalmology* 2001; 132: 427-429. 2001/09/01.
332. Binz N, Graham CE, Simpson K, et al. Long-term effect of therapeutic laser photocoagulation on gene expression in the eye. *FASEB journal : official publication of the Federation of American Societies for Experimental Biology* 2006; 20: 383-385. 2005/12/16. DOI: 10.1096/fj.05-3890fje.
333. Flaxel C, Bradle J, Acott T, et al. Retinal pigment epithelium produces matrix metalloproteinases after laser treatment. *Retina (Philadelphia, Pa)* 2007; 27: 629-634. 2007/06/15. DOI: 10.1097/01.iae.0000249561.02567.fd.
334. Richert E, Koinzer S, Tode J, et al. Release of Different Cell Mediators During Retinal Pigment Epithelium Regeneration Following Selective Retina Therapy. *Investigative ophthalmology & visual science* 2018; 59: 1323-1331. 2018/04/07. DOI: 10.1167/iovs.17-23163.
335. Treumer F, Klettner A, Baltz J, et al. Vectorial release of matrix metalloproteinases (MMPs) from porcine RPE-choroid explants following selective retina therapy (SRT): towards slowing the macular ageing process. *Experimental eye research* 2012; 97: 63-72. 2012/03/06. DOI: 10.1016/j.exer.2012.02.011.
336. Bressler NM, Maguire MG, Murphy PL, et al. Macular scatter ('grid') laser treatment of poorly demarcated subfoveal choroidal neovascularization in age-related macular degeneration. Results of a randomized pilot trial. *Archives of ophthalmology* 1996; 114: 1456-1464. 1996/12/01.
337. Morgan CM and Schatz H. Atrophic creep of the retinal pigment epithelium after focal macular photocoagulation. *Ophthalmology* 1989; 96: 96-103. 1989/01/01.
338. Owens SL, Guymer RH, Gross-Jendroska M, et al. Fluorescein angiographic abnormalities after prophylactic macular photocoagulation for high-risk age-related maculopathy. *American journal of ophthalmology* 1999; 127: 681-687. 1999/06/18.
339. Owens SL, Bunce C, Brannon AJ, et al. Prophylactic laser treatment hastens choroidal neovascularization in unilateral age-related maculopathy: final results of the drusen laser study. *American journal of ophthalmology* 2006; 141: 276-281. 2006/02/07. DOI: 10.1016/j.ajo.2005.08.019.
340. Friberg TR, Musch DC, Lim JI, et al. Prophylactic treatment of age-related macular degeneration report number 1: 810-nanometer laser to eyes with drusen. Unilaterally eligible patients. *Ophthalmology* 2006; 113: 622 e621. 2006/04/04. DOI: 10.1016/j.ophtha.2005.10.066.
341. Hooper CY and Guymer RH. New treatments in age-related macular degeneration. *Clinical & experimental ophthalmology* 2003; 31: 376-391. 2003/10/01.

342. Chhablani J, Roh YJ, Jobling AI, et al. Restorative retinal laser therapy: Present state and future directions. *Survey of ophthalmology* 2018; 63: 307-328. 2017/10/11. DOI: 10.1016/j.survophthal.2017.09.008.
343. Low-Level Light Therapy. MeSH: NCBI, 2002.
344. Grzybowski A and Pietrzak K. From patient to discoverer--Niels Ryberg Finsen (1860-1904) --the founder of phototherapy in dermatology. *Clinics in dermatology* 2012; 30: 451-455. 2012/08/04.
345. Mester E, Mester AF and Mester A. The biomedical effects of laser application. *Lasers in surgery and medicine* 1985; 5: 31-39. 1985/01/01.
346. Karu TI and Kolyakov SF. Exact action spectra for cellular responses relevant to phototherapy. *Photomedicine and laser surgery* 2005; 23: 355-361. 2005/09/08. DOI: 10.1089/pho.2005.23.355.
347. Wong-Riley MT, Liang HL, Eells JT, et al. Photobiomodulation directly benefits primary neurons functionally inactivated by toxins: role of cytochrome c oxidase. *The Journal of biological chemistry* 2005; 280: 4761-4771. 2004/11/24. DOI: 10.1074/jbc.M409650200.
348. Rojas JC and Gonzalez-Lima F. Low-level light therapy of the eye and brain. *Eye and brain* 2011; 3: 49-67. 2011/10/14. DOI: 10.2147/eb.s21391.
349. Karu T. Primary and secondary mechanisms of action of visible to near-IR radiation on cells. *Journal of Photochemistry and Photobiology B: Biology* 1999; 49: 1-17. DOI: https://doi.org/10.1016/S1011-1344(98)00219-X.
350. Albarracin R and Valter K. 670 nm red light preconditioning supports Muller cell function: evidence from the white light-induced damage model in the rat retina. *Photochemistry and photobiology* 2012; 88: 1418-1427. 2012/03/01. DOI: 10.1111/j.1751-1097.2012.01130.x.
351. Kirk D, K., Gopalakrishnan S, Schmitt H, et al. Photobiomodulation reduces photoreceptor death and regulates cytoprotection in early states of P23H retinal dystrophy. In: *SPIE BiOS* (eds Hamblin M, R., Anders J, Carroll J, D., et al.), San Fransisco 2013, SPIE BiOS.
352. Rojas JC, Lee J, John JM, et al. Neuroprotective effects of near-infrared light in an in vivo model of mitochondrial optic neuropathy. *The Journal of neuroscience : the official journal of the Society for Neuroscience* 2008; 28: 13511-13521. 2008/12/17. DOI: 10.1523/jneurosci.3457-08.2008.
353. Lane N. Cell biology: power games. *Nature* 2006; 443: 901-903. 2006/10/27. DOI: 10.1038/443901a.
354. Poyton RO and Ball KA. Therapeutic photobiomodulation: nitric oxide and a novel function of mitochondrial cytochrome c oxidase. *Discovery medicine* 2011; 11: 154-159. 2011/03/02.
355. Huang YY, Nagata K, Tedford CE, et al. Low-level laser therapy (LLLT) reduces oxidative stress in primary cortical neurons in vitro. *Journal of biophotonics* 2013; 6: 829-838. 2013/01/03. DOI: 10.1002/jbio.201200157.
356. Wong-Riley MT, Bai X, Buchmann E, et al. Light-emitting diode treatment reverses the effect of TTX on cytochrome oxidase in neurons. *Neuroreport* 2001; 12: 3033-3037. 2001/09/25.
357. Karu T, Pyatibrat L and Kalendo G. Irradiation with He-Ne laser increases ATP level in cells cultivated in vitro. *Journal of photochemistry and photobiology B, Biology* 1995; 27: 219-223. 1995/03/01.

358. Chow RT, Johnson MI, Lopes-Martins RA, et al. Efficacy of low-level laser therapy in the management of neck pain: a systematic review and meta-analysis of randomised placebo or active-treatment controlled trials. *Lancet (London, England)* 2009; 374: 1897-1908. 2009/11/17. DOI: 10.1016/s0140-6736(09)61522-1.
359. Byrnes KR, Waynant RW, Ilev IK, et al. Light promotes regeneration and functional recovery and alters the immune response after spinal cord injury. *Lasers in surgery and medicine* 2005; 36: 171-185. 2005/02/11. DOI: 10.1002/lsm.20143.
360. Peplow PV, Chung TY and Baxter GD. Laser photobiomodulation of wound healing: a review of experimental studies in mouse and rat animal models. *Photomedicine and laser surgery* 2010; 28: 291-325. 2009/12/10. DOI: 10.1089/pho.2008.2446.
361. Whelan HT, Smits RL, Jr., Buchman EV, et al. Effect of NASA light-emitting diode irradiation on wound healing. *Journal of clinical laser medicine & surgery* 2001; 19: 305-314. 2002/01/05. DOI: 10.1089/104454701753342758.
362. Natoli R, Valter K, Barbosa M, et al. 670nm photobiomodulation as a novel protection against retinopathy of prematurity: evidence from oxygen induced retinopathy models. *PloS one* 2013; 8: e72135. 2013/08/21. DOI: 10.1371/journal.pone.0072135.
363. Albarracin R, Natoli R, Rutar M, et al. 670 nm light mitigates oxygen-induced degeneration in C57BL/6J mouse retina. *BMC neuroscience* 2013; 14: 125. 2013/10/19. DOI: 10.1186/1471-2202-14-125.
364. Ivandic BT and Ivandic T. Low-level laser therapy improves visual acuity in adolescent and adult patients with amblyopia. *Photomedicine and laser surgery* 2012; 30: 167-171. 2012/01/13. DOI: 10.1089/pho.2011.3089.
365. Tang J, Herda AA and Kern TS. Photobiomodulation in the treatment of patients with non-center-involving diabetic macular oedema. *The British journal of ophthalmology* 2014; 98: 1013-1015. 2014/04/01. DOI: 10.1136/bjophthalmol-2013-304477.
366. Tang J, Du Y, Lee CA, et al. Low-intensity far-red light inhibits early lesions that contribute to diabetic retinopathy: in vivo and in vitro. *Investigative ophthalmology & visual science* 2013; 54: 3681-3690. 2013/04/06. DOI: 10.1167/iovs.12-11018.
367. Albarracin R, Eells J and Valter K. Photobiomodulation protects the retina from light-induced photoreceptor degeneration. *Investigative ophthalmology & visual science* 2011; 52: 3582-3592. 2011/03/23. DOI: 10.1167/iovs.10-6664.
368. Eells J, Henry M, Summerfelt P, et al. Therapeutic photobiomodulation for methanol-induced retinal toxicity. In: *National Academy of Sciences* 2003, pp.3439-3444.
369. Ivandic BT and Ivandic T. Low-level laser therapy improves vision in a patient with retinitis pigmentosa. *Photomedicine and laser surgery* 2014; 32: 181-184. 2014/02/18. DOI: 10.1089/pho.2013.3535.
370. Merry G, Dotson R, Devenyi R, et al. Photobiomodulation as a new treatment for dry age related macular degeneration. Results from the toronto and oak ridge photobimodulation study in AMD (TORPA). *Investigative ophthalmology & visual science*. 2012, p. 2049-.
371. Merry GF, Munk MR, Dotson RS, et al. Photobiomodulation reduces drusen volume and improves visual acuity and contrast sensitivity in dry age-related macular degeneration. *Acta ophthalmologica* 2017; 95: e270-e277. 2016/12/19. DOI: 10.1111/aos.13354.

372. Ivandic BT and Ivandic T. Low-level laser therapy improves vision in patients with age-related macular degeneration. *Photomedicine and laser surgery* 2008; 26: 241-245. 2008/07/01. DOI: 10.1089/pho.2007.2132.
373. Markowitz SN, Devenyi RG, Munk MR, et al. A double-masked, randomized, sham-controlled, single-center study with photobiomodulation for the treatment of dry age-related macular degeneration. *Retina* 2020; 40: 1471-1482. 2019/08/14. DOI: 10.1097/iae.0000000000002632.
374. Burton B, Parodi MB, Jürgens I, et al. LIGHTSITE II Randomized Multicenter Trial: Evaluation of Multiwavelength Photobiomodulation in Non-exudative Age-Related Macular Degeneration. *Ophthalmology and therapy* 2023: 1-16. 2023/01/02. DOI: 10.1007/s40123-022-00640-6.
375. Shen W, Teo KYC, Wood JPM, et al. Preclinical and clinical studies of photobiomodulation therapy for macular oedema. *Diabetologia* 2020; 63: 1900-1915. 2020/07/15. DOI: 10.1007/s00125-020-05189-2.
376. Markovets AM, Fursova AZ and Kolosova NG. Therapeutic action of the mitochondria-targeted antioxidant SkQ1 on retinopathy in OXYS rats linked with improvement of VEGF and PEDF gene expression. *PloS one* 2011; 6: e21682. 2011/07/14. DOI: 10.1371/journal.pone.0021682.
377. Geneva II. Photobiomodulation for the treatment of retinal diseases: a review. *International journal of ophthalmology* 2016; 9: 145-152. 2016/03/08. DOI: 10.18240/ijo.2016.01.24.
378. Robbins SG, Conaway JR, Ford BL, et al. Detection of vascular endothelial growth factor (VEGF) protein in vascular and non-vascular cells of the normal and oxygen-injured rat retina. *Growth factors (Chur, Switzerland)* 1997; 14: 229-241. 1997/01/01.
379. Lu YZ, Fernando N, Natoli R, et al. 670nm light treatment following retinal injury modulates Müller cell gliosis: Evidence from in vivo and in vitro stress models. *Experimental eye research* 2018; 169: 1-12. 2018/01/23. DOI: 10.1016/j.exer.2018.01.011.
380. Lopes NN, Plapler H, Chavantes MC, et al. Cyclooxygenase-2 and vascular endothelial growth factor expression in 5-fluorouracil-induced oral mucositis in hamsters: evaluation of two low-intensity laser protocols. *Supportive care in cancer : official journal of the Multinational Association of Supportive Care in Cancer* 2009; 17: 1409-1415. 2009/02/24. DOI: 10.1007/s00520-009-0603-9.
381. Zhang Y, Song S, Fong CC, et al. cDNA microarray analysis of gene expression profiles in human fibroblast cells irradiated with red light. *The Journal of investigative dermatology* 2003; 120: 849-857. 2003/04/26. DOI: 10.1046/j.1523-1747.2003.12133.x.
382. Lavey B, J., Estlack L, E., Schuster K, J. , et al. The response of human retinal pigmented epithelial cells in vitro to changes in nitric oxide concentration stimulated by low levels of red light. *SPIE BiOS*. San Francisco, California, United States: SPIE BiOS, 2013.
383. Kokkinopoulos I, Colman A, Hogg C, et al. Age-related retinal inflammation is reduced by 670 nm light via increased mitochondrial membrane potential. *Neurobiology of aging* 2013; 34: 602-609. 2012/05/19. DOI: 10.1016/j.neurobiolaging.2012.04.014.
384. Muili KA, Gopalakrishnan S, Meyer SL, et al. Amelioration of experimental autoimmune encephalomyelitis in C57BL/6 mice by photobiomodulation induced by

670 nm light. *PloS one* 2012; 7: e30655. 2012/02/01. DOI: 10.1371/journal.pone.0030655.
385. Begum R, Powner MB, Hudson N, et al. Treatment with 670 nm light up regulates cytochrome C oxidase expression and reduces inflammation in an age-related macular degeneration model. *PloS one* 2013; 8: e57828. 2013/03/08. DOI: 10.1371/journal.pone.0057828.
386. Saliba A, Du Y, Liu H, et al. Photobiomodulation Mitigates Diabetes-Induced Retinopathy by Direct and Indirect Mechanisms: Evidence from Intervention Studies in Pigmented Mice. *PloS one* 2015; 10: e0139003. 2015/10/02. DOI: 10.1371/journal.pone.0139003.
387. Whelan HT, Wong-Riley M, Eells J, et al. *DARPA Soldier Self Care: Rapid Healing of Laser Eye Injuries with Light Emitting*. 2004.
388. Merry G, Dotson RS, Devenyi R, et al. Photobiomodulation as a new treatment for dry age related macular degeneration. results from the toronto and oak ridge photobimodulation study in AMD (TORPA). *Investigative ophthalmology & visual science* 2012; 53: 2049.
389. Ryan SJ. The development of an experimental model of subretinal neovascularization in disciform macular degeneration. *Transactions of the American Ophthalmological Society* 1979; 77: 707-745. 1979/01/01.
390. Dobi ET, Puliafito CA and Destro M. A new model of experimental choroidal neovascularization in the rat. *Archives of ophthalmology* 1989; 107: 264-269. 1989/02/01.
391. Edelman JL and Castro MR. Quantitative image analysis of laser-induced choroidal neovascularization in rat. *Experimental eye research* 2000; 71: 523-533. 2000/10/21. DOI: 10.1006/exer.2000.0907.
392. Grossniklaus HE, Kang SJ and Berglin L. Animal models of choroidal and retinal neovascularization. *Progress in retinal and eye research* 2010; 29: 500-519. 2010/05/22. DOI: 10.1016/j.preteyeres.2010.05.003.
393. Elkington A, Frank H and Greaney M. *Clinical optics* 3rd ed. Oxford Blackwell Science 1999.
394. Azoulay K, Pianka P and Loewenstein A. The evolution of retinal laser technology and retinal photocoagulation as therapeutic modality. *Eur Ophth* 2012; 6: 185-189. DOI: http://doi.org/10.17925/EOR.2012.06.03.185.
395. Trujillo-Sanchez GP, Martinez-Camarillo JC, Spee CK, et al. Stereological Method in Optical Coherence Tomography for In Vivo Evaluation of Laser-Induced Choroidal Neovascularization. *Ophthalmic surgery, lasers & imaging retina* 2018; 49: e65-e74. 2018/09/18. DOI: 10.3928/23258160-20180907-09.
396. Mu H, Wang Y, Chu Y, et al. Multivesicular liposomes for sustained release of bevacizumab in treating laser-induced choroidal neovascularization. *Drug delivery* 2018; 25: 1372-1383. 2018/06/06. DOI: 10.1080/10717544.2018.1474967.
397. Bae JH, Hwang AR, Kim CY, et al. Intravitreal itraconazole inhibits laser-induced choroidal neovascularization in rats. *PloS one* 2017; 12: e0180482. 2017/07/01. DOI: 10.1371/journal.pone.0180482.
398. Nakajima T, Hirata M, Shearer TR, et al. Mechanism for laser-induced neovascularization in rat choroid: accumulation of integrin alpha chain-positive cells and their ligands. *Molecular vision* 2014; 20: 864-871. 2014/06/25.
399. Yang XM, Wang YS, Zhang J, et al. Role of PI3K/Akt and MEK/ERK in mediating hypoxia-induced expression of HIF-1alpha and VEGF in laser-induced rat

choroidal neovascularization. *Investigative ophthalmology & visual science* 2009; 50: 1873-1879. 2008/12/23. DOI: 10.1167/iovs.08-2591.
400. Liu T, Hui L, Wang YS, et al. In-vivo investigation of laser-induced choroidal neovascularization in rat using spectral-domain optical coherence tomography (SD-OCT). *Graefe's archive for clinical and experimental ophthalmology = Albrecht von Graefes Archiv fur klinische und experimentelle Ophthalmologie* 2013; 251: 1293-1301. 2012/11/02. DOI: 10.1007/s00417-012-2185-3.
401. Krause TA, Alex AF, Engel DR, et al. VEGF-production by CCR2-dependent macrophages contributes to laser-induced choroidal neovascularization. *PloS one* 2014; 9: e94313. 2014/04/10. DOI: 10.1371/journal.pone.0094313.
402. Zhang NL, Samadani EE and Frank RN. Mitogenesis and retinal pigment epithelial cell antigen expression in the rat after krypton laser photocoagulation. *Investigative ophthalmology & visual science* 1993; 34: 2412-2424. 1993/07/01.
403. Ogata N, Matsushima M, Takada Y, et al. Expression of basic fibroblast growth factor mRNA in developing choroidal neovascularization. *Current eye research* 1996; 15: 1008-1018. 1996/10/01. DOI: 10.3109/02713689609017649.
404. Zhao JF, Hua HR, Chen QB, et al. Impact of fenofibrate on choroidal neovascularization formation and VEGF-C plus VEGFR-3 in Brown Norway rats. *Experimental eye research* 2018; 174: 152-160. 2018/06/03. DOI: 10.1016/j.exer.2018.05.030.
405. Lambert V, Lecomte J, Hansen S, et al. Laser-induced choroidal neovascularization model to study age-related macular degeneration in mice. *Nature protocols* 2013; 8: 2197-2211. 2013/10/19. DOI: 10.1038/nprot.2013.135.
406. Guthrie MJ, Osswald CR, Valio NL, et al. Objective area measurement technique for choroidal neovascularization from fluorescein angiography. *Microvascular research* 2014; 91: 1-7. 2013/12/10. DOI: 10.1016/j.mvr.2013.11.005.
407. Sulaiman RS, Quigley J, Qi X, et al. A Simple Optical Coherence Tomography Quantification Method for Choroidal Neovascularization. *Journal of ocular pharmacology and therapeutics : the official journal of the Association for Ocular Pharmacology and Therapeutics* 2015; 31: 447-454. 2015/06/11. DOI: 10.1089/jop.2015.0049.
408. Ernst C and Christie BR. Isolectin-IB 4 as a vascular stain for the study of adult neurogenesis. *Journal of neuroscience methods* 2006; 150: 138-142. 2005/08/13. DOI: 10.1016/j.jneumeth.2005.06.018.
409. Chidlow G, Daymon M, Wood JP, et al. Localization of a wide-ranging panel of antigens in the rat retina by immunohistochemistry: comparison of Davidson's solution and formalin as fixatives. *J Histochem Cytochem* 2011; 59: 884-898. 2011/08/13. DOI: 10.1369/0022155411418115.
410. Lim JI. Iatrogenic choroidal neovascularization. *Survey of ophthalmology* 1999; 44: 95-111. 1999/12/14. DOI: 10.1016/s0039-6257(99)00077-6.
411. Pennesi ME, Neuringer M and Courtney RJ. Animal models of age related macular degeneration. *Molecular aspects of medicine* 2012; 33: 487-509. 2012/06/19. DOI: 10.1016/j.mam.2012.06.003.
412. Chung EJ, Efstathiou NE, Konstantinou EK, et al. AICAR suppresses TNF-α-induced complement factor B in RPE cells. *Scientific reports* 2017; 7: 17651. DOI: 10.1038/s41598-017-17744-w.

413. Anderson PJ, Watts H, Hille C, et al. Glial and endothelial blood-retinal barrier responses to amyloid-beta in the neural retina of the rat. *Clinical ophthalmology (Auckland, NZ)* 2008; 2: 801-816. 2009/08/12. DOI: 10.2147/opth.s3967.
414. D'Amato R, Wesolowski E and Smith LE. Microscopic visualization of the retina by angiography with high-molecular-weight fluorescein-labeled dextrans in the mouse. *Microvascular research* 1993; 46: 135-142. DOI: 10.1006/mvre.1993.1042.
415. Semkova I, Peters S, Welsandt G, et al. Investigation of laser-induced choroidal neovascularization in the rat. *Investigative ophthalmology & visual science* 2003; 44: 5349-5354. 2003/11/26.
416. Lupidi M, Schiavon S, Cerquaglia A, et al. Real-world outcomes of anti-VEGF therapy in treatment-naïve neovascular age-related macular degeneration diagnosed on OCT angiography: the REVEAL study. *Acta Ophthalmol* 2022; 100: e936-e942. 2021/08/19. DOI: 10.1111/aos.15005.
417. Kashani AH, Chen C-L, Gahm JK, et al. Optical coherence tomography angiography: A comprehensive review of current methods and clinical applications. *Progress in Retinal and Eye Research* 2017; 60: 66-100. DOI: https://doi.org/10.1016/j.preteyeres.2017.07.002.
418. Kim DY, Fingler J, Zawadzki RJ, et al. Optical imaging of the chorioretinal vasculature in the living human eye. *Proc Natl Acad Sci U S A* 2013; 110: 14354-14359. 2013/08/07. DOI: 10.1073/pnas.1307315110.
419. Jia Y, Bailey ST, Wilson DJ, et al. Quantitative optical coherence tomography angiography of choroidal neovascularization in age-related macular degeneration. *Ophthalmology* 2014; 121: 1435-1444. 2014/04/01. DOI: 10.1016/j.ophtha.2014.01.034.
420. Lupidi M, Cerquaglia A, Chhablani J, et al. Optical coherence tomography angiography in age-related macular degeneration: The game changer. *European journal of ophthalmology* 2018; 28: 349-357. 2018/04/07. DOI: 10.1177/1120672118766807.
421. Mrejen S and Spaide RF. Optical coherence tomography: Imaging of the choroid and beyond. *Survey of ophthalmology* 2013; 58: 387-429. DOI: https://doi.org/10.1016/j.survophthal.2012.12.001.
422. Pollack JS, Kim JE, Pulido JS, et al. Tissue effects of subclinical diode laser treatment of the retina. *Archives of ophthalmology* 1998; 116: 1633-1639. 1998/12/31. DOI: 10.1001/archopht.116.12.1633.
423. Eells JT, Henry MM, Summerfelt P, et al. Therapeutic photobiomodulation for methanol-induced retinal toxicity. *Proc Natl Acad Sci U S A* 2003; 100: 3439-3444. 2003/03/11. DOI: 10.1073/pnas.0534746100.
424. Fuma S, Murase H, Kuse Y, et al. Photobiomodulation with 670 nm light increased phagocytosis in human retinal pigment epithelial cells. *Molecular vision* 2015; 21: 883-892. 2015/09/01.
425. Jenkins PA and Carroll JD. How to report low-level laser therapy (LLLT)/photomedicine dose and beam parameters in clinical and laboratory studies. *Photomedicine and laser surgery* 2011; 29: 785-787. 2011/11/24. DOI: 10.1089/pho.2011.9895.
426. Schuster K, J. , Estlack L, E. and Wigle J, C. Exposing human retinal pigmented epithelial cells to red light in vitro elicits an adaptive response to a subsequent 2 μm laser challenge. *SPIE BiOS*. San Francisco, California, United States: SPIE BiOS, 2013.

427. Palanker DV, Blumenkranz MS and Marmor MF. Fifty years of ophthalmic laser therapy. *Archives of ophthalmology* 2011; 129: 1613-1619. 2011/12/14. DOI: 10.1001/archophthalmol.2011.293.
428. Casson RJ, Wood JPM, Ao J, et al. Cone photoreceptor preservation with laser photobiomodulation in murine and human retinal dystrophy. *Clin Transl Med* 2022; 12: e673. 2022/02/21. DOI: 10.1002/ctm2.673.
429. Munk MR, Gonzalez VH, Boyer DS, et al. LIGHTSITE III (Interim Analysis): Evaluation of Multiwavelength Photobiomodulation in Dry Age-Related Macular Degeneration Using the LumiThera Valeda Light Delivery System. *Investigative ophthalmology & visual science* 2022; 63: 379 – F0210-0379 – F0210.
430. Sommer AP, Pinheiro AL, Mester AR, et al. Biostimulatory windows in low-intensity laser activation: lasers, scanners, and NASA's light-emitting diode array system. *Journal of clinical laser medicine & surgery* 2001; 19: 29-33. 2001/09/08. DOI: 10.1089/104454701750066910.
431. Chung H, Dai T, Sharma SK, et al. The nuts and bolts of low-level laser (light) therapy. *Annals of biomedical engineering* 2012; 40: 516-533. 2011/11/03. DOI: 10.1007/s10439-011-0454-7.
432. Yu PK, Cringle SJ, McAllister IL, et al. Low power laser treatment of the retina ameliorates neovascularisation in a transgenic mouse model of retinal neovascularisation. *Experimental eye research* 2009; 89: 791-800. 2009/07/21. DOI: 10.1016/j.exer.2009.07.004.
433. Hattenbach LO, Beck KF, Pfeilschifter J, et al. Pigment-Epithelium-Derived Factor Is Upregulated in Photocoagulated Human Retinal Pigment Epithelial Cells. *Ophthalmic Research* 2005; 37: 341-346. DOI: 10.1159/000088263.
434. Spranger J, Hammes HP, Preissner KT, et al. Release of the angiogenesis inhibitor angiostatin in patients with proliferative diabetic retinopathy: association with retinal photocoagulation. *Diabetologia* 2000; 43: 1404-1407. 2000/12/29. DOI: 10.1007/s001250051546.
435. Miloudi S, Valensi M, El Sanharawi M, et al. Nestin contributes to laser choroidal and retinal neovascularization. *Mol Vis* 2022; 28: 280-299. 2022/10/27.
436. Dusart P, Fagerberg L, Perisic L, et al. A systems-approach reveals human nestin is an endothelial-enriched, angiogenesis-independent intermediate filament protein. *Scientific reports* 2018; 8: 14668. DOI: 10.1038/s41598-018-32859-4.
437. Mokrý J, Cízková D, Filip S, et al. Nestin expression by newly formed human blood vessels. *Stem cells and development* 2004; 13: 658-664. 2005/02/03. DOI: 10.1089/scd.2004.13.658.
438. Suzuki S, Namiki J, Shibata S, et al. The neural stem/progenitor cell marker nestin is expressed in proliferative endothelial cells, but not in mature vasculature. *J Histochem Cytochem* 2010; 58: 721-730. 2010/04/28. DOI: 10.1369/jhc.2010.955609.
439. Lendahl U, Zimmerman LB and McKay RD. CNS stem cells express a new class of intermediate filament protein. *Cell* 1990; 60: 585-595. 1990/02/23. DOI: 10.1016/0092-8674(90)90662-x.
440. Kohno H, Sakai T and Kitahara K. Induction of nestin, Ki-67, and cyclin D1 expression in Muller cells after laser injury in adult rat retina. *Graefe's archive for clinical and experimental ophthalmology = Albrecht von Graefes Archiv fur klinische und experimentelle Ophthalmologie* 2006; 244: 90-95. 2005/06/29. DOI: 10.1007/s00417-005-0030-7.

441. Moon CH, Cho H, Kim YK, et al. Nestin Expression in the Adult Mouse Retina with Pharmaceutically Induced Retinal Degeneration. *Journal of Korean medical science* 2017; 32: 343-351. 2017/01/04. DOI: 10.3346/jkms.2017.32.2.343.
442. Potente M, Gerhardt H and Carmeliet P. Basic and therapeutic aspects of angiogenesis. *Cell* 2011; 146: 873-887. 2011/09/20. DOI: 10.1016/j.cell.2011.08.039.
443. Huxlin KR, Dreher Z, Schulz M, et al. Glial reactivity in the retina of adult rats. *Glia* 1995; 15: 105-118. 1995/10/01. DOI: 10.1002/glia.440150203.
444. Regatieri CV, Branchini L and Duker JS. The role of spectral-domain OCT in the diagnosis and management of neovascular age-related macular degeneration. *Ophthalmic surgery, lasers & imaging : the official journal of the International Society for Imaging in the Eye* 2011; 42 Suppl: S56-66. 2011/07/28. DOI: 10.3928/15428877-20110627-05.
445. Lu YZ, Natoli R, Madigan M, et al. Photobiomodulation with 670 nm light ameliorates Muller cell-mediated activation of microglia and macrophages in retinal degeneration. *Experimental eye research* 2017; 165: 78-89. 2017/09/11. DOI: 10.1016/j.exer.2017.09.002.
446. Kadiu I, Glanzer JG, Kipnis J, et al. Mononuclear phagocytes in the pathogenesis of neurodegenerative diseases. *Neurotoxicity research* 2005; 8: 25-50. 2005/11/02. DOI: 10.1007/bf03033818.
447. Mudhar HS, Pollock RA, Wang C, et al. PDGF and its receptors in the developing rodent retina and optic nerve. *Development (Cambridge, England)* 1993; 118: 539-552. DOI: 10.1242/dev.118.2.539.
448. Gomes NA, do Valle IB, Gleber-Netto FO, et al. Nestin and NG2 transgenes reveal two populations of perivascular cells stimulated by photobiomodulation. *Journal of cellular physiology* 2022; 237: 2198-2210. 2022/01/19. DOI: 10.1002/jcp.30680.
449. Stepanov YV, Golovynska I, Golovynskyi S, et al. Red and near infrared light-stimulated angiogenesis mediated via Ca(2+) influx, VEGF production and NO synthesis in endothelial cells in macrophage or malignant environments. *Journal of photochemistry and photobiology B, Biology* 2022; 227: 112388. 2022/01/26. DOI: 10.1016/j.jphotobiol.2022.112388.
450. Zhao F, Shi B, Liu R, et al. Theme trends and knowledge structure on choroidal neovascularization: a quantitative and co-word analysis. *BMC ophthalmology* 2018; 18: 86. 2018/04/05. DOI: 10.1186/s12886-018-0752-z.
451. Combadiere C, Feumi C, Raoul W, et al. CX3CR1-dependent subretinal microglia cell accumulation is associated with cardinal features of age-related macular degeneration. *The Journal of clinical investigation* 2007; 117: 2920-2928. 2007/10/03. DOI: 10.1172/jci31692.
452. Tuo J, Bojanowski CM, Zhou M, et al. Murine ccl2/cx3cr1 deficiency results in retinal lesions mimicking human age-related macular degeneration. *Investigative ophthalmology & visual science* 2007; 48: 3827-3836. 2007/07/27. DOI: 10.1167/iovs.07-0051.
453. Lutty G, Grunwald J, Majji AB, et al. Changes in choriocapillaris and retinal pigment epithelium in age-related macular degeneration. *Molecular vision* 1999; 5: 35. 1999/11/17.
454. Koleva-Georgieva DN, Sivkova NP and Terzieva D. Serum inflammatory cytokines IL-1beta, IL-6, TNF-alpha and VEGF have influence on the development of diabetic retinopathy. *Folia medica* 2011; 53: 44-50. 2011/07/30.

455. Mysliwiec M, Balcerska A, Zorena K, et al. The role of vascular endothelial growth factor, tumor necrosis factor alpha and interleukin-6 in pathogenesis of diabetic retinopathy. *Diabetes research and clinical practice* 2008; 79: 141-146. 2007/08/25. DOI: 10.1016/j.diabres.2007.07.011.
456. D'Amore PA. Mechanisms of retinal and choroidal neovascularization. *Investigative ophthalmology & visual science* 1994; 35: 3974-3979. 1994/11/01.
457. Roberge FG, Caspi RR and Nussenblatt RB. Glial retinal Müller cells produce IL-1 activity and have a dual effect on autoimmune T helper lymphocytes. Antigen presentation manifested after removal of suppressive activity. *Journal of immunology (Baltimore, Md : 1950)* 1988; 140: 2193-2196. 1988/04/01.
458. Hetier E, Ayala J, Denèfle P, et al. Brain macrophages synthesize interleukin-1 and interleukin-1 mRNAs in vitro. *Journal of neuroscience research* 1988; 21: 391-397. 1988/10/01. DOI: 10.1002/jnr.490210230.
459. Frank RN. Growth factors in age-related macular degeneration: pathogenic and therapeutic implications. *Ophthalmic research* 1997; 29: 341-353. 1997/01/01. DOI: 10.1159/000268032.
460. Frank RN, Amin RH, Eliott D, et al. Basic fibroblast growth factor and vascular endothelial growth factor are present in epiretinal and choroidal neovascular membranes. *American journal of ophthalmology* 1996; 122: 393-403. 1996/09/01. DOI: 10.1016/s0002-9394(14)72066-5.
461. Amin R, Puklin JE and Frank RN. Growth factor localization in choroidal neovascular membranes of age-related macular degeneration. *Investigative ophthalmology & visual science* 1994; 35: 3178-3188. 1994/07/01.
462. Lambooij AC, van Wely KH, Lindenbergh-Kortleve DJ, et al. Insulin-like growth factor-I and its receptor in neovascular age-related macular degeneration. *Investigative ophthalmology & visual science* 2003; 44: 2192-2198. 2003/04/26. DOI: 10.1167/iovs.02-0410.
463. Rosenthal R, Wohlleben H, Malek G, et al. Insulin-like growth factor-1 contributes to neovascularization in age-related macular degeneration. *Biochemical and biophysical research communications* 2004; 323: 1203-1208. 2004/09/29. DOI: 10.1016/j.bbrc.2004.08.219.
464. Seghezzi G, Patel S, Ren CJ, et al. Fibroblast growth factor-2 (FGF-2) induces vascular endothelial growth factor (VEGF) expression in the endothelial cells of forming capillaries: an autocrine mechanism contributing to angiogenesis. *The Journal of cell biology* 1998; 141: 1659-1673. 1998/07/01. DOI: 10.1083/jcb.141.7.1659.
465. Ferrari G, Cook BD, Terushkin V, et al. Transforming growth factor-beta 1 (TGF-beta1) induces angiogenesis through vascular endothelial growth factor (VEGF)-mediated apoptosis. *Journal of cellular physiology* 2009; 219: 449-458. 2009/01/31. DOI: 10.1002/jcp.21706.
466. Brown J, Wallet MA, Krastins B, et al. Proteome bioprofiles distinguish between M1 priming and activation states in human macrophages. *Journal of leukocyte biology* 2010; 87: 655-662. 2009/12/17. DOI: 10.1189/jlb.0809570.
467. Jiang K, Cao S, Cui JZ, et al. Immuno-modulatory Effect of IFN-gamma in AMD and its Role as a Possible Target for Therapy. *Journal of clinical & experimental ophthalmology* 2013; Suppl 2: 0071-0076. 2013/02/26. DOI: 10.4172/2155-9570-s2-007.
468. Lau LI, Chiou SH, Liu CJ, et al. The effect of photo-oxidative stress and inflammatory cytokine on complement factor H expression in retinal pigment epithelial

cells. *Invest Ophthalmol Vis Sci* 2011; 52: 6832-6841. 2011/07/12. DOI: 10.1167/iovs.11-7815.
469. Tobe T, Ortega S, Luna JD, et al. Targeted disruption of the FGF2 gene does not prevent choroidal neovascularization in a murine model. *The American journal of pathology* 1998; 153: 1641-1646. 1998/11/12. DOI: 10.1016/s0002-9440(10)65753-7.
470. Hangai M, Yoshimura N and Honda Y. Increased cytokine gene expression in rat retina following transient ischemia. *Ophthalmic Res* 1996; 28: 248-254. 1996/01/01. DOI: 10.1159/000267910.
471. Bringmann A, Iandiev I, Pannicke T, et al. Cellular signaling and factors involved in Müller cell gliosis: neuroprotective and detrimental effects. *Prog Retin Eye Res* 2009; 28: 423-451. 2009/08/08. DOI: 10.1016/j.preteyeres.2009.07.001.
472. Coorey NJ, Shen W, Chung SH, et al. The role of glia in retinal vascular disease. *Clinical & experimental optometry : journal of the Australian Optometrical Association* 2012; 95: 266-281. 2012/04/24. DOI: 10.1111/j.1444-0938.2012.00741.x.
473. Norden DM, Trojanowski PJ, Villanueva E, et al. Sequential activation of microglia and astrocyte cytokine expression precedes increased Iba-1 or GFAP immunoreactivity following systemic immune challenge. *Glia* 2016; 64: 300-316. 2015/10/16. DOI: 10.1002/glia.22930.
474. Lee JE, Liang KJ, Fariss RN, et al. Ex vivo dynamic imaging of retinal microglia using time-lapse confocal microscopy. *Investigative ophthalmology & visual science* 2008; 49: 4169-4176. 2008/05/20. DOI: 10.1167/iovs.08-2076.
475. Martiney JA, Litwak M, Berman JW, et al. Pathophysiologic effect of interleukin-1b in the rabbit retina. *The American journal of pathology* 1990; 137: 1411-1423.
476. Valle ML, Dworshak J, Sharma A, et al. Inhibition of interleukin-6 trans-signaling prevents inflammation and endothelial barrier disruption in retinal endothelial cells. *Experimental eye research* 2019; 178: 27-36. 2018/09/22. DOI: 10.1016/j.exer.2018.09.009.
477. Aderka D, Le JM and Vilcek J. IL-6 inhibits lipopolysaccharide-induced tumor necrosis factor production in cultured human monocytes, U937 cells, and in mice. *Journal of immunology (Baltimore, Md : 1950)* 1989; 143: 3517-3523. 1989/12/01.
478. Kim I, Ryan AM, Rohan R, et al. Constitutive expression of VEGF, VEGFR-1, and VEGFR-2 in normal eyes. *Investigative ophthalmology & visual science* 1999; 40: 2115-2121. 1999/08/10.
479. Eells JT, Wong-Riley MT, VerHoeve J, et al. Mitochondrial signal transduction in accelerated wound and retinal healing by near-infrared light therapy. *Mitochondrion* 2004; 4: 559-567. 2005/08/27. DOI: 10.1016/j.mito.2004.07.033.
480. Fitzgerald M, Bartlett CA, Payne SC, et al. Near infrared light reduces oxidative stress and preserves function in CNS tissue vulnerable to secondary degeneration following partial transection of the optic nerve. *Journal of neurotrauma* 2010; 27: 2107-2119. 2010/09/09. DOI: 10.1089/neu.2010.1426.
481. Shweiki D, Itin A, Soffer D, et al. Vascular endothelial growth factor induced by hypoxia may mediate hypoxia-initiated angiogenesis. *Nature* 1992; 359: 843-845. 1992/10/29. DOI: 10.1038/359843a0.
482. Campochiaro PA. Ocular neovascularization. *Journal of molecular medicine (Berlin, Germany)* 2013; 91: 311-321. 2013/01/19. DOI: 10.1007/s00109-013-0993-5.

483. Thomas KA. Vascular endothelial growth factor, a potent and selective angiogenic agent. *The Journal of biological chemistry* 1996; 271: 603-606. 1996/01/12. DOI: 10.1074/jbc.271.2.603.
484. Garibyan L and Avashia N. Polymerase chain reaction. *The Journal of investigative dermatology* 2013; 133: 1-4. 2013/02/13. DOI: 10.1038/jid.2013.1.
485. Nolan T, Hands RE and Bustin SA. Quantification of mRNA using real-time RT-PCR. *Nature protocols* 2006; 1: 1559-1582. 2007/04/05. DOI: 10.1038/nprot.2006.236.
486. Zhang SX, Wang JJ, Gao G, et al. Pigment epithelium-derived factor downregulates vascular endothelial growth factor (VEGF) expression and inhibits VEGF-VEGF receptor 2 binding in diabetic retinopathy. *Journal of molecular endocrinology* 2006; 37: 1-12. 2006/08/12. DOI: 10.1677/jme.1.02008.
487. Ablonczy Z, Prakasam A, Fant J, et al. Pigment epithelium-derived factor maintains retinal pigment epithelium function by inhibiting vascular endothelial growth factor-R2 signaling through gamma-secretase. *The Journal of biological chemistry* 2009; 284: 30177-30186. 2009/09/03. DOI: 10.1074/jbc.M109.032391.
488. Farnoodian M, Sorenson CM and Sheibani N. Negative Regulators of Angiogenesis, Ocular Vascular Homeostasis, and Pathogenesis and Treatment of Exudative AMD. *Journal of ophthalmic & vision research* 2018; 13: 470-486. 2018/11/28. DOI: 10.4103/jovr.jovr_67_18.
489. Wang S, Gottlieb JL, Sorenson CM, et al. Modulation of thrombospondin 1 and pigment epithelium-derived factor levels in vitreous fluid of patients with diabetes. *Archives of ophthalmology* 2009; 127: 507-513. 2009/04/15. DOI: 10.1001/archophthalmol.2009.53.
490. Wang S, Sorenson CM and Sheibani N. Lack of Thrombospondin 1 and Exacerbation of Choroidal Neovascularization. *Archives of ophthalmology* 2012; 130: 615-620. DOI: 10.1001/archopthalmol.2011.1892.
491. Sheibani N and Frazier WA. Thrombospondin 1 expression in transformed endothelial cells restores a normal phenotype and suppresses their tumorigenesis. *Proc Natl Acad Sci U S A* 1995; 92: 6788-6792. 1995/07/18. DOI: 10.1073/pnas.92.15.6788.
492. Wang S, Wu Z, Sorenson CM, et al. Thrombospondin-1-deficient mice exhibit increased vascular density during retinal vascular development and are less sensitive to hyperoxia-mediated vessel obliteration. *Developmental dynamics : an official publication of the American Association of Anatomists* 2003; 228: 630-642. 2003/12/04. DOI: 10.1002/dvdy.10412.
493. Wu Z, Wang S, Sorenson CM, et al. Attenuation of retinal vascular development and neovascularization in transgenic mice over-expressing thrombospondin-1 in the lens. *Developmental dynamics : an official publication of the American Association of Anatomists* 2006; 235: 1908-1920. 2006/05/13. DOI: 10.1002/dvdy.20837.
494. Miyajima-Uchida H, Hayashi H, Beppu R, et al. Production and accumulation of thrombospondin-1 in human retinal pigment epithelial cells. *Investigative ophthalmology & visual science* 2000; 41: 561-567. 2000/02/12.
495. Carron JA, Hiscott P, Hagan S, et al. Cultured human retinal pigment epithelial cells differentially express thrombospondin-1, -2, -3, and -4. *The international journal of biochemistry & cell biology* 2000; 32: 1137-1142. 2001/01/04.
496. Park K, Jin J, Hu Y, et al. Overexpression of pigment epithelium-derived factor inhibits retinal inflammation and neovascularization. *The American journal of pathology* 2011; 178: 688-698. 2011/02/02. DOI: 10.1016/j.ajpath.2010.10.014.

497. Dawson DW, Volpert OV, Gillis P, et al. Pigment epithelium-derived factor: A potent inhibitor of angiogenesis. *Science (New York, NY)* 1999; 285: 245-248.
498. Korn C and Augustin HG. Mechanisms of Vessel Pruning and Regression. *Dev Cell* 2015; 34: 5-17. 2015/07/08. DOI: 10.1016/j.devcel.2015.06.004.
499. Lai CC, Wu WC, Chen SL, et al. Suppression of choroidal neovascularization by adeno-associated virus vector expressing angiostatin. *Invest Ophthalmol Vis Sci* 2001; 42: 2401-2407. 2001/08/31.
500. Campochiaro PA, Lauer AK, Sohn EH, et al. Lentiviral Vector Gene Transfer of Endostatin/Angiostatin for Macular Degeneration (GEM) Study. *Human gene therapy* 2017; 28: 99-111. 2016/10/07. DOI: 10.1089/hum.2016.117.
501. Saishin Y, Silva RL, Saishin Y, et al. Periocular gene transfer of pigment epithelium-derived factor inhibits choroidal neovascularization in a human-sized eye. *Hum Gene Ther* 2005; 16: 473-478. 2005/05/06. DOI: 10.1089/hum.2005.16.473.
502. Gehlbach P, Demetriades AM, Yamamoto S, et al. Periocular injection of an adenoviral vector encoding pigment epithelium-derived factor inhibits choroidal neovascularization. *Gene Ther* 2003; 10: 637-646. 2003/04/15. DOI: 10.1038/sj.gt.3301931.
503. Sugita Y, Becerra SP, Chader GJ, et al. Pigment epithelium-derived factor (PEDF) has direct effects on the metabolism and proliferation of microglia and indirect effects on astrocytes. *Journal of neuroscience research* 1997; 49: 710-718. 1997/10/23 22:32. DOI: 10.1002/(sici)1097-4547(19970915)49:6<710::Aid-jnr5>3.0.Co;2-a.
504. Cohen J, Sugita Y, Chader GJ, et al. Recombinant forms of the neurotrophic factor pigment epithelium-derived factor activate cellular metabolism and inhibit proliferation of the RAW macrophage cell line. *Neuroimmunomodulation* 2000; 7: 51-58. 1999/12/22. DOI: 10.1159/000026420.
505. Notari L, Baladron V, Aroca-Aguilar JD, et al. Identification of a lipase-linked cell membrane receptor for pigment epithelium-derived factor. *The Journal of biological chemistry* 2006; 281: 38022-38037. 2006/10/13. DOI: 10.1074/jbc.M600353200.
506. Subramanian P, Notario PM and Becerra SP. Pigment epithelium-derived factor receptor (PEDF-R): a plasma membrane-linked phospholipase with PEDF binding affinity. *Advances in experimental medicine and biology* 2010; 664: 29-37. 2010/03/20. DOI: 10.1007/978-1-4419-1399-9_4.
507. Subramanian P, Locatelli-Hoops S, Kenealey J, et al. Pigment epithelium-derived factor (PEDF) prevents retinal cell death via PEDF Receptor (PEDF-R): identification of a functional ligand binding site. *The Journal of biological chemistry* 2013; 288: 23928-23942. 2013/07/03. DOI: 10.1074/jbc.M113.487884.
508. Yabe T, Herbert JT, Takanohashi A, et al. Treatment of cerebellar granule cell neurons with the neurotrophic factor pigment epithelium-derived factor in vitro enhances expression of other neurotrophic factors as well as cytokines and chemokines. *Journal of neuroscience research* 2004; 77: 642-652. 2004/09/08. DOI: 10.1002/jnr.20196.
509. Muili KA, Gopalakrishnan S, Eells JT, et al. Photobiomodulation induced by 670 nm light ameliorates MOG35-55 induced EAE in female C57BL/6 mice: a role for remediation of nitrosative stress. *PloS one* 2013; 8: e67358. 2013/07/11. DOI: 10.1371/journal.pone.0067358.

510. Beach KM, Wang J and Otteson DC. Regulation of Stem Cell Properties of Müller Glia by JAK/STAT and MAPK Signaling in the Mammalian Retina. *Stem cells international* 2017; 2017: 1610691. DOI: 10.1155/2017/1610691.
511. Kalluri R and Weinberg RA. The basics of epithelial-mesenchymal transition. *The Journal of clinical investigation* 2009; 119: 1420-1428. 2009/06/03. DOI: 10.1172/jci39104.
512. Walcott JC and Provis JM. Müller cells express the neuronal progenitor cell marker nestin in both differentiated and undifferentiated human foetal retina. *Clinical & experimental ophthalmology* 2003; 31: 246-249. 2003/06/06. DOI: 10.1046/j.1442-9071.2003.00638.x.
513. Strzalka W and Ziemienowicz A. Proliferating cell nuclear antigen (PCNA): a key factor in DNA replication and cell cycle regulation. *Annals of Botany* 2010; 107: 1127-1140. DOI: 10.1093/aob/mcq243.
514. Bravo R and Macdonald-Bravo H. Existence of two populations of cyclin/proliferating cell nuclear antigen during the cell cycle: association with DNA replication sites. *J Cell Biol* 1987; 105: 1549-1554. 1987/10/01. DOI: 10.1083/jcb.105.4.1549.
515. Kurki P, Vanderlaan M, Dolbeare F, et al. Expression of proliferating cell nuclear antigen (PCNA)/cyclin during the cell cycle. *Experimental cell research* 1986; 166: 209-219. 1986/09/01. DOI: 10.1016/0014-4827(86)90520-3.
516. Schönenberger F, Deutzmann A, Ferrando-May E, et al. Discrimination of cell cycle phases in PCNA-immunolabeled cells. *BMC Bioinformatics* 2015; 16: 180. 2015/05/30. DOI: 10.1186/s12859-015-0618-9.
517. Umar A, Buermeyer AB, Simon JA, et al. Requirement for PCNA in DNA mismatch repair at a step preceding DNA resynthesis. *Cell* 1996; 87: 65-73. 1996/10/04. DOI: 10.1016/s0092-8674(00)81323-9.
518. Ju W-K, Kim K-Y, Hofmann H-D, et al. Selective Neuronal Survival and Upregulation of PCNA in the Rat Inner Retina Following Transient Ischemia. *Journal of Neuropathology & Experimental Neurology* 2000; 59: 241-250. DOI: 10.1093/jnen/59.3.241.
519. Strunnikova N, Baffi J, Gonzalez A, et al. Regulated heat shock protein 27 expression in human retinal pigment epithelium. *Invest Ophthalmol Vis Sci* 2001; 42: 2130-2138. 2001/08/02.
520. Dean DO and Tytell M. Hsp25 and -90 Immunoreactivity in the Normal Rat Eye. *Investigative Ophthalmology & Visual Science* 2001; 42: 3031-3040.
521. Concannon CG, Gorman AM and Samali A. On the role of Hsp27 in regulating apoptosis. *Apoptosis* 2003; 8: 61-70. 2003/01/03. DOI: 10.1023/a:1021601103096.
522. Bruey JM, Ducasse C, Bonniaud P, et al. Hsp27 negatively regulates cell death by interacting with cytochrome c. *Nat Cell Biol* 2000; 2: 645-652. 2000/09/12. DOI: 10.1038/35023595.
523. Garrido C, Bruey JM, Fromentin A, et al. HSP27 inhibits cytochrome c-dependent activation of procaspase-9. *FASEB journal : official publication of the Federation of American Societies for Experimental Biology* 1999; 13: 2061-2070. 1999/11/02. DOI: 10.1096/fasebj.13.14.2061.
524. Jazwa A and Cuadrado A. Targeting heme oxygenase-1 for neuroprotection and neuroinflammation in neurodegenerative diseases. *Current drug targets* 2010; 11: 1517-1531. 2010/08/14. DOI: 10.2174/1389450111009011517.

525. Huang G, Diao J, Yi H, et al. Signaling pathways involved in HSP32 induction by hyperbaric oxygen in rat spinal neurons. *Redox biology* 2016; 10: 108-118. DOI: https://doi.org/10.1016/j.redox.2016.09.011.
526. Pae HO, Kim EC and Chung HT. Integrative survival response evoked by heme oxygenase-1 and heme metabolites. *Journal of clinical biochemistry and nutrition* 2008; 42: 197-203. 2008/06/12. DOI: 10.3164/jcbn.2008029.
527. Walsh N, Valter K and Stone J. Cellular and Subcellular Patterns of Expression of bFGF and CNTF in the Normal and Light Stressed Adult Rat Retina. *Experimental Eye Research* 2001; 72: 495-501. DOI: https://doi.org/10.1006/exer.2000.0984.
528. Yang P, Peairs JJ, Tano R, et al. Oxidant-mediated Akt activation in human RPE cells. *Investigative ophthalmology & visual science* 2006; 47: 4598-4606. 2006/09/28. DOI: 10.1167/iovs.06-0140.
529. Sreekumar PG, Kannan R, de Silva AT, et al. Thiol regulation of vascular endothelial growth factor-A and its receptors in human retinal pigment epithelial cells. *Biochemical and biophysical research communications* 2006; 346: 1200-1206. 2006/06/24. DOI: 10.1016/j.bbrc.2006.06.021.
530. Wen R, Song Y, Cheng T, et al. Injury-induced upregulation of bFGF and CNTF mRNAS in the rat retina. *J Neurosci* 1995; 15: 7377-7385. 1995/11/01.
531. Yafai Y, Iandiev I, Lange J, et al. Basic Fibroblast Growth Factor Contributes to a Shift in the Angioregulatory Activity of Retinal Glial (Müller) Cells. *PLOS ONE* 2013; 8: e68773. DOI: 10.1371/journal.pone.0068773.
532. Casanovas O, Hicklin DJ, Bergers G, et al. Drug resistance by evasion of antiangiogenic targeting of VEGF signaling in late-stage pancreatic islet tumors. *Cancer cell* 2005; 8: 299-309. 2005/10/18. DOI: 10.1016/j.ccr.2005.09.005.
533. Batchelor TT, Sorensen AG, di Tomaso E, et al. AZD2171, a pan-VEGF receptor tyrosine kinase inhibitor, normalizes tumor vasculature and alleviates edema in glioblastoma patients. *Cancer cell* 2007; 11: 83-95. DOI: 10.1016/j.ccr.2006.11.021.
534. Gerwins P, Sköldenberg E and Claesson-Welsh L. Function of fibroblast growth factors and vascular endothelial growth factors and their receptors in angiogenesis. *Crit Rev Oncol Hematol* 2000; 34: 185-194. 2000/06/06. DOI: 10.1016/s1040-8428(00)00062-7.
535. Suyama K, Shapiro I, Guttman M, et al. A signaling pathway leading to metastasis is controlled by N-cadherin and the FGF receptor. *Cancer cell* 2002; 2: 301-314. 2002/10/26. DOI: 10.1016/s1535-6108(02)00150-2.
536. Costa R, Carneiro BA, Chandra S, et al. Spotlight on lenvatinib in the treatment of thyroid cancer: patient selection and perspectives. *Drug design, development and therapy* 2016; 10: 873-884. 2016/03/26. DOI: 10.2147/dddt.s93459.
537. Koziczak M, Holbro T and Hynes NE. Blocking of FGFR signaling inhibits breast cancer cell proliferation through downregulation of D-type cyclins. *Oncogene* 2004; 23: 3501-3508. 2004/04/30. DOI: 10.1038/sj.onc.1207331.
538. Li Z, Song Y, Chen X, et al. Biological Modulation of Mouse RPE Cells in Response to Subthreshold Diode Micropulse Laser Treatment. *Cell biochemistry and biophysics* 2015; 73: 545-552. 2016/06/29. DOI: 10.1007/s12013-015-0675-8.
539. Natoli R, Zhu Y, Valter K, et al. Gene and noncoding RNA regulation underlying photoreceptor protection: microarray study of dietary antioxidant saffron and photobiomodulation in rat retina. *Molecular vision* 2010; 16: 1801-1822. 2010/09/17.

540. Gamble JR and Vadas MA. Endothelial adhesiveness for blood neutrophils is inhibited by transforming growth factor-beta. *Science (New York, NY)* 1988; 242: 97-99. 1988/10/07. DOI: 10.1126/science.3175638.
541. Ruscetti FW and Palladino MA. Transforming growth factor-beta and the immune system. *Prog Growth Factor Res* 1991; 3: 159-175. 1991/01/01. DOI: 10.1016/s0955-2235(05)80006-7.
542. Merrill JE and Zimmerman RP. Natural and induced cytotoxicity of oligodendrocytes by microglia is inhibitable by TGF beta. *Glia* 1991; 4: 327-331. 1991/01/01. DOI: 10.1002/glia.440040311.
543. Tsunawaki S, Sporn M, Ding A, et al. Deactivation of macrophages by transforming growth factor-beta. *Nature* 1988; 334: 260-262. 1988/07/21. DOI: 10.1038/334260a0.
544. Innamorato NG, Lastres-Becker I and Cuadrado A. Role of microglial redox balance in modulation of neuroinflammation. *Current opinion in neurology* 2009; 22: 308-314. 2009/04/11. DOI: 10.1097/WCO.0b013e32832a3225.
545. Bertolino P, Deckers M, Lebrin F, et al. Transforming Growth Factor-[beta] Signal Transduction in Angiogenesis and Vascular Disorders*. *Chest* 2005; 128: 585S-590S.
546. Müller G, Behrens J, Nussbaumer U, et al. Inhibitory action of transforming growth factor beta on endothelial cells. *Proc Natl Acad Sci U S A* 1987; 84: 5600-5604. 1987/08/01. DOI: 10.1073/pnas.84.16.5600.
547. Behzadian MA, Wang XL, Windsor LJ, et al. TGF-beta increases retinal endothelial cell permeability by increasing MMP-9: possible role of glial cells in endothelial barrier function. *Invest Ophthalmol Vis Sci* 2001; 42: 853-859. 2001/02/27.
548. Spranger J, Meyer-Schwickerath R, Klein M, et al. Deficient activation and different expression of transforming growth factor-beta isoforms in active proliferative diabetic retinopathy and neovascular eye disease. *Experimental and clinical endocrinology & diabetes : official journal, German Society of Endocrinology [and] German Diabetes Association* 1999; 107: 21-28. 1999/03/17. DOI: 10.1055/s-0029-1212068.
549. Pepper MS. Transforming growth factor-beta: vasculogenesis, angiogenesis, and vessel wall integrity. *Cytokine & growth factor reviews* 1997; 8: 21-43. 1997/03/01. DOI: 10.1016/s1359-6101(96)00048-2.
550. Penfold PL, Liew SC, Madigan MC, et al. Modulation of major histocompatibility complex class II expression in retinas with age-related macular degeneration. *Investigative ophthalmology & visual science* 1997; 38: 2125-2133. 1997/10/23.
551. Georges P, Cornish EE, Provis JM, et al. Muller cell expression of glutamate cycle related proteins and anti-apoptotic proteins in early human retinal development. *The British journal of ophthalmology* 2006; 90: 223-228. 2006/01/21. DOI: 10.1136/bjo.2005.078014.
552. Lichtlen P, Lam TT, Nork TM, et al. Relative contribution of VEGF and TNF-alpha in the cynomolgus laser-induced CNV model: comparing the efficacy of bevacizumab, adalimumab, and ESBA105. *Investigative ophthalmology & visual science* 2010; 51: 4738-4745. 2010/04/16. DOI: 10.1167/iovs.09-4890.
553. Chidlow G, Shibeeb O, Plunkett M, et al. Glial cell and inflammatory responses to retinal laser treatment: comparison of a conventional photocoagulator and a novel, 3-

nanosecond pulse laser. *Invest Ophthalmol Vis Sci* 2013; 54: 2319-2332. 2013/02/27. DOI: 10.1167/iovs.12-11204.
554. Ohsawa K, Imai Y, Sasaki Y, et al. Microglia/macrophage-specific protein Iba1 binds to fimbrin and enhances its actin-bundling activity. *J Neurochem* 2004; 88: 844-856. 2004/02/06. DOI: 10.1046/j.1471-4159.2003.02213.x.
555. Arroba AI, Alcalde-Estevez E, Garcia-Ramirez M, et al. Modulation of microglia polarization dynamics during diabetic retinopathy in db/db mice. *Biochimica et biophysica acta* 2016; 1862: 1663-1674. 2016/06/09. DOI: 10.1016/j.bbadis.2016.05.024.
556. Han JW, Choi J, Kim YS, et al. Comparison of the neuroinflammatory responses to selective retina therapy and continuous-wave laser photocoagulation in mouse eyes. *Graefe's archive for clinical and experimental ophthalmology = Albrecht von Graefes Archiv fur klinische und experimentelle Ophthalmologie* 2018; 256: 341-353. 2018/01/13. DOI: 10.1007/s00417-017-3883-7.
557. Ito D, Imai Y, Ohsawa K, et al. Microglia-specific localisation of a novel calcium binding protein, Iba1. *Brain research Molecular brain research* 1998; 57: 1-9. 1998/06/19. DOI: 10.1016/s0169-328x(98)00040-0.
558. Jurga AM, Paleczna M and Kuter KZ. Overview of General and Discriminating Markers of Differential Microglia Phenotypes. *Frontiers in cellular neuroscience* 2020; 14: 198. 2020/08/28. DOI: 10.3389/fncel.2020.00198.
559. Chhor V, Le Charpentier T, Lebon S, et al. Characterization of phenotype markers and neuronotoxic potential of polarised primary microglia in vitro. *Brain, behavior, and immunity* 2013; 32: 70-85. 2013/03/05. DOI: 10.1016/j.bbi.2013.02.005.
560. Jobling AI, Guymer RH, Vessey KA, et al. Nanosecond laser therapy reverses pathologic and molecular changes in age-related macular degeneration without retinal damage. *FASEB journal : official publication of the Federation of American Societies for Experimental Biology* 2015; 29: 696-710. 2014/11/14. DOI: 10.1096/fj.14-262444.
561. Laser treatment in eyes with large drusen: Short-term effects seen in a pilot randomized clinical trial. *Ophthalmology* 1998; 105: 11-23. DOI: https://doi.org/10.1016/S0161-6420(98)90931-9.
562. Laser Treatment in Patients with Bilateral Large Drusen: The Complications of Age-Related Macular Degeneration Prevention Trial. *Ophthalmology* 2006; 113: 1974-1986. DOI: https://doi.org/10.1016/j.ophtha.2006.08.015.
563. Rhodes KM, Weinstein R, Saltzmann RM, et al. Intraocular pressure reduction in the untreated fellow eye after selective laser trabeculoplasty. *Current medical research and opinion* 2009; 25: 787-796. 2009/02/11. DOI: 10.1185/03007990902728316.
564. Ford KM, Saint-Geniez M, Walshe T, et al. Expression and role of VEGF in the adult retinal pigment epithelium. *Investigative ophthalmology & visual science* 2011; 52: 9478-9487. 2011/11/08. DOI: 10.1167/iovs.11-8353.
565. Byeon SH, Lee SC, Choi SH, et al. Vascular endothelial growth factor as an autocrine survival factor for retinal pigment epithelial cells under oxidative stress via the VEGF-R2/PI3K/Akt. *Investigative ophthalmology & visual science* 2010; 51: 1190-1197. 2009/10/17. DOI: 10.1167/iovs.09-4144.
566. Yang X and Cepko CL. Flk-1, a receptor for vascular endothelial growth factor (VEGF), is expressed by retinal progenitor cells. *J Neurosci* 1996; 16: 6089-6099. 1996/10/01. DOI: 10.1523/jneurosci.16-19-06089.1996.

567. Holz FG, Sadda SR, Busbee B, et al. Efficacy and Safety of Lampalizumab for Geographic Atrophy Due to Age-Related Macular Degeneration: Chroma and Spectri Phase 3 Randomized Clinical Trials. *JAMA ophthalmology* 2018; 136: 666-677. 2018/05/26. DOI: 10.1001/jamaophthalmol.2018.1544.
568. Zarbin MA. Anti-VEGF Agents and the Risk of Arteriothrombotic Events. *Asia-Pacific journal of ophthalmology (Philadelphia, Pa)* 2018; 7: 63-67. 2018/02/07. DOI: 10.22608/apo.2017495.